Peter Wellstead
Mathieu Cloutier *Editors*

Systems Biology of Parkinson's Disease

Springer

Systems Biology of Parkinson's Disease

Peter Wellstead • Mathieu Cloutier
Editors

Systems Biology of Parkinson's Disease

Springer

Editors
Peter Wellstead
Hamilton Institute
National University of Ireland
Maynooth, County Kildare, Ireland

Mathieu Cloutier
Ecole Polytechnique de Montreal
Montreal, QC, Canada

ISBN 978-1-4614-3410-8 ISBN 978-1-4614-3411-5 (eBook)
DOI 10.1007/978-1-4614-3411-5
Springer New York Heidelberg Dordrecht London

Library of Congress Control Number: 2012936651

Printed on acid-free paper

Springer is part of Springer Science+Business Media (www.springer.com)

Preface

The term *Systems Biology* first appeared in 1968 [1] and immediately attracted attention in both the life and physical sciences. It was important because it provided a name, and therefore a focus, for an emerging interdisciplinary activity. The intervening years have been fruitful for systems biology. Many countries now have institutes dedicated to the area (some have several!) and the number of interdisciplinary courses linking systems theory and biology continues to expand. Rapid growth is not generally a harmonious affair and so it is with systems biology. There are continuing debates as to what systems biology means, what it should do, and how it can best deliver benefits to society. However, no matter how animated these discussions may become, there is a clear consensus on one point: interdisciplinary effort is essential if we are to adequately understand the complexities of the human body and the diseases that afflict it.

Systems biology in the service of disease research is the motivation for this book. The choice of Parkinson's disease (PD) for the study was determined by the problems that PD, and other neurodegenerative disorders, pose to society. Parkinson's disease affects approximately 0.3% of the world's population and 1% of people over 60 years old. And PD exacts a high price: in the USA for example it costs over 20 billion dollars per year, and this sum will continue to grow as life expectancy increases. Beyond the financial issues, PD brings a considerable long-term personal burden to sufferers: with no cures or preventative strategies, it typically takes more than a decade of decline to run its course. There are interventions to alleviate the principal symptoms of motor dysfunction, but no treatment can prevent its progression.

For medical science, the problems of PD lie with its complexity, variability and multi-factorial origins. Each of these issues presents huge challenges for traditional life science; together they form an immense obstacle to progress and understanding. The aim of this book is to demonstrate how systems biology tools—new measurement methods, mathematical modelling, computer simulation and theoretical analysis—can help in disease research. The chapters in this volume present specific examples of these, as applied to PD. They represent a snapshot of the state-of-the-art in the systems biology of Parkinson's disease.

Background

Because this book addresses two scientific constituencies, we offer two contrasting introductory backgrounds: one for the systems biology community and the other for PD researchers. First for systems biologists.

On Parkinson's Disease

Modern lifestyles and modern healthcare mean that people live longer, and as a consequence, they increasingly fall prey to neurodegenerative conditions like PD. But PD is not a product of modern life styles—ancient Ayurveda literature describes a disease resembling PD [2, 3]. Much later, around 170 A.D., Galen made a good first definition of motor tremor (which would have included PD); distinguishing it from other forms of involuntary movement [4]. Since Galen there have been numerous descriptions of tremor and "shaking palsies," with the first comprehensive attempt in the English language being James Parkinson's famous essay [5]. As part of his important work, Charcot [6] extended Parkinson's description and coined the term Parkinson's disease. Subsequently, Sherringham [7] moved things on considerable by making the link between PD tremors and the specific region of the brain responsible for motor control.

What was going wrong in the motor region remained unknown until the 1960s, when a deficit of dopamine in the motor control circuits of the *basal ganglia* was associated with Parkinsonian tremor [8]. This discovery led to the use of L-dopa as the first effective therapy for PD. L-dopa is a dopamine precursor and was the first of a family of therapies that attempt to regulate dopamine levels in the *striatum*. To this day, these drugs remain the standard treatment.

Further important illumination came in the staging theory [9] in which, by tracing intracellular accumulations of a protein (alphasynuclein) residue, a progressive pattern was observed. This consists of a stage-wise trajectory of PD damage, starting at brain stem and spreading in a sequential manner to different brain sectors. Within the staging process each brain region responds differently, but the dopaminergic neurons of the *substantia nigra* (*SN*) are most vulnerable: it is their death that causes the debilitating tremors associated with PD.

This book is about systems biology used to study the causes of PD and biochemical mechanisms of PD, rather than therapies. However, it is interesting to mention, at least in passing, an important new electrical therapeutic from the 1980s. This takes the form of low intensity periodic (~130 Hz) stimulation of deep-brain elements associated with the motor circuits—particularly the *subthalamic nucleus* [10]. When it works, the technique, known as deep brain stimulation (DBS) is capable of remarkable results, often with complete alleviation of motor tremors. There are a number of plausible DBS theories, but how DBS works in detail is a subject of current research.

Although the causes of PD are unknown, a good deal is known about various environmental, genetic and biological issues that are implicated in the condition. Most of these will be described in detail within the chapters that follow, but an initial overview will provide some orientation. A number of genetic irregularities have been associated with PD. However, the number of truly genetic cases of PD (familial PD) is small (less than 10%). In most instances, the cause of PD is unknown—this is termed idiopathic or sporadic PD. For this majority of sufferers the general view is that advancing age, life-experiences and a number of environmental issues can be responsible. What happens in a neuron during PD is known only in qualitative terms and the general description is of several sets of biochemical species interacting in a "vicious cycle." Why certain neurons are more vulnerable than others is also unknown, although the chapters of this volume will use systems ideas to make some suggestions.

On Systems Biology

This section is for PD specialists and researchers.

In its broadest definition, systems biology is the application to living things of techniques (mathematical modelling, theoretical analysis and computer simulation) originally developed to understand how physical/engineering systems work. Such interdisciplinary transfers of ideas from the physical to the living world (and vice versa) are not new. They occur periodically in the development of science, with a relevant example from 1679 being Borelli's *De Motu Animalium*. In this justly famous work, Borelli used the methods of Galileo's in the field of mechanics to explain movement in humans, animal and fishes.

Attempts to apply ideas from technological systems theory to biology started in earnest during the mid-twentieth century, notably with Norbert Wiener's book, *Cybernetics* [11]. In this important book, Wiener gave accounts of control and communications theory applied to understand biological phenomena. Despite its importance, *Cybernetics* was in fact indicative of a wider interdisciplinary movement, which is typified by other works, such as Schrödinger's *What is Life?* [12]; Cannon's, *The Wisdom of the Body*, [13]; and Hodgkin and Huxley's research [14]. These contributions gave important indicators of how ideas from physics, applied mathematics and technological systems theory could usefully help explain how living things work—with Hodgkin and Huxley showing a "proof of the pudding."

In the 1960s, systems theorists and life scientists began to formalise systems biology as the application of mathematical modelling, dynamical systems analysis and computer simulation in life science [1]. Cheap computing and new sensing technologies became available, and by the last decades of the twentieth century it became feasible to model and analyse complex biological systems on personal computers. This task was made easier by free software and open source directories of models (for example the CellML directory of mathematical models).

The enthusiasm of cheerleaders such as Kitano [15], and others, generated an expectation that systems biology could give deeper understanding of cellular processes and help solve big problems in drug development. In the sequel to the Human Genome Project there was a belief among geneticists that systems biology would help extract hidden information (particularly concerning complex diseases [16]) from genomic and proteomic data. In another fundamental development, many systems biologists hope to elucidate the hidden dynamics of gene expression and cell signalling pathways. In parallel with fundamental research aims, there has always been a "problem-solving" view of systems biology. Features of this include a systems approach to (1) mathematical modelling of entire organs [17], (2) "personalised medicine" for delivery of healthcare [18] and (3) understanding the causes of complex diseases. In the latter context, mathematical models have been used to study HIV-AIDS, with emergent work on systems biology approaches to cancer, diabetes, etc.

Possibly because of their extreme complexity, a systems biology approach to neurodegenerative disorders has been late coming. However, reports such as *Dementia 2010* and others [19] have exposed the social and economic imperatives associated with our ageing populations. Fortunately, and with help from forceful publicity campaigns, neurodegeneration has moved to the front rank of diseases to be addressed with urgency and by every available means. This book is the first to approach Parkinson's disease from a systems viewpoint. We hope that it will create focus and direction for further effort and give a platform for systems approaches to other neurodegenerative conditions.

Layout of the Book

The contributors to this volume approach a range of PD issues from a systems perspective. The complexity and variability of PD make it hard to classify the contributions precisely, but a useful way in which to attempt this is through the temporal and spatial spectrum of PD's features (Fig. 1). Notice in particular that the underlying mechanisms of PD's aetiology and pathology span several orders of magnitude in both time and space. At one end, PD involves imbalances in ion transport at the sub-cellular level, operating in the order of milliseconds. At the other end, physiological changes operate over decades and throughout the entire brain. It is extremely hard, if not impossible, to synthesise all the available knowledge on such a complex disease in a way that would reconcile the time and length scales involved. We do not pretend to resolve this issue, but we do find it useful to organise and present the content of this volume with this consideration in mind. Ultimately, and in the spirit of the Human Physiome project [20], modelling efforts will achieve a certain extent of unification of PD's multiple dimensions. The material presented here is a step in this direction.

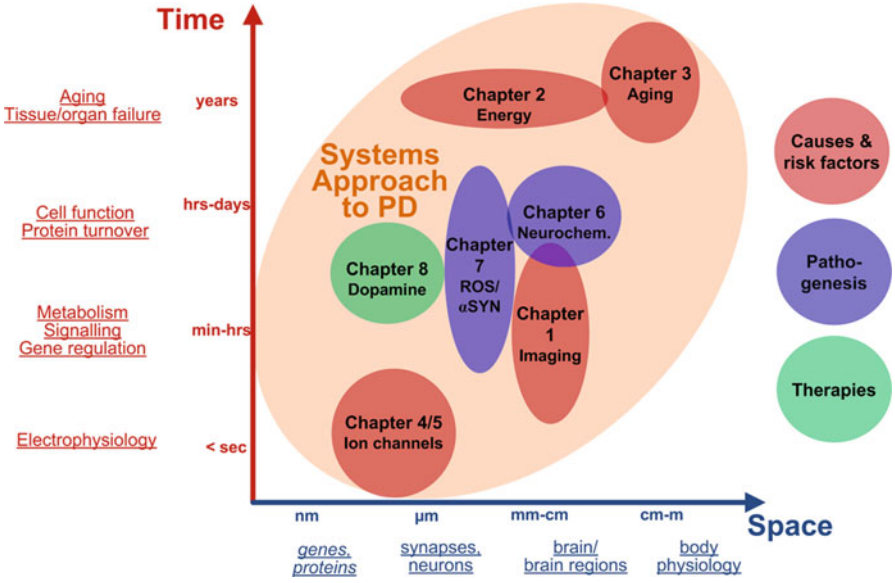

Fig. 1 Overview of the book's content in terms of the spatial and temporal scales involved in Parkinson's disease

As shown with colour codes in Fig. 1, the main features of PD can be sub-divided as follows:

1. The causes and risk factors in PD.
2. The inception (pathogenesis) of the PD state.
3. Dopamine therapies for PD.

With this sub-division in mind, chapters are laid out as follows.

Causes and Risk Factors

Chapter 1 describes how innovative imaging techniques have been able to reveal previously unknown structures of dopaminergic neurons of the *SN*. The dramatic images shown in the chapter reveal new information and give insights into the special vulnerability of SN neurons to energy-stresses and their compensatory redundancy mechanism. These energy-related findings have special implications for Chap. 2, which uses a mathematical model of brain energy metabolism to assess how energy-stress forms a common denominator in PD risk factors. The most common risk factor for PD—advanced age—gets detail treatment in Chap. 3.

Here, the techniques of fuzzy logic are used to develop a mathematical model of ageing phenotypes and assess the implications of cellular ageing for PD.

As noted previously the neurons of the *SN* are most vulnerable to PD damage. A special feature of these neurons is their use of calcium ions to facilitate signalling—in particular pace-making signalling. Chapter 4 takes this as its theme and, using mathematical models of electrochemical signalling, explains the potential part played by dysregulated signalling in the vulnerability of SN neurons. Chapter 5 continues with the role of calcium-facilitated signalling in neurons. It constructs a mathematical model of calcium metabolism in *substantia nigral* neurons and estimates the additional energy budgets associated with calcium signalling.

Pathogenesis of PD

The transition from a healthy neuron with a predisposition to PD, to a neuron where PD is established is termed *pathogenesis*. Whereas, as discussed in Chap. 2, the preconditions for disease can grow over many years, it is generally agreed that pathogenic mechanisms proceed over a period where hours and days are the relevant temporal scale. The measurement of such rapid changes requires special in vivo sensing methods, and Chap. 6 deals with a sensing technology designed for just such purposes. These take the form of electrochemical sensors that produce accurate records of both the short and long-term changes that occur during neuronal and glial cellular transitions. This has important implications for the neurochemical processes of pathogenesis that are modelled in Chap. 7. Here, the interactions between reactive oxygen species and mis-folded alphasynuclein are modelled mathematically and used to demonstrate a neurochemical "switch" associated with the pathogenic transition to the disease state.

Dopamine Therapy

Therapy based on restoring/retaining dopamine levels is the gold standard treatment for PD motor dysfunction. However, design and administration of dopamine therapy require expert knowledge and management. Better, more accurately personalised management of dopamine-related treatments would greatly benefit sufferers. Computational modelling of dopamine metabolism is a strong first step in this direction, and our concluding chapter—Chap. 8—addresses this area. It describes the development of a mathematical model of dopamine metabolism, and illustrates its uses through simulation of a range of PD scenarios.

Acknowledgements This book has its origins in the *Symposium on Systems Approaches to Parkinson's Disease*, which was held at the Hamilton Institute in 2010. The event was made possible by the farsighted actions of Science Foundation Ireland who, in 2003, agreed to fund

speculative research on the systems biology of a then unfashionable disease. We gratefully acknowledge their visionary support and assistance. In addition, we thank the contributing authors to this book, and other collaborators, who are helping to shape the systems biology of Parkinson's disease. As their ideas are collectively developed, and other groups add their contributions, we look forward to further advances in the understanding of Parkinson's disease, and ultimately to a better future for sufferers.

County Kildare, Ireland — Peter Wellstead
Montreal, QC, Canada — Mathieu Cloutier

References

1. Mesarovic MD (1968) Systems theory and biology. Springer, Berlin
2. Gourie M, Ramu MG, Venkataram BS (1991) Treatment of Parkinson's disease in ayurveda. J Roy Soc Med 84:491–492
3. Nagashayana N, Sankarankutty P, Nampoothiri MRV, Mohan PK, Mohanakumar KP (2000) Association of L-dopa with recovery following ayurveda medication in Parkinson's disease. J Neurol Sci 176:124–127
4. Sider D, McVaugh M (1979) Galen on tremor, palpitation, spasm and rigor (English translation from Greek and Latin sources). Trans Stud Coll Phys Phila 1(3):183–210
5. Parkinson J (1817) An essay on the Shaking Palsy. Reprinted as a classic article by American Psychiatric Publishing, Washington, DC
6. Charcot JM (1880) Lecons sur les maladies du systeme nerveux faites a la Salpetrie re: Recueillies et publiees par Bourneville. Tome 1, A Delahaye et Lecrosnier, Paris, Reprinted and published by Adamant Media Corporation, Boston
7. Burke RE (2007) Sir Charles Sherrington's The integrative action of the nervous system: a centenary appreciation. Brain 130:887–894
8. Carlsson A (2000) A half century of neurotransmitter research: impact on neurology and psychiatry, Text of Nobel Lecture (see http://nobelprize.org)
9. Braak H, de Tredici K, Rub U, de Vos RAI, Jansen Steur EN, Braak E (2003) Staging of brain pathology related to sporadic Parkinson's disease. Neurobiol Aging 24(2):197–211
10. Benabid AL (2010) Profile: stimulation and serendipity. The Lancet Neurology, December, 9:1152
11. Wiener N (1948) Cybernetics: or control and communication in the animal and the machine. MIT Press, Cambridge.
12. Schroedinger E (1943) What is life? Cambridge University Press, Cambridge.
13. Cannon WB (1932) The wisdom of the body. Norton, NY.
14. Hodgkin AL, Huxley AF (1952) Currents carried by sodium and potassium ions through the membrane of the giant axon of Loligo. J Physiol 116(4):449–472
15. Kitano H (2002) Systems biology: a brief overview. Science 295:1662–1664
16. Manolio TA, Collins FS, Cox NJ et al. (2009) Finding the missing heritability of complex diseases. Nature 8(7265):747–753
17. Noble D (2002) Modelling the heart. Science 295(5560):1678–1682
18. Auffray C, Chen Z, Hood L (2009) Systems medicine: the future of medical genomics and healthcare. Genome Med 1:2
19. Luengo-Fernadez R, Leal J, Gray A. (2010) Dementia 2010, A report of the Alzheimer's Research Trust www.dementia.org.
20. Hunter P, Robbins P, Noble D (2002) The IUPS human physiome project. Pflügers Archiv 445:1

Contents

Contributors

Fiachra B. Bolger BioAnalytics Laboratory, Department of Chemistry, National University of Ireland Maynooth, Maynooth, County Kildare, Ireland

Mathieu Cloutier GERAD, Ecole Polytechnique de Montreal, Montreal, QC, Canada

Guillaume Drion Laboratory of Neurophysiology, GIGA Neurosciences, Université de Liège, Liège (Sart Tilman), Belgium

Department of Electrical Engineering and Computer Sciences, Université de Liège, Liège, Belgium

Niall J. Finnerty BioAnalytics Laboratory, Department of Chemistry, National University of Ireland Maynooth, Maynooth, County Kildare, Ireland

Febe Francis Hamilton Institute, NUIM, Maynooth, County Kildare, Ireland

Míriam R. García Hamilton Institute, NUIM, Maynooth, County Kildare, Ireland

Andres Kriete School of Biomedical Engineering, Science & Health Systems, Drexel University, Philadelphia, PA, USA

John P. Lowry BioAnalytics Laboratory, Department of Chemistry, National University of Ireland Maynooth, Maynooth, County Kildare, Ireland

Wakoto Matsuda Division of Anatomy and Cell Biology, Department of Anatomy, Shiga University of Medical Science, Otsu, Japan

Richard H. Middleton ARC Centre for Complex Dynamic Systems and Control, University of Newcastle, Newcastle, NSW, Australia

Gary W. Miller Center for Neurodegenerative Disease, Emory University, School of Medicine, Atlanta, GA, USA

Department of Environmental Health, Rollins School of Public Health, Emory University, Atlanta, GA, USA

Zhen Qi Department of Biomedical Engineering, Georgia Institute of Technology, Atlanta, GA, USA

Center for Neurodegenerative Disease, Emory University, Atlanta, GA, USA

Integrative BioSystems Institute, Georgia Institute of Technology, Atlanta, GA, USA

Rodolphe Sepulchre Department of Electrical Engineering and Computer Sciences, University of Liège, Liège, Belgium

Vincent Seutin Laboratory of Neurophysiology, GIGA Neurosciences, Université de Liège, Liège (Sart Tilman), Belgium

Eberhard O. Voit Department of Biomedical Engineering, Georgia Institute of Technology and Emory University Medical School, Atlanta, GA, USA

Integrative BioSystems Institute, Georgia Institute of Technology, Atlanta, GA, USA

Peter Wellstead Hamilton Institute, National University of Ireland, Maynooth, County Kildare, Ireland

Chapter 1
Imaging of Dopaminergic Neurons and the Implications for Parkinson's Disease

Wakoto Matsuda

Abstract The Systems Biology of Parkinson's disease (PD) will be underpinned by new measurement techniques. This is particularly true of the pathology of PD, where recent developments in brain imaging have offered new insights into the morphology of dopaminergic (DA) neurons that have profound implications for the special vulnerability and role of this class of neurons. In this chapter, we describe these new morphological measurement techniques and how they contribute to our understanding of PD.

We begin with an overview of the conventional understanding of the morphology of DA neurons, as seen from a historical perspective. We then describe novel imaging techniques that reveal important new structural information concerning DA neurons. In particular, we outline some new methods for labeling DA neurons, together with the technical aspects of labeling and measuring axonal structure.

Detail morphological images of DA neurons derived from this new approach are used to elucidate the role of DA neurons in PD. First, we point out how the new images reveal how DA neurons have a massive axonal arborization in the striatum. This arborization is on a scale not previously known, and of a form that implies both a particular vulnerability and a redundancy in DA neurons. Second, we describe how the imaging results indicate that DA neurons innervate both the striosome and the matrix compartments of the striatum. This dual innervation has implications for reinforcement learning in the basal ganglia and for how normal behavior is driven and how it may be disrupted by Levodopa PD therapies.

The chapter concludes with a summary of how these results contribute to our understanding of PD and how it forms a part of the Systems Biology of PD.

W. Matsuda (✉)
Division of Anatomy and Cell Biology, Department of Anatomy,
Shiga University of Medical Science, Otsu 520-2192, Shiga, Japan
e-mail: matsuda2@belle.shiga-med.ac.jp

P. Wellstead and M. Cloutier (eds.), *Systems Biology of Parkinson's Disease*,
DOI 10.1007/978-1-4614-3411-5_1,

Introduction

The classic denominator of disorders associated with Parkinsonism (including Parkinson's disease (PD)) is neuronal loss in the substantia nigra (*SN*) of the midbrain, especially of DA neurons in the *SN* that project mainly to the striatum. As seen in the *SN*, the ventrolateral tier of neurons appears to be more vulnerable than medial groups of neurons that send projections to the ventral striatum, forebrain, and the medial temporal lobe [10]. Why DA neurons should be more vulnerable to PD damage than neurons in other brain regions is not well understood, although there is evidence that, in a certain sense, DA neurons exhibit a high degree of redundancy. Clinically, there is prodromal phase in PD [39]. Pathologically, there is also a presymptomatic phase, including a loss of nigrostriatal neurons, which is believed to represent a middle stage of a degenerative process that starts in the lower brainstem and olfactory nuclei and ascends throughout the cortex [6, 38].

In this chapter, the chronological progress of labeling and methods of tracing neurons is described in the field of neuroanatomy (section "Basic Structure and Historical Overview of Morphology of Basal Ganglia and DA Neurons"). A novel virus tracer is outlined in section "New Methods for the Imaging (Labeling) of DA Neurons, Including Technical Aspects of Labeling and Measurement of Axon," along with a detail description of the reconstruction technique of single neuron and axonal arborization. Subsequently, based on anatomical findings from the novel neuronal imaging method, the implications for PD are discussed (section "Implications for PD and Learning Models: Two Aspects of Two Findings"). The chapter concludes with a discussion of preliminary results in DA neurons in the other nucleus of the midbrain, and non-DA neurons in the midbrain (section "Preliminary Results in DA Neurons in the VTA, RRF, and Non-DA Neurons in the Midbrain").

Basic Structure and Historical Overview of Morphology of Basal Ganglia and DA Neurons

Basic Structure of Basal Ganglia and DA Neurons

The basal ganglia are central to the cardinal motor manifestations of PD, comprising bradykinesia, rigidity, resting tremor, and postural instability. They consist of a collection of bilateral subcortical nuclei that are so named because they lie at the base of the forebrain in primates. The major components of this region of the brain are the caudate nucleus, the putamen, the globus pallidus (GP), the subthalamic nucleus (STN), and *SN*. The caudate nucleus and putamen are collectively known as the neostriatum. The term "striatum" is often used to encompass both the neostriatum (also called the dorsal striatum) and ventral striatum, the principal

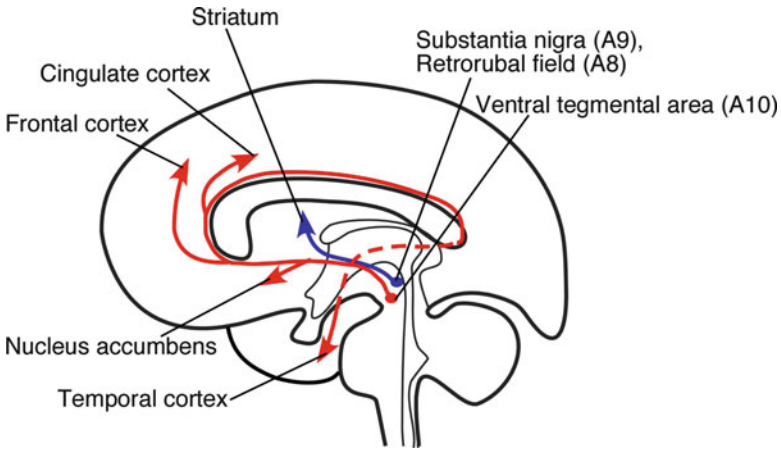

Fig. 1.1 Dopaminergic systems of the brain. Three dopaminergic nuclei associated with Parkinson's disease (PD) occur in the midbrain. The substantia nigra pars compacta (*SNc*) and retrorubral field (RRF) project to the striatum. The ventral tegmental area (VTA) projects to the nucleus accumbens, frontal cortex, cingulate cortex, and temporal cortex

component of which is the nucleus accumbens. The *SN* is located in the midbrain and has two main parts: the pars compacta (*SNc*), which contains DA neurons, and the pars reticulata (*SNr*), which contains gamma-aminobutyric acid (GABA) neurons. The *SN* was given its name because it contains black melanin pigment in its DA neurons.

The neostriatum is a main input nucleus of the basal ganglia circuit. It receives massive cortical and thalamic inputs and sends inhibitory projections to the external segment of the globus pallidus (GPe), entopeduncular nucleus (internal segment of the GP; GPi) and *SNr*. The latter two structures (GPi and *SNr*) are output nuclei of the basal ganglia circuit. The neostriatum is also known to have a mosaic organization, composed of patch/striosome and matrix compartments, which are distinguishable from each other by the expression of neurochemical markers (i.e., opiate receptor binding, acetylcholineseterase) and by their input–output organization [5, 11, 16–21, 23, 25, 30, 32, 33].

Three DA cell groups in the midbrain were originally numbered as if they were a rostral continuation of the noradrenergic system. This occurred because identification was based on histofluorescence, which does not distinguish DA from norepinephrine very well. With reference to Fig. 1.1, the DA cell groups were identified based on their location: the A10, A9, and A8 DA cell groups located respectively in the ventral tegmental area (VTA), *SNc*, and retrorubral field (RRF). They send the major ascending DA inputs to the telencephalon, including the nigrostriatal pathway that arise from the A8 and A9 cell groups and innervates the striatum, which is involved in initiating motor responses. Mesocortical and mesolimbic DA pathways (arising from the A10 cell group) innervate the frontal and temporal cortices and the limbic structures of forebrain (mainly accumbens nucleus) (see Fig. 1.1). These pathways

have been implicated in emotion, thought, and memory storage. Furthermore, DA neurons in the *SNc* are classified as follows: (1) neurons of the dorsal tier of the *SNc* (*SNcd*), which coexpress the calcium binding protein, calbindin as a neurochemical marker, and (2) those of the ventral tier of the *SNc* (*SNcv*).

Historical Overview of Morphology of DA Neurons

In the 1960s, the discovery of dopamine as a neurotransmitter was shown by fluorescent catecholamine histochemical methods [9]. These DA neurons have a strong influence on the following: (1) emotion, motivation, and cognitive processes, mainly by the projection from the VTA to limbic forebrain areas, and (2) motor control, chiefly by the projection from the *SNc* and RRF to the neostriatum [3, 31].

Additional details of the organization of the DA system and other neuroanatomical circuits of the basal ganglia were identified by axonal tracing studies. In particular, neurons in the patch compartment are known to send their inhibitory axons selectively to the *SNc* [17], whereas those in the matrix compartment project directly, or indirectly, to the *SNr* and GPi [1]. On the other hand, axonal tracing studies have demonstrated that DA neuron projections from the VTA, *SNcd*, and RRF provide input to the striatal matrix compartment, whereas projections from *SNcv* provide input to the striatal patch compartment [21].

Up until the 1980s, important insights such as these had been established by pioneering work based on tracing study with conventional bulk-injection methods. In the 1990s and early 2000s, methods gradually became more precise, and single nigrostriatal axons of *SNc* neurons were labeled, and reconstructed, based on a small injection of anterograde tracer, biotinylated dextran-amine [14, 45]. Although these studies showed the reconstructed axons were distributed widely in the striatum, the DA characteristics of nigrostriatal neurons were not examined, and the reconstruction of axon fibers could be incomplete owing to low labeling efficiency associated with the small amounts of the tracer used. As a result, the precise extent of influence that a single DA neuron exerts on striatal neurons had yet to be clarified.

New Methods for the Imaging (Labeling) of DA Neurons, Including Technical Aspects of Labeling and Measurement of Axon

Background of the New Labeling Method

From the previous paragraphs, it should be clear that imaging methods used so far, while insightful, lacked the fine-scale resolution required to reveal the detail structure of individual neuronal connections. In response to this, the author and

his colleagues have in recent years developed a new recombinant viral vector that labels the infected neurons in a Golgi-stain-like fashion [13]. This vector was based upon a replication-defective Sindbis virus and is designed to express green fluorescent protein with a membrane-targeting palmitoylation signal of GAP-43 (palGFP) under the control of a powerful subgenomic promoter of the virus. In this method, a large amount of palGFP is produced and distributed, not only on the somatodendritic membrane, but also on the axonal membrane of infected neurons [13]. As a consequence, the vector has found use as a highly sensitive anterograde tracer in the central nervous system [27, 40–42]. For our investigations, we used the recombinant Sindbis virus vector as a tool for single neuron labeling of DA neurons in the *SNc* and their axonal extensions. More specifically, we determined the DA characteristics of the infected neurons immunocytochemically, and then visualized the highly extensive axonal arborization of single nigrostriatal DA neurons [35]. The axonal arborization was examined further, in association with the patch and matrix compartments of the neostriatum, to clarify whether single DA signals exerted a selective influence upon reinforcement learning.

Essential Points of Labeling Process

The key stages in the process of recombinant viral labeling are described as follows:

Stage 1: Injection of the virus vector, its survival time, and fixation: The Sindbis virus vector for palGFP expression, diluted to an optimal concentration, is injected stereotaxically into the *SN* of rats. After 36–48 h survival, the rat brains are fixed by transcardial perfusion, cut into parasagittal sections and processed for histological analysis. In this procedure, survival time is important. For periods less than 9 h, the immunoreactivity of infected cells is incomplete. Furthermore, glial cells are labeled with palGFP at 4.5–9 h after infection, but the glial cells themselves, and their processes, then disappear almost completely within 36 h after the viral injection (however, no significant loss of cell body of infected neurons are observed after 36 h). For time periods more than 72 h, the infected neurons show degenerative changes, such as beaded dendrites and shrinkage of the cell bodies [13]. Thus, for neuronal labeling results, the best survival time of rats would be around 48 h (e.g., between 18 and 72 h).

Stage 2: Chemical characteristics of the infected neurons, double immunoperoxidase staining for GFP and MOR: In this stage, palGFP-labeled single neurons are first examined for the expression of tyrosine hydroxylase (TH) immunoreactivity (a marker for DA neurons in the *SN*) by the immunofluorescence method. After confirming the DA characteristics, single DA neurons are stained black by the immunoperoxidase method with anti-GFP antibody. Simultaneously, immunoreactivity for the mu-opioid receptor (MOR) is visualized as violet red and used as a marker for the patch compartment of the neostriatum [32].

Confirmation of the chemical characteristics of the cell body of each infected neuron is highly important for reasons that are explained by the following example. Morphological analysis of single nigrostriatal axons were recently reported using a labeling method with a small injection of biotinylated dextran-amine into the rat *SN* [14, 45]. In the study, which used a conventional anterograde tracer, the chemical nature of the injected neurons was, unfortunately, not defined. As a result, although all neurons with axons that were traced did indeed occur in the *SNc*, it was impossible to conclude that they were themselves dopaminergic. The authors of this study acknowledged this possibility, by noting that some of the neurons described might be GABAergic *SNr* neurons, especially those with an axon that arborized profusely at extrastriatal nuclei (including both thalamic and brainstem) levels. A further issue with the staining process is that the surrounding area of the labeled cell body is frequently immunostained darkly, probably due to the extracellular leakage of palGFP. This suggests an extremely strong expression of protein by the subgenomic promoter of Sindbis virus.

Stage 3: Selection and reconstruction of single DA neurons: The first step in reconstruction of a single DA neuron is the examination (at stage 1) of the hemiencephalic sections, including the injection sites, using epifluorescence microscopy. For this purpose, the hemibrains that contained only 1–10 palGFP labeled *SN* neurons (ideally 1–3 labeled neurons) are selected. In the second step, labeled neurons are examined for the expression of TH immunofluorescence, a marker for DA neurons in the *SN* (at stage 2, the first half). And in the third step, the hemiencephalic sections containing these DA neurons are further stained by the immunoperoxidase method with anti-GFP antibody (at stage 2, the second half).

The cell body, dendrites, and the projecting main axon of stained DA neurons are reconstructed under a microscope equipped with a camera lucida apparatus. In particular, the striatal axon fibers are photographed with a digital camera attached to the microscope, and then traced on to the photograph using special-purpose graphics software. A difficulty at this stage is that almost all the stained neurons are entangled or overlapped in the striatum with other neurons. As a result, they are inseparable for reconstruction, leaving only a limited number of neurons that can be unambiguously traced—a task performed using an (as yet) unpublished technique.

In the final process, the axon fibers in a section are reconstructed one-by-one onto a parasagittal plane, and superimposed to create the medial view in the computer. For the frontal and dorsal views, the extent of axon fibers in each section is superimposed on frontal and horizontal planes, respectively (Figs. 1.2 and 1.3), using the software package *Image J* (NIH; http:/rsb.info.nih.gov/ij/). The length of axons was measured by calculating the length of traced lines separately in the patch and matrix compartments. Figures 1.2 and 1.3 show the representative *SNcd* and *SNcv* neuron with the reconstructed DA ones, respectively. The main axon emerges from the cell body (Figs. 1.2b and 1.3b) without local axon collaterals around the cell body. It then passes through the internal

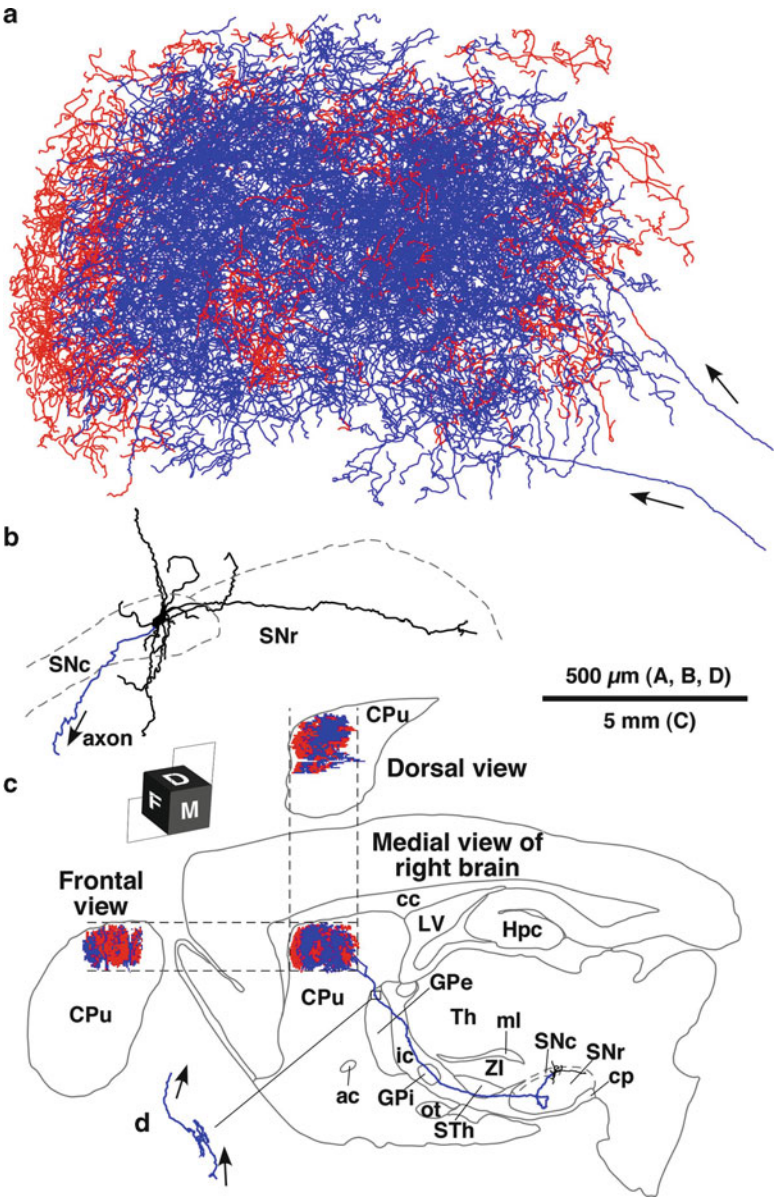

Fig. 1.2 Camera lucida reconstruction of *SNcd* neuron. The axon fibers in the striatum (**a**) and dendrites (**b**) in the *SNc* were projected onto a parasagittal plane and superimposed from the medial side. In (**c**), the dorsal and frontal views of the intrastriatal axonal arborization were reconstructed and compared with the medial view. *Red* and *blue lines* in the striatum indicate the axon fibers located in the striosome and matrix compartments, respectively. *Red* fibers at the most rostral portion in (**a**) were mostly located in the mu-opioid receptor (MOR)-positive subcallosal streak. The axon gave rise to only minor collaterals in the external segment of the globus pallidus (GPe; (**d**)). *ac* Anterior commissure; *cc* corpus callosum; *cp* cerebral peduncle; *CPu* caudate-putamen (neostriatum); *GPi* internal segment of the globus pallidus; *Hpc* hippocampus; *ic* internal capsule; *LV* lateral ventricle; *ml* medial lemniscus; *ot* optic tract; *SNr* substantia nigra pars reticulata; *STh* subthalamic nucleus; *Th* thalamus; *ZI* zona incerta [Adapted and reproduced with permission from Journal of Neuroscience 29(2): 444–453, 2009]

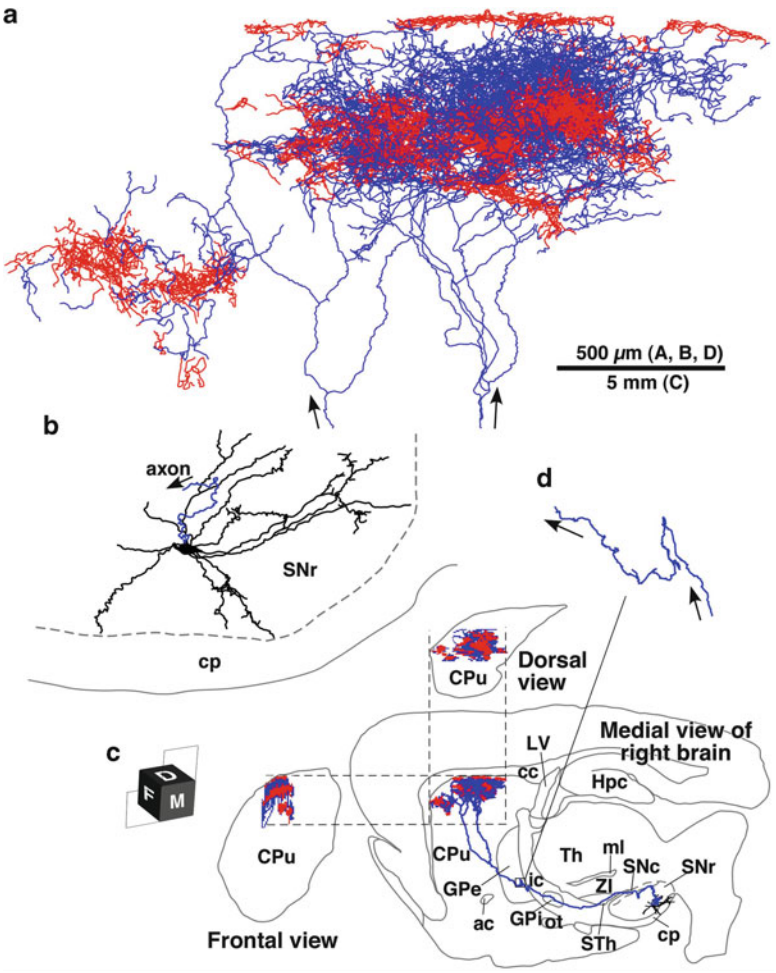

Fig. 1.3 Camera lucida reconstruction of *SNcv* neuron. The axons of this *SNcv* neuron showed the highest preference for the striosome compartment in the present results, and made two bushes in the neostriatum. *Red* fibers at the top of (**a**) were located in MOR-positive subcallosal streaks (see the legend of Fig. 1.2 for further detail) [Adapted and reproduced with permission from Journal of Neuroscience 29(2): 444–453, 2009]

capsule, and then heads directly to the striatum. Both of the imaged axons emitted very short curly collateral projections in the GPe before entering the striatum (Figs. 1.2d and 1.3d). In contrast to the minimal collateral projections within extrastriatal structures, the individual nigrostriatal axons form widespread and highly arborized axonal bushes within the striatum (Figs. 1.2a–1.3a and 1.2c–1.3c). The axonal arborizations reconstructed in the striatum are more extended and much denser than those of the nigrostriatal axons described previously [14, 45].

Throughout the process of infection, cytochemical check and separable tracing, the most important and critical process for this method is the selection (from the enormous volume of brain and slice data) of a few samples that satisfy all the conditions. In this process, it is particularly important to exclude as rigorously as possible the neurons whose axons are entangled, or overlapped, with those of other neurons. Only strict attention to this point can guarantee the quality of single neuron studies.

Other Technical Problems

When comparing viral-vector results with previously reported works [14, 45], the largest difference was in the density of intrastriatal arborization of the nigrostriatal axons. Using the single-fiber method described here, the axon fibers of TH-immunopositive nigrostriatal neurons were distributed in the neostriatum far more densely than the nigrostriatal fibers described in the previous reports. This difference may be caused by the much higher sensitivity of the single-fiber tracing method using the palGFP Sindbis virus vector, when compared with a conventional anterograde tracer. Furthermore, the sensitivity of conventional tracers would be limited by the small amount of injected materials.

It has been suggested that palGFP expression might have some transformational effects on the axonal arborization of DA neurons [15]. However, after close examination of this possibility, it has been concluded that palGFP expression seems to have little morphological influence on DA axon fibers. In particular, a comparative study using GFP Sindbis virus vector, of single GFP-positive nigrostriatal axon fibers showed similar characteristics to palGFP-positive fibers, although the axon fibers were not completely visualized throughout their arborization [35].

Implications for PD and Learning Models: Two Aspects of Two Findings

In our study of the full axonal arborization of single DA neurons, the intrastriatal axon fibers of nigrostriatal neurons were more widely distributed and of a much higher density than those reported in previous studies (Figs. 1.2 and 1.3). In addition, *SNcd* and *SNcv* neurons were revealed principally to innervate both the patch *and* the matrix compartments of the neostriatum, although they both showed some degree of preference for either compartment. In this section, the implications of these two interesting findings are discussed from each of two aspects.

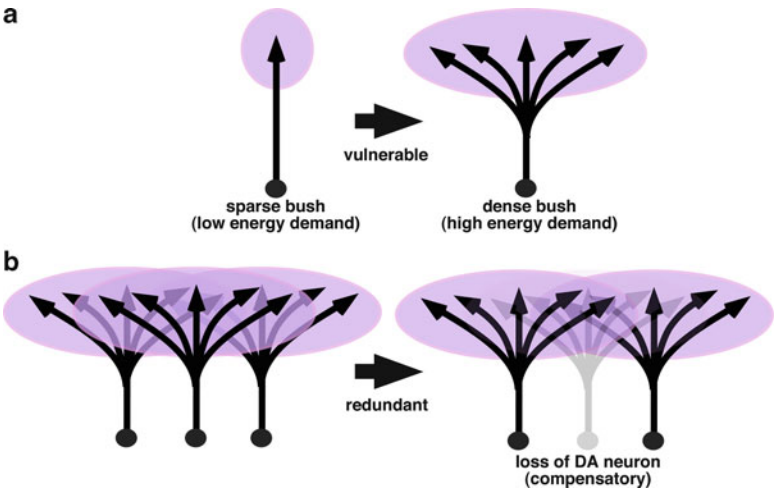

Fig. 1.4 The massive arborizations of the neostriatal extensions of *SNc* neurons would have an enormous energy requirement, as compared with sparse bushing, resulting in its vulnerability (**a**). On the other hand, the highly overlapping innervation of DA neurons may be a safety-margin built-in to the *SN*, resulting in its redundancy (**b**)

Massive Axonal Arborizations of DA Neurons: Vulnerability and Redundancy

Probably the most important unanswered question in PD research is: why are *SNc* DA neurons preferentially damaged in PD? Our study points to a plausible answer to this question in the following way. Results from our viral-tracer imaging indicate that, on average, 2.7% of neostriatal neurons and, at the maximum, 5.7% of neostriatal neurons, are under the strong influence of a single DA neuron [35]. This can be further quantified as follows: the rat neostriatum contains 2,790,000 neurons in one side [43], and the volume innervated by a single DA neuron is, on average, 2.7% of the total neostriatal volume in our study. It follows therefore that approximately 75,000 striatal neurons are influenced by a *single* DA neuron. This high level of connectivity is possible because of the massive arborizations of the neostriatal extensions of *SNc* neurons, and implies that *SNc* neurons have an enormous energy requirement. Compared to other cells, neurons have a higher energy budget that is suggestive of a particularly susceptible to failure if energy systems are compromised ([49]; see also Chap. 2). The especially high energy-stress experienced by *SNc* neurons could thus potentially account for their particular vulnerability to PD damage (Fig. 1.4a). The large number of striatal neurons influenced by a single DA neuron, also implies that the *SN* exercises a high-gain proportional control of innervation. This might be anticipated in a critical area of

brain control, in the same way that high gain loops are used where highly responsive control systems are required [22].

On the other hand, and possibly to compensate for their particularly high levels of energy stress, *SNc* DA neurons also have a high level of redundancy. Specifically, it can be predicted that a neuron in the rat neostriatum might be under the influence of between 95 and 194 DA neurons on average. This figure is calculated using the estimated volume innervated by a single DA neuron (2.7% of the total volume of a neostriatum), and the number of neurons in the *SNc* of a rat (3,500–7,200 neurons in one side [2, 24, 43]). The highly overlapping innervation of DA neurons implied by this estimate suggests that a safety-margin is built into to the *SN* (Fig. 1.4b). Such a safety-margin in human brains would offer redundancy in innervation and also account for the high level of *SN* damage that can occur before diagnosis of idiopathic PD. In particular, the extensive loss (>70%) of neurons in the *SN* observed in most patients with clear parkinsonian symptoms suggests that patients with a less extensive loss of neurons could be asymptomatic [26]. Since neurons are labile elements and are relatively easily lost, it is a natural developmental strategy for a system composed of such highly stressed elements to maintain a high level of redundancy. For *SNc* DA neurons, being probably the most energetic cells in the brain, the redundancy could be because of their standpoint at the "evolutional edge"; a point at which there is not yet a specially developed regulatory mechanism to support their extra demands for activity (Wellstead P., 2011, private communication). Interestingly, mathematical modeling of neuronal energy metabolism also suggests a relatively large range of pathophysiological conditions where neuronal damage can occur, but without a complete collapse at the metabolic level (see Fig. 2.6 of Chap. 2).

The twin issues of vulnerability and redundancy of DA neurons would be implied, not only in idiopathic PD but also more generally in the Parkinson's syndrome. For example, in the field of neurotraumatology, we have previously reported patients with a persistent vegetative state, or minimally conscious state, after severe head injury [29, 36, 37]. These patients recovered from a prolonged disturbance of consciousness after the administration of levodopa, and all had parkinsonian features. Furthermore, magnetic resonance imaging implied that all had a diffuse axonal injury involving the *SN* and VTA. The puzzle that remained for us was: why did they respond to levodopa treatment, in spite of the fact that their DA systems may have been selectively damaged? An explanation would appear to lie in the pathophysiology of the patients, which also implied vulnerability (selective damage) and redundancy (responsiveness to levodopa). These two aspects, vulnerability and redundancy, appear to be "opposite sides of the same coin," and jointly constitute one of the most important characteristics of DA neurons.

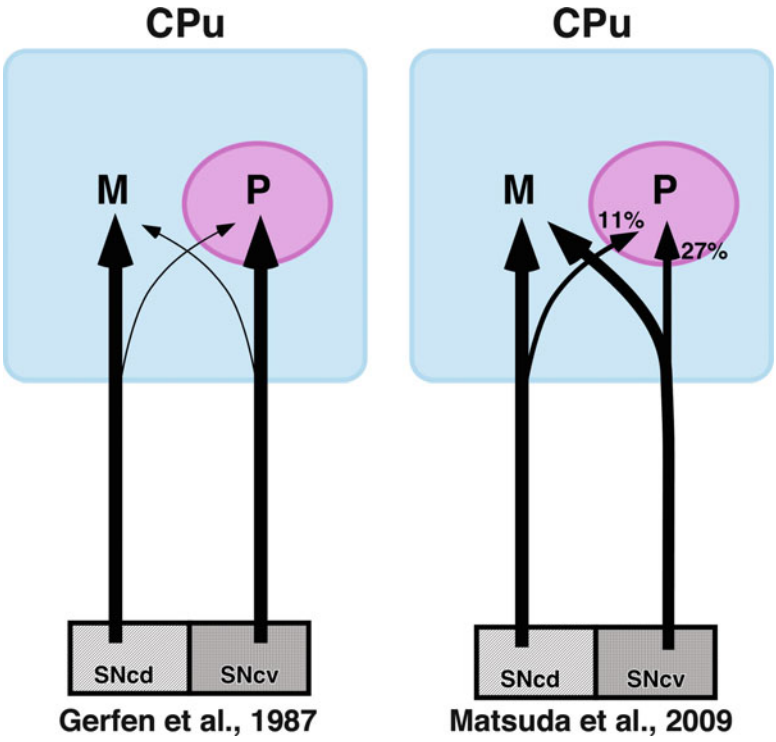

Fig. 1.5 Comparison between single-axon arbors innervating the patch and matrix compartment of the neostriatum. (*Left*) Previous study [20, 21] reported that dopaminergic neurons in the *SNcd* project chiefly to the matrix, while those in the *SNcv* send axons mainly to the patch compartment. (*Right*) Our study revealed that *SNcv* neurons preferred the patch compartment, although proportionally the patch innervation constituted only a minority of their total axonal length [35]. On average, *SNcd* neurons sent approximately 11% of total axon fibers to patch compartment, and *SNcv* neurons projected 27% to patch compartment. *CPu* caudate-putamen (neostriatum); *M* matrix compartment (*blue square*); *P* patch (striosome) compartment (*pink circle*); *SNcd* substantia nigra pars compacta, dorsal tier; *SNcv* substantia nigra pars compacta, ventral tier

DA Neurons Innervate Both the Patch and Matrix Compartments, Resulting in Reinforcement Learning in Basal Ganglia

In the normal state, it is known empirically that rewards always involve motivated behaviors, and in certain disease states this reward–motivation cycle becomes disturbed. Specifically, in the long-term symptomatic therapy of PD patients, an iatrogenic disturbance called dopamine dysregulation syndrome (DDS) has been recently described [44]. Patients with DDS develop an addictive pattern of dopamine replacement therapy use, administering doses in excess of those required to control their motor symptoms. Among the behavioral disturbances associated with DDS is a preoccupation with obsessively repetitive mechanical acts (punding),

such as pathological gambling, hypersexuality, compulsive shopping, and compulsive eating. In these pathological conditions, rewards appear to be integrated with compulsive repetitive activity. Why do these symptoms occur in PD? In the following paragraphs, the causes of these symptoms are discussed based on the anatomical findings of the axonal arborization of DA neurons.

Based on measurements of the rat brain, the nigrostriatal projection has been reported to provide an organizational role, in which DA neurons in the *SNcd* project chiefly to the matrix, while those in the *SNcv* send axons mainly to the patch compartment (Fig. 1.5) [21]. A similar segregation of nigrostriatal projections in association with striosome and matrix compartments has been reported in the cat and primate brains [30, 33]. Interestingly, these reports of segregated organization were only partially supported by our findings. Specifically, we observed that *SNcd* neurons chiefly showed a *preference* for matrix compartment, while *SNcv* neurons showed a similar preference for patch compartment. As illustrated in Fig. 1.5, on average, *SNcd* neurons sent approximately 11% of total axon fibers to the patch compartment, and *SNcv* neurons projected 27% to patch compartment. Thus, rather than a *segregation* of innervation, we consider it more important to emphasize that single *SNcd* or *SNcv* neurons innervated *both* the patch *and* matrix compartments [35]. Dual innervation of this kind means that identical temporal difference (TD) signals[1] are sent simultaneously to a large number of patch and matrix neurons. This point is significant because reinforcement-learning mechanisms have recently been proposed to operate within the neural circuit of the basal ganglia, with the assumption that the dopamine nigrostriatal projection acts as a reinforcement signal pathway [12, 46]. In particular, and on the basis of the TD learning model, neostriatal neurons in the patch/striosome and matrix compartments are presumed to serve as state-value and action-value functions, respectively [12, 46]. The model requires that DA neurons in the *SNc* receives state-value signals from the neostriatum, integrates these signals with reward information to produce a scalar reinforcement signal, and then sends the reinforcement signal back to the neostriatum. The model then suggests that striatal neurons alter their responsiveness to cortical or thalamic inputs according to the DA signal, using the mechanism of dopamine-regulated synaptic plasticity [7, 8], and may learn how to behave in response to such inputs.

A crucial element of this theory will be to understand how many, and which type of, striatal neurons are really under the influence of a single DA neuron, as this would determine the type of learning rule used in the basal ganglia circuit. Our results are relevant to this point, since they showed that every DA neuron projects simultaneously to both the patch and matrix compartments within the wide territory innervated by the neuron. Thus, both patch and matrix neurons, i.e., both state-value and action-value function neurons, at least within the territory, might receive the identical DA signal (as expected by the theoretical model).

[1] TD learning is a well-known reinforcement-learning model [47].

In other preclinical experimental studies [4, 28, 48], the administration of various drugs affecting the dopaminergic system was found to augment motor responses; an observation that was interpreted as behavioral (locomotor) sensitization. These reports would support our finding that single *SNcd* or *SNcv* neurons innervated both the patch and matrix compartments, rather than the previous findings of a segregated organization.

Preliminary Results in DA Neurons in the VTA, RRF, and Non-DA Neurons in the Midbrain

DA neurons in the VTA and RRF that correspond to cell groups A10 and A8 in the mammalian mesencephalon, respectively [9], also mediate a variety of brain functions, such as emotion, motivation and cognitive processes. This is achieved mainly by the projection from the VTA to limbic forebrain areas, while motor control is exercised chiefly by the projection from the RRF to the neostriatum [3, 31]. We studied the axonal arborization of VTA and RRF neurons with Sindbis virus vectors. After injections of the viral vectors into rat VTA and RRF, infected single neurons were first examined for their TH immunoreactivity. They were then visualized completely by the immunoperoxidase method with an anti-GFP antibody and the whole axonal arborizations reconstructed, long the same lines as used for *SNc* neurons.

In the mesolimbic pathway (A10), VTA neurons were classified into three groups in terms of their projection sites. The first groups sent their axons to the limbic cortices, the second to the ventral striatum (accumbens nucleus, olfactory tubercle), and the third to both dorsal and ventral striatum. All the DA neurons in RRF (A8) formed high-density bushes in the dorsal striatum. Many of these neurons were observed to form relatively high-density bushes in their terminal fields, although the densities of the bushes of VTA or RRF neurons had a tendency to be lower than those of *SNc* DA neurons (unpublished data—[34]). These findings also support the neuronal mechanism of the vulnerability of *SN* DA neurons. Additionally, the third type of VTA neuron, which sends its axons to both dorsal and ventral striatum, would also imply that VTA DA neurons integrate the emotion, motivation, and behavior.

On the other hand, non-DA neurons (without TH immunoreactivity) were observed to project their axons to the lateral hypothalamic area, thalamus, and preoptic area. Many of these non-DA neurons were observed to form sparse bushes in their terminal fields. Additionally, the labeled fibers of non-DA neurons possessed many voluminous varicosities, whereas those of DA neurons projecting to ventral and dorsal neostriatum possessed ambiguous ones. Again, this finding also supports the particular vulnerability of *SNc* DA neurons—not through energy stress, but by excessive reactive oxygen species (see also Chaps. 7 and 8). More specifically, mitochondrial-derived oxidative stress (i.e., the major endogenous source of

oxidative stress) will also be higher in brain regions with greater synaptic abundance such as the DA neurons of the *SN* (Wellstead P., 2011, private communication).

Closing Remarks

In this chapter, recent developments in imaging morphology of single DA neurons with the novel virus vector were described from a historical perspective, and in the context of attempts to understand the mechanisms of PD. Two key findings of the virus-vector imaging are reported here. First, DA neurons in the *SNc* form widespread and highly dense axonal arborizations in the neostriatum, implying a particular vulnerability and redundancy in DA neurons. The energetic vulnerability of DA neurons is explained here from quantitative physiological observations and should be compared with Chap. 2 where a mathematical modeling of neuronal energy metabolism will be used to probe similar issues.

Second, *SNcd* and *SNcv* DA neurons innervate both patch/striosome and matrix compartment, implying that rewards and behavior would be integrated in the basal ganglia circuit, not only in a pathological status in PD, but also in the normal conditions. Preliminary results in DA neurons in the mesocorticolimbic pathways would also support an integration of rewards and behavior.

Competing Interest Statements The authors declare that they have no competing financial interests.

Acknowledgments This study was supported by Grants-in-Aid for Scientific Research 22500307, 22500308, 22592041, and General Insurance Association of Japan, ZENKYOREN, Mitsui Sumitomo Insurance Welfare Foundation, and Shiga Prefecture Rehabilitation Centre.

References

1. Alexander GE, Crutcher MD et al (1990) Basal ganglia-thalamocortical circuits: parallel substrates for motor, oculomotor, "prefrontal" and "limbic" functions. Prog Brain Res 85:119–146
2. Anden NE, Hfuxe K et al (1966) A quantitative study on the nigro-neostriatal dopamine neuron system in the rat. Acta Physiol Scand 67(3):306–312
3. Bjorklund A, Dunnett SB (2007) Dopamine neuron systems in the brain: an update. Trends Neurosci 30(5):194–202
4. Blanchet PJ, Calon F et al (1995) Continuous administration decreases and pulsatile administration increases behavioral sensitivity to a novel dopamine D2 agonist (U-91356A) in MPTP-exposed monkeys. J Pharmacol Exp Ther 272(2):854–859
5. Bowen WD, Gentleman S et al (1981) Interconverting mu and delta forms of the opiate receptor in rat striatal patches. Proc Natl Acad Sci U S A 78(8):4818–4822
6. Braak H, Ghebremedhin E et al (2004) Stages in the development of Parkinson's disease-related pathology. Cell Tissue Res 318(1):121–134

7. Calabresi P, Centonze D et al (2000) Synaptic transmission in the striatum: from plasticity to neurodegeneration. Prog Neurobiol 61(3):231–265
8. Calabresi P, Picconi B et al (2007) Dopamine-mediated regulation of corticostriatal synaptic plasticity. Trends Neurosci 30(5):211–219
9. Dahlstroem A, Fuxe K (1964) Evidence for the existence of monoamine-containing neurons in the central nervous system: I. Demonstration of monoamines in the cell bodies of brain stem neurons. Acta Physiol Scand Suppl 232(suppl):231–255
10. Dickson DW (2007) Neuropathology. In: Rajesh Pahwa KEL (ed) Handbook of Parkinson's disease. Informa Healthcare, New York, pp 195–207
11. Donoghue JP, Herkenham M (1986) Neostriatal projections from individual cortical fields conform to histochemically distinct striatal compartments in the rat. Brain Res 365(2):397–403
12. Doya K (2000) Complementary roles of basal ganglia and cerebellum in learning and motor control. Curr Opin Neurobiol 10(6):732–739
13. Furuta T, Tomioka R et al (2001) In vivo transduction of central neurons using recombinant Sindbis virus: Golgi-like labelling of dendrites and axons with membrane-targeted fluorescent proteins. J Histochem Cytochem 49(12):1497–1508
14. Gauthier J, Parent M et al (1999) The axonal arborization of single nigrostriatal neurons in rats. Brain Res 834(1–2):228–232
15. Gauthier-Campbell C, Bredt DS et al (2004) Regulation of dendritic branching and filopodia formation in hippocampal neurons by specific acylated protein motifs. Mol Biol Cell 15(5):2205–2217
16. Gerfen CR (1984) The neostriatal mosaic: compartmentalization of corticostriatal input and striatonigral output systems. Nature 311(5985):461–464
17. Gerfen CR (1985) The neostriatal mosaic: I. Compartmental organization of projections from the striatum to the substantia nigra in the rat. J Comp Neurol 236(4):454–476
18. Gerfen CR (1989) The neostriatal mosaic: striatal patch-matrix organization is related to cortical lamination. Science 246(4928):385–388
19. Gerfen CR, Baimbridge KG et al (1985) The neostriatal mosaic: compartmental distribution of calcium-binding protein and parvalbumin in the basal ganglia of the rat and monkey. Proc Natl Acad Sci U S A 82(24):8780–8784
20. Gerfen CR, Baimbridge KG et al (1987) The neostriatal mosaic: III. Biochemical and developmental dissociation of patch-matrix mesostriatal systems. J Neurosci 7(12):3935–3944
21. Gerfen CR, Herkenham M et al (1987) The neostriatal mosaic: II. Patch- and matrix-directed mesostriatal dopaminergic and non-dopaminergic systems. J Neurosci 7(12):3915–3934
22. Goodwin GC, Graebe SF, Salgado ME (2001) Control system design. Prentice Hall, Englewood Cliffs, 908 p
23. Graybiel AM, Ragsdale CW Jr (1978) Histochemically distinct compartments in the striatum of human, monkeys, and cat demonstrated by acetylthiocholinesterase staining. Proc Natl Acad Sci U S A 75(11):5723–5726
24. Halliday GM, Tork I (1986) Comparative anatomy of the ventromedial mesencephalic tegmentum in the rat, cat, monkey and human. J Comp Neurol 252(4):423–445
25. Herkenham M, Pert CB (1981) Mosaic distribution of opiate receptors, parafascicular projections and acetylcholinesterase in rat striatum. Nature 291(5814):415–418
26. Hirsch E, Graybiel AM et al (1988) Melanized dopaminergic neurons are differentially susceptible to degeneration in Parkinson's disease. Nature 334(6180):345–348
27. Ito T, Hioki H et al (2007) Gamma-aminobutyric acid-containing sympathetic preganglionic neurons in rat thoracic spinal cord send their axons to the superior cervical ganglion. J Comp Neurol 502(1):113–125
28. Izenwasser S, French D (2002) Tolerance and sensitization to the locomotor-activating effects of cocaine are mediated via independent mechanisms. Pharmacol Biochem Behav 73(4):877–882
29. Jellinger KA (2004) Parkinsonism and persistent vegetative state after head injury. J Neurol Neurosurg Psychiatry 75(7):1082; author reply 1082–1083

30. Jimenez-Castellanos J, Graybiel AM (1987) Subdivisions of the dopamine-containing A8-A9-A10 complex identified by their differential mesostriatal innervation of striosomes and extrastriosomal matrix. Neuroscience 23(1):223–242
31. Joel D, Weiner I (2000) The connections of the dopaminergic system with the striatum in rats and primates: an analysis with respect to the functional and compartmental organization of the striatum. Neuroscience 96(3):451–474
32. Kaneko T, Minami M et al (1995) Immunocytochemical localization of mu-opioid receptor in the rat caudate-putamen. Neurosci Lett 184(3):149–152
33. Langer LF, Graybiel AM (1989) Distinct nigrostriatal projection systems innervate striosomes and matrix in the primate striatum. Brain Res 498(2):344–350
34. Matsuda W (2008) Axonal arborization of mesocorticolimbic (A10) dopaminergic pathway: a single-cell study. The 31st annual meeting of the Japan neuroscience society, Elsevier
35. Matsuda W, Furuta T et al (2009) Single nigrostriatal dopaminergic neurons form widely spread and highly dense axonal arborizations in the neostriatum. J Neurosci 29(2):444–453
36. Matsuda W, Komatsu Y et al (2005) Levodopa treatment for patients in persistent vegetative or minimally conscious states. Neuropsychol Rehabil 15(3–4):414–427
37. Matsuda W, Matsumura A et al (2003) Awakenings from persistent vegetative state: report of three cases with parkinsonism and brain stem lesions on MRI. J Neurol Neurosurg Psychiatry 74(11):1571–1573
38. McGeer PL, McGeer EG et al (1977) Aging and extrapyramidal function. Arch Neurol 34(1):33–35
39. Morrish PK, Rakshi JS et al (1998) Measuring the rate of progression and estimating the preclinical period of Parkinson's disease with [18F]dopa PET. J Neurol Neurosurg Psychiatry 64(3):314–319
40. Nakamura K, Matsumura K et al (2002) The rostral raphe pallidus nucleus mediates pyrogenic transmission from the preoptic area. J Neurosci 22(11):4600–4610
41. Nakamura K, Matsumura K et al (2004) Identification of sympathetic premotor neurons in medullary raphe regions mediating fever and other thermoregulatory functions. J Neurosci 24(23):5370–5380
42. Nakamura Y, Nakamura K et al (2005) Direct pyrogenic input from prostaglandin EP3 receptor-expressing preoptic neurons to the dorsomedial hypothalamus. Eur J Neurosci 22(12):3137–3146
43. Oorschot DE (1996) Total number of neurons in the neostriatal, pallidal, subthalamic, and substantia nigral nuclei of the rat basal ganglia: a stereological study using the cavalieri and optical disector methods. J Comp Neurol 366(4):580–599
44. O'Sullivan SS, Evans AH et al (2009) Dopamine dysregulation syndrome: an overview of its epidemiology, mechanisms and management. CNS Drugs 23(2):157–170
45. Prensa L, Parent A (2001) The nigrostriatal pathway in the rat: a single-axon study of the relationship between dorsal and ventral tier nigral neurons and the striosome/matrix striatal compartments. J Neurosci 21(18):7247–7260
46. Schultz W (1998) Predictive reward signal of dopamine neurons. J Neurophysiol 80(1):1–27
47. Sutton RS, Barto AG (1998) Reinforcement learning: an introduction. MIT Press, Cambridge
48. Trujillo KA, Kubota KS et al (2004) Continuous administration of opioids produces locomotor sensitization. Pharmacol Biochem Behav 79(4):661–669
49. Wellstead P, Cloutier M (2011) An energy systems approach to Parkinson's disease. Wiley Interdiscip Rev Syst Biol Med 3(1):1–6

Chapter 2
Modelling and Simulation of Brain Energy Metabolism: Energy and Parkinson's Disease

Peter Wellstead and Mathieu Cloutier

Abstract The brain is the most energy intensive organ in the human body, so it is to be expected that weaknesses in brain energy metabolism could be a potential factor in neurodegenerative conditions. This is the starting point for a systems biology study of how known Parkinson's disease (PD) risks can weaken brain energy metabolism and contribute to the preconditions for disease. We begin by describing PD as a multifactorial condition in which energy deficits form a common denominator for known risk factors. This is followed by a description of a mathematical model of brain energy metabolism, and its structural and dynamic properties. Simulations of the model are then used to illustrate how external risk factors, plus structural and dynamic weaknesses in neural energy supplies, particularly affect neurons most vulnerable to PD damage. Taken together, these issues form the basis of an energy-deficit theory for how the preconditions for PD are formed.

Introduction

For the majority of Parkinson's disease (PD) sufferers, the cause of their condition is unknown. This idiopathic/sporadic form of PD represents around 90% of known occurrences, with the balance being composed of the familial form, where there is a clear genetic mechanism [1]. The causes of idiopathic/sporadic PD are not a complete mystery. It is, for example, known that certain risk factors will raise the likelihood of developing idiopathic/sporadic PD. These risks include advanced age, exposure to certain toxins, head trauma, plus possible other factors [2, 3].

P. Wellstead (✉)
Hamilton Institute, National University of Ireland, Maynooth, County Kildare, Ireland
e-mail: peter.wellstead@nuim.ie

M. Cloutier
GERAD and Ecole Polytechnique de Montreal, Montreal, QC, Canada
e-mail: Mathieu.Cloutier@nuim.ie

P. Wellstead and M. Cloutier (eds.), *Systems Biology of Parkinson's Disease*,
DOI 10.1007/978-1-4614-3411-5_2,

It is generally assumed that risk factors accumulate in some unknown way to create preconditions in which PD can develop. The aim in this chapter is to consider how this happens. In particular, we describe the development of an in silico framework for the study of PD in the form of a mathematical model of brain energy metabolism. This model is then used to probe underlying causal mechanisms for PD, and in particular the search for a common causal denominator that unifies the diverse set of known risks.

PD Is a Multifactorial Condition

PD is a heterogeneous condition that manifests in a variety of ways and with various symptoms. This continues throughout the course of the disease, with the rate and nature of its progress varying from one sufferer to another. Variability, considered with other issues [4, 5], has led to the consensus view that there is no single causal mechanism for PD and that there are a variety issues (risk factors) that contribute to PD in, as yet, undefined multifactorial ways [6].

The existence of a set of possible risk factors for PD presents an opportunity for systems biology. Specifically, if systems biologists can construct a suitable mathematical model it will be possible to apply a computer implementation of the model to systematically investigate in silico the many combinatorial and temporal variations that multifactorial problems present. Based on such a systems biology approach, the viewpoint put forward in this chapter is that (1) individual PD risk factors, if severe, may work alone, or more usually, in multifactorial combination, (2) PD risks factors are "causal" only in the sense that they create the preconditions for pathogenesis to be initiated, and (3) there is a common denominator for all non-genetic PD risk factors in the form of cumulative neuronal energy deficits.

PD Risk Factors

The single most important of risk factor in idiopathic PD is age (see Chap. 3). The statistical risk of developing PD rises significantly as we get older, increasing particularly after the age of 60 years, but decreasing again in extreme old age [7]. In addition to age, there is also strong evidence of risks due to exposure to certain chemicals used in the workplace. This risk associates particularly with toxins associated with land workers [8] and certain industries [9, 10]. How such toxins contribute to PD was revealed by the case of the frozen addicts of California [11]. This concerned the incidence of severe Parkinsonian symptoms in young drug addicts who had injected drugs that include a neurotoxin MPTP (1-methyl-4-phenyl-1,2,3,6-tetrahydropyridine). Subsequent research showed that MPTP creates Parkinsonian symptoms through damage to neuronal mitochondria.

A third risk factor for PD, or at least PD symptoms, is severe head injury (head trauma, see Chap. 1). While this is generally accepted as a risk, it is not supported by strong statistical evidence. In fact, the number of PD sufferers that are known to have experienced head trauma is relatively small, so that it is difficult to gather sufficient evidence to be statistically convincing. Nonetheless, in the case of severe head injury, and in sports that involve repeated violent head impact, there is strong circumstantial evidence. In boxing, Muhammad Ali is the most famous case, with further examples in other high-impact sports. Outside of sport, other sufferers have reported incidents in their formative years during which they received severe blows to the head.

A life-course factor that influences PD risk in a beneficial way is physical fitness. In particular, there is statistical evidence that vigorous physical exercise, particularly in youth, has a protective effect [12]. Unconnected with this protective factor, a number of genes have been implicated in familial PD [1]. However, as suggested by the case of the Ohio Kindred, a high level of genetic damage appears to be required in order to trigger familial PD [13]. An inference drawn from this is that limited irregularity in "PD genes" be tolerated but that they can provide a background level of predisposition, upon which the various risk factors then build [14].

Energy as a Common Denominator

There is a connection between the major risk factor—advancing age—and a decline in energy metabolism. Specifically, the efficiency of the cerebral energy metabolism, and the general effectiveness with which our bodies utilise glucose, reduces with age [15, 16]. The decline in energy generation and utilisation takes place gradually over a person's lifetime (Chap. 3). This suggests a linkage between an increased chance of PD in an ageing brain, and the declining effectiveness of brain energy metabolism in the elderly. On the reverse side, the apparent protective influence of vigorous exercise [12] could be to slow down the rate of metabolic decline—keeping the energy metabolism "on its toes", so to speak.

Age is not the only risk factor to have an energy link. Revisiting other factors—external toxins and head trauma—shows that they too are associated with a compromised brain energy metabolism. In particular, toxins linked to PD are known to selectively damage the energy generating mechanisms of mitochondria [10, 17], weakening their ability to maintain neural ATP (adenosine triphosphate) levels. In addition, damage to the brain's supporting structures of capillary and astrocytic systems may reduce the effectiveness of energy metabolism. As illustrated later, astrocytic damage in particular may compromise transient energy supplies during neuronal signalling.

So far, we have discussed the "supply-side" of energy in the brain. Now, we consider the "demand-side" argument. As far as it is known, neurons are the only

cells to experience Parkinsonian damage. So to understand why energy should be a factor in PD, we consider why neurons are special from an energy demand perspective:

Neurons work harder than other cells: Between 10 and 20 times harder in fact, with most of the additional energy requirement being needed to fuel neural signalling [18]. Their higher work rate implies that neurons would be more susceptible to failure if their energy metabolism were to be deficient.

Substantia nigra neurons work the hardest of all: Dopaminergic neurons in the *substantia nigra* are the most vulnerable to PD damage. And as explained in Chap. 1 and [19], they are, by a very large margin, the most demanding neurons in terms of the energy requirement.

Substantia nigra neurons signal differently: *Substantia nigra* neurons also have a continuous "pace-making" feature and use calcium to facilitate this signalling. As discussed in Chaps. 4 and 5, these two factors further amplify the energy load on *SN* neurons.

Long axons need more energy: Neurons with long and/or lightly protected axons have also been found to be more vulnerable to Parkinsonian damage [20]. This provides another connection between vulnerability and energy requirements, since the longer the axon, the greater the amount of energy needed to perform signalling [21].

Brain Energy Metabolism as a Framework for the Systems Biology of PD

The mathematical modelling of physical systems can be interpreted as the analysis of energy flows within the system [22]. This involves partitioning the system into a central energy supply compartment, plus a set of modules that draw down energy from the supply and use it to perform their function within the system. The same approach can be applied to modelling living systems and, in the current context, to the modelling of PD [23]. Proceeding in this vein, the brain energy metabolism forms the central energy-supply model compartment, while the various cellular and metabolic processes that give neurons their function are the modules that attach to the central compartment.

In the modelling of a particular neurological disease, only those cellular modules implicated in the specific condition need be considered. Thus, for a mathematical model of PD, we would have a central brain energy metabolism model as the framework, and the cellular functions implicated with PD attached to it, as indicated in Fig. 2.1. Because of the strong implication of energy in PD, this chapter concentrates on the construction of a mathematical model of brain energy metabolism. The role of cellular processes implicated in PD is discussed in subsequent chapters of this volume.

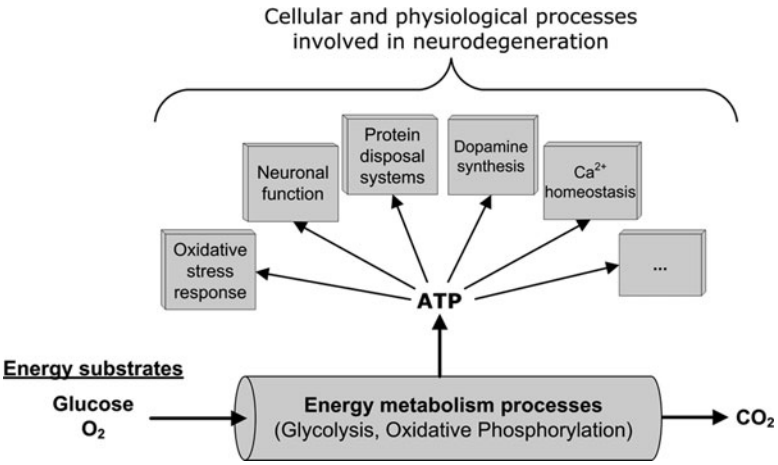

Fig. 2.1 Brain energy metabolism as a modelling framework for neurodegenerative disease. The brain energy metabolism forms a central modelling structure with modules representing cellular functions associated with a particular condition (in this case PD) connected to it by their dependence upon ATP supplies; cross-linkages between modules are used to model interdependence of cellular functions

Brain Energy Metabolism Modelling

Following work by Aubert and co-workers [24], we take a compartmental view, with four main compartments: brain capillaries, neurons, astrocytes and the extracellular space. In the form described here, the brain energy metabolism model is for a generic region within a neuron, with no special features that would associate it with a particular neural function, structural form, or spatial location. A more complete model of PD would recognise the specifically different features of vulnerable neurons, e.g. calcium facilitated signalling (see Chaps. 4 and 5), dopamine metabolism (see Chap. 8), take account of morphological variations (e.g. Chap. 1) and other spatial factors in PD. Since the model is designed to be extended, such features can be accommodated subsequently by modification of model parameters or by the incorporation of new modules as suggested in Fig. 2.1.

The role of astrocytes in brain energy metabolism was suggested in [25, 26] through the proposal for an astrocyte-neuron lactate shuttle (ANLS), whereby lactate from astrocytes supports the neuronal ATP system. Although the ANLS theory is not universally endorsed, the general consensus is that astrocytes play a role in energy metabolism by their release of lactate. This consensus is supported by modelling studies in [27, 28] and experimental observation of extracellular lactate levels during astrocytic blockade, (see Chap. 6 and Fig. 2.3). Later, we comment on the ANLS theory through a developmental argument for the existence of astrocyte support for neuronal ATP.

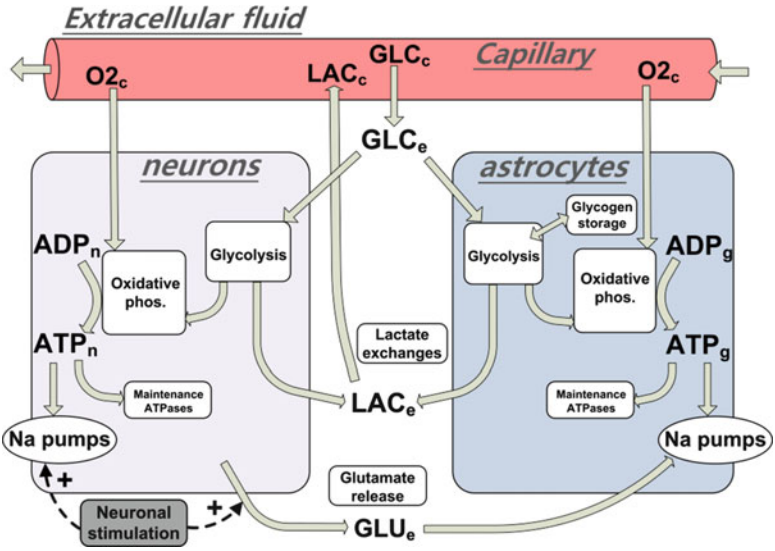

Fig. 2.2 The compartmental structure of the brain energy metabolism model. The model represents a general area within a neuron. Energy substrates glucose and oxygen (GLC, O_2) from the capillary compartment enter the neuronal compartment and astrocyte compartments via the extracellular compartment. There is an additional path for energy substrates directly from capillaries to astrocytes

Brain Energy Metabolism Model

The model outlined here was first developed for the study of neurodegenerative conditions in general [29]. Amongst other features, it includes the representation of the astrocyte–neuron coordination by modelling neuronal and astrocytic activity as a coordinated neurotransmitter cycling (the glutamate loop). A further important feature is the description of astrocytic glycogen dynamics as an astrocytic storage capability. Finally, the model of the central energy metabolism is extended to include a more detailed representation of glycolysis and mitochondrial regulation.

A complete description [29] of the model involves 12 independent states for neurons, 13 for astrocytes, 3 extracellular states and 4 capillary states. In total, 42 kinetic equations are used to describe the metabolic system, and the model has 63 kinetic parameters (reaction constants, maximum reaction rates, affinity constants and regulation parameters). The kinetic rates included in the model also use 27 physical constants (volumes fractions, arterial concentrations, electrochemical constants, etc.). These constants are assumed to be known and representative of the system (see [24, 30], with further details in the CellML metabolism directory).

In the following section, we restrict ourselves to the model design and features as they relate to subsequent discussions of energy and PD. The model structure is

illustrated in the schematic view of Fig. 2.2, and its main characteristics are as follows:

Cerebral compartments and exchange systems
There are four main compartments in the model: neurons (variables indexed "n"), astrocytes (variables indexed "g"), capillaries (variables indexed "c") and extracellular space (variables indexed "e"). Glucose (GLC) is transferred from capillaries to neurons and astrocytes via the extracellular space. In addition, and because of the intimate contact between astrocytes and capillaries, there is an additional direct transfer pathway of GLC. Glucose transport is described by facilitated diffusion, while LAC transport is modelled by the same mechanism, with the exception that chemical gradients are arranged to favour release of LAC, instead of uptake as for GLC. The dynamics of Oxygen (O_2) and carbon dioxide (CO_2) in the extracellular space are ignored so that transport of gaseous species between capillaries and tissue is direct.

Central energy metabolism
In Fig. 2.2, the central energy metabolism of both neurons and astrocytes consists of glucose entering the cells, from where it is converted by glycolysis to pyruvate (PYR). This process is modelled in the sequence: adenosine triphosphate (ATP) is consumed by the hexokinase (HK) and phosphofructokinase (PFK). Glyceraldehyde-3-P (GAP) produced from the PFK reaction is then converted to phosphoenolpyruvate (PEP), with nicotinamide dinucleotide (NADH) regeneration from NAD and, finally, the production of PYR from PEP by the pyruvate kinase. Pyruvate produced by glycolysis can either be converted to LAC, or oxidized in the mitochondria (v_{mito}) to regenerate ATP from ADP (adenosine diphosphate).

The regulation mechanisms and reactions for energy metabolism used in the model are modified forms of those described in [24, 30] and [31]. The modifications involved the addition of inhibition of mitochondrial activity at high ATP–ADP ratio [30] and the removal of secondary activation of mitochondrial activity (model validation tests showed it to be unnecessary). Thus, the model describes mitochondrial regulation from the availability of PYR, O_2 and energetic requirements of the tissue. Energetic metabolism in neurons and astrocytes is buffered by phosphocreatine (PCr), which is used to regenerate ATP during short-term abrupt increases in energy demand. Adenosine monophosphate (AMP) equilibrium with ADP and ATP through the adenylate kinase reaction is neglected. Using kinetic parameters from the literature for adenylate kinase, it was observed that AMP dynamics were negligible in the conditions of this study (simulations results not shown).

Neuronal stimulation system and the glutamate loop
The major "sink" for energy metabolism is the maintenance of ionic gradient in neurons and astrocytes through sodium pumping (Na pumps in Fig. 2.2). The dynamics of sodium are considered in a way that allows the description of the tissue energetic "load" both in resting conditions (Na-ATPases pumps working to maintain Na gradient) and during stimulation (increased Na inflow in neurons). The stimulation of neurons is modelled as a base stimulation rate (flow of Na after neuronal habituation) and a spiking at the onset of stimulation.

As described earlier, an important phenomenon in the ANLS view of brain physiology is the coordination of neuronal and astrocytic response during stimulation. Such a coordination mechanism is implemented through the uptake of glutamate (GLU) by astrocytes (with Na co-transport) after neuronal stimulation. Subsequent to the initial ANLS proposal, the GLU loop has been assessed through NMR measurements [32, 33], with the quantitative importance of the glutamate loop being emphasised in [34]. The model represents the physiological response of the cerebral tissue in the glutamate loop through a series of reactions. As shown in Fig. 2.2, the loop is described by: (1) the release of GLU by neurons, (2) cleaning of extracellular space by astrocytes (with Na co-transport) and (3) non-stimulatory recycling of GLU from astrocytes back to neurons. The GLU loop model is simplified by neglecting the dynamics of glutamine (a non-stimulatory intermediate in the transfer from astrocytes to neurons). This enables the conversion of GLU to glutamine in astrocytes, with transfer to neurons and reconversion to GLU, to be modelled as one reaction.

The GLU loop activates astrocytic metabolism through two mechanisms. First, Na pumps are activated to maintain the Na gradient in the astrocytes, consuming ATP in the process. Second, the conversion of GLU to glutamine requires 1 molecule of ATP per molecule of GLU processed. Thus, the GLU loop allows a proportional activation of astrocytic and neuronal metabolism, with an increase in ATP consumption in both cell types. This increase in energy demand directly activates the PFK through an activation-inhibition kinetic for ATP and potentially the whole glycolytic flux. An increase in the mitochondrial activity is also expected (direct activation by ADP and reduced inhibition by ATP). Including the glutamate loop in this way allows the astrocytes–neurons physiological coordination to be described by a physiologically realistic mechanism.

Glycogen metabolism

The inclusion of astrocytic glycogen (GLY) storage in the model (see Fig. 2.2) was a key mechanism in enabling the model to reproduce the variations of GLC and LAC observed in vivo (see Chap. 6). It proved possible to model GLY dynamics with two reactions: synthesis and breakdown. Synthesis of GLY occurs during "rest" periods, whereas breakdown is activated by "work" periods, e.g. neuronal stimulation periods (induced by noradrenaline). This mechanism allowed an additional input of energy substrate during high-energy demand periods, and proved critical during model validation against experimental data. The modelling of GLY dynamics would however benefit from further analysis of the dynamics of GLC and O_2 consumption and uncoupling phenomenon (GLY is a buffer between the entering GLC flux and its mitochondrial oxidation). In particular, an increase in energy substrate inflow is required to explain how LAC and GLC concentrations could both be higher than their baseline values for a long period of time after neural stimulation. The transfer of GLC between capillary and extracellular space, even though it constitutes the major GLC inflow to the tissue, does not show sufficient variations to explain the GLC profile.

Brain Energy Metabolism: In Silico and In Vivo

Model Calibration

Values of parameters, coefficients and physical constant were, where possible, taken from the literature. Volumes fractions, resting steady-states values, sodium transport parameters and CBF values were considered to be the same as reported in [24] and [30]. Likewise, in calibration routines [35], the initial values for parameters were taken mainly from [24], with the GLU coordination loop parameters initialised to produce a cycling of GLU consistent with values reported in [34] and [30]. Additional parameters on LAC transport and regulation (affinity constants and maximum reaction rates) were obtained from data in [36]. The parameters of glucose transport kinetics were based on glucose transport literature [37]. Literature information on kinetic parameters also ensured that the model operated within a realistic physiological range (when measured in terms of concentrations and fluxes). A second-stage of calibration involved using in vivo time-course histories of GLC and LAC measurements during perturbations experiments with animals. These real-time measurements, as described in Chap. 6, provided time course calibration data for dynamic tuning of the model to the extracellular changes that take place in cerebral metabolism during neural stimulation.

Calibration was performed using in vivo measurements of extracellular cerebral GLC and LAC from data obtained during active neurological stimulation [38, 39]. These time histories were used in the Systems Biology Toolbox [35] to search for model parameter sets that optimally matched the model dynamical performance with the observed time course information in [38, 39]. Examples of the source in vivo data for GLC and LAC in normal conditions, plus the corresponding in silico data are compared in Fig. 2.3b and 3c.

Validation, Prediction and Visualisation

Calibration of the model ensures that it is able to reproduce in vivo data. However, to be acceptable, the model also required validation. This was done by testing its capacity to predict observed behaviour that is outside of its calibration range: that is to say by comparing model outputs with independent experimental data collected in modes of behaviour not included in the calibration. For this, we used the model to predict, in silico, the variations in extracellular GLC and LAC when the astrocytic coupling is reduced using propranolol. Figure 2.3e, f compares predictions with the corresponding independent in vivo measurement of GLC and LAC where astrocyte action is reduced [39]. The two diagrams show how the model predicts

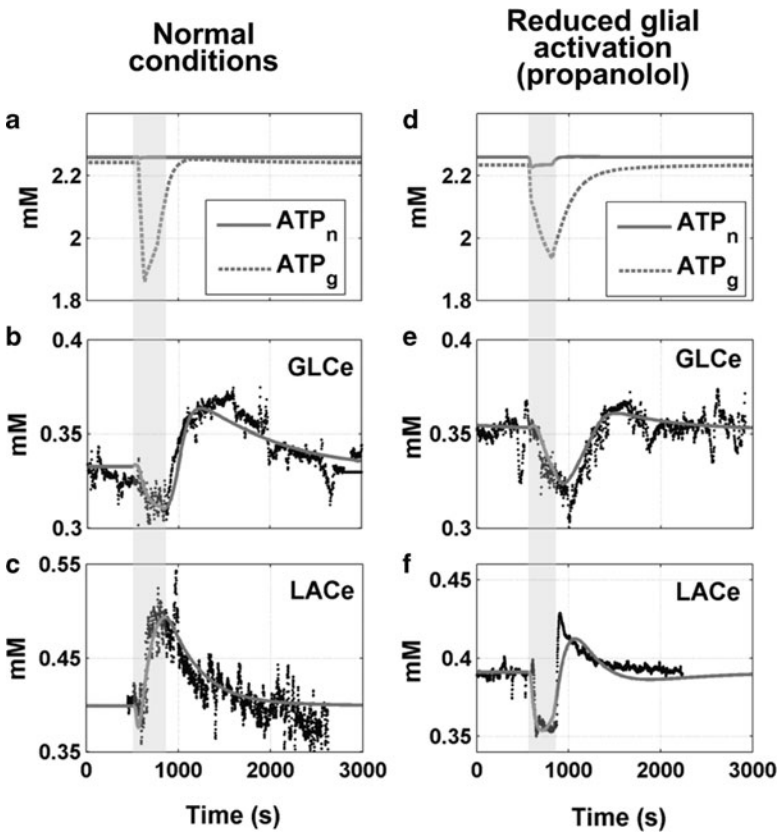

Fig. 2.3 Calibration and validation of the brain energy metabolism model. Plots (**a**, **d**) in row 1 show variations in intracellular ATP variables not measureable in vivo. (**b**, **c**) Calibration data for extracellular GLC and LAC. (**e**, **f**) Validation data obtained by comparing results with reduced astrocytic activity in vivo with in silico predictions

a drop in extracellular LAC that is later observed in vivo. This result is significant: (1) at a fundamental level it supports the ANLS theory and (2) for PD it has implications for head trauma as a risk factor. In particular, it implies that any damage to neuron–astrocyte coordination, such as might be caused by head trauma, will reduce the astrocytic support of neuronal ATP during signalling. Thus, we would expect that head trauma, in addition to direct damage to brain capillaries and neuronal structures mentioned in Chap. 1, would also induce additional energy-stress through astrocyte damage.

The ability to make real-time measurement of dynamic variations inside cells of the living brain could help unlock the secrets of neurodegeneration. In silico tools, such as the brain energy metabolism model, offer hope in this direction. Specifically, in addition to prediction of extracellular variables, the model enables variations in intracellular fluxes to be visualised. For example, Fig. 2.3a, d show

visualisations of neuronal ATP levels. As discussed elsewhere in this volume, such visualisations using in silico models may offer insights into otherwise "hidden" cellular mechanisms. Notice in particular that with astrocytic action reduced (Fig. 2.3b), the neuronal ATP level is temporarily reduced during stimulation.

Systems Properties of Brain Energy Metabolism

The act of mathematical modelling forces a strict discipline on the systems biologist. In a mathematical model, each reaction must be defined in quantitative terms, and related to other reactions involved in the model in a consistent way. A benefit of this discipline is that core systems properties are revealed in useful ways. In the brain energy metabolism model, two such properties are relevant to PD—both concern the consistent supply of neuronal ATP as determined by the mechanisms that control and regulate the brain energy metabolism. Details of brain energy metabolism control are given in [40]; here, we review points that relate to PD.

ATP Regulation

As illustrated in Fig. 2.4, the regulation of ATP is provided by a combination of two feedback loops. The outer feedback loop is a legacy from the control of glycolysis in simple cells and would, on its own, provide relatively poor control [41]. However, the quality of control is greatly strengthened by the second (inner) feedback loop, and the two together ensure ATP supplies are regulated to a consistent and constant homeostatic level during the steady "rest" state, and during slow changes in activity.

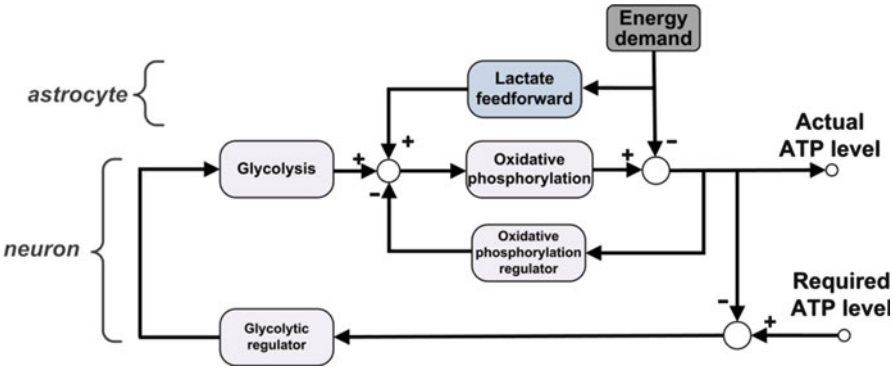

Fig. 2.4 Energy regulation and control structure for brain energy metabolism. Two feedback loops regulate the ATP supplies for the steady homeostatic state. The lactate feedforward loop supplements oxidative phosphorylation during stimulation and enables the neuron to create ATP supplies during rapid, transient, energy demands

This suffices for most human cell types, but good steady-state regulation is not sufficient in neurons: the energy demands of signalling requires transient bursts of extra ATP [42], and these, in turn, requires the brain energy metabolism to accommodate rapid changes in ATP levels. Unfortunately the two feedback loops cannot respond fast enough, and instead the transient demands of energy are met by the fast feedforward lactate loop shown in Fig. 2.4. This coordinated release of astrocytic lactate, supports the specific element of the overall neuronal energy budget associated with rapid transient ATP demands. The implications of this for PD can be seen from the following systems view.

Astrocyte Feedforward

Within the model, astrocytes are activated during signalling by neuronal release of neurotransmitters during signalling, with coordination provided by the uptake by glial cells (astrocytes in particular) of excess neurotransmitters. In order to do this, astrocytes draw upon the efficient glycogen storage mechanism and consequently undergo an increase in glycolytic rate and LAC production. Such increases in LAC have been observed experimentally during high activity periods in the brain [43, 44] and are a feature of our model response (e.g. Fig. 2.3c). The use of a secondary system (e.g. astrocytes) to produce a supplementary energy substrate (LAC) for the main functional system (neuron) is a biological equivalent of feedforward control structures used to regulate technological processes during periods of sudden large demands [45]. In such processes, feedforward is designed to give an early and rapid response to a change that cannot be met quickly enough through the feedback pathway. In brain energy metabolism, the feedback pathway passes through a number of intermediate states that, particularly in glycolysis, incurs a significant time delay. For the neuron, the use of lactate feedforward is a natural cooperative development that short-circuits this delay as follows: the increase in energy loading (i.e. increase in neurotransmitter circulation) is forwarded to astrocytes. The astrocytes respond by drawing upon their glycogen store to produce LAC. In its turn, the higher available LAC concentration then favours neuronal uptake, oxidation in neurons and consequent increase of ATP just when it is required for signalling.

The feedforward mechanism is independent of feedback action within neuronal metabolism (i.e. LAC will increase regardless of ATP levels in neurons) and enables the feedforward loop to bypass the time delays in glycolysis. In classical control, this type of controller can be finely tuned to reject disturbances on the system. Again, analogies for this tuning are found in the systems biology literature, for example in the perfect adaptation system presented in [46].

Figure 2.3c demonstrates, in vivo and in silico, the extracellular LAC variations with the feedforward LAC mechanism. The change in energy demand here is relatively small (25%) as it is reported that the basal metabolic rate in neurons is relatively high (i.e. as much as 90% of the active rate). This corresponds with observations, during physiological stimulations, of a maximum of 20–25% increase in energy demand.

The Role of Glycogen Storage

Astrocytic feedforward works because of glycogen storage. In particular, the additional inflow during stimulation is assumed to be coming from an activation of glycogen breakdown by a molecular signal (noradrenaline) that is known to be involved in sensory response. The amplitude of that GLY breakdown flux during stimulation was found to be of the order of 2×10^{-3} mMol s^{-1}.

The increase in GLY breakdown allows astrocytes to switch from a pure GLC usage to a mix of GLC and GLY usage. The comparison of hexokinase rate and glycogen breakdown in astrocytes provides a clear explanation for the observed triphasic behaviour for GLC. First, at the onset of stimulation, the activation of glycolysis in astrocytes induces an increase in the hexokinase rate that explains the rapid decline in GLC concentration. Then, after a delay, the noradrenaline "signal" induces GLY breakdown, which supplies the excess GLC needed in astrocytes. Thus, the hexokinase rate returns to its steady-state value as soon as the GLY breakdown is initiated, which stabilises the extracellular GLC concentration. After stimulation ends, the noradrenaline signal still activates GLY breakdown, this induces an increase in G6P, which in turn inhibits hexokinase, and results in a fast increase in extracellular GLC.

Using the GLY store during high demand periods allows the cerebral tissue to meet its increased energy requirements with minimal changes in GLC transport from the capillaries. This smoothing action allows GLC level to be maintained in the cerebral environment during stimulation, a factor that is critical for neuronal glycolysis (neurons do not accumulate GLY). The described GLY breakdown (2×10^{-3} mMol s^{-1} for 400 s) would lead to a dip of ~0.8 mMol in astrocytic GLY concentration. This corresponds with the current literature on GLY levels in astrocytes that report GLY concentrations in astrocytes in the range of 1.4–4.2 mMol (adjusted for units consistency) [47]. The model also shows that the GLY pool is easily replenished in resting conditions, thus bringing an overall balance between high and low activity periods (simulations not shown). GLY is thus considered here not as an "infinite" substrate pool, but rather as a dynamic energy reserve that the cerebral tissue can draw upon to buffer its "energy budget" between low and high demand periods.

Simulating PD Risk Factors

Earlier we described how the neurons most vulnerable to PD damage also have the highest energy requirements. Reference was made to the morphological evidence given in Chap. 1, and further in silico evidence from the issues associated with calcium-facilitated signalling (Chaps. 4 and 5). It was further explained that the known PD risk factors each involve impairment of neuronal ATP availability. This was then used to claim energy deficits as the common denominator in the risk

factors that create preconditions for PD. In this section, we use simulations of the brain energy metabolism model to explore this claim. In particular, we demonstrate the influence on neuronal ATP of individual PD risk factors: age, toxin exposure and head trauma as they might be expected to gradually develop over a number of years.

The three risk factors are modelled as follows. (1) *Toxins*: the cumulative impact of a prolonged low-level neurotoxic exposure is simulated by a linear decline in mitochondrial efficiency (from 100 to 50%) over a 10-year period. (2) *Age*: the gradual decline of metabolism with age is represented by a linear reduction (from 100 to 75%) in the efficiency of glucose transport capacity over the same period. (3) *Head trauma*: the potential influence of head trauma is modelled as reduced astrocytic support of brain energy metabolism, and is simulated by a linear reduction in astrocytic activity, (from 100 to 35%) over the same simulation period. The simulations (Fig. 2.5) are in two parts: row two of the figure shows how risk factors influence the regulation of neuronal ATP during the steady "rest" state of the brain. The simulations shown in row three highlight the impact of transient ATP dynamics during neuronal signalling.

Steady-State ATP Regulation

Consider first the steady "rest" state ATP during the gradual metabolic decline associated with age and other risk factors such as head trauma. Figure 2.5 shows the individual application of three known PD related factors: (1) loss of mitochondrial complex I efficiency (Fig. 2.5a), (2) lower glucose transport capacity (Fig. 2.5b), and (3) loss of neuron–astrocyte metabolic interactions (Fig. 2.5c). The key point from these three plots (second row in Fig. 2.5) is that the ATP regulation system (e.g. the two feedback loops in Fig. 2.4) is highly effective maintaining a constant level of ATP even under significant deterioration in brain energy metabolism. Simulations of combinations of risk factors (not shown) indicate that the steady-state regulatory system remains robust during combinations of risk, but is more strongly challenged and fails earlier as more risks are imposed. This in silico result suggests an additive effect when combinations of risk are applied. Moreover, the particular combination of risk is not important since all risks reduce energy availability: it is the number and severity of risks that is important.

Transient ATP Control During Signalling

The two feedback loops in the brain energy metabolism prove themselves robustly capable to supply steady-state ATP requirements. Even with combinations of risk factors, the steady ATP levels maintain a good degree of resilience. However, when

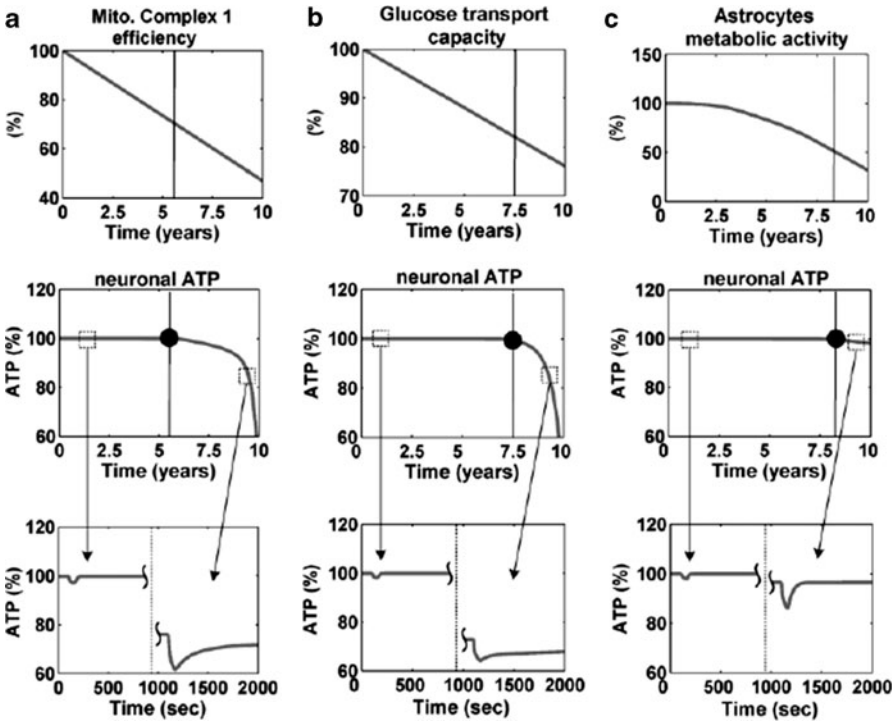

Fig. 2.5 Steady "rest" state regulation and transient control of ATP in brain energy metabolism. Deterioration of energy regulation as PD risks factors grow with time: (**a**) loss of mitochondrial Complex I efficiency; (**b**) lower glucose (GLC) transport; and (**c**) loss of astrocytes connectivity from head trauma. The *second row* shows long term dynamics of ATP (as a % of healthy steady state). The *third row* shows excerpts of short terms dynamics (1-min stimulation) before and after energy regulation is compromised

bursts of energy demand for signalling are added to the rest energy demand, the story changes and the neuronal ATP supplies are less able to respond to demand with sufficient speed. This is illustrated in the third row of Fig. 2.5, which shows the added impact of a transient increase in energy requirement corresponding to neuronal stimulation. Note that these dynamics operate on a very fast time scale (see, e.g., Chap. 6) and are thus not visible on the 10 years scale of the first two rows in Fig. 2.5. The rapid additional energy demand for signalling causes the available ATP levels to drop during the stimulation period, with the drop increasing as the level of a particular risk factor increases (Fig. 2.5a, b). Interestingly, the simulations suggest that steady-state neuronal ATP is particularly robust when the astrocytes contribution is reduced (Fig. 2.5c) but the short-term dynamics reveals a particular vulnerability. In this situation, even though the system maintains its steady state, it is not able to cope with rapid additional perturbations in energy demand and a transient decrease in ATP ensues. From a systems biology viewpoint, this is to be anticipated,

since it is the feedforward function of astrocytes that maintains neuronal ATP during signalling. Taken together, the results of Fig. 2.5 imply that a rigorous investigation of both rapid and long-term dynamics of metabolism in PD is important. This point is covered further in Chap. 7.

Preconditions for PD and Pathogenesis

From the "demand-side", the large energy budgets of vulnerable neurons suggest that energy stress is a precondition for Parkinsonian damage. From the "supply-side", this is reinforced by the observation that the three known PD risk factors are individually associated with a reduced effectiveness of brain energy metabolism, and that their combined impact in creating preconditions would be cumulative. The next question is this: how does the creation of preconditions for PD link to the initiation of the disease state? The pathogenesis of PD is considered in Chap. 7, and as a linkage to that chapter, we now make some bridging remarks between the energy issues discussed here and the cellular mechanisms that are implicated in the pathogenesis of PD.

An insight into the transition between preconditioning and pathogenesis can be gained by considering the two parallel control loops shown in Fig. 2.6a. We consider the class of PD where alpha-synuclein (α-SYN) accumulations are a feature: the upper loop in the figure concerns the energy supply, in which mitochondrial oxidative phosphorylation regenerates ATP from ADP (e.g. the inner feedback loop of Fig. 2.4). The second, lower, loop concerns the positive feedback on reactive oxygen species (ROS), and its implication in the accumulation of mis-folded α-SYN during PD. The full nature of this pathogenic feedback is described in Chap. 7, for the moment it is the linkage between the two feedbacks that is relevant. Specifically, as the energy level at which a neuron operates increases, then the increasing fluxes in the energy supply loop (υ_{op}. υ_{ATP}) drive up the level of oxidative stress, ROS. However, any increase in ROS feeds positively into the level of the protein α-SYN and can stimulate the disease state.

A consequence of the energy/ROS interaction is that the metabolic regimes of oxidative phosphorylation, ATP and ROS overlap. Thus, as shown in Fig. 2.6b in a plot with normalised scales, as ATP flux (υ_{ATP}) increases (corresponding to a larger neuronal energy demand), then so does the flux υ_{op}. The production of ATP can track growing demand (in this synthetic example) for over an order of magnitude change. However, beyond a certain pathogenic point, a rapid growth in ROS is triggered via the ROS feedback. In this "disease" regime, the ROS levels will grow but without an associated energy collapse. How pathogenesis can be triggered in this way is discussed in Chap. 7, the key points suggested by these simulations are the following: (1) a wide level of robustness in ATP supplies exists that can accommodate great variations in energy budgets in different neurons and (2) increasing energy stresses create the preconditions for pathogenesis significantly *before* the energetic capability of the energy metabolism is fully exhausted.

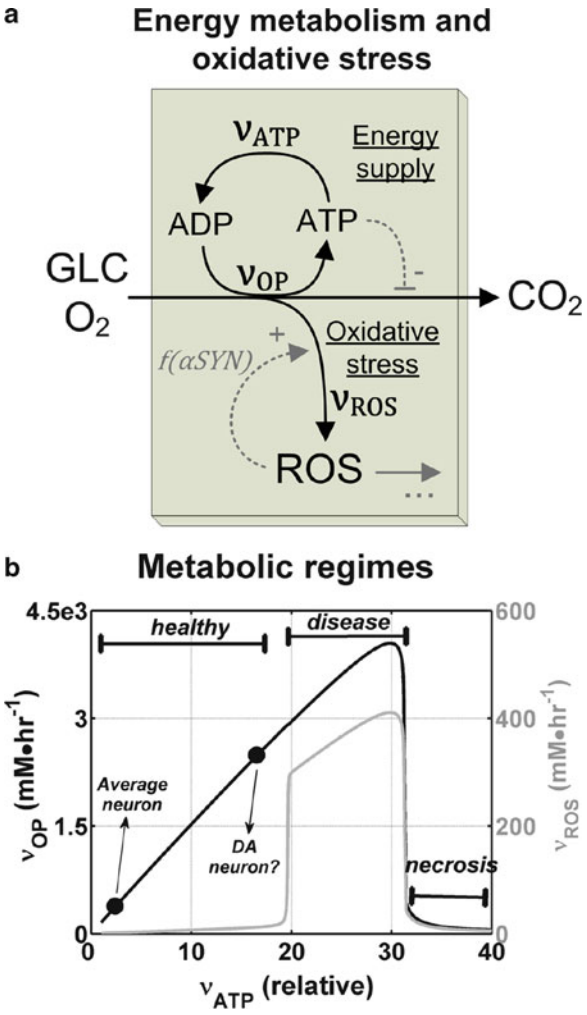

Fig. 2.6 Energy metabolism and oxidative stress. (**a**) Synthetic pathway showing how negative feedback is involved in energy (ATP) regulation and positive feedback is involved in oxidative stress (mediated by α-synuclein as described in Chap. 7). (**b**) Simulations of the system show how energy production (v_{OP}, *black line*) can follow along energy demand (v_{ATP}, *horizontal axis*) for over an order of magnitude, whereas ROS production (v_{ROS}, *grey line*) is initiated at some point before a complete energy collapse occurs. The two points on the energy production line indicate the likely position of the average neuron, and dopaminergic (DA) neurons of the substantia nigra

Discussion

A mathematical model of brain energy metabolism provides a core element in a systems biology approach to neurodegeneration, where multifactorial "wear and tear" is important. In the case of PD, a brain energy metabolism model is particularly relevant since the diversity of risk factors can all be linked to impaired ATP supplies in neurons. Moreover, the brain energy metabolism model provides a quantitative in silico framework for analysing the known risk factors in terms of their impact on brain energy metabolism, and illustrates the proposition that ATP deficits are the common denominator whereby various PD risk factors create the preconditions for pathogenesis. A computer implementation of the model allows

possible mechanisms for risk factors to be simulated over the many years required for them to develop. A structural view of energy metabolism helps to explain the role of rapid signalling in transient ATP deficits. Finally, a consideration of the link between ATP availability and pathogenesis shows how reduced energy levels can feed the process of disease inception (pathogenesis). The descriptions in this chapter are at an overall systems level—further clarity and detail of ageing are given in the following chapter, and relevant cellular mechanisms are explored in other chapters throughout this volume.

Acknowledgements We acknowledge the support of Science Foundation Ireland (Award 03/RP1/I382) for the research described in this chapter.

References

1. von Bohlen und Halbach O, Schober A, Krieglstein K (2004) Genes, proteins, and neurotoxins involved in Parkinson's disease. Prog Neurobiol 73(3):151–177
2. Seidler A, Hellenbrand W, Robra B-P, Vieregge P, Nischan P, Joerg J, Oertel WH, Ulmand G, Schneider E (1996) Possible environmental, occupational, and other etiologic factors for Parkinson's disease. Neurology 47:1275–1285
3. Tanner CM, Ross GW, Jewell SA, Hauser RA et al (2009) Occupation and risk of parkinsonism. Arch Neurol 9(66):1106–1113
4. Litvan I et al (2007) The etiopathogenesis of Parkinson's disease and suggestions for future research. Part 1. J Neuropathol Exp Neurol 66:251–257
5. Hughes AJ, Daniel SE, Kilford L, Lees AJ (1992) Accuracy of clinical diagnosis of idiopathic Parkinson's disease: a clinico-pathological study of 100 cases. J Neurol Neurosurg Psychiatry 55:181–184
6. Semchuk KM, Love EJ, Lee RG (1993) Parkinson's disease: a test of the multifactorial etiology hypothesis. Neurology 43:1173–1180
7. Van den Eeden SK, Tanner CM, Bernstein AL, Fross RD, Leimpeter A, Bloch DA, Nelson LM (2003) Incidence of Parkinson's disease: variation by age, gender and race/ethnicity. Am Jour Epidemiol 11:1015–1022
8. Tanner CM, Kamel F, Ross GW, Hoppin JA, Goldman SM, Korell M et al (2011) Rotenone, paraquat and Parkinson's disease, Environ. Health Perspect 119(6):866–872
9. Lucchini RG, Albini E, Benedetti L et al (2007) High prevalence of Parkinsonian disorders associated to manganese exposure in the vicinities of ferroalloy industries. Am Jour Ind Med 50(11):788–800
10. Gash DM, Rutland K, Hudson NL et al (2008) Trichloroethylene: Parkinsonism and complex 1 mitochondrial neurotoxicity. Ann Neurol 63:184–192
11. Langston JW, Palfreman J (1995) The case of the frozen addicts. Pantheon, New York
12. Thacker EL, Chen H, Patel AV, McCullough ML, Calle EE, Thun MJ, Schwarzschild MA, Ascherio A (2008) Recreational Physical Activity and Risk of Parkinson's disease. Mov Disord 1(23):69–74
13. Singleton AD, Farrer M, Johnson J, Singleton A et al (2003) Alpha-synuclein locus triplication causes Parkinson's disease. Science 302:841–844
14. Foltyne T, Sawcer S, Brayne C, Barker RA (2002) The genetic basis for Parkinson's disease. Journ Neurol Neurosurg Psychiatry 73:363–370
15. Willis MW, Ketter TA, Kimbrell TA, George MS, Herscovitch P, Danielson AL, Benson BE, Post RM (2002) Age, sex and laterality effects on cerebral glucose metabolism in healthy adults. Psychiatric Research: Neuroimaging 114(1):23–37

16. Roberts SB, Rosenberg I (2006) Nutrition and aging: changes in the regulation of energy metabolism with aging. Physiological Review 86:651–667
17. Sherer TB, Betarbet R, Testa CM, Seo BB et al (2003) Mechanisms of toxicity in rotenone models of Parkinson's disease, Jour. Neuroscience 23(24):10756–10764
18. Attwell D, Laughlin SB (2001) An energy budget for signalling in the grey matter of the brain. J Cereb Blood Flow Metab 21:1133–1145
19. Matsuda W, Furuta T, Nakamura KC, Hioki H, Fujiyama F, Arai R, Kaneko T (2009) Single nigrostratal dopaminergic neurons form widely spread and high dense axonal arborisations in the neostriatum, Jour. Neuroscience 29(2):444–453
20. Braak H, Del Tredici K (2004) Poor and protracted myelination as a contributory factor in neurodegenerative disorders. Neurbiology of Aging 25:19–23
21. Kelly M (2010) private communication
22. Paynter HM (1961) Analysis and design of engineering systems. MIT, Cambridge
23. Wellstead P (2010) Systems biology and the spirit of Tustin. IEEE Contr Syst Mag 57–102
24. Aubert A, Costalat R (2002) A model of the coupling between brain electrical activity, metabolism, and hemodynamics: application to the interpretation of functional neuroimaging. Neuroimage 17:1162–1181
25. Pellerin L, Magistretti PJ (1994) Glutamate uptake into astrocytes stimulates aerobic glycolysis: A mechanism coupling neuronal activity to glucose utilization. Proceedings of the National Academy of Science 91:10625–10629
26. Pellerin L, Bouzier-Sore AK, Auber A, Serres S, Merle M, Costalat R, Magistretti PJ (2007) Activity-Dependant Regulation of Energy Metabolism by Astrocytes: An Update. Glia 55:1251–1262
27. Aubert A, Costalat R (2005) Interactions between astrocytes and neurons studied using a mathematical of compartimentalized energy metabolism. J Cereb Blood Flow Metab 25:1476–1490
28. Aubert A, Costalat R, Magistretti PJ, Pellerin L (2005) Brain lactate kinetics: modeling evidence for neuronal lactate uptake upon activation. Proceedings of the National Academy of Science 102(45):16448–16453
29. Cloutier M, Bolger FB, Lowry JP, Wellstead P (2009) An integrative dynamical model of brain energy metabolism using in-vivo neurochemical measurements, Jour of Comp. Neuroscience 27(3):391–414
30. Geddje A (2002) Coupling of Blood Flow to Neuronal Excitability. In: Walz W (ed) The Neuronal Environment: Brain Homeostasis in Health and Disease. Humana Press, Totowa, NJ, USA, p 432
31. Heinrich R, Schuster S (1996) The regulation of cellular systems. ITP Chapman & Hall, New York
32. Shen J, Petersen K, Behar K, Brown P, Nixon T, Mason G, Petroff O, Shulmann G, Shulman R, Rothman D (1999) Determination of the rate of the glutamate/glutamine cycle in the human brain by in vivo 13 C NMR. Proceedings of the National Academy of Science 96:8235–8240
33. Zwingmann C, Butterworth R (2005) An update on the role of brain glutamine synthesis and its relation to cell-specific energy metabolism in the hyperammonemic brain: further studies using NMR spectroscopy. Neurochem Int 47:19–30
34. Hyder F, Patel AB, Gjedde A, Rothman DL, Behar KL, Shulman RG (2006) Neuronal-Glial Glucose Oxidation and Glutamatergic-GABAergic Function. J Cereb Blood Flow Metab 26:865–877
35. Schmidt H, Jirstand M (2006) Systems Biology Toolbox for MATLAB: A computational platform for research in Systems Biology. Bioinformatics 22(4):514–515
36. Simpson IA, Carruthers A, Vannucci SJ (2007) Supply and Demand in Cerebral Energy Metabolism: The Role of Nutrient Transporters. J Cereb Blood Flow Metab 27(11):1766–1791
37. Barros LF, Bittner CX, Loaiza A, Porras OH (2007) A Quantitative Overview of Glucose Dynamics in the Gliovascular Unit. Glia 55:1222–1237

38. Fillenz M, Lowry JP (1998) Studies of the Source of Glucose in the Extracellular Compartment of the Rat Brain. Dev Neurosci 20:365–368
39. Bolger F, Serra PA, O'Neill RD, Fillenz M, Lowry JP (2006) Real-time monitoring of brain extracellular lactate. In: Di Chiara G, Carboni E, Valentini V, Acquas E, Bassareo V, Cadoni C (eds) Monitoring Molecules in Neuroscience. University of Cagliari Press, Cagliara, Italy, pp 286–288
40. Clouter M, Wellstead P (2010) The control systems structures of energy metabolism. J R Soc Interface 7(45):651–665
41. Hess B (1979) The glycolytic oscillator. J Exp Biol 81:7–14
42. Attwell D, Laughlin SB (2001) An energy budget for signalling in the grey matter of the brain. J Cereb Blood Flow Metab 21:1133–1145
43. Hu Y, Wilson GS (1997) A temporal local energy pool coupled to neuronal activity: fluctuations of extracellular lactate levels in rat brain monitored with rapid-response enzyme-based sensor. J Neurochem 69:1484–1490
44. McMahon CP, Rocchitta G, Serra PA, Kirwan SM, Lowry JP, O'Neill RD (2006) Control of the oxygen dependence of an implantable polymer/enzyme composite biosensor for glutamate. Anal Chem 78:2352–2359
45. Seborg DE, Edgar TF, Mellichamp DA (1989) Process dynamics and control (Chapter 18). Wiley, New York
46. Tyson JJ, Chen KC, Novak B (2003) Sniffers, buzzers, toggles and blinkers: dynamics of regulatory and signaling pathways in the cell. Curr Opin Cell Biol 15:221–231
47. Brown AM, Ransom BR (2007) Astrocyte glycogen and brain energy metabolism. Glia 55(12):1263–1271

Chapter 3
Systems Biology of Aging: Opportunities for Parkinson's Disease

Andres Kriete

Abstract Parkinson's disease (PD), like many other dementias, is a disease of old age with neurological-pathological signs and underlying molecular mechanisms that precede cell death. Deciphering PD specifically from an aging perspective has many advantages. PD shares multiple mechanisms with aging, albeit in an accelerated fashion, including accumulation of damage and dysfunction, stress responses, and deficiencies in the maintenance of protein quality. Here, we review the foundations of a new hybrid, phenotypical model, which combines organelle phenotypes with molecular mechanisms associated with the long-term progression of normal aging. Subsequently, we adapt this model to PD and demonstrate the acceleration of dysfunction. On the level of molecular mechanisms, we specifically discuss two pathways that play a key role in the progression of both aging and PD: NF-κB and mTOR. The introduction of comprehensive modeling approaches is expected to make a significant contribution in deciphering the relationship between the different processes and risks factors. In particular, the tight relationship of aging and PD as discussed here sheds new light on future strategies for interventions.

Introduction

Systems biology has become a broad and sustained endeavor to decipher biological complexities in several areas. Most common is the reverse engineering of gene regulatory, signaling, or metabolic processes. A variety of computational tools have been devised to analyze and simulate the dynamic behavior of pathways, and models have evolved from more conceptual to highly detailed representation,

A. Kriete (✉)
School of Biomedical Engineering, Science and Health Systems, Drexel University, 3141 Chestnut Street, Philadelphia, PA 19104, USA
e-mail: ak3652@drexel.edu

P. Wellstead and M. Cloutier (eds.), *Systems Biology of Parkinson's Disease*,
DOI 10.1007/978-1-4614-3411-5_3,

a prime example being the EGF-MAPK pathway [55, 74]. Another area of activity is the compilation of networks based on known protein–protein interactions, allowing us to decipher network topologies, function, and robustness [3]. A third area of interest is the evaluation of basic principles of biological organization, such as scaling laws, feedbacks, and the theory of open systems. Whatever the main thrust chosen, systems approaches offer valuable insights into the progression of aging and those diseases, such as PD, for which aging is a major risk factor.

In contrast to many other fields, computational modeling has not been widely applied to the biology of aging. Increasing interest due to an aging population and dedicated funding initiatives may bolster activities in the systems biology of aging. But researchers also face hurdles that are rooted in the variability and complexity of aging, and which limit demonstration of straightforward solutions. Chance, damage, regulation, genetics, lifestyle, and environment all contribute to the aging process. For the prediction of life span of an individual, or better for our inability to make such prediction, chance is the dominant factor. As a matter of fact, genetically identical cohorts of model organisms, grown under identical conditions, show a wide spectrum of life spans [47]. Currently, neither the main source nor the mechanism contributing to such apparently stochastic variations is well understood. In addition to chance, there is an overall increase in heterogeneity, exemplified by the finding that gene expression between single cells becomes heterogeneous with age [7]. Accordingly, the histological appearance of cells and tissues also becomes more diverse, and, in addition, cells enter age-related cell states such as replicative senescence or they undergo apoptosis. Increases in variation in cell states may continue to show at a physiological level, disturbing the function and interplay of organ systems, while on average almost all physiological parameters show a linear decline with age. Conceivably, these stochastic mechanisms have been only partially considered as a contributing factor to the development of age-related diseases and will need future attention.

Genetic makeup is yet another factor that influences the process of aging. Popularity for the view that genes determine the progression of aging stems from knockout and RNAi screens demonstrating that single genes can increase life span in worms [42]. Genetic variations may modulate life span through modulation of pathways [105], and population studies targeting centenarians have identified specific roles for genetic variations [6, 10]. However, it has been shown in twin studies that the genetic contribution is not strong when compared to environmental and, yet to be identified, stochastic mechanisms. Whether genes have evolved to regulate life span, or are the main cause for differences in life span between species is a matter of debate, particularly when contrasted with allometric considerations relating life span to body mass and metabolism [97]. A related question concerns the genetic coordination of life span to control population sizes competing over limited resources. However, the onset of aging occurs after offspring are produced, and this “evolutionary shadow” would reduce feedback on an evolutionary scale. By the same mechanism, age-related traits that may be beneficial at young age, but detrimental at old age, are not directly under evolutionary pressure and can potentially accumulate. Although only a minority (5–10%) of PD cases have

a clearly identified genetic component, multiple genes have been identified that contribute to the development of the disease, disturbing the fine-tuned homeostasis of multiple and interrelated cellular function, including mitochondrial, proteosomal, and autophagosomal systems [20, 44].

Experimentally more tractable is the investigation of progressive damage accumulation in aging cells, dysfunction, and alterations in pathways. The increase in damage, along with the theory of a vicious cycle, has been discussed elsewhere in this volume [9]. A related question is if, and to what extent, cells respond to the diverse spectrum of damage adaptively or even protectively. This topic is discussed in more detail later in this chapter.

In summary, aging is truly a systems process, and only a sufficiently comprehensive approach is likely to decipher the underlying complexities and dynamic interactions in a way that allows useful predictions. Furthermore, the task of modeling goes beyond the integration of multiple pathways and would also include damage, dysfunction of organelles, regulatory mechanisms, and genetics. Simultaneous measurement of all relevant parameters with sufficient precision will also be a major concern. A whole cell modeling approach would allow integrating interacting biological entities on a broader scale (genes, transcription factors, proteins, pathways, organelle activities, etc.). Multiscale computation and hybrid models seem to offer a productive platform for computational systems biology. Early examples include the combined models of mitochondrial, reactive oxygen species (ROS) production, aberrant proteins, free radicals, and scavengers (MARS model) by Kowald and Kirkwood [59] and the Adaptive Response model by Kriete et al. [60]. We have to realize that we may be able to identify "public" mechanisms prevailing in most cells, but that there are cell and tissue-specific "private" mechanisms. Here, we show that our Adaptive Response model describing "public" mechanisms can be modified to reflect specific "private" mechanisms, consistent with observations of PD. The model is limited to a demonstration of long-term changes in some key aging pathways, however it does not specifically describe alterations in functional properties in neurons and astrocytes as they occur in PD. Chapters 7 and 8 cover this subject in more detail by presenting deterministic models of biochemical regulation in neuronal metabolic processes. This complements the rule-based model of aging adopted here. Also, as demonstrated elsewhere in this volume (see Chaps. 4 and 5), neuronal-physiological models can be developed; thus, both approaches are complementary and reflect different properties and functional levels of disease manifestation.

Hybrid Rule-Based Models of Aging

Computational modeling of the aging process requires the integration of organelle phenotypes such as mitochondrial respiration or autophagy, and molecular regulatory mechanisms such as stress response, along with proteomics and genomics data. The interplay of these factors determines cell physiological alterations on

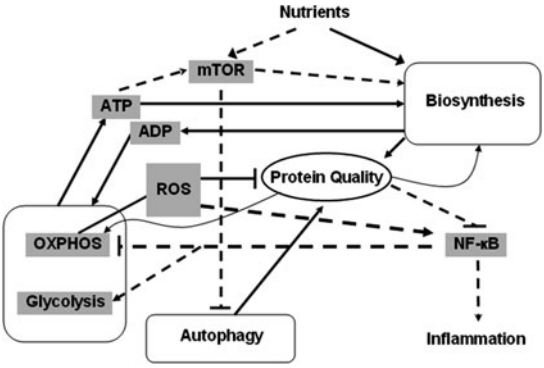

Fig. 3.1 Concept of a cellular network contributing to protein quality. The interplay of organelle activities, metabolic fluxes between compartments (*solid lines*), responses and regulations (*dashed lines*) mediated by NF-κB and mTOR contribute to maintenance of overall cellular energetics, survival and protein quality of the cell. Disturbances in ATP production, caused by dysfunctional mitochondria, alter the operation of the cell from anabolism to catabolism through the involvement of mTOR, while high reactive oxygen species (ROS) levels and oxidized proteins activate the prosurvival NF-κB pathway contributing to a metabolic remodeling from an oxidative phosphorylation (OXPHOS) towards a less energetically efficient glycolysis (cf. Chap. 7). Inhibited activity of mTOR enhances autophagy and the removal of damaged mitochondria and proteins. The interaction between organelles, metabolite turnover, stress responses, regulations and protein renewal rates demonstrates the need to develop hybrid computational models to simulate the aging process

which cell-based functional simulation can be based. Resulting models are hybrid, covering multiple levels of biological organization. Some of the known interactions as they relate to the biology of aging are shown in Fig. 3.1, demonstrating how protein quality is influenced by material and energy fluxes regulated by molecular stress sensors. Protein quality is a determining factor in aging [8, 27].

Fuzzy logic or rule-based modeling has proven particularly applicable where explicit mathematical models cannot be easily derived due to the complexity of the problem [13]. By granulating the parameter space, fuzzy logic modeling provides a way to incorporate data that might otherwise be excluded because of incompleteness or lack of precision. As an example, a continuous variable can be divided into “low,” “middle,” and “high” states. Fuzzy logic models are more robust with respect to noise and variation due to the initial fuzzyfication of parameters [92], but still allow reproducible and precise computation of logical relationships to predict complex system dynamics. We use a rule-based approach in a software environment called Bionet [13], developed specifically for biological networks. Input information for a Bionet model consists of a list of state variables, also called nodes, along with initial values. Each reaction between variables is a fuzzy rule-based inference. A reaction rate is a function of one or more variables and a reaction rate constant. The rate constant scales the reaction rate that is

determined as an output from the fuzzy inference. Rule-based pathway models can be developed to test the logic of interactions even if little is known about rate constants. A strength of this approach is that one can represent entities other than biochemical reactions, such as measured parameters, transcription, regulation, etc., as long as the relationship can be defined.

The Vicious Cycle Model vs. Linear Decline

The Vicious Cycle theory of aging suggests a damage amplification process, by which ROS as a byproduct of metabolism damage, mitochondrial proteins and mtDNA. In return, this leads to an even stronger release of ROS, as outlined in Bandy and Davison [9]. The theory centers on dysfunctional mitochondria [28], and relates expansion of mutations by positive feedback loops to the decline in ATP levels with age mentioned in Chap. 2 [19, 91]. It has not been confirmed that mtDNA mutations spread exponentially within a given cell by clonal expansion; rather, a prevalence of single or a few mtDNA point mutations has been observed [56, 65]. Notably, other types of positive feedbacks have also been suggested. Lower protein output in aged cells may decrease protein turnover, so that the portion of damaged proteins accumulates more quickly, a process which may be further enhanced by less efficient ubiquitination and degradation [40, 95]. Activation of the nonphagocytic NADPH-oxidase system [21, 34] may also contribute to higher levels of free radicals in older cells and exacerbate oxidative damage. As will be discussed in Chap. 7, one of these vicious cycles between ROS and misfolded protein may also operate on a much faster timescale (i.e., a few days) and would exacerbate symptoms of slowly progressing age. This is compatible with the multitimescale nature of biological processes, but does not rule out possible interactions across radically different timescales. For example, important pathogenic mechanisms, such as ion transport deregulation, operate on the much faster timescales of seconds (see Chaps. 4 and 5).

Although conceptually sound, there are no data available to substantiate the idea that the overall development of the aging phenotypes resembles a "vicious cycle" behavior. Experimentally induced oxidative stress in mitochondria increases ROS levels, but not necessarily in an exponential fashion [85]. Mitochondrial function indeed declines with age [73, 89], but the decline was shown to occur in a linear fashion. Related to the decline of mitochondrial function is a linear decline of ATP concentrations, as shown in *Caenorhabditis elegans* [39] and a cross-sectional study of human fibroblasts [38]. If aging were driven by an exponential increase in accumulation of damage and dysfunction, then there should be a noticeable exponential decline on higher levels of biological organization. Again, there is no evidence for an exponential decline on an organ level, as first shown by Nathan Shock [14, 90] and later substantiated in a comprehensive review of loss rates of 445 physiological parameters [87]. These observations share a decline averaging

0.65% per year starting once adulthood is reached. It would be difficult to explain how such an early onset and linear decline would be compatible with an exponential decline on the cellular level. In an attempt to provide an explanation, we suggest that the aging process activates negative feedback loops, working against the positive feedbacks, which in unison give rise to the observed linearity in decline. At the same time, the activation of such feedbacks helps to maintain homeostasis of critical cellular parameters, protein quality and extends life span (see Chap. 2 for a specific example of such a feedback mechanism for ATP regulation).

NF-κB, Feedback, and Inflammation

In the following section, we introduce the concept of an important stress response mechanism: Nuclear Factor kappa-B (NF-κB). NF-κB becomes constitutively active during aging and takes a role as a master regulator on the stress–metabolic–inflammatory axis. NF-κB is activated in response to infectious agents, environmental factors, and cellular stresses, including DNA damage. Activation of NF-κB by proinflammatory cytokines such as TNF and IL-families is termed the canonical pathway, whereas activation of a specific IKK signalosome complex, active in B cells, is a second and alternative pathway. The third group of mechanisms is collectively termed "atypical pathways" and comprises chemical and physiological stress factors [77] as well as oxidative [64], genotoxic [49], and organelle stress, including the endoplasmic overload response [78] and mechanisms related to aging [61]. The main role of NF-κB is in cell protection and prevention of apoptosis. Thus, NF-κB not is only a central mediator of immune responses but also has a more general role as a regulator of stress responses, and thereby a potential role in aging.

NF-κB activity has been shown to be upregulated with age in many tissues, including nuclear fractions in mouse and rat tissues [46]. Similar observations were reported for mouse cardiac muscle [45], rat brain [58], lymphoid organs [93], and gastric mucosa [99]. NF-κB has also been identified as a contributing factor to cellular atrophy such as sarcopenia [17]. Expression of NF-κB with age is consistent with elevated levels of inflammatory markers and a proinflammatory phenotype. Cytokines and chemokine profiles, likely activated by NF-κB, have been observed in gene expression studies of both human and animal tissues including brain [67], lung [5], liver [54], cartilage [53], and coronary arteries [25]. In fact, a review of gene expressions of nine tissue types in mice and humans revealed that the occurrence of the NF-κB motif was most ubiquitous and strongly associated with age [2]. Mediating factors of NF-κB and inflammation include the insulin/IGF pathway, SIRT1 and FOXO, PDC-1 and PPARγ, which are extensively reviewed elsewhere [84]. In support of cell-autonomous causes for age-associated inflammation, expression of inflammatory markers such as cytokine has been observed in cells subjected to replicative senescence in vitro caused by serial passaging [62, 71, 88, 103],

and the senescence-associated secretory phenotype (SASP) has been recently characterized [24].

The role played by a range of different mechanisms has been described in the atypical activation of NF-κB and is reviewed elsewhere [61]. A major stress event in the ER, unfolded protein response (UPR), develops when unfolded and misfolded proteins accumulate in the ER membrane. Such misregulation of protein posttranslational modifications and degradation processes contribute to ER stress. ER stress can be linked to many diseases [104], including type-2 diabetes [76]. As described in Chap. 7, in PD, α-synuclein misfolding and aggregation are specific examples for a loss of protein quality. Since type-2 diabetes, as well as atherosclerosis and neurodegenerative diseases, is age-related, ER-stress and related NF-κB activation and inflammation might also be aging-induced factors for these pathological conditions [33].

A mitochondria-to-nucleus cross talk in yeast, termed retrograde signaling, has been described as a compensatory mechanism to the functional decline of mitochondria [57] by readjusting metabolic activities to extend life span [50]. Retrograde signaling comprises pathways that communicate changes in mitochondrial function to the nucleus [16, 66]. Mitochondria are central in both metabolism and production of oxidized proteins. Mitochondrial stress, defined by altered mitochondrial membrane potential and loss of Complex I efficiency, increased the production of ROS. Moreover, oxidative damage is known to increase with age [52, 72].

While most of the work on retrograde signaling and longevity has been done in yeast [51], altered nuclear expression in response to mitochondrial dysfunction in mammalian cells has also been described. Mitochondrial dysfunction in response to stress in mammalian cells including mtDNA lesions has been found to elevate cytosolic Ca^{2+} and to activate calcineurin, partly due to the inability of stressed mitochondria to participate in Ca^{2+} uptake [11], which can activate the inhibitory protein IκBβ [12]. Calcium levels have been previously reported to decline in aged fibroblasts in vitro [80], but in aging neurons the reduced dynamic of Ca^{2+} fluxes, perturbing functional processes, is likely more important than Ca^{2+} levels [18, 41] (see Chaps. 4 and 5 for further details on Ca^{2+} dynamics and the role of Calcium generally).

It is noteworthy that other compensatory mechanisms have been suggested that may contribute to a negative feedback: inhibition of the mitochondrial electron transport chain (ETC) (as a function of superoxide production) has been suggested by Gardner et al. [35, 36] for example. Recently, this concept has been revisited to explain the absence of life-span reduction in superoxide dismutase (SOD) scavenger knockouts in *C. elegans* [39]. Similarly, aged cells have been found to upregulate uncoupling proteins to mitigate oxidative stress [82]. Furthermore, sestrins, which are conserved proteins activated in cells exposed to stress, have been shown to potentiate adenosine monophosphate-activated protein kinase (AMPK), and inhibit activation of target protein mTOR, while loss of sestrins results in age-related pathologies [63].

Rule-Based Adaptive Response Model

Realizing the importance of negative feedbacks, the VC model was extended, with the adaptive-response (AR) model, to include the stress–response element NF-κB that alters transcription of genes responsible for mitochondrial function, antioxidants and biosynthesis. Initial conditions in the AR model and many basal rates, such as oxidative damage, have been adopted from a previous VC model in order to directly compare the performance of both models. These are identical to the initial conditions used in the VC model. The model also uses the same basic rules for generation of ROS, buildup of oxidative damage, and inhibition of mitochondrial respiration and biosynthesis. The final implementation of the AR model consists of 24 nodes, 47 processes and activators, including 1 for NF-κB activation, 3 negative feedback loops reducing metabolic respiration, biosynthesis and improving ROS scavenging (see Fig. 3.2), a further positive feedback accelerating the relative portion of oxidized proteins through reduced turnover rates of newly formed proteins, a compensatory mechanism stimulating glycolysis, and a secondary autocrine loop activating the NADPH oxidase system.

The first feedback loop mediates regulation of mitochondrial respiration with age. Decrease in functional performance [23, 38] and downregulated gene transcripts of mitochondrial genes coded in nuclear DNA have been reported [67, 81, 96, 101, 102], including lower levels of NADH dehydrogenases, alterations

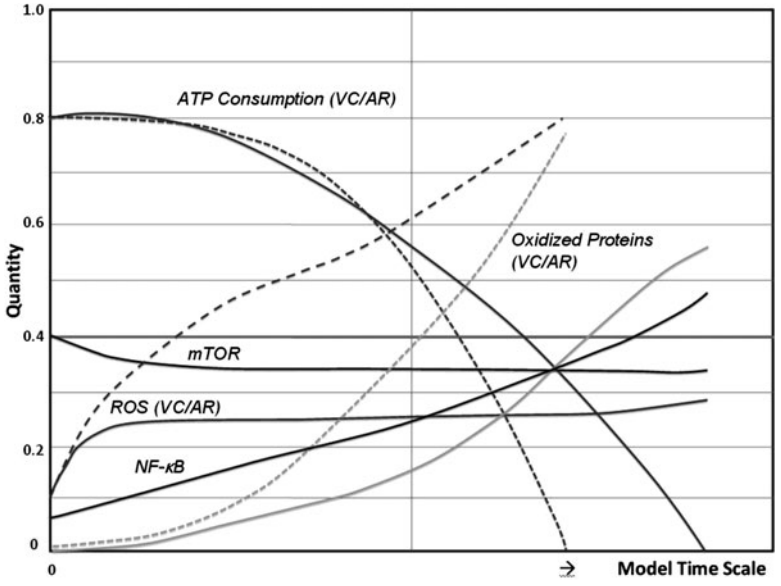

Fig. 3.2 Outcome of simulations of the Vicious Cycle (VC, *dashed lines*) and Adaptive Response (AR, *solid lines*) models, compiled from Kriete et al. [60]. With mTOR, which drops after an initial growth phase of the organism, and the role of NF-κB, ROS levels and oxidized proteins increase only moderately in the AR model as compared to the VC model and extend life span through the maintenance of protein quality

in the TCA cycle and ETC reducing respiration, mitochondrial membrane potential, and ATP production. This is initially counterintuitive, since we may expect an increase in biogenesis in response to dysfunction of damaged mitochondria. However, it fits the notion that an active downregulation, rather than damage only, contributes to the observed progressive decline in mitochondrial energetics. As a compensatory mechanism we incorporated an increase in anaerobic glycolysis into our model. Although NF-κB is not known to have direct target genes related to metabolism, it is known to interact with other transcription factors that have such metabolically related target genes, including c-MYC [32], which is consistent with the observation that glycolysis is increased with age [26, 68].

The second feedback loop concerns the scavenging of free radicals, such as dismutases. For instance, MnSOD has been shown to be increased with age and is NF-κB dependent [100]. Finally, the third feedback loop reduces protein biosynthesis and turnover in the endoplasmic reticulum [67, 69, 101], supported by gene expression studies indicating lower levels of ribosomal transcripts in many, but not all, tissues [101]. In contrast to the VC model, this is an active, regulated mechanism, which operates to mitigate an ongoing damage impairing function.

While, the Vicious Cycle (VC) model causes exponentially increasing cellular stress, inclusion of an adaptive feedback-loop reveals an overall linear behavior as shown in Fig. 3.2. This result adds supports to the idea of a more linear decline of metabolic functions, observed experimentally [38]. Downregulation of oxidative phosphorylation contains ROS, consistent with a retrograde response as a negative feedback loop mechanism. These preliminary results show the feasibility of a rule-based framework for the suggested study. The behavior of the model shows a linearization of decline in mitochondrial function.

Parkinson's Disease: Return of the Vicious Cycle

The AR model was conceived to place decline in metabolism and mitochondrial dysfunction at center stage. Coincidently, alterations in brain energy metabolism and mitochondrial deficiencies are also emerging as central mechanisms in PD (see Chap. 2; [1, 22]), and polymorphisms in some of the experimental models using mitochondrial toxins take this into account [86]. Furthermore, mTOR and NF-κB, key regulators in our model, have emerged as key regulators in PD as well. Thus, the AR model provides a platform to modify specific mechanisms relevant for PD. We identified three specific areas that needed to be adapted to better fit with experimental data in PD:

1. *Decline in mTOR levels*. Experimental observations report lower than normal mTOR levels in PD that have a profound influence on the overall integrity of the cell including nucleolar disruption [83]. A stress regulated protein, RTP801, has been identified to inhibit mTOR in PD, and in experimental models the compound 6-OHDA [79] has been shown to suppress mTOR via RTP801 [70]. Other pathways may be involved such as PTEN, which activates mTOR when ablated [30]. Since mTOR regulates biosynthesis, chronic low levels have a

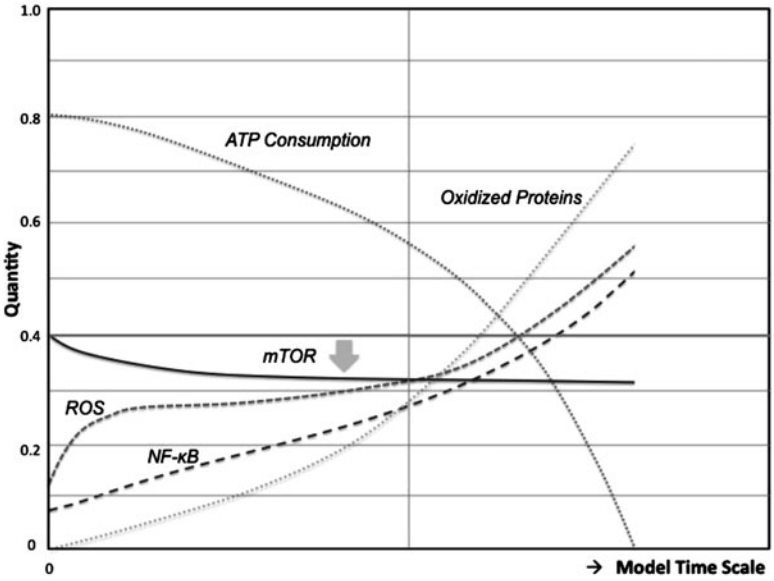

Fig. 3.3 Output of the rule-based model modified for PD. Despite low mTOR activity, ROS and oxidized protein concentration increase rapidly. The simulation predicts high NF-κB activity in the later phase of PD. ATP consumption, an indicator of biogenesis, drops rapidly indicating that the cell enters a vicious cycle of loss in protein quality and energetics, thus limiting cellular life span. Low mTOR levels have been associated with apoptosis in the acute phase of PD

profound impact on the structural and functional integrity of neurons, especially as these do not regenerate.

2. *Interaction between mTOR and NF-κB*. In experimental studies, a direct relationship between inflammation, NF-κB and elevated mTOR levels has been shown. It is known, for example, that when apoptotic rates of neurons are high, NF-κB is hyperactive and it may activate mTOR. However, there is no specific indication of increasing mTOR levels in PD.
3. *Role of autophagy*. While low mTOR activity in PD is an indicator of mitochondrial dysfunction and elevated AMPK levels upstream, it does not appear to have a protective role as they are known from pharmacological interventions of this pathway. Despite low mTOR damage and dysfunction in PD, the clearing activity involving autophagy and lysosomes does not seem to be sufficient. This may have two reasons, either the low mTOR levels do not activate autophagy and lysosomal processes as these levels may suggest, or these clearing mechanisms are unable to take care of the amount, or type, of damage in the mitochondria and specifically formed proteins which continue to accumulate. In this context, the α-synuclein theory of protein aggregation in PD accompanied by parkin-driven proteasome deregulation should be mentioned [1].

The simulation of the refined PD model (Fig. 3.3) predicts a slow decline of mTOR that is not accompanied by an improvement of autophagy so that protein and

mitochondrial dysfunction continue to accumulate. This emphasizes the contribution of mitochondrial and proteasomal/autophagosomal dysfunctions in PD. Rapamycin, caloric restriction, and Sirtuins, all known to suppress the mTOR pathway, can extend life span in model organisms such as yeast [4], *C. elegans* [75], and mice [43], by improving maintenance of protein quality. Similarly long-term inhibition of mTOR has been recognized as a strategy to delay the onset of PD or other dementias. However, in the acute phase of PD, mTOR activity has been observed at very low levels despite rapidly progressing protein damage, indicating that at this stage the regulatory link between mTOR and autophagy is broken. In this situation, the reduced activity of mTOR has been discussed as a risk factor in promoting apoptosis [48]. Therefore, one therapeutic strategy is the administration of growth factors through the Akt pathway, suppressing TSC2 and activating mTOR downstream [15, 31]. Akt activation may also be involved in some of the beneficial effect of nicotine observed in PD [98].

In the final phase of our simulation, PD is characterized by an increasing heterogeneity in the cell population with cells in apoptosis and an increasing imbalance of pro- and anti-inflammatory proteins involving NF-κB (such as iNOS, TNF-α, and IL-1β) which have been shown to play an role in the loss of dopaminergic neurons in MPTP-intoxicated mice and PD patients [29, 94]. Secretion of inflammatory proteins activates NF-κB in other cell, spreading the stress signal. Therefore, the specific inhibition of molecules in the NF-κB pathway has been suggested as another target in PD [37].

Summary

In summary, we show how a phenotypical, hybrid computational approach, developed to investigate mechanisms involved in aging, can be modified to predict aspects in the progression of PD. Both biological phenomena share the importance of maintaining protein quality, which is well balanced in normal aging, but greatly disturbed in PD. Studying complex phenomena by an integrated computational modeling should broaden our understanding of the nature of underlying mechanisms and their dynamic interactions. Such computational approaches are complementary to well-focused experimental investigations. Specifically, computational systems approaches try to integrate the diversity of analyses into a consistent framework. Rule-based approaches, as suggested here, make it possible to connect different levels of biological organization and pieces of knowledge, allowing reliable and reproducible predictions of long-term developments.

Our preliminary results show the feasibility of using a rule-based framework for the suggested studies. Furthermore, the model can be connected to other modeling initiatives describing subprocesses on the one end and functional cell physiological and multicellular interactions on the other end, to cover properties of PD on different timescales. In normal aging, the behavior of the model shows a linearization of the decline in mitochondrial function. Damage in proteins also accumulates

at a linear rate. As soon as the system detects changes in protein quality and organelle dysfunction, it adapts by evolved mechanisms to improve protein clearance and remodeling of metabolism. Thus, the system proceeds in a lock-step fashion, but is still balanced and keeps ROS at low levels. This optimal path of "healthy" aging can be challenged by tissue specific and genetic risks, combined with environmental and lifestyle related risk factors that are often a feature of age-related diseases. In PD, the progression of mitochondrial dysfunction is severe; protein oxidation, misfolding, and aggregation progresses rapidly, and regulatory mechanisms are either overwhelmed or dysfunctional in their attempt to prevent an accelerated decline. As our knowledge about the interaction of these factors deepens, the model can be extended in detail to pinpoint the role of risk factors that in return may suggest new interventions to prevent the disease or delay its progression. Since the aging process is so deeply rooted in PD, a substantial reversal of symptoms or even cure may only be achieved by progress in regenerative medicine.

References

1. Abou-Sleiman PM, Muqit MM, Wood NW (2006) Expanding insights of mitochondrial dysfunction in Parkinson's disease. Nat Rev Neurosci 7:207–219
2. Adler AS, Sinha S, Kawahara TL, Zhang JY, Segal E, Chang HY (2007) Motif module map reveals enforcement of aging by continual NF-kappaB activity. Genes Dev 21:3244–3257
3. Albert R, Jeong H, Barabasi AL (2000) Error and attack tolerance of complex networks. Nature 406:378–382
4. Alvers AL, Fishwick LK, Wood MS, Hu D, Chung HS, Dunn WA Jr, Aris JP (2009) Autophagy and amino acid homeostasis are required for chronological longevity in *Saccharomyces cerevisiae*. Aging Cell 8:353–369
5. Aoshiba K, Nagai A (2007) Chronic lung inflammation in aging mice. FEBS Lett 581:3512–3516
6. Atzmon G, Rincon M, Rabizadeh P, Barzilai N (2005) Biological evidence for inheritance of exceptional longevity. Mech Ageing Dev 126:341–345
7. Bahar R, Hartmann CH, Rodriguez KA, Denny AD, Busuttil RA, Dolle ME, Calder RB, Chisholm GB, Pollock BH, Klein CA, Vijg J (2006) Increased cell-to-cell variation in gene expression in ageing mouse heart. Nature 441:1011–1014
8. Baker BM, Haynes CM (2011) Mitochondrial protein quality control during biogenesis and aging. Trends Biochem Sci 36:254–261
9. Bandy B, Davison AJ (1990) Mitochondrial mutations may increase oxidative stress: implications for carcinogenesis and aging? Free Radic Biol Med 8:523–539
10. Bergman A, Atzmon G, Ye K, MacCarthy T, Barzilai N (2007) Buffering mechanisms in aging: a systems approach toward uncovering the genetic component of aging. PLoS Comput Biol 3:e170
11. Biswas G, Adebanjo OA, Freedman BD, Anandatheerthavarada HK, Vijayasarathy C, Zaidi M, Kotlikoff M, Avadhani NG (1999) Retrograde Ca^{2+} signaling in C2C12 skeletal myocytes in response to mitochondrial genetic and metabolic stress: a novel mode of inter-organelle crosstalk. EMBO J 18:522–533
12. Biswas G, Tang W, Sondheimer N, Guha M, Bansal S, Avadhani NG (2008) A distinctive physiological role for IkappaBbeta in the propagation of mitochondrial respiratory stress signaling. J Biol Chem 283:12586–12594

13. Bosl WJ (2007) Systems biology by the rules: hybrid intelligent systems for pathway modeling and discovery. BMC Syst Biol 1:13
14. Brandfonbrener M, Landowne M, Shock NW (1955) Changes in cardiac output with age. Circulation 12:557–566
15. Burke RE (2007) Inhibition of mitogen-activated protein kinase and stimulation of Akt kinase signaling pathways: two approaches with therapeutic potential in the treatment of neurodegenerative disease. Pharmacol Ther 114:261–277
16. Butow RA, Avadhani NG (2004) Mitochondrial signaling: the retrograde response. Mol Cell 14:1–15
17. Cai D, Frantz JD, Tawa NE Jr, Melendez PA, Oh BC, Lidov HG, Hasselgren PO, Frontera WR, Lee J, Glass DJ, Shoelson SE (2004) IKKbeta/NF-kappaB activation causes severe muscle wasting in mice. Cell 119:285–298
18. Chen M, Nguyen HT, Sawmiller DR (2011) What to look for beyond "pathogenic" factors in senile dementia? A functional deficiency of Ca^{2+} signaling. J Alzheimers Dis 27(4):679–689
19. Chinnery PF, Samuels DC (1999) Relaxed replication of mtDNA: a model with implications for the expression of disease. Am J Hum Genet 64:1158–1165
20. Clark J, Reddy S, Zheng K, Betensky RA, Simon DK (2011) Association of PGC-1alpha polymorphisms with age of onset and risk of Parkinson's disease. BMC Med Genet 12:69
21. Clark RA, Valente AJ (2004) Nuclear factor kappa B activation by NADPH oxidases. Mech Ageing Dev 125:799–810
22. Cloutier M, Bolger FB, Lowry JP, Wellstead P (2009) An integrative dynamic model of brain energy metabolism using in vivo neurochemical measurements. J Comput Neurosci 27:391–414
23. Conley KE, Amara CE, Jubrias SA, Marcinek DJ (2007) Mitochondrial function, fibre types and ageing: new insights from human muscle in vivo. Exp Physiol 92:333–339
24. Coppe JP, Patil CK, Rodier F, Sun Y, Munoz DP, Goldstein J, Nelson PS, Desprez PY, Campisi J (2008) Senescence-associated secretory phenotypes reveal cell-nonautonomous functions of oncogenic RAS and the p53 tumor suppressor. PLoS Biol 6:e301
25. Csiszar A, Ungvari Z, Koller A, Edwards JG, Kaley G (2003) Aging-induced proinflammatory shift in cytokine expression profile in coronary arteries. FASEB J 17:1183–1185
26. D'Aurelio M, Merlo Pich M, Catani L, Sgarbi GL, Bovina C, Formiggini G, Parenti Castelli G, Baum H, Tura S, Lenaz G (2001) Decreased Pasteur effect in platelets of aged individuals. Mech Ageing Dev 122:823–833
27. David DC, Ollikainen N, Trinidad JC, Cary MP, Burlingame AL, Kenyon C (2011) Widespread protein aggregation as an inherent part of aging in *C. elegans*. PLoS Biol 8:e1000450
28. de Grey AD (1997) A proposed refinement of the mitochondrial free radical theory of aging. Bioessays 19:161–166
29. Dehmer T, Lindenau J, Haid S, Dichgans J, Schulz JB (2000) Deficiency of inducible nitric oxide synthase protects against MPTP toxicity in vivo. J Neurochem 74:2213–2216
30. Domanskyi A, Geissler C, Vinnikov IA, Alter H, Schober A, Vogt MA, Gass P, Parlato R, Schutz G (2011) Pten ablation in adult dopaminergic neurons is neuroprotective in Parkinson's disease models. FASEB J 25:2898–2910
31. Du Y, Li X, Yang D, Zhang X, Chen S, Huang K, Le W (2008) Multiple molecular pathways are involved in the neuroprotection of GDNF against proteasome inhibitor induced dopamine neuron degeneration in vivo. Exp Biol Med (Maywood) 233:881–890
32. Duyao MP, Kessler DJ, Spicer DB, Sonenshein GE (1990) Binding of NF-KB-like factors to regulatory sequences of the c-myc gene. Curr Top Microbiol Immunol 166:211–220
33. Finch CE (2006) A perspective on sporadic inclusion-body myositis: the role of aging and inflammatory processes. Neurology 66:S1–S6
34. Finkel T, Holbrook NJ (2000) Oxidants, oxidative stress and the biology of ageing. Nature 408:239–247

35. Gardner R, Moradas-Ferreira P, Salvador A (2006) Why does superoxide dismutase overexpression often increase hydrogen peroxide concentrations? An alternative explanation. J Theor Biol 242:798–800
36. Gardner R, Salvador A, Moradas-Ferreira P (2002) Why does SOD overexpression sometimes enhance, sometimes decrease, hydrogen peroxide production? A minimalist explanation. Free Radic Biol Med 32:1351–1357
37. Ghosh A, Roy A, Liu X, Kordower JH, Mufson EJ, Hartley DM, Ghosh S, Mosley RL, Gendelman HE, Pahan K (2007) Selective inhibition of NF-kappaB activation prevents dopaminergic neuronal loss in a mouse model of Parkinson's disease. Proc Natl Acad Sci U S A 104:18754–18759
38. Greco M, Villani G, Mazzucchelli F, Bresolin N, Papa S, Attardi G (2003) Marked aging-related decline in efficiency of oxidative phosphorylation in human skin fibroblasts. FASEB J 17:1706–1708
39. Gruber J, Ng LF, Fong S, Wong YT, Koh SA, Chen CB, Shui G, Cheong WF, Schaffer S, Wenk MR, Halliwell B (2011) Mitochondrial changes in ageing *Caenorhabditis elegans*—what do we learn from superoxide dismutase knockouts? PLoS One 6:e19444
40. Grune T, Jung T, Merker K, Davies KJ (2004) Decreased proteolysis caused by protein aggregates, inclusion bodies, plaques, lipofuscin, ceroid, and 'aggresomes' during oxidative stress, aging, and disease. Int J Biochem Cell Biol 36:2519–2530
41. Guzman JN, Sanchez-Padilla J, Wokosin D, Kondapalli J, Ilijic E, Schumacker PT, Surmeier DJ (2011) Oxidant stress evoked by pacemaking in dopaminergic neurons is attenuated by DJ-1. Nature 468:696–700
42. Hansen M, Hsu AL, Dillin A, Kenyon C (2005) New genes tied to endocrine, metabolic, and dietary regulation of lifespan from a *Caenorhabditis elegans* genomic RNAi screen. PLoS Genet 1:119–128
43. Harrison DE, Strong R, Sharp ZD, Nelson JF, Astle CM, Flurkey K, Nadon NL, Wilkinson JE, Frenkel K, Carter CS, Pahor M, Javors MA, Fernandez E, Miller RA (2009) Rapamycin fed late in life extends lifespan in genetically heterogeneous mice. Nature 460:392–395
44. Hatano T, Kubo S, Sato S, Hattori N (2009) Pathogenesis of familial Parkinson's disease: new insights based on monogenic forms of Parkinson's disease. J Neurochem 111:1075–1093
45. Helenius M, Hanninen M, Lehtinen SK, Salminen A (1996) Aging-induced up-regulation of nuclear binding activities of oxidative stress responsive NF-kB transcription factor in mouse cardiac muscle. J Mol Cell Cardiol 28:487–498
46. Helenius M, Hanninen M, Lehtinen SK, Salminen A (1996) Changes associated with aging and replicative senescence in the regulation of transcription factor nuclear factor-kappa B. Biochem J 318(pt 2):603–608
47. Herndon LA, Schmeissner PJ, Dudaronek JM, Brown PA, Listner KM, Sakano Y, Paupard MC, Hall DH, Driscoll M (2002) Stochastic and genetic factors influence tissue-specific decline in ageing *C. elegans*. Nature 419:808–814
48. Huang S, Shu L, Easton J, Harwood FC, Germain GS, Ichijo H, Houghton PJ (2004) Inhibition of mammalian target of rapamycin activates apoptosis signal-regulating kinase 1 signaling by suppressing protein phosphatase 5 activity. J Biol Chem 279:36490–36496
49. Janssens S, Tschopp J (2006) Signals from within: the DNA-damage-induced NF-kappaB response. Cell Death Differ 13:773–784
50. Jazwinski SM (2000) Metabolic control and ageing. Trends Genet 16:506–511
51. Jazwinski SM (2002) Growing old: metabolic control and yeast aging. Annu Rev Microbiol 56:769–792
52. Kakkar P, Singh BK (2007) Mitochondria: a hub of redox activities and cellular distress control. Mol Cell Biochem 305:235–253
53. Kato H, Matsumine A, Wakabayashi T, Hasegawa M, Sudo A, Shintani K, Fukuda A, Kato K, Ide N, Orita S, Hasegawa T, Matsumura C, Furukawa M, Tasaki T, Sonoda H, Uchida A (2007) Large-scale gene expression profiles, differentially represented in osteoarthritic synovium of the knee joint using cDNA microarray technology. Biomarkers 12:384–402

54. Kelder B, Boyce K, Kriete A, Clark R, Berryman DE, Nagatomi S, List EO, Braughler M, Kopchick JJ (2007) CIDE-A is expressed in liver of old mice and in type 2 diabetic mouse liver exhibiting steatosis. Comp Hepatol 6:4
55. Kholodenko BN (2000) Negative feedback and ultrasensitivity can bring about oscillations in the mitogen-activated protein kinase cascades. Eur J Biochem 267:1583–1588
56. Khrapko K, Bodyak N, Thilly WG, van Orsouw NJ, Zhang X, Coller HA, Perls TT, Upton M, Vijg J, Wei JY (1999) Cell-by-cell scanning of whole mitochondrial genomes in aged human heart reveals a significant fraction of myocytes with clonally expanded deletions. Nucleic Acids Res 27:2434–2441
57. Kirchman PA, Kim S, Lai CY, Jazwinski SM (1999) Interorganelle signaling is a determinant of longevity in *Saccharomyces cerevisiae*. Genetics 152:179–190
58. Korhonen P, Helenius M, Salminen A (1997) Age-related changes in the regulation of transcription factor NF-kappa B in rat brain. Neurosci Lett 225:61–64
59. Kowald A, Kirkwood TB (1996) A network theory of ageing: the interactions of defective mitochondria, aberrant proteins, free radicals and scavengers in the ageing process. Mutat Res 316:209–236
60. Kriete A, Bosl WJ, Booker G (2010) Rule-based cell systems model of aging using feedback loop motifs mediated by stress responses. PLoS Comput Biol 6:e1000820
61. Kriete A, Mayo K (2009) Atypical mechanisms of NF-kB activation and aging. Exp Gerontol 44(4):250–255
62. Krtolica A, Campisi J (2002) Cancer and aging: a model for the cancer promoting effects of the aging stroma. Int J Biochem Cell Biol 34:1401–1414
63. Lee JH, Budanov AV, Park EJ, Birse R, Kim TE, Perkins GA, Ocorr K, Ellisman MH, Bodmer R, Bier E, Karin M (2010) Sestrin as a feedback inhibitor of TOR that prevents age-related pathologies. Science 327:1223–1228
64. Li N, Karin M (1999) Is NF-kappaB the sensor of oxidative stress? FASEB J 13:1137–1143
65. Lin MT, Simon DK, Ahn CH, Kim LM, Beal MF (2002) High aggregate burden of somatic mtDNA point mutations in aging and Alzheimer's disease brain. Hum Mol Genet 11:133–145
66. Liu Z, Butow RA (2006) Mitochondrial retrograde signaling. Annu Rev Genet 40:159–185
67. Lu T, Pan Y, Kao SY, Li C, Kohane I, Chan J, Yankner BA (2004) Gene regulation and DNA damage in the ageing human brain. Nature 429:883–891
68. Luptak I, Yan J, Cui L, Jain M, Liao R, Tian R (2007) Long-term effects of increased glucose entry on mouse hearts during normal aging and ischemic stress. Circulation 116:901–909
69. Makrides SC (1983) Protein synthesis and degradation during aging and senescence. Biol Rev Camb Philos Soc 58:343–422
70. Malagelada C, Jin ZH, Greene LA (2008) RTP801 is induced in Parkinson's disease and mediates neuron death by inhibiting Akt phosphorylation/activation. J Neurosci 28:14363–14371
71. Mariotti M, Castiglioni S, Bernardini D, Maier JA (2006) Interleukin 1 alpha is a marker of endothelial cellular senescent. Immun Ageing 3:4
72. Melov S (2000) Mitochondrial oxidative stress. Physiologic consequences and potential for a role in aging. Ann N Y Acad Sci 908:219–225
73. Navarro A, Boveris A (2007) The mitochondrial energy transduction system and the aging process. Am J Physiol Cell Physiol 292:C670–C686
74. Oda K, Matsuoka Y, Funahashi A, Kitano H (2005) A comprehensive pathway map of epidermal growth factor receptor signaling. Mol Syst Biol 1:2005.0010
75. Onken B, Driscoll M (2010) Metformin induces a dietary restriction-like state and the oxidative stress response to extend *C. elegans* Healthspan via AMPK, LKB1, and SKN-1. PLoS One 5:e8758
76. Ozcan U, Cao Q, Yilmaz E, Lee AH, Iwakoshi NN, Ozdelen E, Tuncman G, Gorgun C, Glimcher LH, Hotamisligil GS (2004) Endoplasmic reticulum stress links obesity, insulin action, and type 2 diabetes. Science 306:457–461
77. Pahl HL (1999) Activators and target genes of Rel/NF-kappaB transcription factors. Oncogene 18:6853–6866

78. Pahl HL, Baeuerle PA (1995) A novel signal transduction pathway from the endoplasmic reticulum to the nucleus is mediated by transcription factor NF-kappa B. EMBO J 14:2580–2588
79. Perese DA, Ulman J, Viola J, Ewing SE, Bankiewicz KS (1989) A 6-hydroxydopamine-induced selective parkinsonian rat model. Brain Res 494:285–293
80. Peterson C, Goldman JE (1986) Alterations in calcium content and biochemical processes in cultured skin fibroblasts from aged and Alzheimer donors. Proc Natl Acad Sci U S A 83:2758–2762
81. Preston CC, Oberlin AS, Holmuhamedov EL, Gupta A, Sagar S, Syed RH, Siddiqui SA, Raghavakaimal S, Terzic A, Jahangir A (2008) Aging-induced alterations in gene transcripts and functional activity of mitochondrial oxidative phosphorylation complexes in the heart. Mech Ageing Dev 129:304–312
82. Ramanujan VK, Herman BA (2007) Aging process modulates nonlinear dynamics in liver cell metabolism. J Biol Chem 282:19217–19226
83. Rieker C, Engblom D, Kreiner G, Domanskyi A, Schober A, Stotz S, Neumann M, Yuan X, Grummt I, Schutz G, Parlato R (2011) Nucleolar disruption in dopaminergic neurons leads to oxidative damage and parkinsonism through repression of mammalian target of rapamycin signaling. J Neurosci 31:453–460
84. Salminen A, Huuskonen J, Ojala J, Kauppinen A, Kaarniranta K, Suuronen T (2008) Activation of innate immunity system during aging: NF-kB signaling is the molecular culprit of inflamm-aging. Ageing Res Rev 7:83–105
85. Sanz A, Caro P, Gomez J, Barja G (2006) Testing the vicious cycle theory of mitochondrial ROS production: effects of H_2O_2 and cumene hydroperoxide treatment on heart mitochondria. J Bioenerg Biomembr 38:121–127
86. Schober A, Peterziel H, von Bartheld CS, Simon H, Krieglstein K, Unsicker K (2007) GDNF applied to the MPTP-lesioned nigrostriatal system requires TGF-beta for its neuroprotective action. Neurobiol Dis 25:378–391
87. Sehl ME, Yates FE (2001) Kinetics of human aging: I. Rates of senescence between ages 30 and 70 years in healthy people. J Gerontol A Biol Sci Med Sci 56:B198–B208
88. Shelton DN, Chang E, Whittier PS, Choi D, Funk WD (1999) Microarray analysis of replicative senescence. Curr Biol 9:939–945
89. Shigenaga MK, Hagen TM, Ames BN (1994) Oxidative damage and mitochondrial decay in aging. Proc Natl Acad Sci U S A 91:10771–10778
90. Shock NW, Yiengst MJ (1955) Age changes in basal respiratory measurements and metabolism in males. J Gerontol 10:31–40
91. Shoubridge EA, Karpati G, Hastings KE (1990) Deletion mutants are functionally dominant over wild-type mitochondrial genomes in skeletal muscle fiber segments in mitochondrial disease. Cell 62:43–49
92. Sokhansanj BA, Wilson DM III (2004) Oxidative DNA damage background estimated by a system model of base excision repair. Free Radic Biol Med 37:422–427
93. Spencer NF, Poynter ME, Im SY, Daynes RA (1997) Constitutive activation of NF-kappa B in an animal model of aging. Int Immunol 9:1581–1588
94. Sriram K, Matheson JM, Benkovic SA, Miller DB, Luster MI, O'Callaghan JP (2002) Mice deficient in TNF receptors are protected against dopaminergic neurotoxicity: implications for Parkinson's disease. FASEB J 16:1474–1476
95. Stadtman ER (1992) Protein oxidation and aging. Science 257:1220–1224
96. Welle S, Brooks AI, Delehanty JM, Needler N, Thornton CA (2003) Gene expression profile of aging in human muscle. Physiol Genomics 14:149–159
97. West GB, Savage VM, Gillooly J, Enquist BJ, Woodruff WH, Brown JH (2003) Physiology: why does metabolic rate scale with body size? Nature 421:713; discussion 714
98. West KA, Brognard J, Clark AS, Linnoila IR, Yang X, Swain SM, Harris C, Belinsky S, Dennis PA (2003) Rapid Akt activation by nicotine and a tobacco carcinogen modulates the phenotype of normal human airway epithelial cells. J Clin Invest 111:81–90

99. Xiao ZQ, Majumdar AP (2000) Induction of transcriptional activity of AP-1 and NF-kappaB in the gastric mucosa during aging. Am J Physiol Gastrointest Liver Physiol 278:G855–G865
100. Xu Y, Kiningham KK, Devalaraja MN, Yeh CC, Majima H, Kasarskis EJ, St Clair DK (1999) An intronic NF-kappaB element is essential for induction of the human manganese superoxide dismutase gene by tumor necrosis factor-alpha and interleukin-1beta. DNA Cell Biol 18:709–722
101. Zahn JM, Poosala S, Owen AB, Ingram DK, Lustig A, Carter A, Weeraratna AT, Taub DD, Gorospe M, Mazan-Mamczarz K, Lakatta EG, Boheler KR, Xu X, Mattson MP, Falco G, Ko MS, Schlessinger D, Firman J, Kummerfeld SK, Wood WH III, Zonderman AB, Kim SK, Becker KG (2007) AGEMAP: a gene expression database for aging in mice. PLoS Genet 3:e201
102. Zahn JM, Sonu R, Vogel H, Crane E, Mazan-Mamczarz K, Rabkin R, Davis RW, Becker KG, Owen AB, Kim SK (2006) Transcriptional profiling of aging in human muscle reveals a common aging signature. PLoS Genet 2:e115
103. Zhang H, Pan KH, Cohen SN (2003) Senescence-specific gene expression fingerprints reveal cell-type-dependent physical clustering of up-regulated chromosomal loci. Proc Natl Acad Sci U S A 100:3251–3256
104. Zhang K, Kaufman RJ (2008) From endoplasmic-reticulum stress to the inflammatory response. Nature 454:455–462
105. Nuzhdin SV, Brisson JA, Pickering A, Wayne ML, Harshman LG, McIntyre LM (2009) Natural genetic variation in transcriptome reflects network structure inferred with major effect mutations: insulin/TOR and associated phenotypes in Drosophila melanogaster. BMC Genomics. 2009 Mar 24;10:124–136

Chapter 4
Mitochondrion- and Endoplasmic Reticulum-Induced SK Channel Dysregulation as a Potential Origin of the Selective Neurodegeneration in Parkinson's Disease

Guillaume Drion, Vincent Seutin, and Rodolphe Sepulchre

Abstract Mitochondrial dysfunction and metabolic issues are known to have strong implications in the pathogenesis of Parkinson's disease (PD). But it is also known that the neuronal loss leading to PD symptoms is selective for particular areas of the brain (see Chap. 1). In particular, the characteristic motor symptoms of PD are mainly due to abnormal neuronal activity in the basal ganglia, through the degeneration of substantia nigra pars compacta (SNc), but not ventral tegmental area (VTA), dopaminergic (DA) neurons. How a metabolic dysfunction triggers such a selective loss is considered from a range of perspectives in several contributions to this volume. The aim of this chapter is to investigate the potential role of small conductance calcium-activated potassium (SK) channels in this selective degeneration.

Based on a recently proposed model and experimental data, we underline the fundamental role of SK channels in regulating the excitability of SNc DA neurons. The fact that SK channels do not play this regulating role in VTA DA neurons

G. Drion (✉)
Laboratory of Neurophysiology, GIGA Neurosciences, Université de Liège, Avenue de l'Hôpital 1, Bâtiment B36, 1er étage, Liège (Sart Tilman) B-4000, Belgium

Department of Electrical Engineering and Computer Sciences,
University of Liège, Liège, Belgium
e-mail: gdrion@ulg.ac.be

V. Seutin
Laboratory of Neurophysiology, GIGA Neurosciences, Université de Liège, Avenue de l'Hôpital 1, Bâtiment B36, 1er étage, Liège (Sart Tilman) B-4000, Belgium
e-mail: v.seutin@ulg.ac.be

R. Sepulchre
Department of Electrical Engineering and Computer Sciences,
University of Liège, Liège, Belgium
e-mail: R.Sepulchre@ulg.ac.be

P. Wellstead and M. Cloutier (eds.), *Systems Biology of Parkinson's Disease*,
DOI 10.1007/978-1-4614-3411-5_4,

suggests the hypothesis that one reason for the preferential vulnerability of SNc DA neurons in Parkinson's disease is that SK channels, which have a profound influence on their firing physiologically, are dysregulated by a dysfunction of mitochondria and/or endoplasmic reticulum.

Introduction

Mitochondrial dysfunction and metabolic issues are known to have a strong implication in the pathogenesis of PD [1–10]. Indeed, since the first postmortem description of complex I deficiency in the substantia nigra [1–3], platelets [3–5], and skeletal muscle [3, 6] of PD patients, many mitochondrial proteins or proteins associated with mitochondria have been associated with familial forms of PD. These include *Parkin*, PINK1 (PTEN-induced putative kinase 1), DJ-1, and HtrA2/Omi, inter alia [7]. Moreover, toxins used to create animal models of PD, and which are thought to increase the incidence of the disease in humans, are known to target mitochondria [11–16].

An intriguing hallmark of PD is that, despite the fact that mitochondrial dysfunction and expression of PD associated genes is a general feature [9], the resulting neurodegeneration is still strongly localized. Indeed, Braak staging and other studies have shown that many brain areas are affected—but that SN is most vulnerable to damage and with visible manifestation (see Chap. 1 and [17, 18]). Namely, the characteristic motor symptoms of PD are mainly due to abnormal neuronal activity in the basal ganglia, through the degeneration of substantia nigra pars compacta (SNc) dopaminergic (DA) neurons and, to a lesser extent, other basal ganglia/brainstem neurons [19, 20].

The mechanisms by which metabolic and/or mitochondrial dysfunction triggers such selective vulnerability remains unclear [21], even if many modeling and experimental results have highlighted the enhanced vulnerability of SNc DA neurons (see Chaps. 1 and 2). Further results in [10, 22–33] suggest the involvement of cytoplasmic calcium accumulation in degeneration [10, 26–33]. Indeed, calcium accumulation induces mitochondrial stress, one role of this organelle being to regulate the cytoplasmic concentration $[Ca^{2+}]_{cyt}$, through the pumping or release of calcium. In addition, an increasing body of experimental data highlights the involvement of endoplasmic reticulum (ER) stress in PD [34–37], the other intracellular stores of calcium, which supports the previous idea.

Besides its well-known physiological role as a second messenger and its pathophysiological role in case of overload, $[Ca^{2+}]_{cyt}$ is a major regulator of cell excitability. Indeed, the relative variations of $[Ca^{2+}]_{cyt}$, although tightly regulated, are much larger than those of all other ions. Moreover, a number of ion channels are calcium-regulated, which suggests a major role for this ion in the firing regulation of excitable cells such as SNc DA neurons.

SNc DA neurons are slow pacemaker cells, i.e., they exhibit spontaneous firing in vitro (in the absence of excitatory inputs) (0.5–5 Hz), and intracellular calcium

variations are a key element of their pacemaker activity [28, 38–41]. In other words, these neurons have a proper endogenous rhythm, which relies on the $[Ca^{2+}]_{cyt}$ variations. Moreover, they are able to exhibit two specific firing patterns in vivo, namely single-spike firing and burst firing [39, 42]. Burst firing is defined as a sequence of high frequency periods separated by quiescent hyperpolarized periods. One important feature is that the intraburst firing frequency is much higher than single-spike firing rate.

In addition, the firing pattern of SNc DA neurons is regulated by a specific category of ion channels, the so-called small conductance calcium-activated (SK) potassium channels. The gating of SK channels is solely regulated by the intracellular calcium concentration in the vicinity of their intracellular C terminus. Indeed, these channels are tightly associated with the protein calmodulin, which accounts for the calcium sensitivity [43, 44]. On the other hand, their gating is insensitive to variations of the membrane potential, which makes these channels quite unique. As a consequence, their activity is an image of the $[Ca^{2+}]_{cyt}$ variations in what is called their nanodomain, and therefore linked to the endogenous rhythm of the cell. In addition, the EC50 for the activation by Ca is rather low, ~300 nM [45] meaning that, physiologically, these channels will operate during a large portion of the pacemaker cycle, as opposed to, e.g., BK channels, which are much less sensitive to calcium and therefore close at the end of the fast afterhyperpolarization (AHP) (a few ms after the end of each action potential).

SK channels are important and prevalent in a large set of neurons (see [46]). In hippocampal CA1 pyramidal cells, these channels are located close to NMDA receptors and mediate a negative feedback loop by hyperpolarizing the membrane when calcium flows through NMDA channels. This hyperpolarization, in turn, reduces the NMDA conductance [47]. They are therefore thought to regulate the ability of nearby synapses to undergo LTP or LTD. Their role in SNc DA neurons is different in the sense that they operate even in the absence of synaptic afferents. An inhibition of the SK current affects both the excitability and the firing pattern [48–54]. In vitro, SK channel blockade usually induces irregularities in the firing and potentiates the response of the cell to excitatory stimuli. In vivo, the blockade also strongly affects the firing pattern. In particular, it causes a switch from low-frequency single spike firing to bursting, with a relatively high intraburst firing frequency.

In summary, these experimental observations show that $[Ca^{2+}]_{cyt}$ is a key messenger for the regulation of the firing patterns of SNc DA neurons. However, particularly high calcium concentrations during firing of these cells have been pointed out to be a potential origin of the specific vulnerability of SNc DA neurons in PD. Therefore, it is of critical importance to understand how a dysregulation of $[Ca^{2+}]_{cyt}$ variations might affect the electrophysiological activity of these cells, as well as their metabolism. Given that the reverse interaction may also occur, there is a clear possibility for a vicious cycle to be initiated, a subject that will be investigated in other parts of this volume. More specifically, Chap. 5 explores the energy balance of Ca^{2+} pace-making activity and potential effects of reduced energy on the overall

Ca^{2+} balance. In addition, Chap. 7 addresses related biochemical issues arising from a high energy budget coupled to mitochondrial stresses. We argue here that one important pathophysiological change could actually be a change in the temporal pattern of calcium fluxes within SNc DA neurons.

Analysis of the Mechanisms Underlying SNc DA Neuron Firing

A Simple Model of SNc DA Neurons

In [55], we propose a simple model that only contains the minimal set of conductances that are essential to reproduce the firing patterns exhibited by SNc DA neurons. This model has been shown to successfully reproduce experimental observations made with SNc DA neurons, and to reconcile apparently discrepant experimental results concerning the spike generation origin in pacemaker firing [53]. In particular, it underlines the important cooperation between sodium and calcium channels in the spontaneous generation of action potentials in vitro.

The model follows a scheme based on the Hodgkin–Huxley (HH) model [56]. The membrane of excitable cells is modeled as a set of varying conductances g_{ion} representing ion channels, in parallel to a capacitance C_{m} accounting for the ion-impermeable phospholipid bilayer of the membrane. Therefore, the variations of the membrane potential V_{m} obey the following electrical circuit law:

$$C_{\text{m}} \frac{\text{d}V_{\text{m}}}{\text{d}t} = -\sum I_{\text{ions}} + I_{\text{app}}$$

with

$$I_{\text{ion}} = g_{\text{ion}}(V_{\text{m}} - V_{\text{ion}}),$$

where V_{ion} accounts for the resting potential of each ion, which is generated by the concentration gradient of this ion across the membrane, and I_{app} represents a stimulation current. The ionic conductance can vary according to the membrane potential, in the case of voltage-gated channels, or when activated by particular ions or macromolecules, in the case of ligand-gated channels. To date, this modeling scheme has (largely successfully) been used to quantitatively model the behavior of many neurons and predict experimental outcomes [57–62].

An equivalent circuit of the model developed in [55] is shown in Fig. 4.1. It is composed of voltage-gated sodium channels I_{Na} and delayed-rectifier potassium channels $I_{\text{K,DR}}$, which are responsible for the rising and the falling phases of action potentials, respectively. The equations for these currents are identical for those of the HH model, where time constants are tuned to fit DA neuron specifics ($\tau_{\text{DA}} = 0.25 \times \tau_{\text{HH}}$, see [55] for detailed equations).

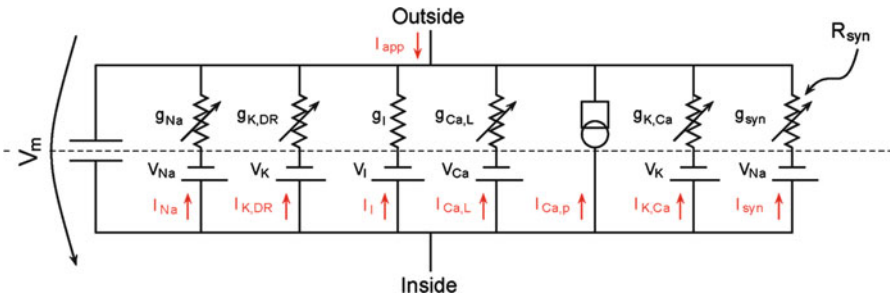

Fig. 4.1 Equivalent circuit diagram of the model. The model is composed of one compartment containing the conductances shown, in parallel with a membrane capacitance. Taken from [55]

Because the endogenous rhythm of SNc DA neurons strongly relies on variations of intracellular calcium concentration, we added calcium dynamics to the HH model:

$$\frac{\mathrm{d}[Ca^{2+}]_{\mathrm{cyt}}}{\mathrm{d}t} = -k_1(I_{\mathrm{Ca,L}} + I_{\mathrm{Ca,pump}}) - k_{\mathrm{c}}[Ca^{2+}]_{\mathrm{cyt}}.$$

Calcium enters into the cell through voltage-gated calcium channels $I_{\mathrm{Ca,L}}$ and is pumped out of the cell by calcium pumps $I_{\mathrm{Ca,pump}}$. We choose a particular category of calcium channels; called L-type calcium channels, because they have been shown to play an important role in the pacemaking of SNc DA neurons [28, 40, 41, 55]. The kinetics of these channels are

$$I_{\mathrm{Ca,L}} = \bar{g}_{\mathrm{Ca,L}} d_{\mathrm{L}} f_{\mathrm{L}} (V_{\mathrm{m}} - V_{\mathrm{Ca}})$$

where

$$\frac{\mathrm{d}d_{\mathrm{L}}}{\mathrm{d}t} = \frac{d_{\mathrm{L},inf} - d_{\mathrm{L}}}{\tau_{d_{\mathrm{L}}}}$$

$$d_{\mathrm{L},inf} = \frac{1}{1 + \exp(-(V_{\mathrm{m}} + 55)/3)}$$

$$\tau_{d_{\mathrm{L}}} = 72\ \exp(-(V_{\mathrm{m}} + 45)^2/400) + 6$$

account for the voltage-activation of the channels, and

$$f_{\mathrm{L}} = \frac{K_{\mathrm{M,L}}}{K_{\mathrm{M,L}} + [Ca^{2+}]_{\mathrm{cyt}}}$$

accounts for the calcium-inactivation of the channels [58]. The current of the calcium pump is given by:

$$I_{\mathrm{Ca,pump}} = I_{\mathrm{Ca,pump},max}\left(1 + \frac{K_{\mathrm{M,P}}}{[Ca^{2+}]_{\mathrm{cyt}}}\right)^{-1}.$$

In addition, the model contains a SK-type calcium-activated potassium current $I_{\mathrm{K,Ca}}$, which has been shown to regulate the electrophysiological behavior of these neurons (see above):

$$I_{\mathrm{K,Ca}} = \bar{g}_{\mathrm{K,Ca}}\left(\frac{[Ca^{2+}]_{\mathrm{cyt}}}{K_{\mathrm{D}} + [Ca^{2+}]_{\mathrm{cyt}}}\right)^{2}(V_{\mathrm{m}} - V_{\mathrm{K}}).$$

In agreement with experimental results, this current is calcium-activated, but not voltage-gated. Finally, a depolarizing current activated by an external input R_{syn} was added to mimic synaptic stimulations:

$$I_{\mathrm{syn}} = R_{\mathrm{syn}}\bar{g}_{\mathrm{syn}}(V_{\mathrm{m}} - 0).$$

The external input R_{syn} can have different shapes: deterministic shapes, such as step or square wave inputs; or a stochastic shape. The latter is designed to mimic physiological synaptic stimulations, which can be modeled through a Poisson stochastic process. The chosen rate for the stimulations is about 50 events per seconds. For the jth event that occurs at time t_j, the marginal activation r_j is given by:

$$\begin{aligned} r_j(t) &= 0, & t < t_j \\ r_j(t) &= p_{\mathrm{syn}}\ \exp((t_j - t)/\tau_{\mathrm{syn}}), & t \geq t_j. \end{aligned}$$

The global synaptic input R_{syn} is given by the sum of the $nr(t)$ corresponding to the n events of the Poisson stochastic process:

$$R_{\mathrm{syn}}(t) = \sum_{j=1}^{n} r_j(t).$$

The values of the parameters used for these currents are given in Table 4.1.

Comparison between simulations of the simple model in different conditions and experimental data are shown in Fig. 4.2 (adapted from [55]). In this very simple configuration, the model adequately captures the basic firing mechanisms of SNc DA neurons, namely pacemaker firing in vitro and SK channel blockade induced switch from low frequency single spike firing to bursting in vivo.

Based upon the validation in Fig. 4.2, we now use this model to analyze the mechanisms underlying the regulation of SNc DA neuron electrophysiology.

Table 4.1 Parameter values of the model (taken from [55])

Parameter	Value	Parameter	Value
C_m	10^{-3} μF/cm^2	V_{Na}	50 mV
V_K	−95 mV	V_l	−54.3 mV
V_{Ca}	120 mV	$\bar{g}_l$	0.3×10^{-3} S/cm^2
$\bar{g}_{Na}$	0.16 S/cm^2	$\bar{g}_{K,DR}$	0.024 S/cm^2
k_1	0.1375×10^{-3}	$I_{Ca,pump,max}$	0.0156 mA/cm^2
k_c	0	$K_{M,P}$	0.0001 mM
$\bar{g}_{Ca,L}$	2×10^{-3} S/cm^2	$\bar{g}_{K,Ca}$	5×10^{-3} S/cm^2
$K_{M,L}$	0.00018 mM	K_D	0.4×10^{-3} mM
$\bar{g}_{syn}$	0.1×10^{-3} S/cm^2	τ_{syn}	45 ms
p_{syn}	1.2		

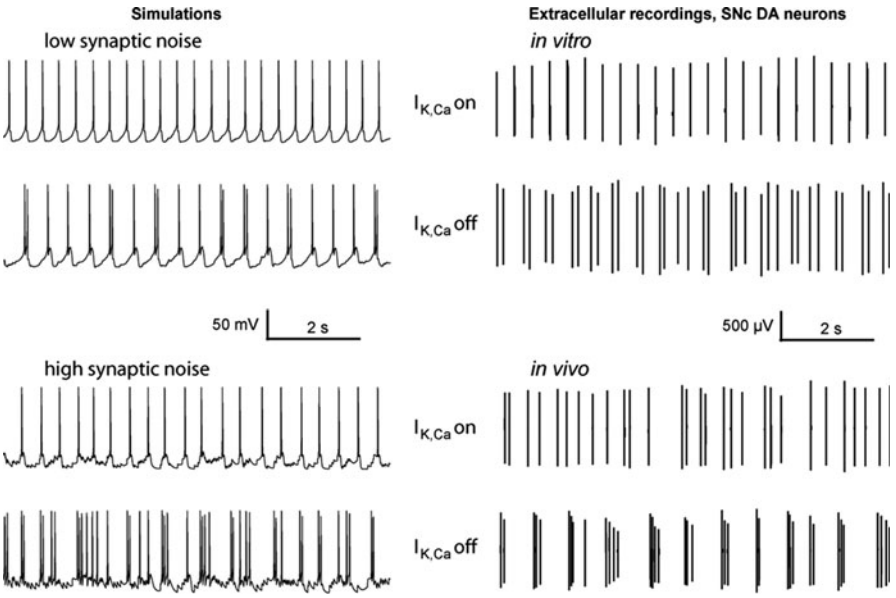

Fig. 4.2 Comparison of the behavior of the simple model in vitro and in vivo (*left*) with experimental data obtained from SNc DA neurons (*right*). In both cases, the neuron fires regularly in single spikes in vitro, and an inhibition of a calcium-activated potassium induces burst firing in vivo (adapted from [55])

Mechanisms of Calcium-Regulated Pacemaking

Whereas the involvement of sodium and delayed-rectifier potassium channels in the generation of action potentials is a well-known feature of the HH model, the low-frequency pacemaker activity is a specific behavior of the model shown in Fig. 4.1. This spontaneous activity is shown in Fig. 4.3 in the absence of SK channels, these

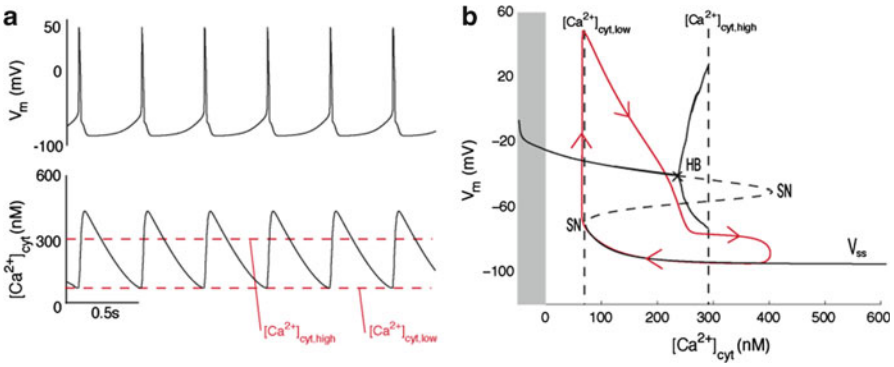

Fig. 4.3 Calcium-regulated spontaneous firing of the simple model. (**a**) Variations of the membrane potential (*top*) and the intracellular calcium concentration (bottom) over time. (**b**) Sketch of the bifurcation diagram of the minimal model, with $[Ca^{2+}]_{cyt}$ as the bifurcation parameter. The *gray* part corresponds to negative values of $[Ca^{2+}]_{cyt}$, which is nonphysiological. V_{ss} denotes the steady-state curve for each value of the bifurcation parameters. The dotted part of V_{ss} shows its unstable part. HB denotes a Hopf bifurcation and SN a saddle node bifurcation. The trajectory of the membrane potential is plotted in *red* (adapted from [55])

channels having little effect on this firing pattern when no synaptic afferents are present [55, 59]. As illustrated in Fig. 4.3a, an action potential is spontaneously generated when the cytoplasmic calcium concentration reaches a minimal value: the low threshold $[Ca^{2+}]_{cyt,low}$. The generated action potential thus induces an entry of calcium into the cell through calcium channels, which has to be pumped out of the cell before a new action potential can be spontaneously generated. As a consequence, the endogenous firing frequency (i.e., endogenous rhythm) of the cell is fixed by the kinetics of calcium entries and exits.

This behavior can be understood with the help of a bifurcation diagram (Fig. 4.3b). This diagram displays the possible steady state of the model for a fixed value of $[Ca^{2+}]_{cyt}$. When $[Ca^{2+}]_{cyt}$ is below the low threshold $[Ca^{2+}]_{cyt,low}$, the only stable steady state is depolarization block or fast firing, which corresponds to a high state of excitation of the cell. In contrast, when $[Ca^{2+}]_{cyt,low}$ is above a high threshold $[Ca^{2+}]_{cyt,high}$, the only stable steady state is an hyperpolarized fixed point, which corresponds to a weakly excitable cell. Finally, when $[Ca^{2+}]_{cyt}$ is between these two thresholds, both steady states are stable (the model is said to be bistable). The pacemaker activity results from the fact that $[Ca^{2+}]_{cyt}$ is not a fixed parameter, but a state variable that itself oscillates spontaneously between the two thresholds. The generation of a single action potential is sufficient for $[Ca^{2+}]_{cyt}$ to exceed $[Ca^{2+}]_{cyt,high}$, which explains why the cell exhibits single-spike firing rather than endogenous bursting, as it is the case for traditional models of endogenous bursting neurons [58].

Physiologically, the calcium low and high thresholds are mainly dependent on the regulation of calcium channels and calcium pumps by the cytoplasmic calcium concentration. Thus, in the model, a rise of the intracellular calcium concentration

induces an inactivation of the L-type calcium channels, which reduces the amount of inward (i.e., depolarizing) current, and an activation of calcium pumps, which increase the amount of outward (i.e., repolarizing) current. As a consequence, excitability of the cell decreases when $[Ca^{2+}]_{cyt}$ rises. A variation of $[Ca^{2+}]_{cyt}$ that exceeds the high threshold will induce a switch from firing to the resting state. The high threshold thus defines the maximum possible intracellular calcium concentration compatible with firing.

The analysis of the pacemaker behavior of SNc DA neurons highlights the critical role of $[Ca^{2+}]_{cyt}$ in the regulation of cell endogenous rhythm. The pacemaker activity of these neurons is strongly different from those of other pacemaker neurons, such as inter alia, pacemaker neurons of the sinoatrial node of the heart. Indeed, the spontaneous activity of the latter do not rely on $[Ca^{2+}]_{cyt}$, but depend fully on voltage-gated channels [61, 62]. This difference is of critical importance: voltage-gated pacemaking ensures a spontaneous activity robust to external noise, which is critical for the regulation of the heart beat; whereas calcium-regulated pacemaking allows the generation of very different firing patterns in the presence of external stimulations (see below), which is a critical component of the signaling of these neurons.

On the other hand, the calcium that enters into the cell during calcium-regulated pacemaking might be a source of mitochondrial stress, as suggested experimentally [10, 33]. Therefore, as mentioned in previous chapters, SNc DA neurons might be more sensitive to metabolic stress, and might, therefore, be the first to degenerate in such pathological conditions.

The Mechanisms of Exogenous Bursting

Calcium-regulated pacemakers are able to exhibit various firing patterns in the presence of external stimulations [42]. This is mainly due to the fact that the kinetics of action potential generation, which is fully voltage-gated, is somewhat decoupled from the endogenous rhythm of the cell, which is regulated by cytoplasmic calcium. In addition, these two variables evolve on very different timescales, $[Ca^{2+}]_{cyt}$ variations being >100 times slower than V_m variations. As a consequence, the neuron has two reachable states, namely hyperpolarization and fast firing, and the switch between these states is regulated by $[Ca^{2+}]_{cyt}$ variations. In the absence of external stimulation, we saw that this mechanism generates single-spike pacemaker firing.

Excitatory stimulations profoundly affect the endogenous mechanisms of the neuronal cell, as illustrated in Fig. 4.4 (note that at this stage, SK channels are not yet integrated into the model). Figure 4.4a shows the response of the model to a step input of synaptic current. A step of synaptic input of sufficient amplitude strongly increases the firing frequency of the cell (accompanied by a dramatic increase in $[Ca^{2+}]_{cyt}$) and the neuron does not hyperpolarize spontaneously until the

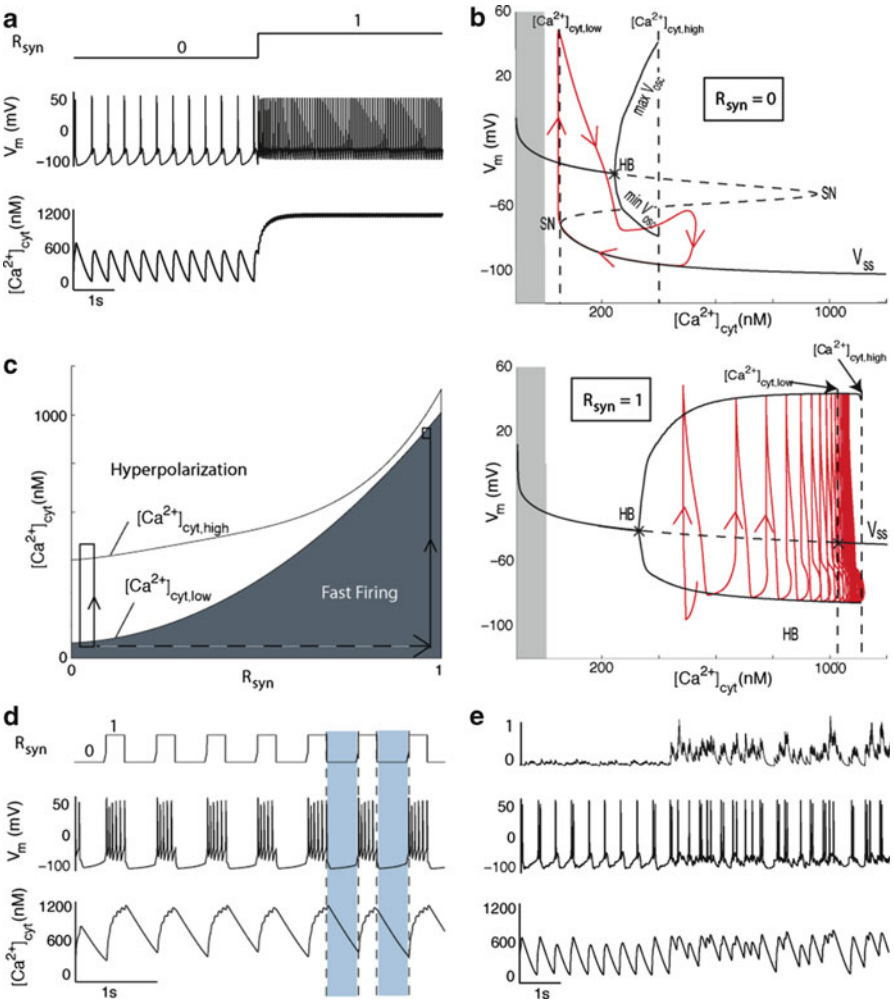

Fig. 4.4 Behavior of the model in in vivo conditions, in the absence of SK channels. (**a**) Variations of the synaptic input, the membrane potential and the intracellular calcium concentration over time, from top to bottom. (**b**) Sketch of the bifurcation diagram of the minimal model for $R_{syn} = 0$ (*top*) and $R_{syn} = 1$ (*bottom*), with $[Ca^{2+}]_{cyt}$ as the bifurcation parameter. (**c**) Variation of the calcium thresholds in the simple model according to the synaptic input. (**d**, **e**) Variations of the synaptic input, the membrane potential and the intracellular calcium concentration over time, from *top* to *bottom*. In the absence of SK channels, variations of the synaptic input are critical for the burst and irregular firing patterns, and the bursting quality is regulated by the interaction between synaptic inputs and the endogenous rhythm of the cell

stimulation is relaxed. This result is in agreement with experimental observations of SNc DA neurons [41, 63, 64].

Through the analysis of the effect on the bifurcation diagram of the system, Fig. 4.4b shows how a step input of synaptic current affects the endogenous rhythm

of the neuron. In the presence of synaptic current, both the low and high calcium thresholds are significantly increased by the new current balance (Fig. 4.4c). As a consequence, several action potentials are necessary before calcium accumulates to the value of the high threshold. In this situation, the high-frequency firing of the cell is governed by the fast dynamics, until the calcium concentration reaches the new threshold $[Ca^{2+}]_{cyt,high}$. If the inward current is large enough, the calcium balance can even stabilize the calcium concentration below the high threshold, resulting in sustained high frequency firing, as it is the case in Fig. 4.4a.

Importantly, whereas a step input of excitatory synaptic current induces fast firing, no spontaneous hyperpolarization is observed. A constant input is therefore not able to induce a burst-firing pattern alone. This observation has largely been confirmed experimentally [41, 63, 64]. Therefore, variations of synaptic inputs are needed. This phenomenon is illustrated in Fig. 4.4d. During the stimulation, the cell exhibits fast firing, and calcium accumulates into the cytoplasm. When the stimulation is released, the cell stops firing, and the accumulated calcium is pumped out. The shape of each burst is determined by the amplitude and shape of the input combined with the amount of calcium that is present in the cytoplasm at the stimulation time. As a consequence, bursts induced by an identical input can have different shapes (compare the second and third bursts of Fig. 4.4d).

To summarize, variations of the synaptic input are needed for the burst and irregular firing patterns of SNc DA neurons, and the bursting quality is regulated by the interaction between synaptic inputs and the endogenous rhythm of the cell. This is the definition of an exogenous burster, and is well illustrated by the application of a physiological stimulation to the model (Fig. 4.4e). As seen in experiments, a low level of noise (modeling in vitro conditions) induces irregularities in the firing rate, whereas a high level of noise (modeling in vivo conditions) induces bursting. Note that the calcium oscillations are larger in bursting mode. Therefore, mitochondrial and endoplasmic reticulum stress would be maximal when the neuron exhibits this firing pattern. The fact that the firing pattern can change rapidly means that energy demand will also vary significantly within short timescales and the metabolic regulation in that context is extremely important. Chapter 7 presents some of the biochemical mechanisms for this regulation and implications for neuroprotective therapies.

Role of SK Channels in the Regulation of Neuronal Entrainability

Experimental observations have shown that bursting of SNc DA neurons is preferentially observed during SK channel inhibition in vivo (in anesthetized animals) [52–54], whereas these cells exhibit irregular single-spike in control conditions. However, during these experiments, the tone of synaptic inputs is likely to be constant, which suggests that SK channels may play a role in the filtering of these inputs. This property is indeed predicted in our simple model.

In contrast to Fig. 4.4, in the presence of SK channels, the calcium thresholds that define the firing regions of the neuron are barely affected by the input (Fig. 4.5b). As a consequence, a similar step of synaptic current activation barely affects the firing of the cell, which persists in a low frequency single-spike firing pattern (Fig. 4.5a). Physiologically, the opening of L-type calcium channel by supra-threshold synaptic inputs, (as demonstrated experimentally in [65]) activates the SK channels through the rise of cytoplasmic calcium concentration. In addition, SK channel gating being insensitive to membrane potential variations, they are never fully deactivated, their calcium sensitivity being maintained at very high levels. A consequence is that they instantaneously react to any synaptically induced depolarization of the cell, through a change in the potassium driving force. The resulting outward current balances the inward current induced by these inputs, in a manner that explains why excitatory inputs barely affect the firing rate and pattern of the cell in the presence of SK channels (Fig. 4.5a). In other words, SK channels protect the endogenous rhythm of the cell against external excitatory inputs.

This regulatory mechanism might have a critical impact on neuronal synchrony of specific subpopulations of neurons. Indeed, if a group of calcium-regulated pacemaker neurons are stimulated by a same set of glutamatergic excitatory inputs, SK channels could play an important role in opposing collective bursting and synchronization. This hypothesis is investigated in Fig. 4.5c, through the simulation of modeled neurons with different endogenous firing rates, but subjected to a same excitatory synaptic input.

The figure illustrates the behavior of such a population of neurons stimulated by a common excitatory input. As expected, when SK channels are present, each neuron fires in single-spikes, following its proper endogenous rhythm. These rhythms, being different from one cell to the other, are not synchronized. On the other hand, when SK channels are blocked, the neurons become highly sensitive to the common synaptic inputs, and start to exhibit synchronized burst firing, until SK channel downregulation is removed. In other words, the network is in its excited state and faithfully integrates and transmits the information provided by the synaptic afferents. As a consequence, neuronal subpopulation whose SK channels are not fully active would exhibit pathological bursting and synchrony. Note that this phenomenon remains to be demonstrated experimentally.

SK Channels Fully Adapt to the Endogenous Rhythm of the Neuron

Our previous analysis suggests that SK channels act as a filter against excitatory inputs in the simple model, in a manner that is in agreement with experimental results obtained in SNc DA neurons. In particular, these channels protect the endogenous rhythm of the cell. However, the endogenous firing rate might differ from one DA neuron to the other, ranging from 0.5 to 5 Hz, and the way SK channels adapt to a particular endogenous rhythm is not obvious.

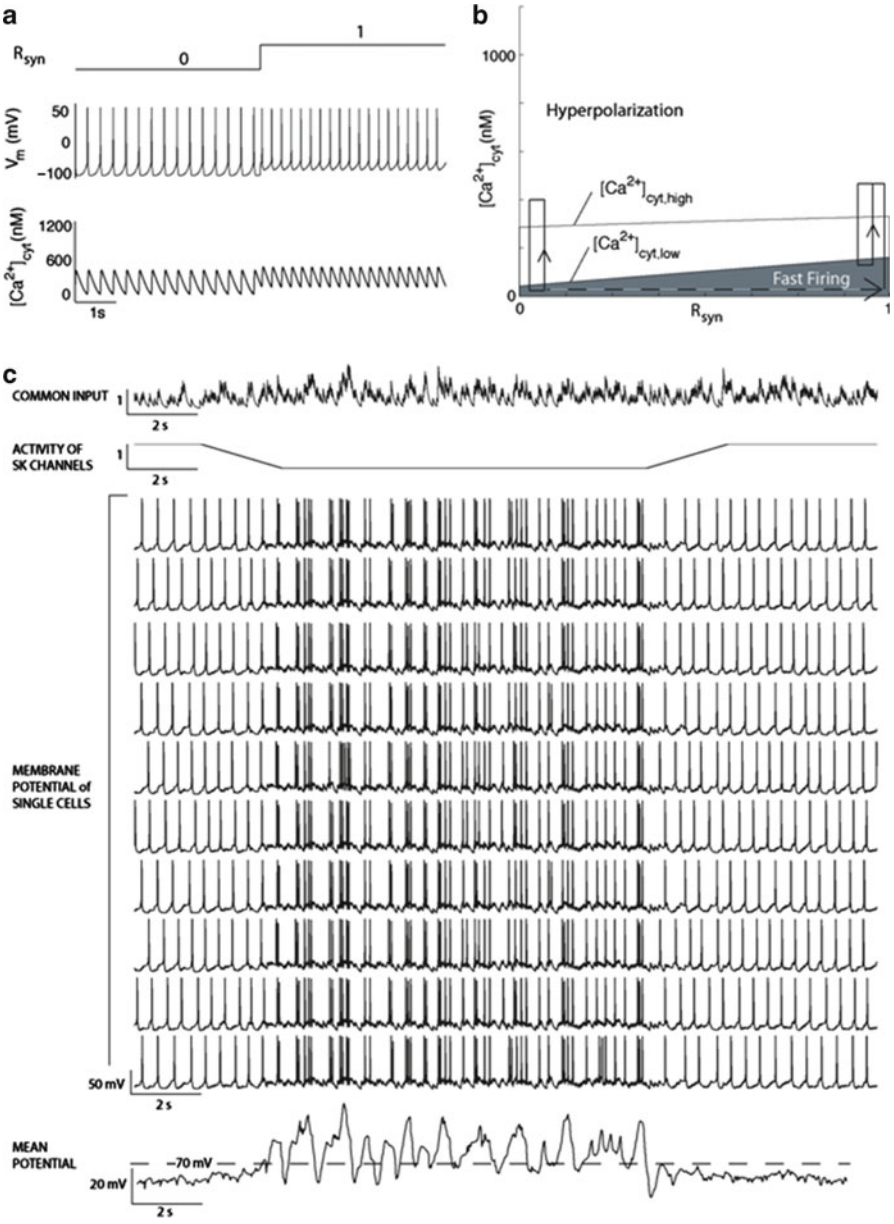

Fig. 4.5 Effect of SK channel modulation on neuronal entrainability. (**a**) Variations of the synaptic input, the membrane potential and the intracellular calcium concentration over time, from *top* to *bottom*, in the presence of SK channels. (**b**) Variation of the calcium thresholds in the simple model according to the synaptic input in the presence of SK channels. (**c**) Variations of neuronal firing pattern and synchrony during a downregulation of SK channels. From *top* to *bottom*: common activation of excitatory inputs, variations of SK channels activity over time, variations of membrane potential of each cells of the network ($n = 10$) over time, and mean electrical activity of the network. A downregulation of SK channels simultaneously induces bursting and synchrony in all cells of the network, resulting in a significant change in the global electrical activity of the population

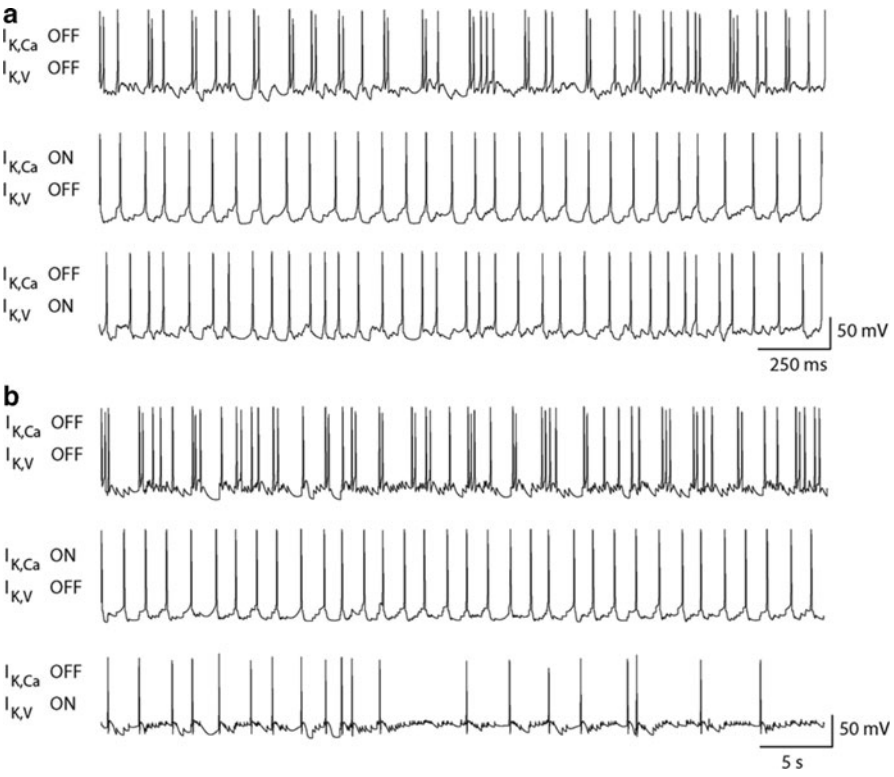

Fig. 4.6 Adaptation of SK channel activity to the endogenous rhythm of the cell. (**a**, **b**) From *top* to *bottom*: Membrane potential variations over time in the absence of $I_{K,Ca}$ and $I_{K,V}$, in the exclusive presence of $I_{K,Ca}$ and in the exclusive presence of $I_{K,V}$, respectively. Note that the time scale in (**b**) is 20 times larger than in (**a**). SK channels fully adapt to neuron endogenous rhythm, in contrast to voltage-gated channels

The critical parameter that makes SK channels very "adaptive" is that their gating is solely regulated by the intracellular calcium concentration in their nanodomain. Indeed, their gating is not affected by many parameters that critically differ from one neuron to the other, such as the resting potential, the action potential amplitude and width, the presence of other ion channels, etc. In contrast, these differences would strongly affect a voltage-gated channel.

This specific feature of SK channels is illustrated in Fig. 4.6. This figure shows an in vivo simulation of the simple model when SK channels are absent, present, or replaced by a voltage-gated potassium current (from top to bottom). As shown in Fig. 4.6a, the voltage-gated current is designed to play a similar role as SK channels in the simple model (the equations for this current are similar to those of the HH potassium current, with $\tau_{K,V} = 0.16 \times \tau_{K,DR}$). In Fig. 4.6b, all time constants are modified similarly (except those of $I_{K,Ca}$ and $I_{K,V}$), in order to change the firing rate by a factor of 20 without affecting the behavior of the modeled neuron.

A comparison of Fig. 4.6a, b shows that SK channels play a similar role in both conditions, regardless of the timescale differences between the two neurons. In contrast, the role of the voltage-gated potassium current is dramatically deteriorated, which shows that the radical changes in the firing rate and action potential shape of the neuron solely affects the behavior of the voltage-gated current. Because of this, the kinetics of voltage-gated currents have to be specific to the neuron, whereas voltage-insensitive calcium-activated channels might be similar in cells having different endogenous rhythms.

Physiologically, the adaptation of SK channels to the endogenous rhythm is due to the fact that these channels are activated by intracellular calcium, and $[Ca^{2+}]_{cyt}$ varies several times slower than the kinetics of activation of SK channels. This activation can be considered as instantaneous compared to $[Ca^{2+}]_{cyt}$ variations. In addition, the gating might be controlled by the neuron itself, through the tight regulation of $[Ca^{2+}]_{cyt}$ in SK channel nanodomains ($[Ca^{2+}]_{cyt,SK}$) by intracellular calcium stores, such as mitochondria and endoplasmic reticulum, as outlined below.

A Possible Interplay Between Calcium Channels and Intracellular Calcium Stores in the Regulation of SK Channel Activation

Correlation Between the Intensity of Neurodegeneration and the Degree of Expression of SK Channels

As mentioned above, although mitochondrial dysfunction is global in PD, the degree of neurodegeneration of DA neurons is extremely variable within the ventral midbrain. There is a wealth of studies that have tried to understand the mechanisms of this heterogeneity. Many potential mechanisms have been suggested, including a variable neuronal size, variables extent of axonal arborization, etc. (see Chap. 1). Recent in situ hybridization, electrophysiological and cell imaging data suggest a further possibility based on the observations that

1. SK channels are expressed to a much greater extend in subregions where neurodegeneration is very prominent [66].
2. In these regions, neuronal pacemaking seems to rely heavily on L-type calcium channels [28].

In our opinion, a link can be made between these observations and the pathophysiology of PD. Indeed, we have shown that SK channels regulate cell entrainability, their inhibition inducing a hyperexcitability of the neuron. In particular, a SK channel blockade induces (synchronized) bursting in vivo in these cells. In addition, Bishop and colleagues analyzed the effect of the deletion of PD-associated genes encoding for mitochondrial proteins on the firing of SNc DA neurons, VTA DA neurons, and GABAergic neurons of mouse brain slices [64].

They observed that the time to peak (TTP) of SK channel-dependent AHP in PINK1- and HtrA2/Omi-Deficient Mouse SNc DA neurons was significantly reduced as compared to control conditions, whereas the maximum peak value was unaffected. As a consequence, SNc DA neurons displayed irregular firing patterns in vitro and were hyperexcitable in ex vivo brain slices and in vivo [67]. Moreover, they showed that an inhibition of ER Ca^{2+} release or mitochondrial Na^{+}/Ca^{2+} exchanger-mediated Ca^{2+} release reduces the amount of spike-generated SK currents in SNc DA neurons of mouse brain slices [67].

On the other hand, deletion of these genes did not affect either VTA DA neuron or GABAergic neuron electrophysiology [67]. The reason for VTA DA neuron unresponsiveness to gene deletions is that SK channels do not, as mentioned above, play an important role in these cells. In contrast, whereas SK channels play an important role in GABAergic neuron excitability [67], their activation does not rely on CICR [64]; an observation that explains why they are spared in these conditions. Indeed, blockade of ER Ca^{2+} release does not affect SK channel activity in GABAergic neurons [67], whereas apamin, a SK channel blocker, strongly affects the firing of the latter [67].

These observations highlight an important role for intracellular stores of calcium in the regulation of SK channels in SNc DA neurons, but not in GABAergic neurons. In addition, the idea that intermediates exist between the entry of calcium through calcium channels and the activation of SK channels is supported by various experimental observations. Namely, the SK channel-dependent AHP has strongly varying kinetics from one neuron to the other. For instance, the maximum peak of the AHP of SNc DA neurons, which express the SK3 subunit [59], is significantly smaller to the one of substantia nigra pars reticulata (SNr) GABAergic neurons [67], which express the SK2 subunit [68]. However, the calcium-activation kinetics of these SK channel subunits are very similar [69]. Therefore, it is clear that the kinetics of $[Ca^{2+}]_{cyt,SK}$ are strongly different in these two neurons. This can probably not be explained specifically by a difference in calcium channel density.

A Potential Regulation Mechanism of SK Channel Activity by Mitochondria and ER

On the one hand, it is commonly accepted that activation of SK channels requires the entry of calcium into the cell through voltage-gated calcium channels. Indeed, a substitution of calcium in the extracellular space, i.e., by cobalt or cesium, has been shown to almost completely block the medium AHP in most of the SK expressing neurons [70], this AHP being generated by an activation of these SK channels [49].

On the other hand, the experimental and modeling results previously mentioned suggest an interaction between calcium channels and intracellular stores of calcium, such as mitochondria and ER, for the regulation of $[Ca^{2+}]_{cyt,SK}$. This hypothesis is illustrated in Fig. 4.7a. One could imagine that calcium entering through calcium

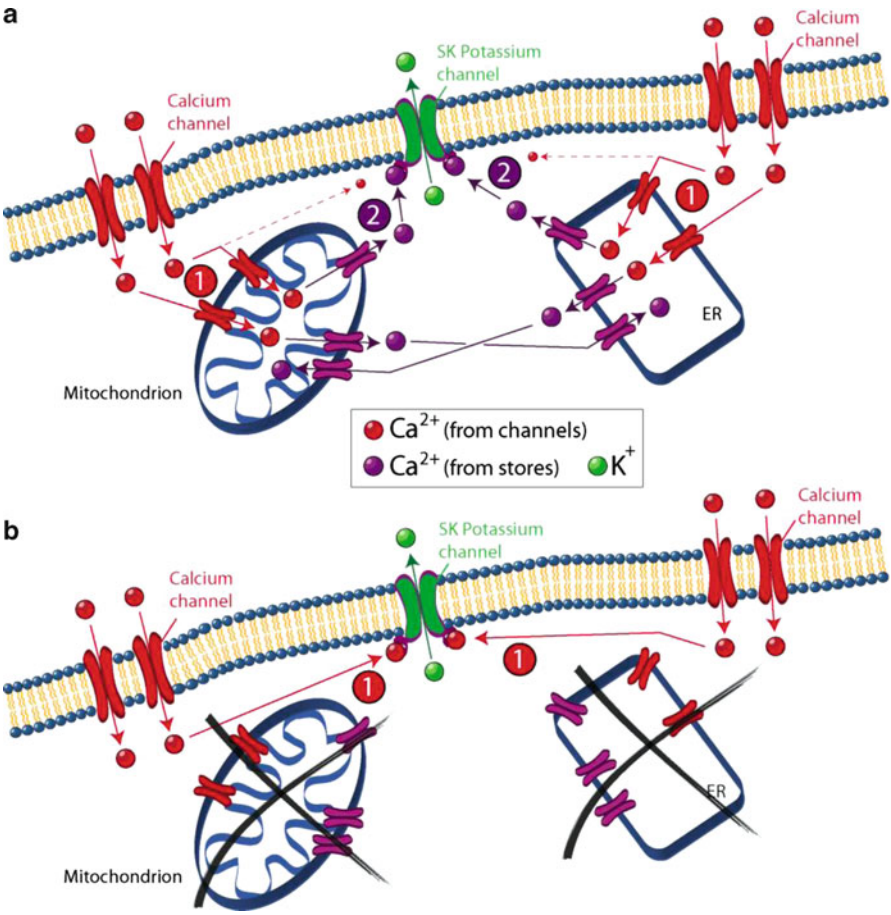

Fig. 4.7 Potential regulation mechanism of SK channel activity by mitochondria and ER. (**a**, **b**) The scheme illustrates a portion of neuron membrane and intracellular space, including a mitochondrion and the ER. A *red dot* represents a calcium ion entering into the cell through calcium channels (in *red*), a *magenta dot* a calcium ion released by intracellular stores, and a *green dot* a potassium ion passing through SK potassium channels (in *green*). Note that the scheme is very simplified, since, for example, ion channel pores are surrounded by accessory subunits and modulating proteins such as kinases and phosphatases

channels is first collected by mitochondria and ER (see Chap. 3). As a consequence, $[Ca^{2+}]_{cyt,SK}$ does not rise much at that time, and SK channels are not strongly activated yet. At a second time, this accumulation of calcium in the stores induces a calcium-induced calcium release (CICR) in the SK nanodomain, which activates SK channels through the increase of $[Ca^{2+}]_{cyt,SK}$. In this configuration, SK channels would be activated after a delay, and their kinetic of activation would be controlled by mitochondria and ER. Strong arguments in favor of CICR exist in cardiac myocytes and in a number of other cell types, including neurons [71–74]. However, any dysregulation of CICR would affect neuron excitability.

Indeed, if the calcium entering through calcium channels is not collected by mitochondria and ER, this calcium immediately diffuses to the SK channel nanodomain (Fig. 4.7b). As a consequence, $[Ca^{2+}]_{cyt,SK}$ rises significantly at that time, and SK channels are strongly activated. This calcium subsequently diffuses, or is pumped out of the SK nanodomain, and thus deactivates SK channels. In this configuration, SK channels are quickly activated and deactivated, in a way that generates a lower AHP TTP after the spike generation. As a consequence, the excitability of the cell is strongly enhanced, making the latter prone to excitotoxicity.

Mitochondrion- and Endoplasmic Reticulum-Induced SK Channel Dysregulation as a Potential Origin of the Selective Neurodegeneration in PD

This phenomenon is of particular relevance in PD. Indeed, as mentioned above, it has recently been shown that deletion of two PD-associated genes, through their effect on the coupling between mitochondrial Na^+/Ca^{2+} exchanger and SK channels, affect the excitability of the PD-affected SNc DA neurons, but not the PD-spared VTA DA neurons and GABAergic neurons [66]. These results suggest that this mitochondrion-induced SK channel dysregulation might contribute to the selective loss of SNc DA cells in PD.

Indeed, global dysfunctions of mitochondria and ER, which affect the metabolism of all cells, may specifically enhance the excitability of these particular pacemaker neurons. Once in a hyperexcited state, their metabolic demand is increased. In turn, this rise of metabolic demand increases mitochondrial and ER stress, which then affects their ability to regulate the intracellular calcium concentration even more [69], and amplifies neuron hyperexcitability. The potentially damaging effect would be exacerbated by the morphological evidence that DA neurons have a very high energy budget (see Chap. 1). This is the beginning of a vicious circle that may lead to the selective degeneration of SNc DA neurons observed in PD. The specific role of energy in this cascade is investigated further in Chap. 5 and the downstream effects of mitochondrial stress (in the form of reactive oxygen species), are explored further in Chap. 7. A relevant link that with Chap. 7 is the fact that the rapid firing dynamics (such as described here) are involved in the mismanagement of oxidative stress by the neurons.

Moreover, this hypothesis can be generalized to many neurons affected in PD. Among the loss of SNc DA cells, other cell types are selectively affected in the disease, such as subthalamic nucleus neurons [75], mitral cells of the olfactory bulb [76], serotonergic neurons of the dorsal raphe [77], motoneurons of the Vagus [17], and interstitial cells of Cajal of the myenteric plexus [18]. Indeed, these cells, among their functional, electrophysiological, and topographic differences, share one important electrophysiological characteristic: their firing is strongly regulated by SK channels [78–82].

Acknowledgments This work is supported by grant 9.4560.03 from the F.R.S.-FNRS (V.S.) and by two grants from the Belgian Science Policy (IAP6/31 (V.S.) and IAP6/4 (R.S.)).

References

1. Schapira AH, Cooper JM, Dexter D, Jenner P, Clark JB, Marsden CD (1989) Mitochondrial complex I deficiency in Parkinson's disease. Lancet 1:1267
2. Schapira AH, Mann VM, Cooper JM, Dexter D, Daniel SE, Jenner P, Clark JB, Marsden CD (1990) Anatomic and disease specificity of NADH CoQ1 reductase (complex I) deficiency in Parkinson's disease. J Neurochem 55:2142–2145
3. Mann VM, Cooper JM, Krige D, Daniel SE, Schapira AH, Marsden CD (1992) Brain, skeletal muscle and platelet homogenate mitochondrial function in Parkinson's disease. Brain 115:333–342
4. Mizuno Y, Ohta S, Tanaka M, Takamiya S, Suzuki K, Sato T, Oya H, Ozawa T, Kagawa Y (1989) Deficiencies in complex I subunits of the respiratory chain in Parkinson's disease. Biochem Biophys Res Commun 163:1450–1455
5. Parker WD Jr, Boyson SJ, Parks JK (1989) Abnormalities of the electron transport chain in idiopathic Parkinson's disease. Ann Neurol 26:719–723
6. Bindoff LA, Birch-Machin M, Cartlidge NE, Parker WD Jr, Turnbull DM (1989) Mitochondrial function in Parkinson's disease. Lancet 2:49
7. Abou-Sleiman PM, Muqit MM, Wood NW (2006) Expanding insights of mitochondrial dysfunction in Parkinson's disease. Nat Rev Neurosci 7:207–219
8. Schapira AH (2008) Mitochondria in the aetiology and pathogenesis of Parkinson's disease. Lancet Neurol 7:97–109
9. Sterky FH, Lee S, Wibom R, Olson L, Larsson NG (2011) Impaired mitochondrial transport and Parkin-independent degeneration of respiratory chain-deficient dopamine neurons in vivo. Proc Natl Acad Sci U S A 108:12937–12942
10. Guzman JN, Sanchez-Padilla J, Wokosin D, Kondapalli J, Ilijic E, Schumacker PT, Surmeier DJ (2010) Oxidant stress evoked by pacemaking in dopaminergic neurons is attenuated by DJ-1. Nature 468:676–680
11. Burns RS, Chiueh CC, Markey SP, Ebert MH, Jacobowitz DM, Kopin IJ (1983) A primate model of parkinsonism-selective destruction of dopaminergic-neurons in the pars compacta of the substantia nigra by n-methyl-4-phenyl-1,2,3,6-tetrahydropyridine. Proc Natl Acad Sci U S A 80:4546–4550
12. Javitch JA, D'Amato RJ, Strittmatter SM, Snyder SH (1985) Parkinsonism-inducing neurotoxin, N-methyl-4-phenyl-1,2,3,6-tetrahydropyridine-uptake of the metabolite N-methyl-4-phenylpyridine by dopamine neurons explains selective toxicity. Proc Natl Acad Sci U S A 82:2173–2177
13. Betarbet R, Sherer TB, MacKenzie G, Garcia-Osuna M, Panov AV, Greenamyre JT (2000) Chronic systemic pesticide exposure reproduces features of Parkinson's disease. Nat Neurosci 3:1301–1306
14. Dawson TM, Ko HS, Dawson VL (2010) Genetic animal models of Parkinson's disease. Neuron 64:646–661
15. Bezard E, Przedborski S (2011) A tale on animal models of Parkinson's disease. Mov Disord 26:993–1002
16. Martinez TN, Greenamyre JT (2012) Toxin models of mitochondrial dysfunction in Parkinson's disease. Antioxid Redox Signal. 16:920–934
17. Braak H, Del Tredici K, Rüb U, de Vos RA, Jansen Steur EN, Braak E (2002) Staging of brain pathology related to sporadic Parkinson's disease. Neurobiol Aging 24:197–211

18. Braak H, de Vos RA, Bohl J, Del Tredici K (2005) Gastric alpha-synuclein immunoreactive inclusions in Meissner's and Auerbach's plexuses in cases staged for Parkinson's disease-related brain pathology. Neurosci Lett 396:67–72
19. Obeso JA, Rodríguez-Oroz MC, Benitez-Temino B, Blesa FJ, Guridi J, Marin C, Rodriguez M (2008) Functional organization of the basal ganglia: therapeutic implications for Parkinson's disease. Mov Disord 23(Suppl 3):S548–S559
20. Fearnley JM, Lees AJ (1991) Ageing and Parkinson's disease: substantia nigra regional selectivity. Brain 114:2283–2301
21. Obeso JA, Rodriguez-Oroz MC, Goetz CG, Marin C, Kordower JH, Rodriguez M, Hirsch EC, Farrer M, Schapira AH, Halliday G (2010) Missing pieces in the Parkinson's disease puzzle. Nat Med 16:653–661
22. Liss B, Haeckel O, Wildmann J, Miki T, Seino S, Roeper J (2005) K-ATP channels promote the differential degeneration of dopaminergic midbrain neurons. Nat Neurosci 8:1742–1751
23. Lu L, Neff F, Fischer DA, Henze C, Hirsch EC, Oertel WH, Schlegel J, Hartmann A (2006) Regional vulnerability of mesencephalic dopaminergic neurons prone to degenerate in Parkinson's disease: a post-mortem study in human control subjects. Neurobiol Dis 23:409–421
24. González-Hernández T, Afonso-Oramas D, Cruz-Muros I (2009) Phenotype, compartmental organization and differential vulnerability of nigral dopaminergic neurons. J Neural Transm Suppl 73:21–37
25. González-Hernández T, Cruz-Muros I, Afonso-Oramas D, Salas-Hernandez J, Castro-Hernandez J (2010) Vulnerability of mesostriatal dopaminergic neurons in Parkinson's disease. Front Neuroanat 4:140
26. Surmeier DJ (2007) Calcium, ageing, and neuronal vulnerability in Parkinson's disease. Lancet Neurol 6:933–938
27. Chan CS, Guzman JN, Ilijic E, Mercer JN, Rick C, Tkatch T, Meredith GE, Surmeier DJ (2007) 'Rejuvenation' protects neurons in mouse models of Parkinson's disease. Nature 447:1081–1086
28. Guzman JN, Sánchez-Padilla J, Chan CS, Surmeier DJ (2009) Robust pacemaking in substantia nigra dopaminergic neurons. J Neurosci 29:11011–11019
29. Chan CS, Gertler TS, Surmeier DJ (2009) Calcium homeostasis, selective vulnerability and Parkinson's disease. Trends Neurosci 32:249–256
30. Chan CS, Gertler TS, Surmeier DJ (2010) A molecular basis for the increased vulnerability of substantia nigra dopamine neurons in aging and Parkinson's disease. Mov Disord 25(Suppl 1): S63–S68
31. Surmeier DJ, Guzman JN, Sanchez-Padilla J (2010) Calcium, cellular aging, and selective neuronal vulnerability in Parkinson's disease. Cell Calcium 47:175–182
32. Surmeier DJ, Guzman JN, Sanchez-Padilla J, Goldberg JA (2010) What causes the death of dopaminergic neurons in Parkinson's disease? Prog Brain Res 183:59–77
33. Ilijic E, Guzman JN, Surmeier DJ (2011) The L-type channel antagonist isradipine is neuroprotective in a mouse model of Parkinson's disease. Neurobiol Dis 43:364–369
34. Calì T, Ottolini D, Brini M (2011) Mitochondria, calcium, and endoplasmic reticulum stress in Parkinson's disease. Biofactors 37:228–240
35. Yuan Y, Cao P, Smith MA, Kramp K, Huang Y, Hisamoto N, Matsumoto K, Hatzoglou M, Jin H, Feng Z (2011) Dysregulated LRRK2 signaling in response to endoplasmic reticulum stress leads to dopaminergic neuron degeneration in *C. elegans*. PLoS One 6(8):e22354
36. Wang HQ, Takahashi R (2007) Expanding insights on the involvement of endoplasmic reticulum stress in Parkinson's disease. Antioxid Redox Signal 9:553–561
37. Arduíno DM, Esteves AR, Cardoso SM, Oliveira CR (2009) Endoplasmic reticulum and mitochondria interplay mediates apoptotic cell death: relevance to Parkinson's disease. Neurochem Int 55:341–348
38. Grace AA, Bunney BS (1984) The control of firing pattern in nigral dopamine neurons: single spike firing. J Neurosci 4:2864–2876

39. Brazhnik E, Shah F, Tepper JM (2008) GABAergic afferents activate both GABAA and GABAB receptors in mouse substantia nigra dopaminergic neurons in vivo. J Neurosci 28:10386–10398
40. Puopolo M, Raviola E, Bean BP (2007) Roles of subthreshold calcium current and sodium current in spontaneous firing of mouse midbrain dopamine neurons. J Neurosci 27:645–656
41. Putzier I, Kullmann PH, Horn JP, Levitan ES (2009) Cav1.3 channel voltage dependence, not Ca2+ selectivity, drives pacemaker activity and amplifies bursts in nigral dopamine neurons. J Neurosci 29:15414–15419
42. Grace AA, Bunney BS (1984) The control of firing pattern in nigral dopamine neurons: burst firing. J Neurosci 4:2877–2890
43. Schumacher MA, Rivard AF, Bächinger HP, Adelman JP (2001) Structure of the gating domain of a Ca2+-activated K+ channel complexed with Ca2+/calmodulin. Nature 410:1120–1124
44. Maylie J, Bond CT, Herson PS, Lee WS, Adelman JP (2004) Small conductance Ca2+-activated K+ channels and calmodulin. J Physiol 554:255–261
45. Köhler M, Hirschberg B, Bond CT, Kinzie JM, Marrion NV, Maylie J, Adelman JP (1996) Small-conductance, calcium-activated potassium channels from mammalian brain. Science 273:1709–1714
46. Vogalis F, Storm JF, Lancaster B (2003) SK channels and the varieties of slow after-hyperpolarizations in neurons. Eur J Neurosci 18:3155–3164
47. Ngo-Anh TJ, Bloodgood BL, Lin M, Sabatini BL, Maylie J, Adelman JP (2005) SK channels and NMDA receptors form a Ca2+-mediated feedback loop in dendritic spines. Nat Neurosci 8:550
48. Shepard PD, Bunney BS (1988) Effect of apamin on the discharge properties of putative dopamine-containing neurons in vitro. Brain Res 463:380–384
49. Shepard PD, Bunney BS (1991) Repetitive firing properties of putative dopamine-containing neurons in vitro: regulation by an apamin-sensitive Ca2+-activated K+ conductance. Exp Brain Res 86:141–150
50. Nedergaard S, Flatman JA, Engberg I (1993) Nifedipine- and omegaconotoxin-sensitive Ca2+ conductances in guinea-pig substantia nigra pars compacta neurones. J Physiol 464:707–747
51. Seutin V, Johnson SW, North RA (1993) Apamin increases NMDA-induced burst firing of rat mesencephalic dopamine neurons. Brain Res 630:341–344
52. Waroux O, Massotte L, Alleva L, Graulich A, Thomas E, Liégeois JF, Scuvée-Moreau J, Seutin V (2005) SK channel control the firing pattern of midbrain dopaminergic neurons in vivo. Eur J Neurosci 22:3111–3121
53. Ji H, Hougaard C, Herrik KF, Strøbaek D, Christophersen P, Shepard PD (2009) Tuning the excitability of midbrain dopamine neurons by modulating the Ca2+ sensitivity of SK channels. Eur J Neurosci 29:1883–1895
54. Herrik KF, Christophersen P, Shepard PD (2010) Pharmacological modulation of the gating properties of small conductance Ca2+-activated K+ channels alters the firing pattern of dopamine neurons in vivo. J Neurophysiol 104:1706–1735
55. Drion G, Massotte L, Sepulchre R, Seutin V (2010) How modeling can reconcile apparently discrepant experimental results: the case of dopaminergic neurons. PLoS Comput Biol 7(5):e1002050
56. Hodgkin AL, Huxley AF (1952) A quantitative description of membrane current and its application to conduction and excitation in nerve. J Physiol 117:500–544
57. Sejnowski TJ, Koch C, Churchland PS (1988) Computational neuroscience. Science 241:1299–1306
58. Hille B (2001) Ion channels of excitable membranes. Sinauer, Sunderland, MA, pp 95–129
59. Wolfart J, Neuhoff H, Franz O, Roeper J (2001) Differential expression of the small-conductance, calcium-activated potassium channel SK3 is critical for pacemaker control in dopaminergic midbrain neurons. J Neurosci 21:3443–3456

60. Izhikevich EM (2007) Dynamical systems in neuroscience: the geometry of excitability and bursting. The MIT, Cambridge, MA, pp 325–378
61. Noble D (1984) The surprising heart: a review of recent progress in cardiac electrophysiology. J Physiol 353:1–50
62. Noma A (1996) Ionic mechanisms of the cardiac pacemaker potential. Jpn Heart J 37:653–682
63. Blythe SN, Wokosin D, Atherton JF, Bevan MD (2009) Cellular mechanisms underlying burst firing in substantia nigra dopamine neurons. J Neurosci 29:15531–15541
64. Lobb CJ, Wilson CJ, Paladini CA (2010) A dynamic role for GABA receptors on the firing pattern of midbrain dopaminergic neurons. J Neurophysiol 104:403–413
65. Magee JC, Johnston D (1995) Synaptic activation of voltage-gated channels in the dendrites of hippocampal pyramidal neurons. Science 268:301–304
66. Sarpal D, Koenig JI, Adelman JP, Brady D, Prendeville LC, Shepard PD (2004) Regional distribution of SK3 mRNA-containing neurons in the adult and adolescent rat ventral midbrain and their relationship to dopamine-containing cells. Synapse 53:104–113
67. Bishop MW, Chakraborty S, Matthews GA, Dougalis A, Wood NW, Festenstein R, Ungless MA (2010) Hyperexcitable substantia nigra dopamine neurons in PINK1- and HtrA2/Omi-deficient mice. J Neurophysiol 104:3009–3020
68. Yanovsky Y, Zhang W, Misgeld U (2005) Two pathways for the activation of small-conductance potassium channels in neurons of substantia nigra pars reticulata. Neuroscience 136:1027–1036
69. Stocker M (2004) Ca(2+)-activated K+ channels: molecular determinants and function of the SK family. Nat Rev Neurosci 5:758–768
70. Scuvée-Moreau J, Waroux O, Alleva L, Boland A, Graulich A, Liégeois JF, SeutinV (2005) T-type calcium channels do not play a major role in the activation of SK channels in rat midbrain dopaminergic neurons. Program No. 376.13. 2005 Neuroscience Meeting Planner. Society for Neuroscience, Washington, DC, 2005. Online
71. Friel D (2004) Interplay between ER Ca2+ uptake and release fluxes in neurons and its impact on [Ca2+] dynamics. Biol Res 37:645–674
72. Coulon P, Herr D, Kanyshkova T, Meuth P, Budde T, Pape HC (2009) Burst discharges in neurons of the thalamic reticular nucleus are shaped by calcium-induced calcium release. Cell Calcium 46:333–346
73. Lee KH, Cho JH, Choi IS, Park HM, Lee MG, Choi BJ, Jang IS (2010) Pregnenolone sulfate enhances spontaneous glutamate release by inducing presynaptic Ca2+-induced Ca2+ release. Neuroscience 169:106–116
74. Barsukova AG, Bourdette D, Forte M (2011) Mitochondrial calcium and its regulation in neurodegeneration induced by oxidative stress. Eur J Neurosci 34:437–447
75. Steigerwald F, Pötter M, Herzog J, Pinsker M, Kopper F, Mehdorn H, Deuschl G, Volkmann J (2008) Neuronal activity of the human subthalamic nucleus in the parkinsonian and nonparkinsonian state. J Neurophysiol 100:2515–2524
76. Duda JE (2009) Olfactory system pathology as a model of Lewy neurodegenerative disease. J Neurol Sci 289:49–54
77. Huot P, Fox SH, Brotchie JM (2011) The serotonergic system in Parkinson's disease. Prog Neurobiol 95(2):163–212
78. Hallworth NE, Wilson CJ, Bevan MD (2003) Apamin-sensitive small conductance calcium-activated potassium channels, through their selective coupling to voltage-gated calcium channels, are critical determinants of the precision, pace, and pattern of action potential generation in rat subthalamic nucleus neurons in vitro. J Neurosci 23:7525–7542
79. Maher BJ, Westbrook GL (2005) SK channel regulation of dendritic excitability and dendrodendritic inhibition in the olfactory bulb. J Neurophysiol 94:3743–3750
80. Rouchet N, Waroux O, Lamy C, Massotte L, Scuvée-Moreau J, Liégeois JF, Seutin V (2008) SK channel blockade promotes burst firing in dorsal raphe serotonergic neurons. Eur J Neurosci 28:1108–1115

81. Sah P, McLachlan EM (1992) Potassium currents contributing to action potential repolarization and the afterhyperpolarization in rat vagal motoneurons. J Neurophysiol 68:1834–1841
82. Fujita A, Takeuchi T, Saitoh N, Hanai J, Hata F (2001) Expression of Ca(2+)-activated K(+) channels, SK3, in the interstitial cells of Cajal in the gastrointestinal tract. Am J Physiol Cell Physiol 281:C1727–C1733

Chapter 5
Energetics of Ion Transport in Dopaminergic *Substantia nigra* Neurons

Febe Francis, Míriam R. García, and Richard H. Middleton

Abstract Cytosolic calcium ion levels are critical in sustaining neuronal activity. They have an intricate relationship with the neuronal energy systems, and Parkinson's disease (PD) probably involves a dysfunctional energy system in the pacemaking neurons of the *Substantia nigra*. This chapter explores the association of repetitive firing pattern of these neurons and cytosolic calcium using a mathematical model. In particular, a theory is examined that proposes a role of low voltage activated L-type calcium channel in creating an energy stress within vulnerable neurons.

Introduction

Biological organisms are known to function by the optimal utilization of available resources, and the high degree of activity that occur in neurons calls for particularly efficient management of energy [2]. Within the brain, the dopaminergic neurons of the *substantia nigra pars compacta* (*SNc*) are among the most energy intensive structures. They are typically the earliest and most seriously affected neurons in Parkinson's disease (PD), and their degeneration is a hallmark of the condition.

Although PD affects many brain areas, there are certain physiological features that make neurons of the *SNc* particularly vulnerable to this chronic condition.

F. Francis (✉) • M.R. García
Hamilton Institute, National University of Ireland, Maynooth, County Kildare, Ireland
e-mail: febe.francis@nuim.ie; miriam.garcia@nuim.ie

R.H. Middleton
ARC Centre for Complex Dynamic Systems and Control, University of Newcastle, Newcastle, NSW 2308, Australia
e-mail: richard.middleton@newcastle.edu.au

P. Wellstead and M. Cloutier (eds.), *Systems Biology of Parkinson's Disease*,
DOI 10.1007/978-1-4614-3411-5_5,

In particular, as discussed in Chap. 4, they are known for their spontaneous pacemaker-like activity. This pacemaking supports the normal functioning of the *basal ganglia* by providing an uninterrupted supply of dopamine. It is probably for this reason that *SNc* neurons are extensively arborized in a way that provides both an abundance of dopamine, and built-in redundancy (see Chap. 1 and [23]). However, extensive arborisation, combined with continuous pacemaking, also forms a high-stress combination that places the management of neuronal energy under pressure. Specifically, we expect these neurons to be chronically energy-stressed, such that any extra energy demand, or an inefficiency of cellular energy metabolism, could have serious consequences. A potential factor in energy stress is the use of calcium ions to maintain tonic activity.

Cytosolic calcium levels have always been at the crux of regulatory aspects of eukaryotic cells. As a secondary messenger, calcium is significant in numerous cellular functions, and as a result, calcium needs to be kept under control. *SNc* neurons in particular have an unusual reliance on calcium ions for their continuous slow and spontaneous firing (see Chap. 4 and [7, 33, 40, 41]). Much of the experimental and modelling studies performed on these neurons suggest that the level of cytosolic calcium affects pacemaking behaviour. As a result, there are apparently multiple cellular storage mechanisms that compensate for short-term surges of calcium above control levels. These include (1) sequestration by mobile protein buffers, (2) the endoplasmic reticulum and (3) ultimately the mitochondria [44]. The involvement of mitochondrial processes in the development of PD and the susceptibility of mitochondria to calcium stress illustrates the importance of precise calcium regulation in these neurons [11, 13, 35, 38].

For *SNc* neurons, a significant portion of the energy budget is devoted to the maintenance of pacemaking activity and regulating intracellular calcium at low levels [40, 45]. An impaired energetic regulation (a subject covered in Chap. 2) would thus directly impact this pacemaking activity and contribute to PD pathology. Some of the current attempts at modelling the pacemaker current of *SNc* neurons include Amini et al. [1], Canavier and Landry [5], Komendantov et al. [18], Kuznetsova et al. [19], Drion et al. [8]. Each of these models has been developed as a means of explaining observations from different individual experiments. Possibly because of this, it is difficult to effectively link these specific models to a general model that would account for energy utilization in the *SNc*. As a consequence there is a need for a "baseline model" of the entire process: a model that can reproduce the basic firing pattern and yet also includes the different pumps and exchangers. In short, a model that is capable of capturing the overall impact of calcium signalling on *SNc* energy metabolism, and in turn, upon neurodegeneration.

Wellstead and Cloutier [45] introduced the concept of energy metabolism as a unifying basis for developing a theory for neurodegeneration in PD. In this chapter, we develop this concept as it relates to the energy implications of membrane ion-transport by the neurons of *SNc*. In this context, an aspect of *SNc* behaviour, important for robust pacemaking, is the utilization of heterogeneous channels [12]. Experiments suggest that the neurons exhibit pacemaking behaviour even if L-type calcium channels are blocked, and despite the fact that these channels are considered

important for generating the voltage patterns (see Chan et al. [6]). Chan's study also suggests the use of drug-targets for calcium channels that would reduce the calcium stress experienced by *SNc* neurons. The study presented here, inter alia, considers whether this proposal has any specific energetic advantage.

Model Description

A popular mathematical representation for the cell membrane is as a capacitor (representing charge accumulation), connected in parallel with resistances (representing ion transport), with voltage sources to represent the driving forces. The original model of this form (see [14]) established a dynamic relationship between the transmembrane potential and transmembrane ionic currents. This differential formulation may be replaced with an algebraic equation relating the transmembrane potential to intracellular ion concentrations [15] as

$$V = \frac{F v_{\text{cyt}}}{C_{\text{m}}} \sum_{s \in S} z_s [s_{\text{i}} - s_{\text{e}}], \tag{5.1}$$

where $s \in S = \{\text{Na, Ca, K, A}\}$, represents sodium, calcium, potassium and anions, respectively (Table 5.1). This explicit relation of the transmembrane potential in terms of ionic concentration is obtained by assuming that the cell shape is retained by an osmotic equilibrium [30]. Assuming that outer ionic concentrations are constant, the membrane potential is predominantly a function of the intracellular ionic concentrations.

The transport of ionic species across the membrane depends on the ionic concentration gradient and electrical field. This flux density can be described by the Nernst–Planck equation in which, for a constant electric field along the width of the membrane, the flux of species s is defined by

$$J_s = -D_s \left(\frac{\mathrm{d}s}{\mathrm{d}x} + \frac{z_s F}{RT} s \frac{V}{L} \right), \tag{5.2}$$

where D_s is the diffusivity of species s and V is the voltage across the membrane of length L. The Nernst potential represents the equilibrium voltage at which the net transport of the species across the membrane is zero:

$$\widehat{V}_s = \frac{V_\tau}{z_s} \ln \frac{s_{\text{e}}}{s_{\text{i}}} \quad s \in S, \tag{5.3}$$

where $V_\tau = RT/F$, is a temperature defined thermodynamic entity. The dynamics of the transport of s may be written as

$$\frac{\mathrm{d}s}{\mathrm{d}t} = \frac{1}{z_s F v_{\text{cyt}}} \sum_{x \in X_s} I_x, \tag{5.4}$$

Table 5.1 Glossary of abbreviations

C_{m}	Membrane capacitance (pF)
D_s	Diffusivity of species s (m^2/s)
ε	Membrane permittivity (m/s)
F	Faraday constant (C/mol)
G	Gibb's free energy (J)
γ_x	Channel conductance in the Hodgkin–Huxley model (nS)
g_x	Channel conductance in the electrodiffusivity model (nS)
Γ_x	Coupling coefficient for facilitated transport
J_s	Mass flux of species s (mmol/(m^2s))
L	Membrane thickness (μm)
$\widehat{\mu}_{\mathrm{s}}$	Electrochemical potential (J/mol)
ψ	Electrical potential (J/mol)
O_x	Channel open probability (dimensionless)
R	Gas constant (J/(mol K))
s_i	Intracellular concentration of s (mM)
s_e	Extracellular concentration of s (mM)
T	Absolute temperature (K)
V	Transmembrane potential (mV)
V_τ	RT/F (mV)
$\widehat{V}_{\mathrm{s}}$	Nernst potential of species s (mV)
v_{cyt}	Cytosolic volume (pL)
z_s	Valency of ionic species s (dimensionless)

where I_x is the ionic flux (current) of species s and X_s includes all mechanisms by which species s are transported across the membrane. The transport could be passive, driven by existing electrochemical force fields along ion channels, or one facilitated by the functioning of membrane proteins that constitute the pumps and exchangers.

Ion Channels

The flux of ions of species s across the membrane, through ion-channels, may be represented as

$$I_{s,c} = O_c(V).f_{s,c}(V, s_{\mathrm{e}}, s_{\mathrm{i}}), \tag{5.5}$$

where the sub-index c takes the name of the different ion channels to be considered. Here, f_s is a function that defines the transport influenced by the given electrochemical field and O_c represents the probability of channel c being open at the given membrane potential, or concentrations of s in the given environment. We describe the possible forms of both terms in the following sections.

Electrochemical Transport

Hodgkin and Huxley [14] observed that the electric current crossing a membrane could be described as a sum of ionic components, of which the currents carried by sodium and potassium were the most important. In a series of experiments, they found that these currents depended on voltage, approximately linearly, for an instantaneous response over a limited range according to the conductance relationship

$$f_{s,c} = \gamma_{s,c}(V - \widehat{V}_s), \tag{5.6}$$

where γ is the channel conductance.

Goldman–Hodgkin–Katz Equation

The Nernst–Planck equation (5.2) may be integrated to generate the electrodiffusion model for channel conduction

$$f_{s,c} = \varepsilon_c z_s^2 F \frac{V}{V_\tau} \frac{[s]_\mathrm{i} - [s]_\mathrm{e} \exp\left(-z_s \frac{V}{V_\tau}\right)}{1 - \exp\left(-z_s \frac{V}{V_\tau}\right)}. \tag{5.7}$$

This equation may also be expressed using the hyperbolic sine (sinh) function[1] as

$$f_{s,c} = z_s g_{s,c} \sqrt{[s]_\mathrm{i}[s]_\mathrm{e}} \frac{\sin\mathrm{h}\left(z_s \frac{V - \widehat{V}_s}{2V_\tau}\right)}{\sin\mathrm{hc}\left(z_s \frac{V}{2V_\tau}\right)}. \tag{5.8}$$

The electrical circuit model (5.6) is the most commonly used in the literature and the Goldman–Hodgkin–Katz (GHK) equation (5.8) is typically used when there are significant differences in the ion dynamics inside the cell, usually when calcium dynamics are considered. Our model employs the modified form of the GHK equation for practically all channels, except for those whose gating characteristics have been adopted from literature.

[1] $\sin\mathrm{hc}(x) = \dfrac{\sin\mathrm{h}(x)}{x}$.

Channel Gating

Ion channels are pore-forming protein ensembles that are responsible for the task of regulating, or gating, ion flows. Gating arises from conformational changes in the proteins that comprise the channel. These conformational changes are driven by variations in the electric field, or by ligands that bind to the protein. For this reason ion-channels are often classified as either voltage-gated or ligand-gated. In the case of voltage-gated channels, for a particular range of membrane potentials they adopt a conformation with a central hole that forms a channel for the free movement of ions. Such an "open" state is further defined by certain "selectivity filters" (often amino acids) that provides ion specificity to the protein. At other membrane potentials, the flow of ionic current is blocked by "closed" or "inactive" conformations of the channel. A channel protein can thus adopt various conformational states with varying degrees of conductance, and can spontaneously switch between these states.

Hodgkin–Huxley Gating

In the Hodgkin–Huxley formalism the channel "gates" are of two types: those that *activate* the channels (m) and those that *inactivate* them (h). The probability that the channels are open (O_c) is thus a function of these gates:

$$O_c(V) = [m_c(t)]^{a_c}[h_c(t)]^{b_c}, \tag{5.9}$$

where a_c and b_c are the number of activation and inactivation gates for channel c, respectively. The dynamics of each of the gating variables (m_c, h_c) may be described by a first-order differential equation:

$$\frac{dy}{dt} = \frac{y_\infty - y}{\tau_y} \quad y \in m_c, h_c.$$

The steady state values of these variables are thought to be best represented by a Boltzmann-type equation. The dependence of the time-constant, τ_y on voltage is mostly expressed empirically, and one popular way of approximating the time constant is by a Gaussian function [17].

Channel Gating as Markov Transitions

The opening of an individual gate may also be represented as a simple Markov transition between two states, with voltage-dependent transition rates, $\alpha(V)$ in the forward direction and $\beta(V)$ in the reverse direction. We can represent the dynamics of these transitions as

$$O_c(V) = \prod_{i=1}^{n_c} \left[m_c^{\{i\}}(V) \right]$$
$$\frac{\mathrm{d}y}{\mathrm{d}t} = \alpha_y(1-y) - \beta_y y \quad y = m_c^{\{i\}} \quad i = 1, \ldots, n_c \tag{5.10}$$

Approximations for these rates of transition [43] are,

$$\alpha = \alpha_0 \exp\left(-\frac{z\delta VF}{RT}\right) = \alpha_0 \exp\left(\frac{z_a V}{V_\tau}\right)$$
$$\beta = \beta_0 \exp\left(\frac{z(1-\delta)VF}{RT}\right) = \beta_0 \exp\left(-\frac{z_b V}{V_\tau}\right) \tag{5.11}$$

Here, z_a and z_b are charges associated with the transition energy barrier located asymmetrically in the electric field of the membrane. For activation gates, $z_{am}, z_{bm} > 0$, and for inactivation gates, $z_{ah}, z_{bh} < 0$. Note that for $\tau_y = 1/(\alpha + \beta)$, the open probabilities for both the gating models remain the same.

Calcium-Dependent Potassium SK Channels

Calcium-activated potassium channels are gated by intracellular calcium ions, thereby coupling intracellular calcium levels and membrane potential. The slow afterhyperpolarization that follows an action potential is generated by the activation of calcium-activated potassium channels. Afterhyperpolarization limits the firing frequency of repetitive action potentials (spike-frequency adaptation) and is essential for normal neurotransmission (see Chap. 4 and [48]).

SNc dopaminergic neurons have at least two forms of potassium currents that are controlled by intracellular calcium [26, 39]: (1) the apamin-sensitive, small-conductance (SK), calcium-activated potassium current and (2) the apamin-insensitive large-conductance (BK) calcium-activated potassium current that is blocked by tetraethylammonium. BK channel current is less essential for producing the slow underlying oscillations as they are less sensitive to cytosolic calcium and are hence excluded from our model.

SK channels are voltage-independent and activated by sub-micro-molar concentrations of intracellular calcium, and are not gated by calcium binding directly to the channel α-subunits. Instead, the functional SK channels are heteromeric complexes with calmodulin, which is associated with the α-subunits in a calcium-independent manner [48]. These two components are thought to have been structurally and functionally paired at an early stage of eukaryotic evolution. Hence, it can be reasonably assumed that calcium indirectly controls the functioning of these channels via calmodulin.

A popular way of modelling SK-channel gating is by using the Hill expression:

$$O_{k,\mathrm{sk}} = \frac{Ca_i^n}{K_{0.5}^n + Ca_i^n}. \tag{5.12}$$

Previous attempts to model the pacemaking of dopaminergic neurons [19, 46] have employed $K_{0.5}$ of 0.25 μM and a Hill coefficient (n) of 4. An experiment conducted on SK channels co-expressed with calmodulin [48], suggests parameters of $K_{0.5} = 0.35$ μM and a Hill coefficient $= 4.2$.

Pumps and Exchangers

Extrusion of cations from cells against their gradient occurs, in essence, by two transport mechanisms. The first of these, calcium ATPases of the plasma membrane (PMCA) and endoplasmic reticulum (ERCA), are active transporters that expel calcium from the cytoplasm using energy from the hydrolysis of adenosine triphosphate (ATP). The sodium–potassium ATPase (NaK), also uses the energy from ATP hydrolysis to transport sodium and potassium ions against their gradient. In the second mechanism, sodium–calcium exchangers (NaCax) found on the cell membrane, as well as across the outer mitochondrial membrane, are antiporters that utilize the gradient of sodium to extrude calcium. A third mechanism exists in the mitochondria to transport calcium released from the endoplasmic reticulum into its inner matrix. The mitochondrial uniporter opens in response to a stimulus and allows the free flow of calcium along its gradient.

The PMCA is a high-affinity calcium removal system that compensates for small and moderate changes of calcium concentration from its control level. However, excessive changes in calcium levels are handled by the low-affinity NaCax. Again, the activation of PMCA is comparatively slow, and hence, the relative contribution of NaCax to calcium removal is more important during the early stages of calcium increase [37]. Later in this section, we describe in detail the functional aspects of these transport processes from an energetic perspective.

Energetics of Exchange

The free energy changes in a system are directly related to the changes in its molecular components and may be represented as

$$\mathrm{d}G = \sum_i \left(\frac{\partial G}{\partial n}\right)_{T,p} \mathrm{d}n_\mathrm{i}.$$

The first derivative of the Gibbs free energy, G. with respect to the molar concentration of component n_i is its chemical potential μ_i (for neutral species) or the electrochemical potential, $\widehat{\mu}_\mathrm{i}$(for charged species). In the presence of an electric field of potential ψ, the electrochemical potential is given by [36],

$$\widehat{\mu}_{\mathrm{i}} = \mu_{\mathrm{i}}^{0} + \frac{RT}{z_s} \ln [s]_{\mathrm{i}} + F\psi,$$

where $\mu_{\mathrm{i}}{}^{0}$ represents the standard chemical potential. Electrochemical potential is a measure of energy and its difference acts as the driving force for ionic transport across membranes [28]. A transport against this gradient requires energy. The ATPase transporters are enzymes that engage the translocation of ions by utilizing energy released by the hydrolysis of ATP. Antiporters, on the other hand, couple a transport in the direction of the gradient with a transport against gradient.

The Sodium–Calcium Exchanger

NaCax is an antiporter responsible for transporting calcium across a membrane against its gradient by using the electrochemical gradient of sodium. In the calcium exit mode, the exchange is defined as an external sodium (Na_e)-dependent calcium efflux. The hydrolysis of ATP is not required to power the calcium extrusion. However, cytosolic ATP seems to slightly influence the kinetics by phosphorylating the exchanger and altering its affinity for the ions [3].

In the case of the sodium calcium exchanger, the energy to drive calcium ions out of the cell is gained by the translocation of sodium into the cytoplasm. The free energy change associated with this transport is given by the difference in the electrochemical potentials of the two ionic species across the membrane ($\Delta G_{\mathrm{i}} = z_{\mathrm{i}}(\widehat{\mu}_{\mathrm{i,out}} - \widehat{\mu}_{\mathrm{i,in}})$):

$$\begin{aligned} \Delta G_{\mathrm{Na}} &= RT \ln \frac{Na_{\mathrm{e}}}{Na_{\mathrm{i}}} - z_{\mathrm{Na}} FV = z_{\mathrm{Na}} F(\widehat{V}_{\mathrm{Na}} - V) \\ \Delta G_{\mathrm{Ca}} &= RT \ln \frac{Ca_{\mathrm{e}}}{Ca_{\mathrm{i}}} - z_{\mathrm{Ca}} FV = z_{\mathrm{Ca}} F(\widehat{V}_{\mathrm{Ca}} - V) \end{aligned}.$$

Theoretically, for a system in which the flux of one calcium ion is coupled to the counter flow of sodium ions, the transport would be favourable when:

$$z_{\mathrm{Na}} \Gamma_{\mathrm{naca}} (\widehat{V}_{\mathrm{Na}} - V) > z_{\mathrm{Ca}} (\widehat{V}_{\mathrm{Ca}} - V),$$

where, Γ_{naca} is the coupling coefficient (no. of moles of sodium transported for a mole of calcium), typically 3. The effective reversal potential, a result of the gradient of sodium in the forward direction and the gradient of calcium in the reverse direction, is $V_{\mathrm{naca}} = (\Gamma_{\mathrm{naca}} \widehat{V}_{\mathrm{Na}} - 2\widehat{V}_{\mathrm{Ca}})/(\Gamma_{\mathrm{naca}} - 2)$.

The directionality of transport is defined by the apparent driving force ($V_{\mathrm{naca}} - V$). Calcium efflux would be favoured when $V_{\mathrm{naca}} > V$ and in the opposite

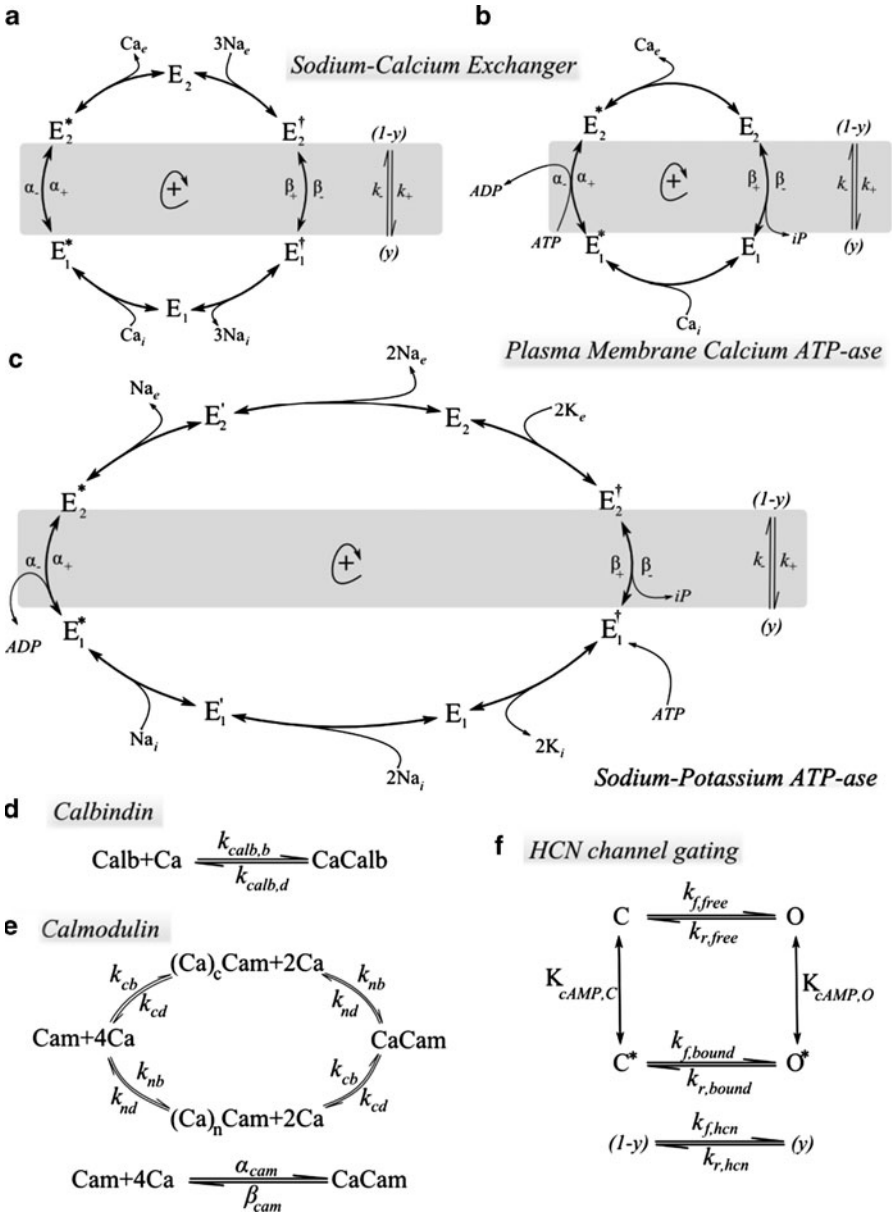

Fig. 5.1 (**a**–**c**) Schemes of different facilitated transport used in the model. (**d**–**e**) Dynamics of calcium buffering. (**f**) Scheme for the gating dynamics of HCN channel

case, calcium entry to the cell would be favoured. Under normal physiological conditions, V_{naca} is more positive than the resting membrane potential; the exchanger will work in Ca extrusion/Na influx mode in resting neurons. During an action potential, NaCax briefly works in Ca entry/Na exit mode.

NaCax has been popularly represented by models that incorporate the voltage dependence and approximate the affinity of the proteins to the cations [1, 21]. There have also been attempts to represent the NaCax function by entirely electrogenic models (for example, [9]). Such models ignore the limits imposed by the binding of ions to these proteins. For instance, the concentration of calcium within the cell is quite small, (around 100 nM), a figure that is 10,000 times lower than extra-neuronal calcium [7]. Hence, it is quite possible that the net rate of transport is limited by the binding of intracellular calcium to the transporter. The electrogenicity of these transporters is primarily associated with sodium translocation [31] and probably a minor component arising from calcium occlusion/deocclusion. Models by Powell et al. [31], and more recently, Matsuoka et al. [24], employ Markov concepts to model NaCax. Assuming that the membrane-crossing step of the process to be rate-limiting, this model lumps a few states together to give a two-state transition process (Fig. 5.1a). We have adapted this representation for our model (see Appendix).

The Plasma Membrane Calcium ATPase

The PMCA is a membrane protein responsible for the efflux of calcium ions against its gradient and is powered by the energy associated with the hydrolysis of an ATP molecule. It has a high affinity for calcium (with K_{m} of 100–200 nM), but does not remove calcium at a very fast rate.

The active transport of calcium ions mediated by these proteins may be approximately represented as

$$Ca_{\text{i}}^{2+} + Mg \cdot \text{ATP} \underset{H_2O}{\longleftrightarrow} Ca_{\text{e}}^{2+} + Mg \cdot \text{ADP} + i\text{P}.$$

The free energy changes significant to this transport are

$$\begin{aligned} \Delta G_{\text{Ca}} &= RT \ln \frac{Ca_{\text{e}}}{Ca_i} - z_{\text{Ca}} FV = z_{\text{Ca}} F(\widehat{V}_{\text{Ca}} - V) \\ \Delta G_{\text{atp}} &= -RT \ln(\kappa_{\text{atp}}) = RT \ln \frac{[Mg \cdot \text{ADP}][i\text{P}]}{[Mg \cdot \text{ATP}]} = FV_{\text{atp}} \end{aligned} \tag{5.13}$$

where κ_{atp} is the equilibrium constant for ATP hydrolysis (approximately 10^5 M). V_{atp} is a voltage equivalent of the hydrolytic energy. Reported values for neuronal cytoplasmic ATP–ADP ratio tend to be between 10 and 100 [4, 25] and in vitro studies suggest a Mg·ATP–Mg·ADP ratio around 2,300 [22]. The inorganic

phosphate concentration average is around 10 mM (An experiment in cardiac cells by [47], shows that it varies between 0.3 and 18 mM). Accordingly, the value of V_{atp} is roughly −330 mV at normal physiological temperatures. (The value used in [9], is around −450 mV, which would push the ATP–ADP ratio to a high value).

Transport is feasible when it is favourably coupled to the energy from ATP hydrolysis, or when $\Gamma_{pmca}\Delta G_{atp} > \Delta G_{Ca}$; Γ_{pmca} being the coupling coefficient (our model employs Γ_{pmca} value of 1, i.e. one mole of ATP per mole of calcium transported). For the condition of feasibility, the apparent driving energy would be

$$\Delta G_{pmca} = F\left(V_{atp} + 2\widehat{V}_{Ca} - 2V\right).$$

Since V_{atp} is much larger than other terms in the equation, the voltage dependence of the pump is apparently small. There are only two ways that net transport can be voltage dependent: either a rate-limiting step in the transport cycle is itself voltage dependent or a voltage-dependent step controls the level of the enzyme intermediate entering the rate-limiting step.

An important feature of PMCA activity is its regulation by the calcium signalling protein calmodulin (CaM). CaM reversibly binds and activates PMCA in a calcium-dependent manner. This association is regarded as stimulating the release of an auto-inhibitory domain from the ATP-binding site of PMCA [29], thereby increasing its affinity and turnover rate.

The mathematical representation of PMCA's function has often been by simple equations similar to the one in the Luo–Rudy model [21]. These models represent the pump in terms of a binding process between the ions and the protein. Models using Markov principles can elaborate the binding process, since they incorporate voltage dependence if needed and can also incorporate finer details of the mechanism, such as the influence of calmodulin on PMCA activity. The Kyoto model [24] is a four-state illustration of the transport mechanism of PMCA. This is further reduced to a two-state model by assuming fast binding of calcium ions (Fig. 5.1b). Based on the Kyoto model, PMCA behaviour is described as shown in the appendix.

The Sodium–Potassium ATPase

The sodium pump, or Na^+/K^+ ATPase, is responsible for the formation and maintenance of electrochemical gradient in animal cells. The enzyme transports three ions of sodium from, and two potassium into, the intracellular space for every molecule of ATP hydrolyzed. The apparent driving potential for this transport is

$$\Delta G_{nak} = F(V_{atp} + 3\widehat{V}_{Na} - 2\widehat{V}_{K} - V).$$

As in the case of PMCA, a large V_{atp} would suggest that the pumps' voltage dependence is negligible. Experiments indicate that dependence of membrane potential on pump rate is seen only in the presence of external sodium. [34]

elaborates on this observation based on a molecular system that assigns the voltage dependence of the pump to the step at which the first sodium ion is released to the outside (Fig. 5.1c).

The sodium pump exists in two conformational states characterized by differences in their interactions with the ions and ATP. Sodium and ATP bind with very high affinity on to the E1 conformation. Equilibrium binding of two sodium ions facilitates the electrogenic binding of the third sodium ion. The phosphorylation of the enzyme in this bound state leads to a conformational change, which renders the sodium ions open to the external space. Unbinding and release of sodium ions leads to the binding of potassium ions on to the E2 conformation. This then leads to the dephosphorylation of the enzyme and a conformational change. The equilibrium binding of the ATP molecule to this structure promotes the release of the potassium ions and completes the cycle. Our model of the sodium pump (based on the model by [24]) incorporates these concepts.

Buffering of Intracellular Calcium

Calcium-dependent signalling pathways control several cellular processes [28]. Hence, it is essential for the cell to regulate the levels of intracellular calcium. In particular, in addition to being spatially limited, calcium extrusion systems are too slow to deal with a sudden upsurge of calcium, so that calcium buffering mechanisms within the cell are required to cushion such effects. Intracellular uptake of calcium is handled by mobile buffers such as calbindin and ultimately by organelles, such as the endoplasmic reticulum and mitochondria, which act as fixed buffers.

The dopaminergic neurons of *SNc* do not have a particularly high intrinsic calcium binding capacity; according to observations of Foehring et al. [10], up to 1% of calcium entering the neuron remains free at steady state. These neurons are known to express traditional calcium binding proteins and data suggests that neurons of the *SNc* that express high levels of calbindin are less vulnerable to PD damage [49].

Pacemaking models of *SNc* have often taken into account the influence of buffers: for example, Amini et al. [1] take into account a single representative buffer and assume linear binding dynamics. Wilson and Callaway [46] assume that buffers are non-saturable and adopt a simple representation for the effect of both mobile and fixed buffers. Kuznetsova et al. [19] implicitly model calcium buffering by defining a control parameter that gives the fraction of free calcium in the respective compartments.

In our model, we employ the binding dynamics of two calcium-binding proteins that appear to be significant in the generation of spontaneous membrane activity. Calbindin is a fast buffer of calcium and its significance in these neurons is evident. Calmodulin, which is the primary decoder of calcium levels within the cell, is also taken into account, while levels of the calcium–calmodulin complex define other calcium-dependent mechanisms in the cell.

Table 5.2 A list of cation channel α subunits expressed in Human *substantia nigra* based on the datasets of Moran et al. [26] and Lesnick et al. [20]

Description	Gene symbol
L-type calcium channel	CACNA1C ($Ca_v1.2$), CACNA1D ($Ca_v1.3$)
T-type calcium channel	CACNA1G ($Ca_v3.1$),CACNA1I ($Ca_v3.3$)
P/Q-type calcium channel	CACNA1A ($Ca_v2.1$)
N-type calcium channel	CACNA1B ($Ca_v2.2$)
Sodium channel	SCN1A ($Na_v1.1$), SCN2A ($Na_v1.2$), SCN3A ($Na_v1.3$), SCN9A ($Na_v1.9$), SCN11A ($Na_v1.11$)
Leak channels	NALCN (Voltage-independent, nonselective channel mostly responsible for sodium leak)
Potassium delayed rectifier	KCNA1 ($K_v1.1$, Shaker-related), KCNA6 ($K_v1.6$, Shaker-related), KCNB1 ($K_v2.1$, Shab-related), KCNC1 ($K_v3.1$, Shaw-related), KCNC4 ($K_v3.4$, Shaw-related)
A-type potassium channel	KCND2 ($K_v4.2$, Shal-related), KCND3 ($K_v4.3$, Shal-related)
Inward-rectifying potassium channel	KCNJ2 ($K_{ir}2.1$), KCNJ10 ($K_{ir}4.1$), KCNJ14 ($K_{ir}2.4$), KCNH2 ($K_v11.1$), KCNH7 ($K_v11.3$)
G protein-coupled inwardly rectifying potassium channel	KCNJ6 ($K_{ir}3.2$), KCNJ9 ($K_{ir}3.3$)
Calcium-activated potassium channel	KCNN2 ($K_{ca}2.2$, SK), KCNN3 ($K_{ca}2.3$, SK), KCNMA1 ($K_{ca}1.1$, BK)
Tandem pore domain potassium channel	KCNK1 ($K_{2p}1.1$), KCNK10 ($K_{2p}10.1$), KCNK12 ($K_{2p}12.1$), KCNK17 ($K_{2p}17.1$)
Hyperpolarization-activated cyclic nucleotide gated channel	HCN1, HCN2, HCN4
Two pore segment channel	TPCN1, TPCN2

Choosing Model Components

Neurons of the *SNc* express a wide variety of cation channels, some of which play a significant role in the autonomous pacemaking behaviour. Based on the datasets of Moran et al. [26] and Lesnick et al. [20], Table 5.2 provides a comprehensive list of the type of cation channels expressed in the *SN* neuron on account of the α subunits expressed.

For our model (see Fig. 5.2), we select channels based on their reported influence in generating the pacemaking current [1, 19, 32, 46]. These includes a representative sodium channel, three types of calcium channels (L-type, T-type and high voltage activated (HVA) type), a calcium-dependent potassium channel (SK), three types of voltage-gated potassium channels (delayed rectifier, inward rectifier and A-type transient channel), hyperpolarization activated cyclic nucleotide gated (HCN) channel and a leakage channel. A sodium–calcium exchanger, along with a calcium and sodium pump, works towards establishing ionic gradients across the membrane. We also include two mobile calcium buffers that are important for the calcium dynamics.

For our model, we consider a single compartment representative of the soma of an acutely dissociated *SNc* neuron. Extracellular ionic concentrations are presumed

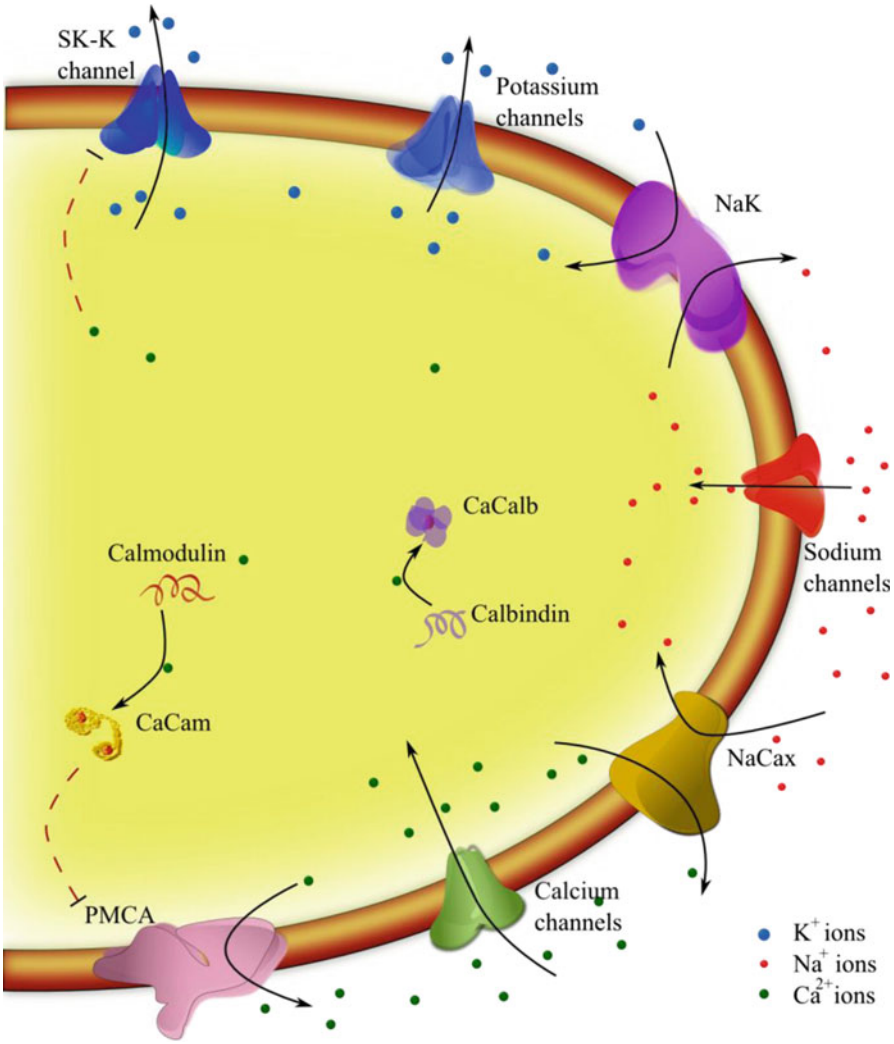

Fig. 5.2 A cartoon representation of the scheme of events considered in the model

constant and the cell is assumed to be in an osmotic equilibrium, thus rendering the cell dimensions constant.

Parameter Estimation

Puopolo et al. [32] describes spontaneous firing in dissociated dopaminergic neurons of the *SNc*, and provides useful information on sodium and calcium

Table 5.3 Numerical Parameters of the model

Parameter	Value	Units
Faraday's constant (F)	96,485.31	C/mol
Gas constant (R)	8,314.472	J/kmol K
Body temperature (T)	37	°C
z_{Ca}	2	–
z_{Na}	1	–
z_{K}	1	–
Somatic diameter	30	μm
Cytosolic volume		
Specific membrane capacitance (C_m)	0.9	μF/cm^2
Anionic offset (anoff)	−0.0118	mM
Ca_e	1.8	mM
Na_e	137	mM
K_e	5.4	mM
Buffer kinetics		
$k_{calb,b}$	10	1/(mM ms)
$k_{calb,d}$	2×10^{-3}	1/(ms)
$k_{cam,cb}$	12,000	1/(mM^2 ms)
$k_{cam,cd}$	0.003	1/(ms)
$k_{cam,nb}$	3.7×10^{6}	1/(mM^2 ms)
$k_{cam,nd}$	3	1/(ms)
Initial conditions		
Ca_i	0.00015	mM
Na_i	6	mM
K_i	140	mM
[calb]	0.0011	mM
[cam]	0.0487	mM

currents from dynamic clamp experiments. In particular, Puopolo's data can be put to use to estimate significant parameters for the corresponding ion-channels. Note that, in the data, currents of sodium and calcium are always negative. This would mean that, according to (5.4), there will be an accumulation of both cations. We therefore assume that, in these measurements, there is no contribution from the pumps or exchangers.

Parameters (Tables 5.3 and 5.4) were estimated sequentially, beginning with the data on sodium current. The sodium current, obtained from a study using Tetrodotoxin that blocks fast sodium channels, is modelled by using a Markovian gating scheme (5.11) for a representative sodium channel. Calcium channels, however, have varied voltage dependences, and hence, their contribution to the calcium current needs to be accounted for separately. Again, the nature of the available data makes it difficult to estimate all parameters for calcium channels in an identifiable manner. Because of this, gating models of the T-type and HVA calcium channel were adopted from the literature. Parameters for the Hodgkin–Huxley

Table 5.4 Model parameters used to fit the data

Parameter	Value	Units
Channel conductances		
g_{Na}	395.14	pA/mM
$g_{Na,leak}$	0.0039	pA/mM
$g_{Na,HCN}$	3	pA/mM
$g_{Ca,L}$	1158.2	pA/mM
$g_{Ca,T}$	10	pA/mM
$g_{Ca,HVA}$	78.5	pA/mM
$g_{K,sk}$	15	pA/mM
$g_{K,HCN}$	7	pA/mM
$\gamma_{k,dr}$	10	pA/mV
$\gamma_{k,a}$	0.2234	pA/mV
$\gamma_{k,ir}$	5	pA/mV
Transporter conductances		
k_{naca}	25	pA ms
k_{pmca}	10	pA ms
k_{nak}	200	pA ms
Buffers		
$[calb]_{total}$	0.002	mM
$[cam]_{total}$	0.0489	mM

gating of low voltage activated L-type channels ($Ca_v1.3$) were identified from experimental data. The HVA current is representative of the high voltage activated L-type channel ($Ca_v1.2$), and P/Q type channel.

In the next stage, parameters for the cation pumps, exchanger and potassium channels were estimated by fitting against the command voltage used for generating the current characteristics. To avoid identifiability issues, the number of potassium channel types was kept to a minimum and their parameters adopted from the literature.

Although the use of a linear conductance model is more popular, the GHK equation is better suited when mass fluxes are concerned. Again, the same gating parameters of a channel can evoke moderately different responses when used along with the two separate formulations for channel current. For this reason, we employ the linear conductance relation (5.6) to express only those channel currents in our model for which the gating parameters correspond to models in the literature that employ the linear relationship. For the rest we employ the GHK equation (5.7).

Model Outcomes

Currently available models of pacemaking in *SNc* have adequately represented experimental studies with pharmacological manipulations and reproduced significant features of neuronal functions. However, the influence of molecular entities

that balance the flux of important cations, namely, the pumps, exchangers and buffers, are mostly ignored in these models.

In addition, the electrical activity of an individual neuron is frequently represented by means of the dynamics of the membrane potential. However, this overlooks the fact that membrane potential is directly determined by the membrane capacitance and ionic concentrations. The response of the system is ultimately dependent on electrical forces and molecular diffusion. For this reason, our model is based on the dynamics of the important ions involved, rather than dynamics of membrane voltage. As a result, in common with other electrophysiological models of membrane potential in the algebraic form [9, 15, 30], our model provides more representative insights into the processes involved.

Some Important Features of the Model

Regular Pacemaking

The role of calcium as the major charge carrier for spontaneous pacemaking in *SNc* neurons has been demonstrated by various studies involving pharmaceutical blockers, as well as experiments involving calcium imaging [16, 46]. Results (shown Fig. 5.3b) that fit our model, confirm that L-type calcium channels that open at relatively depolarized membrane potentials ($Ca_v1.3$) are the most crucial in driving spontaneous pacemaking [33]. From the calcium data fits, the contribution from the L-type calcium channel appeared to be the most important. The HVA calcium channels, however, seem to have a small role in supporting the somatic calcium spikes. The T-type calcium channels apparently have a limited role during spiking; however, they were important in maintaining the levels of calcium during the interspike interval. According to Verkhratsky and Toescu [44], among excitatory neurons, L-type calcium channels are predominantly harboured in the soma, whereas the high voltage activated N and P/Q calcium channels are mostly observed on dendrites and presynaptic terminals. Hence, it is possible that the HVA current of the soma is mostly due to the high voltage activated L-type channel ($Ca_v1.2$) rather than P/Q type channels.

The contribution of the different currents in generating the spontaneous pacemaking is shown in Fig. 5.4a. The role of calcium currents in the generation of oscillation has been demonstrated by blocking the fast sodium currents by the application of Tetrodotoxin (TTX) (Fig. 5.4b). The TTX blocking action is implemented in our model by setting the value of g_{Na} to zero. This leads to the change of oscillations from a spike-firing mode to slow oscillatory potential as demonstrated in previous experiments [1, 16].

Another important feature that may be noticed (and as mentioned by [6]) is that the neurons can switch back to spontaneous pacemaking even without relying on the L-type channel. An increase in the level of *cyclic adenosine monophosphate* (cAMP) activates the HCN channels to a higher degree and makes them drive

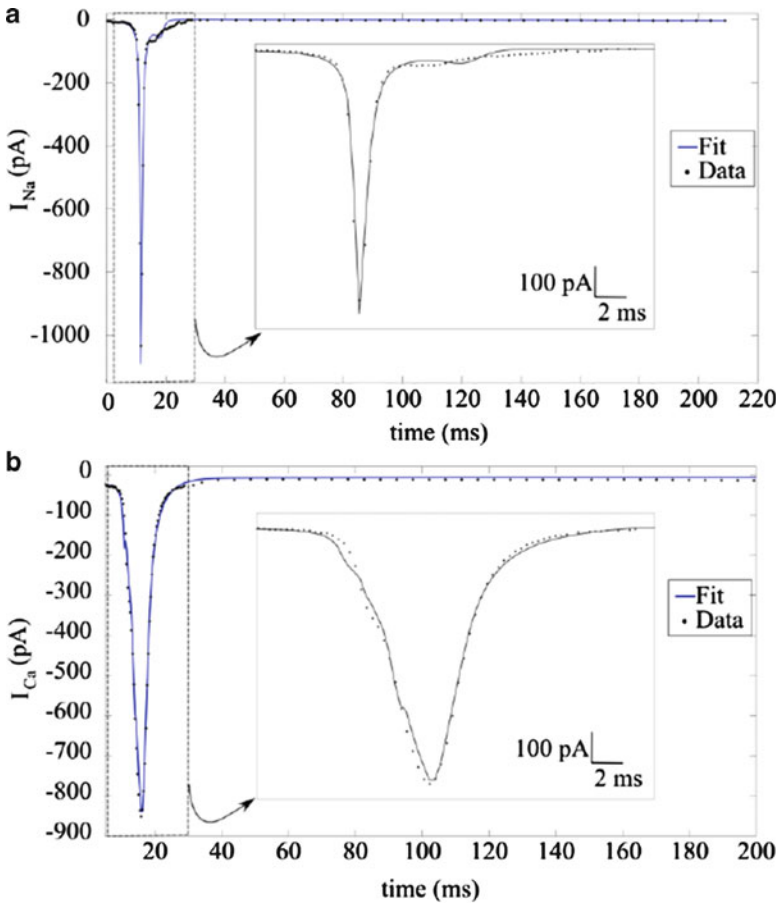

Fig. 5.3 Data fits of currents in acutely dissociated *SNc* neurons determined using the action potential clamp technique (**a**) Fitting of the Tetrodotoxin-sensitive sodium current using Markovian gating dynamics and GHK current equation (**b**) Fitting of the cobalt-sensitive current by employing Hodgkin–Huxley type gating dynamics and GHK current equation

pacemaking (Fig. 5.4c). As we shall see later, this switch could have important energy implications.

Estimates of Energy Use

A quantitative understanding of the energy expenditure in a neuron can be generated by calculation of ATP consumption. Attwell and Laughlin [2] use such calculations to compare different functional aspects of neuronal signalling. In this section, ATP utilization by membrane transport proteins is analyzed.

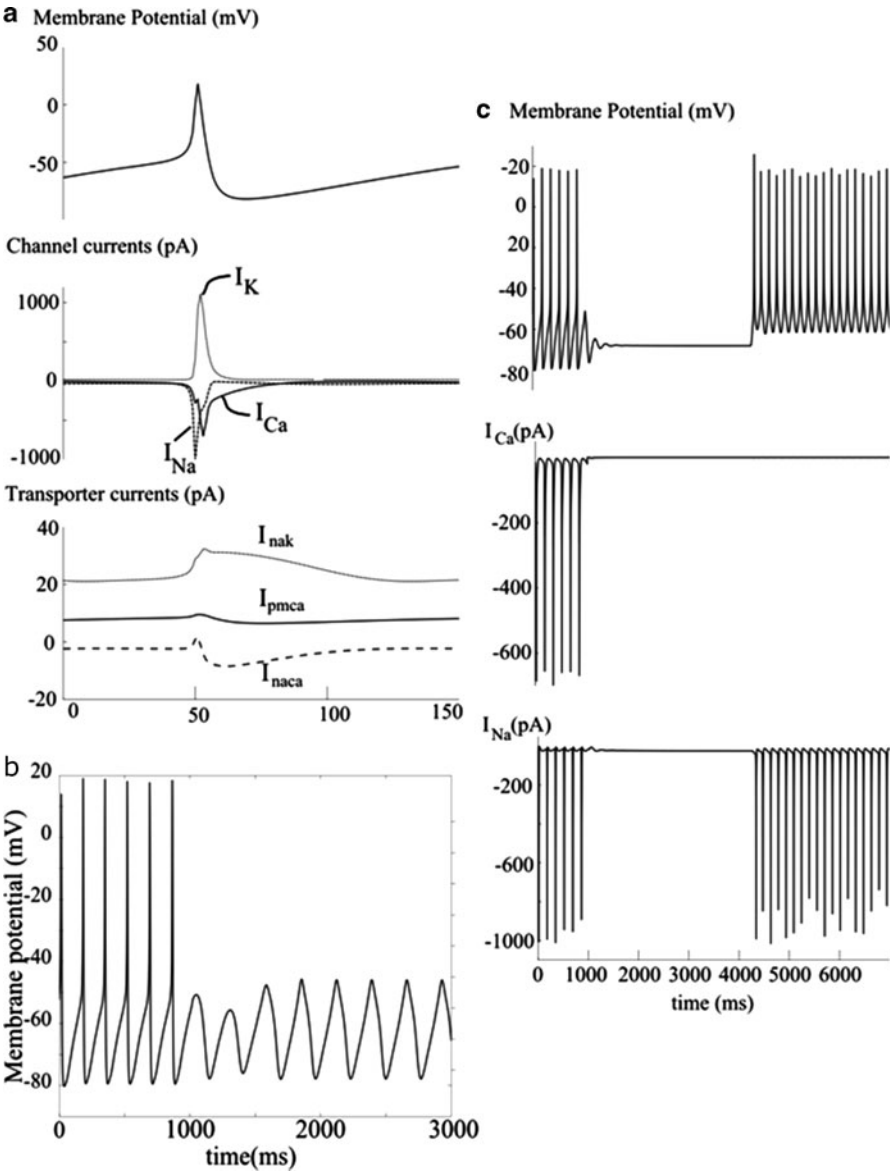

Fig. 5.4 (**a**) Simulated response of the model: Membrane potential, Channel currents contributing to the pacemaking for a single spike and corresponding currents from the molecular transport mechanisms responsible for maintaining ionic fluxes. (**b**) Simulated block of fast sodium current by TTX (gNa is set to zero from 1,000 ms). (**c**) Simulated block of L-type and HVA calcium channels. (gCa,L and gCa,hva are set to zero from 1,000 ms, an increase in cAMP concentration at 4,200 ms revives the pacemaking, now driven by sodium currents activated by the HCN channels)

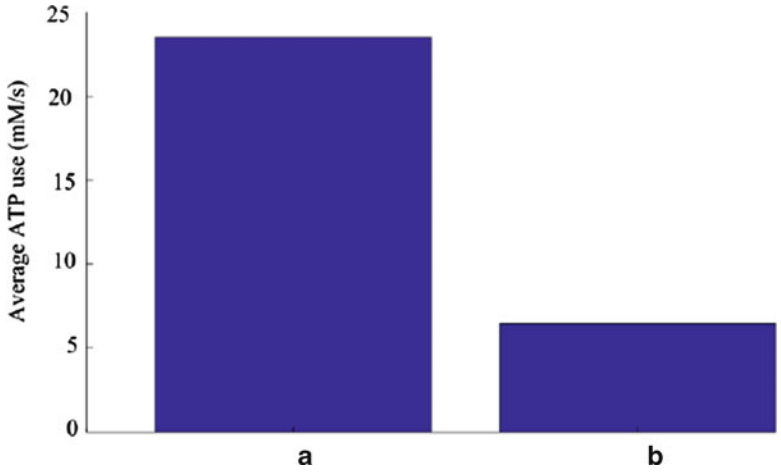

Fig. 5.5 Average energy usage by membrane transport proteins calculated from the model (**a**) Normal pacemaking mode of *SNc* neurons when the L-type calcium current drives pacemaking (**b**) Pacemaking is driven by the HCN channels when the L-type calcium channels are blocked

If $\mathrm{ATP}_{\mathrm{spike}}$ represents the ATP consumed per spike by the *SNc* neuron, we may represent it as:

$$\mathrm{ATP}_{\mathrm{spike}} = \frac{1}{F v_{\mathrm{cyt}}} \int_0^{T_{\mathrm{spike}}} (I_{\mathrm{nak}} + I_{\mathrm{pmca}}) \mathrm{d}t. \tag{5.14}$$

Figure 5.5 shows the variations of average ATP use by the pumps calculated from the model. In particular, it shows that there is a substantial reduction in the use of energy when the neurons pace-make in a calcium-dependent manner, compared to when they pace-make under the influence of sodium fluctuations via HCN channels. This reduction in energy requirement supports the recent proposal [7, 12] to use hypertensive drugs that blocking L-type calcium channels as a preventive measure against the progression of PD in prospective patients. Our energy budget predictions in Fig. 5.5 suggest that this would reduce the energy stress on vulnerable *SNc* neurons through a reduced calcium entry. However, the reduced calcium entry may have other biochemical implications.

Conclusions

The tonic firing by the *SNc* dopaminergic neurons play a crucial role in motor activity control in mammals. However, the dependence of this activity on calcium ions makes these cells particularly vulnerable to calcium-dependent pathophysiology [40].

The study described in this chapter, examines these issues in silico, through a mathematical model of calcium metabolism in *SNc* neurons. In particular, we incorporate the flux balance mechanisms of the neuron in detail by the use of algebraic forms of voltage expression (5.1). This contrasts with previous work in which models of pacemaking in the *SNc* have been based on the differential method [1, 19].

Our advocacy of modelling with the algebraic form brings into focus the transport aspects of contributing ions and easily relates to various aspects of cellular function, including energetics. Most significantly, the study reported here confirms the notion that calcium-driven pacemaking of *SNc* comes with a high energy requirement. It has been shown when the L-type calcium channels are blocked, then *SNc* neurons are able to maintain pacemaking with the help of HCN channels. We show that blocking the L-type calcium channel significantly reduces energy stress in the neuron in a way that may have a neuroprotective affect, thus supporting the notion of calcium channel blocking as a PD therapy.

A general question that needs to be answered is this: why do *SNc* neurons resort to a process that apparently strains its resources and creates an important potential stress factor for degeneration? In this context, an interesting aspect of *SNc* pacemaking is its reliance on the voltage-independent calcium activated SK channels in regulating the frequency of the spike train. As demonstrated by Drion et al. [8], these channels act as a filter of external excitatory signals and preserve the endogenous rhythm in these neurons. Furthermore, in Chap. 4 of this volume, Drion et al. also demonstrate how these channels are critical for these neurons to retain their individuality and how their absence would lead to synchronization of the neuronal network. In contrast, these channels would have hardly any role in maintaining the frequency of sodium driven pacemaking. Hence, when *SNc* neurons are deprived of the L-type channel activity, an increase in cAMP levels is sufficient to return these neurons to pacemaking, but at the cost of being sensitive to excitatory inputs and synchrony among these neurons. Furthermore, a sustained high cAMP will activate protein kinase A, which is involved in the regulation of multiple metabolic processes, include energy metabolism. This suggests an intricate linkage between calcium regulation and metabolism that requires further analysis.

The model we have described here does not account for all features exhibited by the *SNc* neuron pacemaker. It is only representative of the ion-channels expressed in neurons based on the data from Puopolo et al. [32]. Including more ion-channels would give more degrees of freedom to get precise fits to data, but at the expense of the model's complexity, identifiability and ultimately its predictive ability.

Available models on *SNc* pacemaking do not pay much attention to the energy aspects of the activity even though they partially contribute in developing a framework for molecular pathogenesis in PD. As a multifactorial condition, PD pathogenesis needs to be studied by giving due consideration to all sub-systems that contribute to the condition. In this spirit, our model is a step in building a larger framework to analyze the pathology from a systems perspective [45].

Acknowledgments Work support by Science Foundation Ireland, grant SFI 07/IN.1/I1838.

Appendix: Model Formulation

Membrane Dynamics

Membrane potential

$$V = \frac{Fv_{\text{cyt}}}{C_{\text{m}}}[K_{\text{i}} - K_{\text{e}} + Na_{\text{i}} - Na_{\text{e}} + 2(Ca_{\text{i}} - Ca_{\text{e}}) + an_{\text{offset}}]. \tag{5.15}$$

Intracellular cations

$$\begin{aligned}
\frac{\mathrm{d}Ca_i}{\mathrm{d}t} &= \frac{1}{z_{\text{Ca}}Fv_{\text{cyt}}}\left[I_{\text{Ca}} + 2I_{\text{pmca}} - 2I_{\text{naca}}\right] - (J_{\text{calb}} + 4J_{\text{cam}}) \\
\frac{\mathrm{d}Na_i}{\mathrm{d}t} &= \frac{1}{z_{\text{Na}}Fv_{\text{cyt}}}\left[I_{\text{Na}} + 3I_{\text{nak}} + 3I_{\text{naca}}\right] \\
\frac{\mathrm{d}K_i}{\mathrm{d}t} &= \frac{1}{z_{\text{K}}Fv_{\text{cyt}}}\left[I_{\text{K}} - 2I_{\text{nak}}\right]
\end{aligned} \tag{5.16}$$

Membrane currents from ion-channels

$$\begin{aligned}
I_{\text{Ca}} &= \left[\sum_{\text{c}} g_{\text{Ca,c}}O_{\text{Ca,c}}\right]\sqrt{Ca_{\text{e}}Ca_{\text{i}}}\frac{\sin\text{h}\left(\left(V - \widehat{V}_{\text{Ca}}\right)/V_{\tau}\right)}{\sin\text{h}c(V/V_{\tau})} \\
I_{\text{Na}} &= \left[\sum_{\text{c}} g_{\text{Na,c}}O_{\text{Na,c}}\right]\sqrt{Na_{\text{e}}Na_{\text{i}}}\frac{\sin\text{h}\left(\left(V - \widehat{V}_{\text{Na}}\right)/2V_{\tau}\right)}{\sin\text{h}c(V/2V_{\tau})} \\
I_{\text{K}} &= \left[\sum_{\text{c}} g_{\text{K,c}}O_{\text{K,c}}\right]\sqrt{K_{\text{e}}K_{\text{i}}}\sin\text{h}\frac{\left((V - \widehat{V}_{\text{k}})/2V_{\tau}\right)}{\sin\text{h}c(V/2V_{\tau})} + \left[\sum_{\text{c}} \gamma_{\text{K,c}}O_{\text{K,c}}\right]\left(V - \widehat{V}_{\text{K}}\right)
\end{aligned} \tag{5.17}$$

Gating Dynamics

L-type calcium channel [1]

$$O_{\text{cal}} = m_{\text{cal}}h_{\text{cal}} \qquad \tau_{\text{m,cal}} = 0.943 + 10\exp\left(-\left[\frac{V + 86.4}{23.2}\right]^2\right).$$

$$m_{\infty,\text{cal}} = \left[1 + \exp\left(-\frac{V + 15}{7}\right)\right]^{-1} \qquad h_{\text{cal}} = \frac{0.00045}{0.00045 + Ca_{\text{i}}}$$

High voltage activated calcium channel [1]

$$O_{\mathrm{ca,hva}} = m_{\mathrm{ca,hva}} h_{\mathrm{ca,hva}}$$
$$m_{\infty,\mathrm{cahva}} = \left[1 + \exp\left(-\frac{V+10}{10}\right)\right]^{-1} \qquad \tau_{\mathrm{m,cahva}} = 0.05 + 0.1\exp\left(-\left[\frac{V+62}{13}\right]^2\right)$$
$$h_{\infty,\mathrm{cahva}} = \left[1 + \exp\left(\frac{V+48}{5}\right)\right]^{-1} \qquad \tau_{\mathrm{h,cahva}} = 0.5 + 0.5\exp\left(-\left[\frac{V+55.6}{18}\right]^2\right)$$

T-type calcium channel [6]

$$O_{\mathrm{cat}} = m_{\mathrm{cat}} h_{\mathrm{cat}}$$
$$m_{\infty,\mathrm{cat}} = \left[1 + \exp\left(-\frac{V+63}{1.5}\right)\right]^{-1} \qquad \tau_{\mathrm{m,cat}} = 12 + 65\exp\left(-\left[\frac{V+68}{6}\right]^2\right)$$
$$h_{\infty,\mathrm{cat}} = \left[1 + \exp\left(\frac{V+76.2}{3}\right)\right]^{-1} \qquad \tau_{\mathrm{h,cat}} = 10 + 50\exp\left(-\left[\frac{V+72}{10}\right]^2\right)$$

Sodium channel

$$O_{\mathrm{Na}} = m_{\mathrm{na}}^3 h_{\mathrm{na}} \quad \alpha_{\mathrm{mna}} = 1.965\exp\left(1.713\frac{V}{V_\tau}\right) \qquad \beta_{\mathrm{mna}} = 0.0424\exp\left(-1.558\frac{V}{V_\tau}\right)$$
$$\alpha_{\mathrm{hna}} = 9.566\times10^{-5}\exp\left(-2.432\frac{V}{V_\tau}\right) \quad \beta_{\mathrm{hna}} = 0.53\exp\left(1.187\frac{V}{V_\tau}\right)$$

Small conductance calcium gated potassium channel

$$O_{\mathrm{k,sk}} = \frac{Ca_{\mathrm{i}}^4}{(0.00035)^4 + Ca_{\mathrm{i}}^4}.$$

Delayed rectifier potassium channel [1]

$$O_{\mathrm{kdr}} = m_{\mathrm{kdr}}^3$$
$$m_{\infty,\mathrm{kdr}} = \left[1 + \exp\left(-\frac{V+25}{12}\right)\right]^{-1} \qquad \tau_{\mathrm{m,kdr}} = 18\left[1 + \exp\left(\frac{V+39}{8}\right)\right]^{-1} + 1$$

Transient A-type potassium channel [1]

$$O_{\mathrm{ka}} = m_{\mathrm{ka}}^3 h_{\mathrm{ka}}$$
$$m_{\infty,\mathrm{ka}} = \left[1 + \exp\left(-\frac{V+43}{24}\right)\right]^{-1} \qquad \tau_{\mathrm{m,ka}} = 1.1 + 2\exp\left(-\left[\frac{V+50}{23.45}\right]^2\right)$$
$$h_{\infty,\mathrm{ka}} = \left[1 + \exp\left(\frac{V+56}{8}\right)\right]^{-1} \qquad \tau_{\mathrm{h,ka}} = 20$$

Internal rectifying potassium channel [6]

$$O_{\mathrm{kdr}} = \left[1 + \exp\left(\frac{V+90}{12.1}\right)\right]^{-1}$$

HCN channels (based on [6]; see Fig. 5.1f)

$$O_{\mathrm{hcn}} = y \qquad \frac{\mathrm{d}y}{\mathrm{d}t} = k_{\mathrm{f,hcn}}y - k_{\mathrm{r,hcn}}(1-y)$$

$$k_{\mathrm{f,hcn}} = k_{\mathrm{f,free}}\mathrm{P}(C) + k_{\mathrm{f,bnd}}[1-\mathrm{P}(C)] \qquad k_{\mathrm{r,hcn}} = k_{\mathrm{r,free}}\mathrm{P}(O) + k_{\mathrm{r,bnd}}[1-\mathrm{P}(O)]$$

$$\mathrm{P}(C) = \left[1 + \frac{\mathrm{cAMP}}{1.163\times10^{-3}(\mathrm{mM})}\right]^{-1} \qquad \mathrm{P}(O) = \left[1 + \frac{\mathrm{cAMP}}{1.45\times10^{-3}(\mathrm{mM})}\right]^{-1}$$

$$k_{\mathrm{f,free}} = \frac{0.006}{1+\exp\left(\frac{V+87.7}{6.45}\right)} \qquad k_{\mathrm{r,free}} = \frac{0.08}{1+\exp\left(-\frac{V+51.7}{7}\right)}$$

$$k_{\mathrm{f,bnd}} = \frac{0.0268}{1+\exp\left(\frac{V+94.2}{13.3}\right)} \qquad k_{\mathrm{r,bnd}} = \frac{0.08}{1+\exp\left(-\frac{V+35.5}{7}\right)}$$

Dynamics of Facilitated Transport

Sodium–calcium exchanger (Model modified from [24])

$$I_{\mathrm{naca}} = k_{\mathrm{naca}}\left[\beta_{-}\mathrm{P}(E_1')y - \beta_{+}\mathrm{P}(E_2')(1-y)\right]. \tag{5.18}$$

$$\frac{\mathrm{d}y}{\mathrm{d}t} = k_{-}(1-y) - k_{+}y$$

$$k_{+} = \alpha_{+}\mathrm{P}(E_1^*) + \beta_{-}\mathrm{P}(E_1') \qquad k_{-} = \alpha_{-}\mathrm{P}(E_2^*) + \beta_{+}\mathrm{P}(E_2')$$

$$\mathrm{P}(E_1^*) = \left[1 + \frac{0.00138}{Ca_{\mathrm{i}}}\left(1 + \left(\frac{Na_{\mathrm{i}}}{8.75}\right)^3\right)\right]^{-1} \qquad \mathrm{P}(E_2^*) = \left[1 + \frac{1.38}{Ca_{\mathrm{e}}}\left(1 + \left(\frac{Na_{\mathrm{e}}}{87.5}\right)^3\right)\right]^{-1}$$

$$\mathrm{P}(E_1') = \left[1 + \left(\frac{8.75}{Na_{\mathrm{i}}}\right)^3\left(1 + \frac{Ca_{\mathrm{i}}}{0.00138}\right)\right]^{-1} \qquad \mathrm{P}(E_2') = \left[1 + \left(\frac{87.5}{Na_{\mathrm{e}}}\right)^3\left(1 + \frac{Ca_{\mathrm{e}}}{1.38}\right)\right]^{-1}$$

$$\alpha_{+} = \exp((1-0.32)V/V_\tau) \qquad \beta_{+} = \exp(-0.32V/V_\tau)(\mathrm{ms}^{-1})$$

$$\alpha_{-} = \exp(-0.32V/V_\tau) \qquad \beta_{-} = \exp((1-0.32)V/V_\tau)(\mathrm{ms}^{-1})$$

Plasma membrane calcium *ATP-ase*

$$I_{\text{pmca}} = k_{\text{pmca}} A_{\text{pmca}} \left[\alpha_+ \text{P}\left(E_1^*\right) y - \alpha_- \text{P}\left(E_2^*\right)(1-y)\right]. \tag{5.19}$$

$$\frac{\text{d}y}{\text{d}t} = k_-(1-y) - k_+ y$$

$$k_+ = \alpha_+ \text{P}\left(E_1^*\right) + \beta_- \text{P}(E_1) \qquad k_- = \alpha_- \text{P}\left(E_2^*\right) + \beta_+ \text{P}(E_2)$$

$$\text{P}\left(E_1^*\right) = \left[1 + \frac{k_{\text{pmca,cai}}}{Ca_i}\right]^{-1} \qquad \text{P}(E_1) = 1 - \text{P}\left(E_1^*\right)$$

$$\text{P}\left(E_2^*\right) = \left[1 + \frac{2}{Ca_e}\right]^{-1} \qquad \text{P}(E_2) = 1 - \text{P}\left(E_2^*\right)$$

$$A_{\text{pmca}} = \frac{10.56 \times [cacam]}{[cacam] + 0.00005} + 1.2(pA)$$

$$k_{\text{pmca,cai}} = \frac{(180 - 6.4) \times 10^{-5}}{1 + [cacam]/0.00005} + 6.4 \times 10^{-5}(\text{mM})$$

$$\alpha_+ = \left(1 + \frac{0.1}{[ATP]}\right)^{-1} \qquad \beta_+ = 0.001(\text{ms}^{-1})$$

$$\alpha_- = 0.001 \quad \beta_- = 1(\text{ms}^{-1})$$

Sodium–potassium *ATP-ase*

$$I_{\text{nak}} = k_{\text{nak}} \left[\alpha_+ \text{P}\left(E_1^*\right) y - \alpha_- \text{P}\left(E_2^*\right)(1-y)\right]. \tag{5.20}$$

$$\frac{\text{d}y}{\text{d}t} = k_-(1-y) - k_+ y$$

$$k_+ = \alpha_+ \text{P}\left(E_1^*\right) + \beta_- \text{P}\left(E_1'\right) \qquad k_- = \alpha_- \text{P}\left(E_2^*\right) + \beta_+ \text{P}\left(E_2'\right)$$

$$\text{P}\left(E_1^*\right) = \left[1 + \frac{4.05}{Na_{\text{i}}}\left(1 + \frac{K_{\text{i}}}{32.88}\right)\right]^{-1} \qquad \text{P}\left(E_1'\right) = \left[1 + \frac{32.88}{K_{\text{i}}}\left(1 + \frac{Na_{\text{i}}}{4.05}\right)\right]^{-1}$$

$$\text{P}\left(E_2^*\right) = \left[1 + \frac{69.8}{Na_{\text{eff}}}\left(1 + \frac{K_{\text{e}}}{0.258}\right)\right]^{-1} \qquad \text{P}\left(E_2'\right) = \left[1 + \frac{0.258}{K_{\text{e}}}\left(1 + \frac{Na_{\text{eff}}}{69.8}\right)\right]^{-1}$$

$$Na_{\text{eff}} = Na_{\text{e}} \exp(-0.82V/V_\tau)$$

$$\alpha_+ = 0.37\left(1 + \frac{0.094}{[ATP]}\right)^{-1} \qquad \beta_+ = 0.165(\text{ms}^{-1})$$

$$\alpha_- = 0.04 \qquad \beta_- = 0.01(\text{ms}^{-1})$$

Buffer Dynamics

Calbindin

The dynamics of binding of calcium to the fast buffer, calbindin is modelled using mass action kinetics (Fig. 5.1d) and the kinetic parameters for the high affinity binding adopted from Nagerl et al. [27],

$$J_{\text{calb}} = k_{\text{calb,b}}[Ca]_{\text{i}}[Calb] - k_{\text{calb,d}}[cacalb].$$

Calmodulin

Calcium has four binding sites on calmodulin. Two of these are located on the C-terminal lobe and two on the N-terminal. However, the binding and dissociation rates to each of these lobes are different. We model the simultaneous binding of calcium [42] as a four state Markov process, and further reduce the model to two states, assuming quasi-steady state for the intermediary states (Fig. 5.1e).

$$J_{\text{cam}} = \alpha_{\text{cam}}[Cam] - \beta_{\text{cam}}[cacam]$$

$$\alpha_{\text{cam}} = k_{\text{cb}}k_{\text{nb}}\left[\frac{1}{k_{\text{cb}} + k_{\text{nd}}} + \frac{1}{k_{\text{cd}} + k_{\text{nb}}}\right] \qquad \beta_{\text{cam}} = k_{\text{cd}}k_{\text{nd}}\left[\frac{1}{k_{\text{cb}} + k_{\text{nd}}} + \frac{1}{k_{\text{cd}} + k_{\text{nb}}}\right]$$

$$k_{\text{cb}} = k_{\text{cam,cb}}[Ca]_{\text{i}}^2 \qquad k_{\text{nb}} = k_{\text{cam,nb}}[Ca]_{\text{i}}^2$$

References

1. Amini B, Clark J Jr, Canavier C (1999) Calcium dynamics underlying pacemaker-like and burst firing oscillations in midbrain dopaminergic neurons: a computational study. J Neurophysiol 82(5):2249
2. Attwell D, Laughlin SB (2001) An energy budget for signalling in the grey matter of the brain. J Cereb Blood Flow Metab 21:1133–1145
3. Blaustein MP, Lederer WJ (1999) Sodium/calcium exchange: Its physiological implications. Physiol Rev 79(3):763–854
4. Brown GC (1992) Control of respiration and ATP synthesis in mammalian mitochondria and cells. Biochem J 284(Pt 1):1–13
5. Canavier CC, Landry RS (2006) An increase in ampa and a decrease in SK conductance increase burst firing by different mechanisms in a model of a dopamine neuron in vivo. J Neurophysiol 96(5):2549–2563. doi:10.1152/jn.00704.2006
6. Chan CS, Guzman JN, Ilijic E, Mercer JN, Rick C, Tkatch T, Meredith GE, Surmeier DJ (2007) 'Rejuvenation' protects neurons in mouse models of Parkinson's disease. Nature 447:1081–1086
7. Chan CS, Gertler TS, Surmeier DJ (2009) Calcium homeostasis, selective vulnerability and Parkinson's disease. Trends Neurosci 32:249–256

8. Drion G, Massotte L, Sepulchre R, Seutin V (2011) How modeling can reconcile apparently discrepant experimental results: the case of pacemaking in dopaminergic neurons. PLoS Comput Biol 7(5):e1002050. doi:10.1371/journal.pcbi.1002050
9. Endresen LP, Hall K, Hoye JS, Myrheim J (2000) A theory for the membrane potential of living cells. Eur Biophys J 29:90–103
10. Foehring R, Zhang X, Lee J, Callaway J (2009) Endogenous calcium buffering capacity of substantia nigral dopamine neurons. J Neurophysiol 102(4):23–26
11. Green DR, Wang R (2010) Calcium and energy: making the cake and eating it too? Cell 142:200–202
12. Guzman JN, Sánchez-Padilla J, Chan CS, Surmeier DJ (2009) Robust pacemaking in substantia nigra dopaminergic neurons. J Neurosci 29:11011–11019
13. Guzman JN, Sanchez-Padilla J, Wokosin D, Kondapalli J, Ilijic E, Schumacker PT, Surmei-er DJ (2010) Oxidant stress evoked by pacemaking in dopaminergic neurons is attenuated by DJ-1. Nature 468:676–680
14. Hodgkin AL, Huxley AF (1952) A quantitative description of membrane current and its application to conduction and excitation in nerve. J Physiol 117(4):500–544
15. Hund TJ, Kucera JP, Otani NF, Rudy Y (2001) Ionic charge conservation and long-term steady state in the Luo-rudy dynamic cell model. Biophys J 81:3324–3331
16. Ibanez-Sandoval O, Carrillo-Reid L, Galarraga E, Tapia D, Mendoza E, Gomora JC, Aceves J, Bargas J (2007) Bursting in substantia nigra pars reticulata neurons in vitro: possible relevance for Parkinson disease. J Neurophysiol 98:2311–2323
17. Izhikevich E (2007) Dynamical systems in neuroscience: the geometry of excitability and bursting. Computational neuroscience, MIT Press
18. Komendantov AO, Komendantova OG, Johnson SW, Canavier CC (2004) A modeling study suggests complementary roles for gabaa and nmda receptors and the SK channel in regulating the firing pattern in midbrain dopamine neurons. J Neurophysiol 91(1):346–357
19. Kuznetsova AY, Huertas MA, Kuznetsov AS, Paladini CA, Canavier CC (2010) Regulation of firing frequency in a computational model of a midbrain dopaminergic neuron. J Comput Neurosci 28(3):389–403
20. Lesnick TG, Papapetropoulos S, Mash DC, Ffrench-Mullen J, Shehadeh L, de Andrade M, Henley JR, RoccaWA AJE, Maraganore DM (2007) A genomic pathway approach to a complex disease: axon guidance and Parkinson disease. PLoS Genet 3(6):e98
21. Luo C, Rudy Y (1994) A dynamic model of the cardiac ventricular action potential. i. Simulations of ionic currents and concentration changes. Circ Res 74(6):1071
22. Manchester KL (1980) Free energy atp hydrolysis and phosphorylation potential. Biochem Educ 8(3):70–72. doi:10.1016/0307-4412(80)90043-6
23. Matsuda W, Furuta T, Nakamura KC, Hioki H, Fujiyama F, Arai R, Kaneko T (2009) Single nigrostriatal dopaminergic neurons form widely spread and highly dense axonal arborizations in the neostriatum. J Neurosci 29:444–453
24. Matsuoka S, Jo H, Kuzumoto M, Takeuchi A, Saito R, Noma A (2007) Modeling energetics of ion transport, membrane sensing and systems biology of the heart, Wiley-VCH Verlag GmbH & Co. KGaA, pp 435–455. DOI 10.1002/9783527621095.ch13
25. McLaughlin BA, Nelson D, Erecinska M, Chesselet MF (1998) Toxicity of dopamine to striatal neurons in vitro and potentiation of cell death by a mitochondrial inhibitor. J Neurochem 70:2406–2415
26. Moran L, Duke D, Deprez M, Dexter D, Pearce R, Graeber M (2006) Whole genome expression profilling of the medial and lateral substantia nigra in parkinsons disease. Neurogenetics 7:1–11
27. Nagerl UV, Novo D, Mody I, Vergara JL (2000) Binding kinetics of calbindin-D(28 k) determined by flash photolysis of caged Ca^{2+}. Biophys J 79:3009–3018
28. Nelson D, Cox M (2004) Lehninger principles of biochemistry. v. 116–202, W.H. Freeman
29. Osborn KD, Zaidi A, Mandal A, Urbauer RJ, Johnson CK (2004) Single-molecule dynamics of the calcium-dependent activation of plasma-membrane Ca^{2+}-ATPase by calmodulin. Biophys J 87:1892–1899

30. Poignard C, Silve A, Campion F, Mir LM, Saut O, Schwartz L (2011) Ion fluxes, transmembrane potential, and osmotic stabilization: a new dynamic electrophysiological model for eukaryotic cells. Eur Biophys J 40:235–246
31. Powell T, Noma A, Shioya T, Kozlowski RZ (1993) Turnover rate of the cardiac Na^+-Ca^{2+} exchanger in guinea-pig ventricular myocytes. J Physiol (Lond) 472:45–53
32. Puopolo M, Raviola E, Bean B (2007) Roles of subthreshold calcium current and sodium current in spontaneous firing of mouse midbrain dopamine neurons. J Neurosci 27(3):645
33. Putzier I, Kullmann PH, Horn JP, Levitan ES (2009) Cav1.3 Channel voltage dependence, not Ca2+ selectivity, drives pacemaker activity and amplifies bursts in nigral dopamine neurons. J Neurosci 29:15414–15419
34. Rakowski RF, Gadsby DC, De Weer P (1997) Voltage dependence of the Na/K pump. J Membr Biol 155:105–112
35. Schapira AH, Cooper JM, Dexter D, Jenner P, Clark JB, Marsden CD (1989) Mitochondrial complex I deficiency in Parkinson's disease. Lancet 1:1267
36. Schultz S (1980) Basic principles of membrane transport. IUPAB biophysics series, Cambridge University Press
37. Sedova M, Blatter LA (1999) Dynamic regulation of Ca^{2+} by plasma membrane Ca^{2+}-ATPase and Na^+/Ca^{2+} exchange during capacitative Ca^{2+} entry in bovine vascular endothelial cells. Cell Calcium 25:333–343
38. Sherer TB, Betarbet R, Greenamyre JT (2002) Environment, mitochondria, and Parkinson's disease. Neuroscientist 8:192–197
39. Silva NL, Pechura CM, Barker JL (1990) Postnatal rat nigrostriatal dopaminergic neurons exhibit five types of potassium conductances. J Neurophysiol 64:262–272
40. Surmeier DJ (2007) Calcium, ageing, and neuronal vulnerability in Parkinson's disease. Lancet Neurol 6:933–938
41. Surmeier DJ, Guzman JN, Sanchez-Padilla J (2010) Calcium, cellular aging, and selective neuronal vulnerability in Parkinson's disease. Cell Calcium 47:175–182
42. Tadross MR, Dick IE, Yue DT (2008) Mechanism of local and global Ca^{2+} sensing by calmodulin in complex with a Ca^{2+} channel. Cell 133:1228–1240
43. Varghese A, Boland L (2002) Computing transient gating charge movement of voltage-dependent ion channels. J Comput Neurosci 12(2):123–137
44. Verkhratsky A, Toescu E (1998) Integrative aspects of calcium signalling, Plenum Press
45. Wellstead P, Cloutier M (2011) An energy systems approach to Parkinson's disease. Wiley Interdiscip Rev Syst Biol Med 3:1–6
46. Wilson C, Callaway J (2000) Coupled oscillator model of the dopaminergic neuron of the substantia nigra. J Neurophysiol 83(5):3084–3100
47. Wu F, Zhang EY, Zhang J, Bache RJ, Beard DA (2008) Phosphate metabolite concentrations and atp hydrolysis potential in normal and ischaemic hearts. J Physiol 586(17):4193–4208. doi:10.1113/jphysiol.2008.154732
48. Xia XM, Fakler B, Rivard A, Wayman G, Johnson-Pais T, Keen JE, Ishii T, Hirschberg B, Bond CT, Lutsenko S, Maylie J, Adelman JP (1998) Mechanism of calcium gating in small-conductance calcium-activated potassium channels. Nature 395:503–507
49. Yamada T, McGeer PL, Baimbridge KG, McGeer EG (1990) Relative sparing in Parkinson's disease of substantia nigra dopamine neurons containing calbindin-D28K. Brain Res 526:303–307

Chapter 6
Real-Time *In Vivo* Sensing of Neurochemicals

Fiachra B. Bolger, Niall J. Finnerty, and John P. Lowry

Abstract The brain is one of the most complex biological structures known to science. How it works or, more specifically, how the physical brain gives rise to the properties of mind remains an unanswered question. However, it is clear that many drugs used empirically in the treatment of neurological disorders, such as Parkinson's disease, work through their specific chemical actions on nerve cells in the brain. Thus, if we are to understand brain function and drug performance, there is a need to measure chemical signalling in the brain. Measurement technologies for neurochemical studies in the living brain include spectroscopy, such as NMR, sampling techniques, such as cerebral microdialysis, and the topic of this chapter - *in situ* electrochemical monitoring using long-term *in vivo* electrochemistry (LIVE). With LIVE, a microvoltammetric sensor is implanted in a specific brain region to monitor local changes in the concentration of specific substances in the extracellular fluid. It can do this with sub-second time resolution and with measurement periods extending over many hours, potentially days. Spatially, localised, high-temporal resolution, long-term sensing of this kind allows investigations of the functions of chemicals in neuronal signalling, drug actions and well-defined behaviours. In this chapter, we give an overview of the different electrochemical sensor types, the techniques used and the principal neurochemicals potentially associated with Parkinson's disease that can be measured *in vivo*.

F.B. Bolger (✉) • N.J. Finnerty • J.P. Lowry
BioAnalytics Laboratory, Department of Chemistry, National University of Ireland Maynooth, Maynooth, County Kildare, Ireland
e-mail: fiachra.bolger@nuim.ie; niall.finnerty@nuim.ie; john.lowry@nuim.ie

P. Wellstead and M. Cloutier (eds.), *Systems Biology of Parkinson's Disease*,
DOI 10.1007/978-1-4614-3411-5_6,

Abbreviations

3MT	3-Methoxytyramine
5HIAA	5-Hydroxyindoleacetic acid
5HT	5-Hydroxytryptamine
AA	Ascorbic acid
CAT	Catalase
CEE	Carbon epoxy electrode
CFE	Carbon fibre electrode
CNS	Central nervous system
CPA	Constant potential amperometry
CPE	Carbon paste electrode
CV	Cyclic voltammetry
DA	Dopamine
DOPAC	3,4-Dihydroxyphenylacetic acid
DPA	Differential pulse amperometry
DPV	Differential pulse voltammetry
ECF	Extracellular fluid
FCV	Fast cyclic voltammetry
GA	Glutaraldehyde
GluOx	Glutamate oxidase
GOx	Glucose oxidase
HPLC	High-performance liquid chromatography
HVA	Homovanillic acid
LIVE	Long-term *in vivo* electrochemistry
L-NAME	N^{ω}-nitro-L-arginine methyl ester
LSV	Linear sweep voltammetry
NA	Noradrenaline
NMR	Nuclear magnetic resonance spectroscopy
NO	Nitric oxide
NOS	Nitric oxide synthase
o-PPD	Poly(*o*-phenylenediamine)
PD	Parkinson's disease
SCE	Saturated calomel electrode
SCV	Staircase voltammetry
UA	Uric acid

Introduction

The mammalian brain is a highly complex structure and understanding its diverse functions is one of science's greatest challenges. The brain's complexity lies principally in the processing of signals, and although electrical signalling is often considered to be the primary function of brain neurons, intercellular chemical

signalling plays a major role in determining the properties of neural networks. Nerve terminals release one, or more, of a large variety of identified primary chemical messengers (e.g. neurotransmitters) that may activate, or inhibit, cellular systems via a range of ionotropic and metabotropic receptor complexes. This combination of diverse neurotransmitters and receptors is one of the factors that enables the central nervous system (CNS) to function over timescales ranging from "real-time" sensory processing and behavioural responses to the long-term retention of information (e.g. memories) over many decades. The importance of neurochemistry for CNS function is clear from the many drugs used empirically in the treatment of neurological disorders, including Parkinson's disease (PD), schizophrenia and depression. Such drugs are designed to have specific chemical actions on nerve cells, and their widespread use demonstrates the central role of chemical signalling in determining the function of neural networks.

Most of our understanding of neuronal chemical signalling pathways has been gathered through studies of isolated nerve cells and tissues *in vitro*. However, an intrinsic feature of CNS functionality is the integration and interconnectivity over many scales of structure that occurs *in vivo*: between neuronal and glial cells to form tissues or "brain regions" (*cortex*, *cerebellum*, etc.); between the different tissues to form the CNS and so on . . .. Almost all of these levels of coupling are lost in *in vitro* preparations, and yet (as described in Chap. 1) it is crucial to consider them if we are to understand brain function and, by implication, disease.

To fully understand cerebral function, we need to complement *in vitro* investigations (such as presented in Chap. 4) with measurements of chemical events within the living brain. Despite the technical challenges of performing *in vivo* measurement in such a sensitive organ, a number of sensing methodologies exist. These include spectroscopy—such as nuclear magnetic resonance (NMR) [1]; sampling techniques—such as cerebral microdialysis [2]; and electrochemical sensors [3] used in the intact living brain. Each of these approaches to *in vivo* neurochemical analysis has advantages and disadvantages. For example, NMR is non-invasive, but lacks the ability of implanted microdialysis, or electrochemical sensors, to measure at well-defined spatial locations within the brain. Of these two invasive techniques, microdialysis has the advantage that a wide range of compounds (including neurotransmitters, neuromediators, metabolites, drugs, etc.) can be collected simultaneously in a sample and subsequently separated and measured [4]. The main disadvantages of dialysis are the relatively large probe size (typical minimum dia. ~200 μm) and the poor time resolution, which ranges from 2 to 10 min (although about 1 min has been achieved [4]).

In comparison, electrochemical sensors have superior spatial (~10 μm) and temporal (~milliseconds) resolutions. They also have the additional advantage of good long-term stability, which allows continuous monitoring *in vivo* over several weeks; such long-term investigations would be impossible with microdialysis. Since PD is a multi-timescale condition with underlying dynamical biological processes operating on both rapid (see Chaps. 4 and 5) and slow (see Chaps. 3 and 7) timescales, *in vivo* neurochemistry is a promising technique with which to probe such processes. A traditional limitation of long-term *in vivo*

electrochemistry (LIVE) was its restriction to electroactive analytes. However, this limitation is being overcome as enzyme-modified electrodes or biosensors are developed [5]. A number of reviews on the principles and applications of LIVE analysis of the extracellular fluid (ECF) have been published, and a minimal selection is cited here [6, 7].

History

The concept of applying voltammetric techniques to monitor changes in the concentration of electroactive species in brain ECF is generally attributed to Adams et al. [8]. However, reports of electrochemistry in the living brain date back at least as far as 1958, when Leland C. Clark demonstrated the feasibility of voltammetric recording in brain tissue *in vivo* [9, 10]. Clark's 1958 experiments reporting changes in O_2 at a noble metal electrode were followed in 1965 by a paper using "brain polarography" to measure O_2 cathodically with a glassy carbon electrode. In separate experiments, changes in an anodic signal were also observed and attributed to fluctuations in brain ascorbic acid (AA) levels.

Almost a decade later, Adams and co-workers described attempts to detect dopamine in anaesthetised rat brain using a carbon-based sensor (CPE) and an electrochemical technique known as cyclic voltammetry. Even at this early stage in the technology, the authors successfully identified many of the problems and factors affecting the shape of voltammograms recorded in brain tissue. Thus, they make reference to thin-layer behaviour caused by depletion of the ECF around the electrode by the electrochemical voltage, tortuous diffusion in the tissue, heterogeneous distribution of target analytes in various compartments in the brain, overlap of different signals and perturbation of the tissue by the implanted electrodes. Quite inspirationally, the authors also suggested a number of strategies to address some of these problems—such as the use of permselective membranes and immobilised enzymes; approaches that have subsequently proved to be sound.

Long-Term *In Vivo* Electrochemistry

With electrochemical techniques, a potential is applied across an electrode–solution interface (the working electrode) to oxidise or reduce species present in solution. The Faradic current resulting from the redox processes is then related to the chemical identity of the redox species (based on the applied potential where the redox reaction takes place). Finally, the magnitude of the current (at a given potential) can be then related to the analyte's concentration (see Fig. 6.1). In this manner, LIVE provides both a qualitative and quantitative assay for electroactive species.

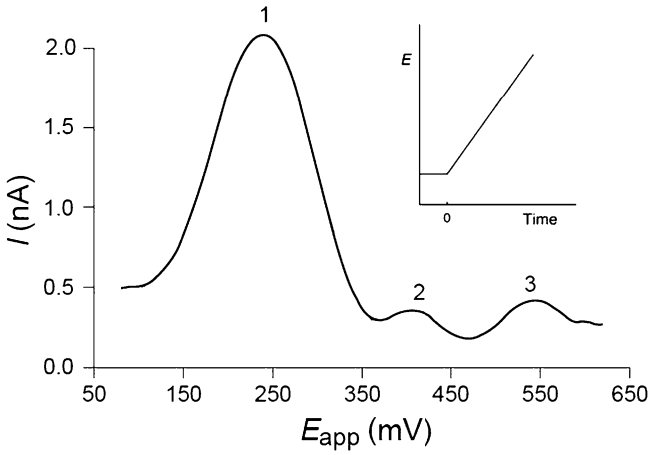

Fig. 6.1 Typical current (nA) data obtained using a scanning potential (linear sweep) LIVE technique. Oxidation peak 1 is essentially due to AA, peak 2 due to 5-hydroxyindoleacetic acid (5HIAA) and peak 3 due to the DA metabolite homovanillic acid (HVA). Increases in the extracellular concentration of catechols, DA and 3,4-dihydroxyphenylacetic acid (DOPAC) increase the current between peaks 1 and 2. *Inset:* Potential waveform for linear sweep voltammetry (LSV)

At least one other electrode is required with respect to which the potential is applied, and to complete the circuit for current flow. These two functions are not ideally suited to a single electrode, as current flowing through a reference interface would perturb the reference potential. Consequently, three electrodes are generally used: (a) a working electrode (sensor) at which the redox reaction of interest occurs, (b) a second (reference) electrode through which no current flows and (c) a third auxiliary (counter) electrode which completes the circuit. A potentiostat maintains the desired relative potential between the working and reference electrodes. This potential ensures that the auxiliary electrode is kept at a sufficient potential to drive the appropriate oxidation or reduction reaction (usually of water) to balance the current produced at the working electrode. For currents of picoamperes produced by ultramicroelectrodes of diameter less than 1 μm, LIVE can be carried out with two-electrode systems without significant disturbance of the reference potential.

Neurochemicals Detected Using LIVE

One of the main problems associated with producing identifiable electrochemical signals *in vivo* is that the ECF contains a wide variety of electroactive species (see Fig. 6.1) that are capable of oxidising or reducing at similar potentials on many electrode materials. These include ascorbic acid, which has a range of general

antioxidant and specific neurochemical functions; neurotransmitter catecholamines, such as dopamine (DA), noradrenaline (NA) and their metabolites 3,4-dihydroxyphenylacetic acid (DOPAC), 3-methoxytyramine (3MT) and homovanillic acid (HVA); the 5-hydroxyindole neurotransmitter 5-hydroxytryptamine (5HT) and its metabolite 5-hydroxyindoleacetic acid (5HIAA); and the purine metabolite uric acid (UA). These compounds are distributed heterogeneously through the tissue in different compartments and in concentrations ranging from high μM (e.g. AA, 100–500 μM) to low nM (e.g. DA, 1–50 nM). In this context, high selectivity and sensitivity are achieved by using appropriate LIVE techniques (see below) and an adequate working electrode (often chemically modified to incorporate coupled enzymatic reactions [5]). LIVE electrodes are usually employed as the working electrode (sensor) in a three-electrode potentiostat configuration with a reference and auxiliary electrode. For a comprehensive overview of electrode developments, the reader is referred to review articles which focus on advances, directions and strategies for sensors in neurochemical applications [5, 6, 11].

LIVE Techniques

In LIVE, one is usually interested in changes in the concentration of a particular neurochemical on a timescale from milliseconds to days. Frequently, experiments start from a baseline at which a particular perturbation is induced (stimulation, injection of a toxin, etc.) and the dynamic response to the stress recorded over a period of time. The choice of electrochemical technique to be used is determined by the time resolution needed, in addition to other factors, such as how well the working electrode can discriminate between the different electroactive species present in the ECF. Since the vast majority of substances of interest in LIVE studies undergo oxidation rather than reduction reactions, the majority of the techniques applied have focused on oxidative electrochemistry.

Different forms of electrochemistry [5, 6] can be categorized on the basis of the time resolution achieved for detecting changes in the concentration of species in the ECF. Fast techniques with resolutions of the order of seconds, or less, are chronoamperometry, fast cyclic voltammetry (FCV), differential pulse amperometry (DPA) and constant potential amperometry (CPA). These methods are generally used to detect stimulated changes in neurotransmitter overflow. Slow techniques with time resolutions of the order of several minutes are linear sweep (LSV, see Fig. 6.1), staircase (SCV), differential pulse (DPV) and differential normal pulse (DNPV) voltammetries at low scan rates. The latter options are usually used in studies of neurotransmitter metabolites as well as AA and UA. The minimum interval between scans is limited, not only by the sweep time, but also by the time taken for the concentration of the electrolysed species in the compartment around the implanted electrode tip to return to its unperturbed value by means of tortuous diffusion through the tissue matrix [12].

Monitoring Neurochemicals Using LIVE

Despite applications in the measurement of a wide range of neurochemicals (e.g. electrochemically active catecholamines, including DA, norepinephrine and their metabolites), LIVE has not yet made a significant contribution to our understanding of diseases such as Parkinson's. However, numerous substances present in brain tissues, including glucose, lactate, glutamate, nitric oxide (NO), O_2 and hydrogen peroxide (H_2O_2), are relevant to PD and are easily measured. Thus, LIVE analysis of these energy metabolities may play an important role in understanding the pathogenesis and progress of the disease. For example, Chap. 2 of this volume provides details on the importance of assessing the dynamics of lactate in energy regulation, with a focus on how it is dysregulated in PD. In the same vein, Chap. 7 presents modelling results that suggest an important role for the dynamics of reactive oxygen species (ROS), with the observation that both slow (weeks) and rapid (seconds) dynamics may be relevant. The mathematical models presented in Chaps. 2 and 7 were calibrated using energy metabolites data obtained from LIVE techniques. While not exhaustive, the following provides an overview of some of these measurements with respect to NO, H_2O_2, O_2, glutamate and lactate. Details with respect to other analytes can be found in previously published review articles [5, 6, 11, 13].

Nitric Oxide

Since its characterisation as the endothelium-derived relaxing factor in the late 1980s, nitric oxide has been elucidated as having various other biomedical roles, both intracellular and extracellular. Typical examples include a neurological function in synaptic plasticity, neurotransmission, learning and memory. In addition, NO has a primary role in non-specific immunity, penile erection and platelet aggregation inhibition.

To date, the majority of techniques used for monitoring NO provide indirect analysis. Electron paramagnetic resonance (EPR) spectroscopy, chemiluminescence and UV spectroscopic techniques (e.g. the Griess reagent and the methemoglobin assay) have all been used to detect NO. However, the aforementioned techniques do not provide the possibility of real-time *in vivo* monitoring of NO. Consequently, the possibility of using microelectrochemical sensors for direct real-time NO measurement has recently gained considerable interest. This is primarily because of their speed and sensitivity, which are particularly important for NO as it is present at picomolar-to-micromolar concentrations and has a half-life of 2–6 s *in vivo*. One of the difficulties associated with detecting this free radical is its short half-life (<1 min) in tissues containing oxygen. Although NO can be reduced at approximately −900 mV vs. SCE, interference by molecular oxygen at this potential means that a reduction mode is not suitable for NO detection *in vivo*. Monitoring is, therefore, normally carried out at high anodic potentials.

The need for high potentials makes it difficult to avoid interference from a range of species, including AA, UA, DA, NO_2^- and 5HT and electroactive amino acids such as tyrosine and tryptophan. The potential for interference of this kind emphasises the need for high sensitivity and selectivity for NO sensors used for LIVE. The concept of tissue concentration of such a reactive species is questionable, but estimates lie in the range of 10–100 nM for brain ECF.

Shibuki reported the first sensor design for NO detection [14], based on a miniature version of Clark's O_2 electrode [15]. However, the internal filling solution (30 mM NaCl and 0.3 mM HCl) prevented the sensor from being miniaturised for use *in vivo*. Further advances in NO sensor design were made by Malinski and Taha, who incorporated nickel porphyrin and Nafion® polymer membranes onto carbon fibre electrode (CFE) surfaces [16]. Gonzalez-Mora constructed a sensor designed on similar lines to Malinski and Taha, incorporating Nafion® in the application step. This allowed the successful determination of NO in the corpus cavernosum of Sprague-Dawley rats [17]. The electrochemical signal also responded in a predictable manner to pharmacological interventions having well-known stimulatory (L-arginine) and inhibitory (L-NAME) effects on NO production. In 1992, the first commercial NO electrode-based amperometric detection system was developed by World Precision Instruments (WPI). A number of different commercially available sensors were subsequently introduced; however, the majority fall short of the required selectivity for *in vivo* analysis. Friedemann et al. described a novel method for drying Nafion® that enhanced the adherence of the polymer to a CFE surface combined with poly(*o*-Phenylenediamine) (*o*-PPD) and greatly increased the selectivity ratio of NO over the various electroactive interferents [18].

Park and co-workers developed an NO sensor based on a non-conducting *meta* polymer (*m*-PPD)—modified CFE [19]. Due to the permselective characteristics of the electropolymerised film, it was incorporated to protect the sensor against interference and fouling from other chemicals. Further modification with Nafion® and Resorcinol resulted in excellent selectivity for NO over AA, DA and NO_2^-. Due to the efficient stability characteristics of the composite polymer layer, the sensor was implanted for direct monitoring in the rat brain. Further work carried out by Pontie et al. investigated two microsensors utilising combinations of NiTSPc-, *o*-PD- and Nafion®-based layers to modify the surface of a CFE [20]. They found that the sensitivity of the carbon electrode to NO decreased when using Nafion® alone while it increased when using both Nafion®/*o*-PD and NiTSPc/Nafion® coatings. They also confirmed that the main forces dominating the sensitivity of a composite coating to NO are hydrophobic interactions. The hydrophobic nature of NO is undoubtedly central to its physiological function, permitting the small molecule to pass freely across cell boundaries and hydrophobic boundaries.

Brown and co-workers have reported the *in vitro* development [21] and characterisation [22] of a Nafion®-modified Pt sensor designed for real-time monitoring of brain extracellular NO. Application of Nafion® (5% commercial solution) using a thermally annealing procedure involving 5 pre-coats and 2 subsequent dip-bake layers results in a sensor (Nafion®(5/2)) which has a response time suitable for *in vivo* monitoring. An extensive characterisation has been carried out in the

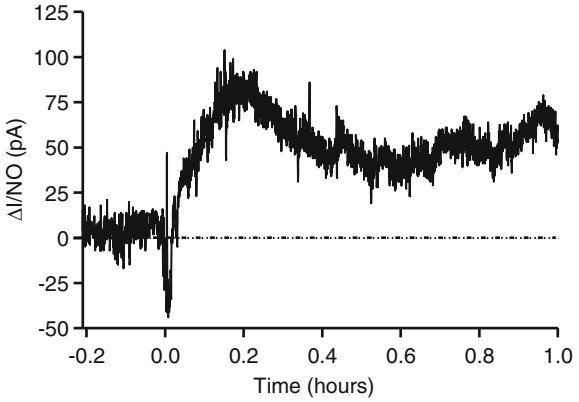

Fig. 6.2 An example of the effect of an intraperitoneal injection of the NO precursor L-Arginine (300 mg/kg) on the response (background subtracted) of a Nafion®(5/2)-modified Pt electrode implanted in the *striatum* of a freely moving Wistar rat. Time 0 is the point of injection

striatum of Wistar rats and significant NO changes were recorded following systemic and local administrations of stock NO and the precursor for NO production, L-arginine (see Fig. 6.2).

A recent report utilising this NO sensor in an animal model of schizophrenia provides direct evidence that L-NAME inhibits NO production following systemic administration of Phencyclidine [23]. This study provides the first direct biochemical evidence for an involvement of NO in the effects of the psychotomimetic drug, a feature that has previously been suggested from behavioural pharmacology data and indirect measures of NO activity [24].

Hydrogen Peroxide

Hydrogen Peroxide has been assumed to have a neuromodulatory function, similar to that of nitric oxide, in various aspects of brain function [25]. When present at high concentrations, H_2O_2 (along with other ROS) can result in oxidative stress, suggesting the hypothesis that it is involved in the etiopathology of neurodegenerative disorders such as PD. Recent studies using microdialysis have revealed that the concentration of H_2O_2 in brain ECF can reach micromolar levels under certain conditions [26, 27] and that brain H_2O_2 levels can be altered by antioxidants, including ascorbic acid [28]. Also, there is a need to measure endogenous H_2O_2 levels in order to validate measurements obtained with amperometric biosensors that rely on oxidase enzymes to generate H_2O_2 for the detection of species, such as glucose, lactate, glutamate and choline [29].

Over the last decade, extensive research has been carried out on the hypothesis that H_2O_2 is an endogenous modulator of synaptic neurotransmitter release. A neuromodulatory role for H_2O_2 has been proposed based on its effects on evoked

release of neurotransmitter from brain slices [25]. Thus, a picture is emerging in which the H_2O_2, formed from a variety of biochemical processes, can reach micromolar levels in brain ECF and modulate brain function [25]. This finding has potential implications in neurodegeneration, and for this and other reasons, there is a growing interest in the detection of H_2O_2 in living brain tissue. Unfortunately, there are few experimental tools for the direct measurement of dynamic H_2O_2 fluctuations in intact tissue. Recently, the electrochemical detection of H_2O_2 has gained widespread interest, but limited *in vivo* evidence has been reported.

Kulagina et al. designed an implantable carbon microelectrode coated with a cross-linked redox polymer (RP) that contains pendant, non-diffusing, osmium-centred polypyridyl complexes and HRP. An additional layering of ascorbate oxidase and Nafion® was incorporated into the design to improve selectivity and stability, respectively [30]. To ensure that there is no interference from the respective electroactive species present in the brain ECF, the sensor operates at an applied potential of −100 mV (relative to an Ag/AgCl reference electrode). Experiments demonstrated that electrical stimulation of dopaminergic axons in the medial forebrain bundle evoked a rapid transient response at the HRP/RP microsensor, but not at the blank RP sensor that lacks HRP. The stimulus-evoked response is attributed to a change in the extracellular concentration of a reducible substrate of HRP, most likely to be H_2O_2 produced by the oxidation of dopamine (see Chap. 8 for related issues investigated from a mathematical modelling viewpoint). Thorough *in vitro* calibration experiments have confirmed that these sensors do not respond to dopamine and that dopamine does not affect their response.

O'Brien and co-workers designed a simple, mediatorless H_2O_2 biosensor based on the enzyme catalase, where Nafion® and *o*-PPD layers block interference from endogenous reducing agents such as ascorbic acid [31]. One electrode has catalase adsorbed onto the surface (CAT) for the decomposition of H_2O_2. The other electrode (the blank electrode) lacks the enzyme and is used for the detection of H_2O_2. The H_2O_2 sensitivity of the overall sensor design is calculated by subtracting the CAT electrode current (I_{CAT}) from the blank electrode current (I_{BLANK}). When implanted *in vivo*, the two electrodes were situated in close proximity and the current from each were recorded simultaneously. The CAT and blank electrodes were adhered to a microdialysis probe (for localised H_2O_2 perfusion) and implanted into the *striatum* of Wistar rats. The design was validated in anaesthetised animals and then used in freely moving animals, taking care not to administer toxic levels of H_2O_2. Local perfusion of varying H_2O_2 concentrations produced current changes that resulted in an overall increase in H_2O_2 signal following subtraction. A typical example is shown in Fig. 6.3 below.

Recently, Sanford and colleagues presented the first voltammetric recordings of H_2O_2 at single, uncoated, carbon fibre microelectrodes in brain tissue [32]. FCV was employed to provide chemical selectivity, temporal resolution and high sensitivity. The CFE (with a limit of detection of 1.9 ± 0.1 μM) was inserted into a section of brain tissue that encompassed the *striatum*. A micropipette containing 50 μM of H_2O_2 was positioned in the tissue and pressure ejection used to introduce the exogenous H_2O_2 to the electrode surface.

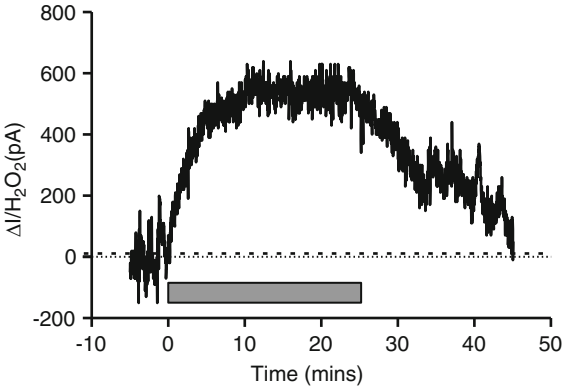

Fig. 6.3 An example of the effect of local perfusion of H_2O_2 (200 μM) on the response (background subtracted) of a H_2O_2 biosensor ($I_{BLANK}-I_{CAT}$) implanted in the *striatum* of a Wistar rat. The period of perfusion is indicated by the *grey* bar. Data from O'Riordan, Finnerty and Lowry (unpublished)

Oxygen

Oxygen is an important substrate for many biochemical reactions, and was one of the first substances detected voltammetrically *in vivo*, both in brain [8, 9] and peripheral tissue [33]. Brain tissue oxygen is delivered by the blood and responds to a range of perturbations, including electrical stimulation and neuromediator release. Changes in tissue oxygen concentration are governed by the balance between supply and utilisation. Moreover, the anatomical distribution of concentrations throughout the brain varies upon the position of the sensor within the brain and the heterogeneity of the tissue, with the *cerebral cortex* having a greater turnover rate compared to other areas. The reported distribution of concentration for brain tissue ranges from 40 to 80 μM [34].

Noble metals such as Au or Pt are the transducer of choice for Clark-type O_2 electrodes. However, carbon-based O_2 electrodes such as CFE, carbon epoxy (CEE), glassy carbon and carbon paste (CPE) have been reported [34]. Despite a literature consensus indicating Pt electrode poisoning in biological tissues, a recent report detailing biocompatibility studies comparing bare Pt vs. membrane-coated Pt electrodes indicates minimal evidence of fouling of the active surface in the *in vitro* environment [35].

Previous reports demonstrate that CPEs can be used to cathodically monitor real-time changes in brain tissue O_2 during neuronal activation (resulting from physiological stimulation) in freely moving rodents using both DPA [36, 37] and CPA [38]. The increases observed with DPA were also found to correlate with increases in regional cerebral blood flow measured using the H_2 clearance technique [38]. A recent finding involving CPA with CPEs coupled with imaging studies highlights that a carbon-based O_2 sensor can serve as an index of changes

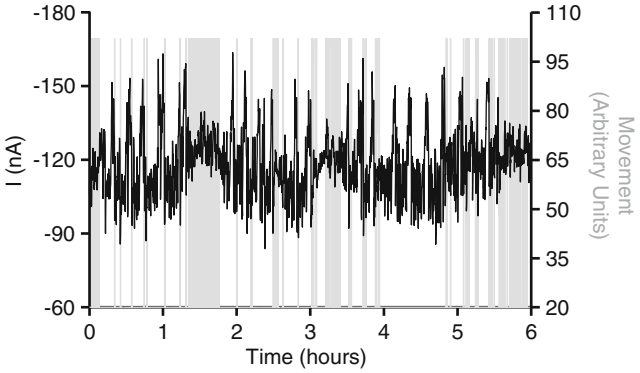

Fig. 6.4 Typical example of continuous real-time O_2 recording showing changes in signal associated with naturally occurring behaviour (movement). Data recorded using a carbon paste electrode (CPE) and constant potential amperometry (CPA) at −650 mV (vs. saturated calomel electrode (SCE)). *Grey* areas indicate periods of movement

in the magnitude of the blood oxygenation level-dependent (BOLD) functional magnetic resonance imaging (fMRI) response [39]. The amperometric O_2 signal, thus, provides a reliable awake animal surrogate of human fMRI experimentation, and is an effective translational tool that can better enable the comparison of preclinical and clinical research.

Carbon epoxy has been used in the fabrication of oxygen sensors for the development of a biotelemetric device for the amperometric detection of brain tissue oxygen [40]. *In vivo* tail-pinch and grooming responses were observed which corroborated previously reported data for these behavioural paradigms. Modified Clark-type oxygen microelectrodes with a guard cathode for tissue oxygen tension have been used due to their small probe size and the fact that the built-in guard cathode removes all oxygen from the electrolyte reservoir [41]. Lauritzen and co-workers recently used similar electrodes to investigate oxygen consumption in various regions of the brain [42, 43].

While stable CPE oxygen signals are observed throughout a 24-h period with CPA, it is important to point out that the signal is subject to naturally occurring deviations from baseline levels. Observed changes can be rapid, occurring over periods ranging from seconds to minutes, or they can be more prolonged, lasting one or more hours (see Fig. 6.4). Rapid changes tend to be associated with physiological phenomena such as grooming, feeding and even sleep while the latter occurs mainly with periods of intense activity. Both are reflective of the fact that the measured real time [O_2] is the dynamic balance between supply and utilisation. As will be seen with a mathematical modelling approach in Chap. 7, rapid changes in neuronal metabolic activity (such as those shown in Fig. 6.4) can lead to short-term increases in mitochondrial-derived ROS that have to be alleviated by neurons. Simulations suggest that the mechanisms operating at this timescale could have implications in the development of neuroprotective strategies.

Glutamate

Various research groups have designed biosensors for the electrochemical detection of glutamate (facilitated by the incorporation of the oxidase enzyme, glutamate oxidase (GluOx)). Wilson and co-workers used glutamate-sensitive microelectrodes to monitor changes in ECF glutamate in the brains of anaesthetised rats [44]. This biosensor was constructed using a previously published glucose sensor as a model biosensor and the biological component altered to detect the new species [45, 46]. Initial layers consisting of Nafion® and cellulose acetate were incorporated into the design and GluOx was deposited on the active surface of the electrode. A working potential of +600 mV (vs. Ag/AgCl) was used and the biosensor displayed a rapid response time (about 1 s) and a high degree of sensitivity (<2 μM) and selectivity. Implantation of the biosensor in the *dentate gyrus* of the *hippocampus* led to the detection of both KCl-induced release of glutamate and release induced by electrical stimulation of the perforant pathway.

The direct entrapment of GluOx on a Pt electrode surface (125-μm diameter) with an *o*-PPD film has been reported as a viable biosensor design for *in vivo* glutamate monitoring similar to the method described by Lowry et al. [47, 48]. Detailed characterisation studies of this sensor in the *in vitro* environment have been performed indicating similar characteristics (sensitivity, selectivity and stability) to the Pt/*o*-PPD/Glucose oxidase (GOx) biosensor. Preliminary *in vivo* experiments to detect glutamate in the *striatum* of the awake, freely moving rat at 1-s intervals using a mild stressor (10-s tail pinch) have been reported for this device [49, 50].

Kulagina et al. have reported the development of a glutamate biosensor in which a CFE was coated with a cross-linked redox hydrogel polymer containing the enzyme GluOx [51]. Initial acute *in vivo* experiments were performed that confirmed that the microsensors were able to detect neuronally derived extracellular glutamate. The Westerink group has improved the glutamate biosensor initially developed by Kulagina et al. by optimising its performance and reproducibility via investigation of the hydrogel composition [52], improvement of the utilisation of an automatic dip-coating machine [53] and purification of ascorbate oxidase [54]. The improved sensors were able to detect extracellular glutamate throughout a wide range of pharmacological studies. In anaesthetised rat brain, dynamic glutamate changes were demonstrated using different pharmacological perturbations, including local application of exogenous glutamate, KCl, the glutamate reuptake inhibitor DL-threo-β-benzyloxyaspartate and the sodium channel blocker tetrodotoxin [55, 56].

More recently, Gerhardt and co-workers have reported the use of ceramic-based multisite microelectrode arrays in the acute brain monitoring of extracellular glutamate [57]. Elsewhere, a glutamate-sensitive dialysis electrode was developed to prevent the direct implantation of a biosensor into the brain [58]. Various other groups have subsequently used this approach to monitor brain glutamate [59–61].

Lactate

In the classical model of brain energy metabolism, lactate is merely a by-product. This was challenged in a theory published by Pellerin and Magestretti (the astrocyte-neuron lactate shuttle (ANLS) hypothesis) postulating that activated neurons use the lactate provided by astrocytes [62]. This hypothesis has been subjected to much debate in recent times, as highlighted by numerous publications [63], both supporting [64] and challenging [65] the ANLS hypothesis. Obviously, *in vivo* detection of lactate will eventually help clarify the matter, as will other arguments. In the latter connection, an analysis of the role of lactate as a dynamical compensatory mechanism during high-activity periods is reviewed elsewhere in this volume (see Chap. 2 and references therein).

To date, direct measurement of lactate in the brain has been performed using microdialysis [66]. However, there are few published reports regarding lactate biosensors implanted in the brain. Wilson and co-workers report a lactate biosensor measuring brain extracellular lactate in anaesthetised animals. The sensor was used to examine changes due to neuronal activity in the *dentate gyrus* of the *hippocampus* after electrical stimulation of the perforant pathway [46]. This lactate biosensor was fabricated by substituting lactate oxidase for GOx in their original biosensor design [45]. Burmeister and co-workers describe a lactate biosensor design based on ceramic multisite microelectrodes [67]. In this design, an initial layer of Nafion® was cast onto the ceramic-based microelectrodes to provide an endogenous electroactive interference-rejecting layer. Lactate oxidase was incorporated into the fabrication protocol, along with bovine serum albumin and glutaraldehyde, thereby creating a sensitivity to lactate. In order to limit oxygen dependency altering the linear range of the electrodes, a final layer of polyurethane was coated onto the microelectrode. Self-referencing was used to further improve the selectivity of the microelectrodes, in a manner similar to the glutamate electrode previously developed by this group [57].

Based on a previous procedure for manufacture of glutamate biosensors [68], Serra and co-workers describe the design of a telemetric lactate biosensor where high sensitivity and good selectivity towards lactate were reported [69]. Implantation of the biosensor into the *striatum* of a freely moving rat, and the subsequent recording of a 5-min tail pinch, indicated a response of the biosensor in the detection of the release of lactate following neuronal activation. Shram et al. have previously developed and described a method for the construction of a biosensor for monitoring glucose in the brain [70]. Subsequent replacement of the GOx with lactate oxidase has resulted in a biosensor that is sensitive and selective for monitoring brain lactate in anaesthetised rats [71] and freely moving rats [72]. Ikegami has utilised a variation of the dialysis electrode reported by Albery et al. [58] and monitored ECF lactate during chemical stimulus of the nucleus tractus solitarii [73].

Lactate variations in the *striatum* of the freely moving rat have been reported by Bolger et al., with the stimulus being a 5-min tail pinch [74]. Figure 6.5 below

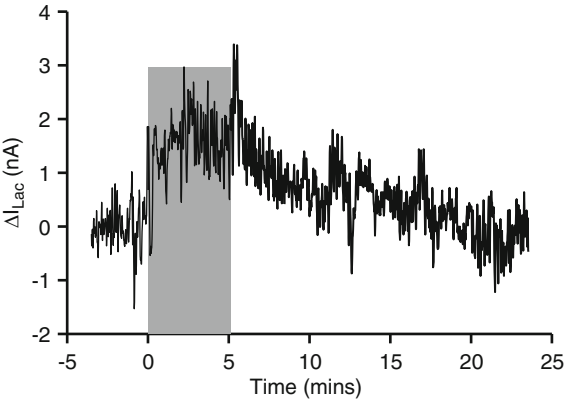

Fig. 6.5 Typical example of the extracellular lactate response to a 5-min restraint stress recorded using a lactate biosensor implanted in the *striatum* of a Wistar rat. The *grey* area indicates the period of induced stress

shows the response of a similar lactate biosensor implanted in the *striatum* of a freely moving rat to a 5-min restraint stress. See [75] and Chaps. 2 and 7, which use similar real-time lactate data recorded with these biosensors.

Discussion

Oxidative stress and mitochondrial dysfunction have been strongly implicated in Parkinson's pathogenesis. Oxidative stress results from increased production, or decreased detoxification, of extremely reactive free radicals, including ROS and peroxynitrite. Free radicals produce oxidative damage by reacting with DNA, lipids and proteins. ROS may be formed during a number of cellular processes, including mitochondrial oxidative respiration and DA metabolism. Electrons leak at several sites along the mitochondrial electron transport chain. These electrons may combine with molecular oxygen and form ROS, such as superoxide (O_2^-) and hydrogen peroxide. In addition, the activities of tyrosine hydroxylase and monoamine oxidase, two enzymes involved in dopamine metabolism, produce hydrogen peroxide as a normal by-product. Moreover, auto-oxidation of DA results in the formation of ROS, which can participate in a positive feedback loop of progressive oxidative damage (see Chaps. 7 and 8). For this reason, dopaminergic neurons and their nerve terminals, the primary targets in PD, are believed to exist in a constant state of oxidative stress.

Through its ability to measure dynamic changes in brain energy metabolism and oxidative stress, LIVE can make a significant contribution to our understanding of PD. Current results have been with single-sensor tests. However, utilising several sensors for different analytes in the same animal model may provide a more complete picture of interactions between different chemical species. For example, dynamic DA transmission in dorsolateral *striatum* is regulated on a sub-second

timescale by glutamate via H_2O_2 signalling, which activates ATP-sensitive potassium channels to inhibit dopamine release [76]. Understanding these interactions and how they are perturbed by disruption of metabolism and ROS may be the key to finally understand the disease mechanisms and the development of new therapies.

References

1. Crespi F, Croce AC, Fiorani S, Masala B, Heidbreder C, Bottiroli G (2004) Autofluorescence spectrofluorometry of central nervous system (CNS) neuromediators. Lasers Surg Med 34:39
2. Parkin MC, Hopwood SE, Strong AJ, Boutelle MG (2003) Resolving dynamic changes in brain metabolism using biosensors and on-line microdialysis. Trends Anal Chem 22:487
3. O'Neill RD, Chang SC, Lowry JP, McNeil CJ (2004) Comparisons of platinum, gold, palladium and glassy carbon as electrode materials in the design of biosensors for glutamate. Biosens Bioelectron 19:1521
4. Lada MW, Kennedy RT (1996) Quantitative in vivo monitoring of primary amines in rat caudate nucleus using microdialysis coupled by a flow-gated interface to capillary electrophoresis with laser-induced fluorescence detection. Anal Chem 68:2790
5. Pantano P, Khur WG (1995) Enzyme-modified microelectrodes for in vivo neurochemical measurements. Electroanalysis 7:405
6. O'Neill RD, Lowry JP, Mas M (1998) Monitoring brain chemistry in vivo: voltammetric techniques, sensors, and behavioral applications. Crit Rev Neurobiol 12:69
7. Lowry JP, O'Neill RD (2005) Neuroanalytical chemistry in vivo using biosensors. In: Grimes CA and Dickey EC (eds) Encyclopedia of sensors. American Scientific Publishers, CA, ISBN: 1-58883-062-4, pp. 501–524
8. Kissinger PT, Hart JB, Adams RN (1973) Voltammetry in brain tissue–a new neurophysiological measurement. Brain Res 55:209
9. Clark LC Jr, Misrahy G, Fox RP (1958) Chronically implanted polarographic electrodes. J Appl Physiol 13:85
10. Clark LC Jr, Lyons C (1965) Studies of a glassy carbon electrode for brain polarography with observations on the effect of carbonic anhydrase inhibition. Ala J Med Sci 2:353
11. Ronkainen NJ, Halsall HB, Heineman WR (2010) Electrochemical biosensors. Chem Soc Rev 39:1747
12. Nicholson C, Sykova E (1998) Extracellular space structure revealed by diffusion analysis. Trends Neurosci 21:207
13. Michael AC, Borland LM (2007) Electrochemical methods for neuroscience. CRC Press, Boca Raton, FL
14. Shibuki K (1990) An electrochemical microprobe for detecting nitric oxide release in brain tissue. Neurosci Res 9:69
15. Clark LC Jr (1956) Monitor and control of blood and tissue O_2 tensions. T Am Soc Art Int Org 2:41
16. Malinski T, Taha Z (1992) Nitric oxide release from a single cell measured in situ by a porphyrinic-based microsensor. Nature 358:676
17. Mas M, Escrig A, Gonzalez-Mora JL (2002) In vivo electrochemical measurement of nitric oxide in corpus cavernosum penis. J Neurosci Methods 119:143
18. Friedemann MN, Robinson SW, Gerhardt GA (1996) o-Phenylenediamine-modified carbon fiber electrodes for the detection of nitric oxide. Anal Chem 68:2621
19. Park JK, Tran PH, Chao JK, Ghodadra R, Rangarajan R, Thakor NV (1998) In vivo nitric oxide sensor using non-conducting polymer-modified carbon fiber. Biosens Bioelectron 13:1187
20. Pontie M (2000) Electrochemical nitric oxide microsensors: sensitivity and selectivity characterisation Anal Chim Acta 411:175

21. Brown FO, Lowry JP (2003) Microelectrochemical sensors for in vivo brain analysis: an investigation of procedures for modifying Pt electrodes using Nafion. Analyst 128:700
22. Brown FO, Finnerty NJ, Lowry JP (2009) Nitric oxide monitoring in brain extracellular fluid: characterisation of Nafion-modified Pt electrodes in vitro and in vivo. Analyst 134:2012
23. Palsson E, Finnerty N, Fejgin K, Klamer D, Wass C, Svensson L, Lowry J (2009) Increased cortical nitric oxide release after phencyclidine administration. Synapse 63:1083
24. Fejgin K, Palsson E, Wass C, Svensson L, Klamer D (2007) Nitric oxide signaling in the medial prefrontal cortex is involved in the biochemical and behavioral effects of phencyclidine. Neuropsychopharmacology 33:1874
25. Chen BT, Avshalumov MV, Rice ME (2001) H(2)O(2) is a novel, endogenous modulator of synaptic dopamine release. J Neurophysiol 85:2468
26. Hyslop PA, Zhang ZY, Pearson DV, Phebus LA (1995) Measurement of striatal H_2O_2 by microdialysis following global forebrain ischemia and reperfusion in the rat: correlation with the cytotoxic potential of H_2O_2 in vitro. Brain Res 671:181
27. Lei BP, Adachi N, Nagaro T, Arai T (1997) The effect of dopamine depletion on the H_2O_2 production in the rat striatum following transient middle cerebral artery occlusion. Brain Res 764:299
28. Layton ME, Pazdernik TL, Samson FE (1997) Cerebral penetration injury leads to H_2O_2 generation in microdialysis samples. Neurosci Lett 236:63
29. O'Neill RD, Lowry JP, Rocchitta G, McMahon CP, Serra PA (2008) Designing sensitive and selective polymer/enzyme composite biosensors for brain monitoring *in vivo*. Trends Anal Chem 27:78
30. Kulagina NV, Michael AC (2003) Monitoring hydrogen peroxide in the extracellular space of the brain with amperometric microsensors. Anal Chem 75:4875
31. O'Brien KB, Killoran SJ, O'Neill RD, Lowry JP (2007) Development and characterization in vitro of a catalase-based biosensor for hydrogen peroxide monitoring. Biosens Bioelectron 22:2994
32. Sanford AL, Morton SW, Whitehouse KL, Oara HM, Lugo-Morales LZ, Roberts JG, SombersLA (2010) Voltammetric detection of hydrogen peroxide at carbon fiber microelectrodes. Anal Chem 82:5205–5210
33. Clark LC Jr, Clark EW (1964) Epicardial oxygen measured with a pyrolytic graphite electrode. Ala J Med Sci 1:142
34. Bolger FB, McHugh SB, Bennett R, Li J, Ishwari K, Francois J, Conway MW, Gilmour G, Bannerman DM, Fillenz M, Tricklebank M, Lowry JP (2011) Characterisation of carbon paste electrodes for real-time amperometric monitoring of brain tissue oxygen. J Neurosci Methods 195:135
35. Bolger FB, Bennett R, Lowry JP (2011) An in vitro characterisation comparing carbon paste and Pt microelectrodes for real-time detection of brain tissue oxygen. Analyst 136:4028
36. Lowry JP, Boutelle MG, O'Neill RD, Fillenz M (1996) Characterization of carbon paste electrodes in vitro for simultaneous amperometric measurement of changes in oxygen and ascorbic acid concentrations in vivo. Analyst 121:761
37. Bolger FB, Lowry JP (2005) Brain tissue oxygen: in vivo monitoring with carbon paste electrodes. Sensors 5:473 567
38. Lowry JP, Boutelle MG, Fillenz M (1997) Measurement of brain tissue oxygen at a carbon paste electrode can serve as an index of increases in regional cerebral blood flow. J Neurosci Methods 71:177
39. Lowry JP, Griffin K, McHugh SB, Lowe AS, Tricklebank M, Sibson NR (2010) Real-time electrochemical monitoring of brain tissue oxygen: a surrogate for functional magnetic resonance imaging in rodents. Neuroimage 52:549
40. Bazzu G, Puggioni GGM, Dedola S, Calia G, Rocchitta G, Migheli R, Desole MS, Lowry JP, O'Neill RD, Serra PA (2009) Real-time monitoring of brain tissue oxygen using a miniaturized biotelemetric device implanted in freely moving rats. Anal Chem 81:2235
41. Revsbech NP (1989) An oxygen microsensor with a guard cathode. Limnol Oceanogr 34:474

42. Offenhauser N, Thomsen K, Caesar K, Lauritzen M (2005) Activity-induced tissue oxygenation changes in rat cerebellar cortex: interplay of postsynaptic activity and cerebral blood flow. J Physiol 565:279
43. Piilgaard H, Lauritzen M (2009) Persistent increase in oxygen consumption and impaired neurovascular coupling after spreading depression in rat neocortex. J Cereb Blood Flow Metab 29:1517
44. Hu Y, Mitchell KM, Albahadily FN, Michaelis EK, Wilson GS (1994) Direct measurement of glutamate release in the brain using a dual enzyme-based electrochemical sensor. Brain Res 659:117
45. Hu Y, Wilson GS (1997) Rapid changes in local extracellular rat brain glucose observed with an in vivo glucose sensor. J Neurochem 68:1745
46. Hu Y, Wilson GS (1997) A temporary local energy pool coupled to neuronal activity: fluctuations of extracellular lactate levels in rat brain monitored with rapid-response enzyme-based sensor. J Neurochem 69:1484
47. Lowry JP, McAteer K, El Atrash SS, Duff A, O'Neill RD (1994) Characterization of glucose oxidase-modified poly(phenylenediamine)-coated electrodes in vitro and in vivo: homogeneous interference by ascorbic acid in hydrogen peroxide detection. Anal Chem 66:1754
48. Lowry JP, Miele M, O'Neill RD, Boutelle MG, Fillenz M (1998) An amperometric glucose-oxidase/poly(o-phenylenediamine) biosensor for monitoring brain extracellular glucose: in vivo characterisation in the striatum of freely-moving rats. J Neurosci Methods 79:65
49. Lowry JP, Ryan MR, O'Neill RD (1998) Behaviourally induced changes in extracellular levels of brain glutamate monitored at 1 s resolution with an implanted biosensor. Anal Commun 35:87
50. Lowry JP, Ryan MR, O'Neill RD (2001) Interference in biosensor detection of brain glutamate in vivo: possible role of endogenous ECF hydrogen peroxide. Monitoring molecules in neuroscience. University College Dublin, Dublin, Ireland.
51. Kulagina NV, Shankar L, Michael AC (1999) Monitoring glutamate and ascorbate in the extracellular space of brain tissue with electrochemical microsensors. Anal Chem 71:5093
52. Oldenziel WH, Westerink BHC (2005) Improving glutamate microsensors by optimizing the composition of the redox hydrogel. Anal Chem 77:5520
53. Oldenziel WH, Beukema W, Westerink BHC (2004) Improving the reproducibility of hydrogel-coated glutamate microsensors by using an automated dipcoater. J Neurosci Methods 140:117
54. Oldenziel WH, de Jong LAA, Dijkstra G, Cremers TIFH, Westerink BHC (2006) Improving the performance of glutamate microsensors by purification of ascorbate oxidase. Anal Chem 78:2456
55. Oldenziel WH, Dijkstra G, Cremers TIFH, Westerink BHC (2006) In vivo monitoring of extracellular glutamate in the brain with a microsensor. Brain Res 1118:34
56. Oldenziel WH, Dijkstra G, Cremers TIFH, Westerink BHC (2006) Evaluation of hydrogel-coated glutamate microsensors. Anal Chem 78:3366
57. Burmeister JJ, Gerhardt GA (2001) Self-referencing ceramic-based multisite microelectrodes for the detection and eliminiation of interferences from the measurement of L-glutamate and other analytes. Anal Chem 73:1037
58. Albery WJ, Boutelle MG Galley PT (1992) The dialysis electrode—a new method for in vivo monitoring. J Chem Soc, Chem Commun 12:900
59. Walker MC, Galley PT, Errington ML, Shorvon SD, Jefferys JGR (1995) Ascorbate and glutamate release in the rat hippocampus after perforant path stimulation: a "dialysis electrode" study. J Neurochem 65
60. Asai S, Iribe Y, Kohno T, Ishikawa K (1996) Real time monitoring of biphasic glutamate release using dialysis electrode in rat acute brain ischemia. Neuroreport 7:1092
61. Kohno T, Asai S, Iribe Y, Hosoi I, Shibata K, Ishikawa K (1998) An improved method for the detection of changes in brain extracellular glutamate levels. J Neurosci Methods 81:199

62. Pellerin L, Magistretti PJ (1994) Glutamate uptake into astrocytes stimulates aerobic glycolysis: a mechanism coupling neuronal activity to glucose utilization. Proc Natl Acad Sci 91:10625
63. Fillenz M (2005) The role of lactate in brain metabolism. Neurochem Int 47:413
64. Pellerin L (2003) Lactate as a pivotal element in neuron-glia metabolic cooperation. Neurochem Int 43:331
65. Chih C-P, Lipton P, Roberts EL Jr (2001) Do active cerebral neurons really use lactate rather than glucose? Trends Neurosci 24:573
66. Demestre M, Boutelle MG, Fillenz M (1997) Stimulated release of lactate in freely moving rats is dependent on the uptake of glutamate. J Physiol 499:825
67. Burmeister JJ, Palmer M, Gerhardt GA (2005) L-Lactate measures in brain tissue with ceramic-based multisite microelectrodes. Biosens Bioelectron 20:1772
68. McMahon CP, Rocchitta G, Serra PA, Kirwan SM, Lowry JP, O'Neill RD (2006) The efficiency of immobilised glutamate oxidase decreases with surface enzyme loading: an electrostatic effect, and reversal by a polycation significantly enhances biosensor sensitivity. Analyst 131:68
69. Serra PA, Puggioni G, Bazzu G, Calia G, Migheli R, Rocchitta G (2010) Design and construction of a distributed sensor NET for biotelemetric monitoring of brain energetic metabolism using microsensors and biosensors. Biosensors 241
70. Shram NF, Netchiporouk LI,Martelet C, Jaffrezic-Renault N, Cespuglio R (1997) Brain glucose: voltammetric determination in normal and hyperglycaemic rats using a glucose microsensor. Neuroreport 8:1109
71. Shram NF, Netchiporouk LI, Martelet C, Jaffrezic-Renault N, Bonnet C, Cespuglio R (1998) In vivo voltammetric detection of rat brain lactate with carbon fiber microelectrodes coated with lactate oxidase. Anal Chem 70:2618
72. Shram N, Netchiporouk L, Cespuglio R (2002) Lactate in the brain of the freely moving rat: voltammetric monitoring of the changes related to the sleep–wake states. Eur J Neurosci 16:461
73. Ikegami Y, Maeda M, Yokota A, Hayashida Y (1997) Cerebral extracellular lactate concentration and blood flow during chemical stimulation of the nucleus tractus solitarii in anesthetized rats. Brain Res 758:33
74. Bolger FB, Serra PA, O'Neill RD, Fillenz M, Lowry JP (2006) Real-time monitoring of brain extracellular lactate. In: Di Chiara G, Carboni E, Valentini V, Acquas E, Bassareo V, Cadoni C (eds) Monitoring molecules in neuroscience. University of Cagliari, Cagliari, Italy, p 286
75. Cloutier M, Bolger F, Lowry J, Wellstead P (2009) An integrative dynamic model of brain energy metabolism using in vivo neurochemical measurements.J Comput Neurosci 27:391
76. Bao L, Avshalumov MV, Patel JC, Lee CR,Miller EW, Chang CJ, RiceME (2009) Mitochondria are the source of hydrogen peroxide for dynamic brain-cell signaling. J Neurosci 29:9002

Chapter 7
Modeling Protein and Oxidative Metabolism in Parkinson's Disease

Mathieu Cloutier and Peter Wellstead

Abstract Elevated levels of reactive oxygen species (ROS) and accumulation of misfolded α-synuclein (αSYN) are recurrent features in a majority of Parkinson's disease cases. Building on the brain energy metabolism framework in Chap. 2, a mathematical model is constructed of these key neurochemical players and their interactions. A computer implementation of the model is used to simulate and visualize the dynamics of ROS, αSYN, and their nonlinear interaction within a positive feedback loop. The most important observation from this modeling is that the homogenous nature of known biomarkers (ROS/αSYN) can be reconciled with the heterogeneous nature of the underlying risk factors, including aging, genetics, and toxins. More specifically, our model uses risk factors (aging, toxins) as "inputs" and then provides estimates of PD susceptibility based on their propensity to destabilize the model system. The stability of the model is then used as a criterion to quantify the level of various risks. The importance of rapid biochemical dynamics in evaluating the impact of neuroprotective strategies is also highlighted, with simulations demonstrating the synergistic effect of creatine and antioxidants in buffering ROS levels during transient conditions.

Introduction

Although the etiopathology of PD is still not completely elucidated [1], the biochemistry of affected (dopaminergic) neurons exhibits certain recurring features. The most frequently cited of these include elevated oxidative stress, mitochondrial

M. Cloutier (✉)
GERAD, Ecole Polytechnique de Montreal, Montreal, QC, Canada
e-mail: mathieu.cloutier@nuim.ie

P. Wellstead
Hamilton Institute, National University of Ireland, Maynooth, County Kildare, Ireland
e-mail: peter.wellstead@nuim.ie

P. Wellstead and M. Cloutier (eds.), *Systems Biology of Parkinson's Disease*,
DOI 10.1007/978-1-4614-3411-5_7,

dysfunction, and the accumulation of misfolded αSYN [2–7]. Furthermore, from experimental investigations in animal and cellular models of the disease, it is clear that dynamic interactions between causal factors are important [8–10]. Although experimental investigations yield critical information on basic underlying mechanisms of PD onset and progression, the analysis is often subject to uncertainty and context-dependent assumptions. A particular issue is the causal relationship between ROS, αSYN, and mitochondrial dysfunction, which is not completely explained by qualitative interaction diagrams (such as presented in [1, 2]). In this chapter, we investigate how mathematical modeling can be used to improve our understanding of such interactions, their impact on PD dynamics and causality, and as a means of generating further hypotheses for research on novel therapeutic approaches.

Biochemical Features of Dopaminergic Neurons in PD

A biomarker for the progression of PD is the presence of intracellular inclusions of misfolded αSYN, known as Lewy Bodies (LB) [11]. These protein inclusions are observed in approximately 75% of PD sufferers [12]. The protein αSYN is involved in vesicles fusion and is present in neurons at a relatively high level of concentration (≈100 μM). As αSYN is concentrated in synapses, it is probable that "local" concentrations are even higher. Moreover, the protein has a short half-life (about 2 h) [13], implying a high turnover rate. Thus, in addition to its abundance, αSYN is continuously produced by neurons and can accumulate if misfolds are not disposed of properly (i.e., through proteasomal or lysosomal pathways). Incidentally, one of the major genes involved in PD, the *parkin* gene, is a functional component of the proteasome disposal pathway.

The major mechanisms by which proteins are misfolded include oxidative and nitrative stresses. In this chapter, we concentrate our analysis on oxidative stress, but it should be kept in mind that similar conclusions would be obtained for nitrative stress. The mechanisms by which proteins are misfolded by ROS in aging and disease are relatively well understood [14]. Although oxidative stress continuously occurs in most tissues and plays an important physiological role, an imbalance in ROS is not desirable and can contribute to premature aging and disease [15]. Mitochondria are the major endogenous source of ROS. In particular, approximately 0.1–2% of the O_2 flux through the mitochondrial electron transport chain (ETC) is released as highly reactive superoxide (O_2^-), which in turn is converted to less reactive (but still damaging) hydrogen peroxide (H_2O_2). It is thus perfectly reasonable to posit that dopaminergic neurons are more likely to accumulate high levels of ROS on the basis of their higher energy budget (see Chaps. 1 and 2). Moreover,

the degradation products of dopamine can also increase ROS levels (see Chap. 8) in a manner that contributes further to the specific susceptibility of dopaminergic neurons in PD.

Dynamical Feedback Interactions Between PD-Related Pathways

From this sketch of the major biochemical features of dopaminergic neurons in PD, it is possible to build a complex web of interactions (see, e.g., [2, 16]). First, as mentioned previously, the link from ROS to misfolded protein is straightforward. Regarding αSYN specifically, oxidative damage leads to the formation of misfolded monomers of the protein, which can then aggregate to form oligomers (with 2–8 units of αSYN). These oligomers are highly damaging, with a pore-like structure that binds to various membranes, including mitochondria, vesicles, and lysosomes [17, 18]. The kinetics of binding have been characterized in [18], showing that relatively low levels of misfolded oligomers (1–10 μM, and much lower than the total αSYN pool) are sufficient to induce significant membrane damage.

As highlighted in multiple reviews [2, 8, 10, 16], this damaging effect of αSYN is central to the possible feedback interactions between PD-related factors and pathways. For example, it has been shown that αSYN can interact with mitochondrial complex I and induce the release of ROS [8, 9]. Also, mice genetically modified to suppress expression of αSYN were shown to be more resistant to oxidative insults [10]. In dopaminergic neurons, misfolded αSYN oligomers could potentially increase the permeability of dopamine vesicles in a manner that would increase oxidative stress from the intracellular sequestration of dopamine (see [16] and Chap. 8). This deleterious effect of misfolded αSYN is often qualitatively described as the "vicious cycle" of neurodegeneration, whereby misfolded αSYN and ROS promote the formation of each other.

Finally, protein disposal pathways need energy (in the form of ATP) in order to operate properly. This provides further linkage between energy metabolism and disease progression. Impairment in energy metabolism (especially oxidative phosphorylation) due to aging or other stresses could thus have a "double effect" in PD, whereby it increases ROS levels *and* decreases ATP levels. This twin attack would be further exacerbated by the relatively "low priority" of protein disposal pathways, compared to other energy consuming pathways. For example, the affinity of proteases for ATP (in the mM range [19]) is at least 2–3 orders of magnitude lower than the affinity of ions pumps for ATP (in the μM range [20]). As a result, a reduction in ATP concentration will most likely impair proteases long before it affects the ion pumps. From this observation, it is possible to posit that misfolded proteins can accumulate for a long time (i.e., when ATP levels are slowly decreasing, but still in the mM range), whereas neuronal integrity and function (i.e., ion pumping, etc.) are still

maintained. As presented in Fig. 6 of Chap. 2, this allows a "range" for disease to develop as energy production continues, but with high ROS levels (and therefore protein misfolding).

The Role of Mathematical Modeling

Chapter 2 described how brain energy metabolism can form a framework in which to integrate the biological pathways and mechanisms involved in PD. As mentioned previously, energy metabolism (more specifically oxidative phosphorylation) is the major source of both ATP and ROS. With this in mind, the authors developed an integrative and detailed modeling of energy metabolism [21], as well as a control systems understanding of energy regulation [22]. We then used the energy metabolism modeling as a framework for the development of an energy systems approach to PD [23] and further developed a detailed model of PD biochemistry [24]. This, in turn, led to the identification and mathematical description of a positive feedback loop between ROS and αSYN [25]. In this current chapter, we present a relatively simplified model of PD-related pathways and energy metabolism, with the objective of minimizing the number of parameters while still reproducing experimental results. As the model is based on ordinary differential equations (ODEs), one of its characteristic features is an ability to reproduce both the steady-state and dynamic conditions in the brain. This integration of dynamic factors will have a critical role in our understanding of disease onset (pathogenesis) and its subsequent progression.

As mentioned throughout this volume, mathematical modeling can be a powerful tool for both experimental biology and systems analysis. More specifically, experimental biologists benefit from a model that can first reproduce experimental data and then generate hypotheses and predict further experimental outcomes. On the other hand, an ODE model is a compact and unequivocal translation of the underlying biological processes. Moreover, ODE models of biology are a form that most engineers can use, even with minimal understanding of the details of disease biology. The model presented here was developed along these lines; the objective is to represent crucial dynamical factors in PD, but with a minimum of equations and parameters.

The following section presents the model and an example of calibration with in vivo LAC data (see Chap. 6 and Fig. 3 of Chap. 2). We then present simulations of neuronal biochemistry under conditions known to increase the risk of PD. More specifically, two cases will be considered: (1) transient exposure to toxins such as MPTP [26]; (2) effect of aging (see Chap. 3). As observed in previous works [24, 25], the "vicious cycle" between ROS/αSYN when translated into a mathematical model, forms a positive feedback loop that exhibits bistability for a wide range of conditions. The implications of this for disease will be briefly discussed. Finally, we use the model as a tool to generate hypotheses on the inner functioning of some neuroprotective strategies, with emphasis on the underlying dynamics.

Combining Energy Metabolism, ROS, and αSYN Dynamics in PD

Model Presentation, Scope, and Implementation

Our mathematical model of energy metabolism with ROS and αSYN dynamics is based on a simplified version of previous works [21–23] and the brain energy metabolism model in Chap. 2. The simplification is done in a way that highlights the key feedback interactions between ROS and αSYN, as shown in Fig. 7.1a (the corresponding ODEs and kinetic equations are given in Tables 7.1 and 7.2, respectively). This section describes some general aspects of the model's scope and implementation, while the following subsections provide details of the model construction and calibration.

The model uses concentrations units for all the biochemical species (i.e., μM) and is limited to a generic set of reactions and pathways found in all neurons. This is to ensure that the model is scalable and adaptable for further studies. In particular, the goal of this study is to give a deterministic "baseline" model upon which subsequent studies will be built. In this context, it is important to note that the parameters of our ODE model, and the ensuing simulations, are representative of what could occur in a generic scenario. Variations between individuals (either animal models or human patients) are obviously expected and in our modeling framework, this would be implemented by fine-tuning the parameters (given that data is available). Note that most parameters of the model (Table 7.3) are chosen to be representative of physiologically measurable entities, such as biochemical reaction rates, affinity constants, etc.

The model was implemented in the Matlab scientific computing environment (The Mathworks, Inc.) using the Systems Biology Toolbox [27], including the provided subroutines for model calibration. A curated implementation of the model is available at www.cellml.org.

Brain Energy Metabolism Regulation

For the purposes of this chapter, the major components of brain energy metabolism are simplified into four processes: glycolysis (v_0), oxidative phosphorylation (v_1), energy consumption (v_2), and possible LAC exchanges between neurons and astrocytes (v_3, v_4, and v_5). Glycolysis is regulated by the ATP concentration with activation–inhibition kinetics [21, 22] (see Table 7.2). The form of this kinetic equation has been verified extensively from in vitro analysis [28] and is used frequently in mathematical modeling [29]. Here, we assume a sufficient glucose (GLC) supply and lump the glycolytic pathway in one reaction which produces pyruvate (PYR) molecules and ATP. Oxidative phosphorylation (v_1 in Table 7.2) is

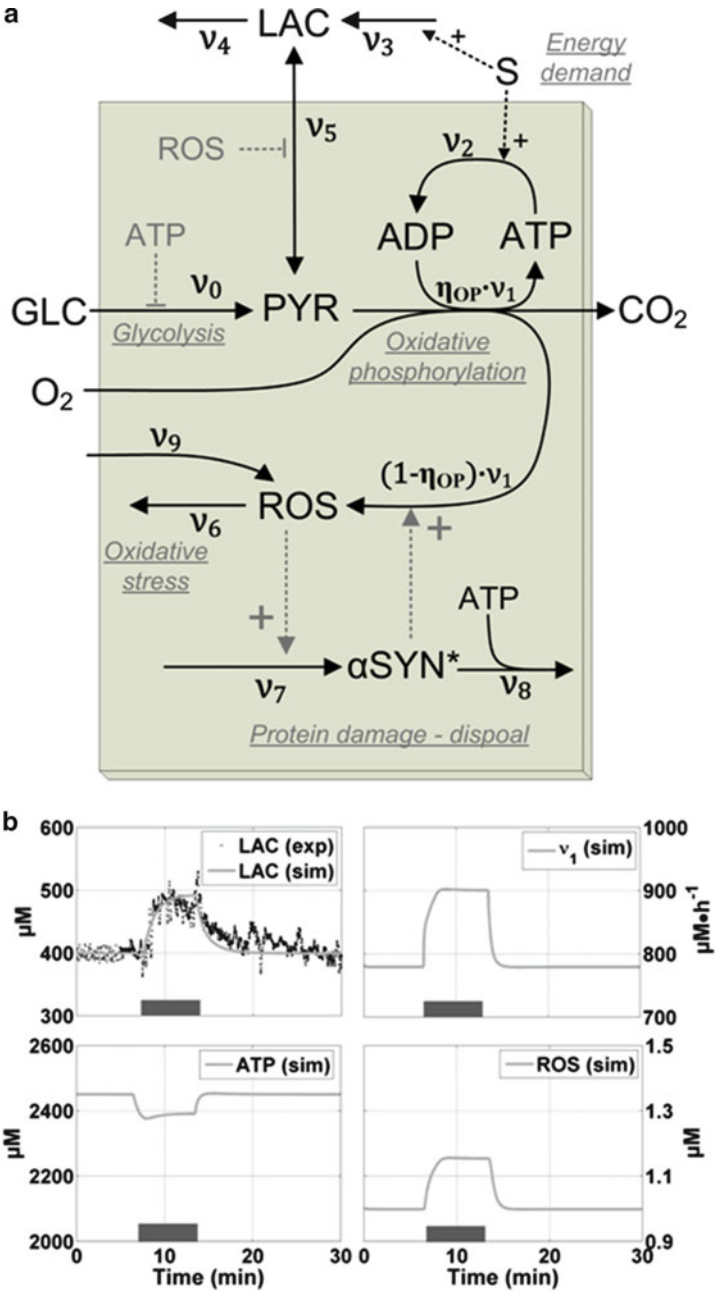

Fig. 7.1 Model of PD-related pathways and energy metabolism. (**a**) Model pathways: note that GLC, O_2, and CO_2 dynamics are not modeled in this work. (**b**) Calibration of the model with in vivo LAC data (see Chap. 6). The *gray band* highlights a period of sensory stimulation in a freely moving animal. This is reproduced in the model by increasing the energy demand by ≈15%

Table 7.1 Mass balances of the model

Variable		Steady-state value (μM)	Differential equation
PYR	Pyruvate	105	$\frac{\mathrm{dPYR}}{\mathrm{d}t} = v_0 - v_1 - v_5$
ATP	Adenosine triphosphate	2450	$\frac{\mathrm{dATP}}{\mathrm{d}t} = 2v_0 + 15\eta_{\mathrm{OP}} \times v_1 - v_2 - 25v_8 + v_{10}$
ADP	Adenosine diphosphate	50	$\mathrm{ADP} = \mathrm{ATP_{TOT}} - \mathrm{ATP}$
LAC[a]	Lactate	400	$\frac{\mathrm{dLAC}}{\mathrm{d}t} = R_{\mathrm{NE}} \times v_5 - v_4 + v_3$
ROS[b]	Reactive O_2 species	1	$\frac{\mathrm{dROS}}{\mathrm{d}t} = (1 - \eta_{\mathrm{OP}}) \times v_1 - v_6 + v_9 - v_{11}$
αSYN*	Misfolded αSYN	1	$\frac{\mathrm{d}\alpha\mathrm{SYN}_*}{\mathrm{d}t} = v_7 - v_8$
PCr	Phosphocreatine	4500	$\frac{\mathrm{dPCr}}{\mathrm{d}t} = -v_{10}$
Cr	Creatine	500	$\mathrm{Cr} = \mathrm{Cr_{TOT}} - \mathrm{PCr}$
AOx	Antioxidant buffer	495	$\frac{\mathrm{dAOx}}{\mathrm{d}t} = -v_{11}$
AOx*	Oxidized AOx	5	$\mathrm{AOx*} = \mathrm{AOx_{TOT}} - \mathrm{AOx}$

[a] R_{NE} (=2.25) is the volumetric ratio of neurons (45% of brain volume) to extracellular fluid (20% of brain volume)

[b] v_9 is a user-defined flux that can be manipulated to reproduce exposition to toxins (see Fig. 7.2). η_{OP} is the mitochondrial ETC efficiency, i.e., the fraction of O_2 consumption that goes to energy production. The other fraction ($1 - \eta_{\mathrm{OP}}$) is converted to ROS. This variable is defined in Table 7.2

Table 7.2 Kinetic equations for fluxes of energy and PD-related pathways

Reaction	Kinetic equation
Glycolysis	$v_0 = k_0 \times \left[\frac{1-(\mathrm{ATP}/K_{\mathrm{I,ATP}})^4}{1+(\mathrm{ATP}/K_{\mathrm{I,ATP}})^4}\right]$
Ox. phos.	$v_1 = k_1 \times \mathrm{PYR} \times \left[\frac{1}{1+0.01(\mathrm{ATP}/\mathrm{ADP})}\right]$
ETC efficiency	$\eta_{\mathrm{op}} = \eta_{\mathrm{op,max}} - \beta_{\mathrm{op},\alpha\mathrm{syn}} \times \left[\frac{\alpha\mathrm{SYN}_*{}^4}{\alpha\mathrm{SYN}_*{}^4 + K_{\alpha\mathrm{SYN}}{}^4}\right]$
Energy consumption	$v_2 = k_2 \times \left[\frac{\mathrm{ATP}}{\mathrm{ATP}+K_{\mathrm{M1,ATP}}}\right] \times S$
Astrocytes LAC production	$v_3 = k_3 \times S$
LAC efflux to blood stream	$v_4 = k_4 \times \mathrm{LAC}$
LAC dehydrogenase	$v_5 = \left[k_{\mathrm{f},5} \times \mathrm{PYR} - k_{\mathrm{r},5} \times \mathrm{LAC}\right] \times \left(1 - \beta_{\mathrm{ldh,ros}} \times \left[\frac{\mathrm{ROS}^4}{\mathrm{ROS}^4 + K_{\mathrm{ROS}}{}^4}\right]\right)$
ROS removal	$v_6 = k_6 \times \mathrm{ROS}$
aSYN misfolding	$v_7 = k_7 \times \mathrm{ROS}$
aSYN removal	$v_8 = k_8 \times aSYN* \times \left[\frac{\mathrm{ATP}}{\mathrm{ATP}+K_{m2,\mathrm{ATP}}}\right]$
Creatine kinase	$v_{10} = k_{\mathrm{f},10} \times \mathrm{PCr} \times \mathrm{ADP} - k_{\mathrm{r},10} \times \mathrm{Cr} \times \mathrm{ATP}$
AOx	$v_{11} = k_{\mathrm{f},11} \times \mathrm{AOx} \times \mathrm{ROS} - k_{\mathrm{r},11} \times \mathrm{AOx}*$

regulated by the ATP/ADP ratio [30] and PYR availability, as presented elsewhere [21, 22]. This slightly different regulation between v_0 and v_1 implies that the intermediate PYR needs an additional "degree of freedom" in order to avoid intracellular accumulation or depletion. The enzyme lactate dehydrogenase

Table 7.3 Parameters of the model

Parameter	Numerical values	Units	References
k_0	1.7x10^6	μM h^{-1}	Model calibration
k_1	467	h^{-1}	Model calibration
k_2	8.2×10^5	μM h^{-1}	Neuronal energy demand [21]
k_3	1.2×10^5	μM h^{-1}	Model calibration and [21]
k_4	30	h^{-1}	Model calibration and [21]
$k_{f,5}$	30	h^{-1}	Model calibration and [21]
$k_{r,5}$	11.25	h^{-1}	Model calibration and [21]
k_6	235	h^{-1}	[24, 25, 42]
k_7	7×10^{-3}	h^{-1}	[24, 25, 38, 39, 41]
k_8	9.86×10^{-3}	h^{-1}	[24, 25, 38, 39, 41]
$k_{f,10}$	2	μM^{-1} h^{-1}	[21, 22]
$k_{r,10}$	0.367	μM^{-1} h^{-1}	[21, 22]
$k_{f,11}$	0.2	μM^{-1} h^{-1}	Model calibration and [51]
$k_{r,11}$	24.9	h^{-1}	Model calibration and [51]
$K_{I,ATP}$	1000	μM	[21, 22]
$K_{M1,ATP}$	100	μM	[19]
$K_{M2,ATP}$	1000	μM	[20, 21]
$\eta_{OP,max}$	0.995	–	[15]
$\beta_{OP,\alpha SYN}$	0.08	–	Estimated from [44]
$K_{\alpha SYN}$	8.5	μM	Estimated from [18]
$\beta_{ldh,ros}$	0.5	–	[33]
K_{ROS}	10	μM	[33]

(v_5 in Fig. 7.1 and Table 7.2) provides such a mechanism. For example, during intense exercise, O_2 transport to muscle cells limits oxidative phosphorylation and excess PYR is excreted as lactate (LAC). In neurons, the mechanism is still a topic for debate, with the balance of probability being that neurons consume excess LAC produced by astrocytes during stimulation (v_3) (a theory presented as the "astrocyte-neuron LAC shuttle" [31]). In Chap. 2, we reviewed some previous works that showed how this mechanism improves ATP regulation in transient conditions by acting as a feedforward controller [21, 22]. Finally, ATP is consumed by a generic ATPase reaction (v_2) that lumps all the neuronal energy consuming reactions. ATP is also involved in protein removal (v_8 in Fig. 7.1a and Table 7.2).

Oxidative Stress and αSYN Misfolding

Oxidative phosphorylation (v_1) is the major source of oxidative stress in animal tissues. In normal physiological conditions, approximately 0.1–2% of the flux v_1 can leak to form ROS [15]. We describe this in the model by using a coefficient for oxidative phosphorylation efficiency (η_{OP} in Table 7.2). This coefficient represents the fraction of v_1 that goes to energy production, while the remainder (i.e., $(1 - \eta_{OP})v_1$) is the flux of ROS production. ROS are removed by a generic

antioxidative reaction (v_6). We also consider that ROS levels can increase in the presence of external toxins such as MPTP. This reaction is modeled with reaction v_9 and is set to 0 by default, but can be modulated to represent continuous or transient toxic exposure.

ROS will have two major effects in this model. First, it will lead to the misfolding of αSYN (v_7), a reaction we describe with mass action kinetics [32]. Misfolded αSYN (αSYN* in Fig. 7.1 and Tables 7.1 and 7.2) is then removed by a generic proteasomal reaction (v_8), again using mass action kinetics for αSYN* and a low affinity Michaelis–Menten kinetic for ATP [19] (see Table 7.2). Elevated ROS can also cause damage to proteins and reduced enzymatic activity (this has been characterized for LAC dehydrogenase in the brain [33]), we represent this by an inhibition kinetic for v_5 (see Table 7.2). Other enzymes are most probably affected as well, but are not included here.

Finally, we close the aforementioned "vicious cycle" of oxidative stress and protein misfolding by assuming that αSYN* can increase endogenous ROS release from reaction (v_1). To this end, we use a nonlinear Hill equation, for which the parameters are estimated as described below and in previous works [24, 25].

Parameters Estimation and Model Calibration

The model presented in Fig. 7.1 has 5 states, 9 reactions, and 15 kinetic parameters. Note that we will implement two additional reactions in a later section but these reactions are for rapid dynamics (i.e., seconds) and do not affect the model calibration described here. Many of the parameters can be determined from the literature on enzyme kinetics. For example, the inhibition of (v_0) by ATP requires an inhibition constant (K_{IATP}) that we determine from kinetic data [28], and as detailed in other modeling studies [21, 22]. The same approach is applied for the regulation of oxidative phosphorylation (v_1), whereas the kinetic data comes from in vitro experiments on isolated mitochondria [30]. As mentioned previously, the affinity constant for ATPases ($K_{\mathrm{M1,ATP}}$ in v_2) is known to be in the μM range [20], consequently we have used a value of 100 μM for this parameter.

Regarding energy metabolism, the major uncertainty rests with the kinetic reaction rate constants (k_0–k_5 in Tables 7.2 and 7.3) for which in vivo measurement is practically impossible. Various methods can be used to estimate these rate constants. For example, the enzyme abundance can be combined with known enzymatic turnover rates in order to estimate the maximal enzymatic activity, thus providing a constraint on possible values for the actual metabolic flux [34]. Other constraints (including thermodynamics) can also be implemented [35], however, these are more suited to genome scale metabolic reconstructions (such as in [35]) and could be misleading if applied to our highly simplified reactions. To avoid this issue, we used an approach that combines literature data about the metabolic steady state in the brain and in vivo LAC data that provides information

about the dynamic response during brain stimulation. This approach can be divided into three major steps:

- Set parameter k_2 such that the model reproduces the neuronal ATP consumption rate.
- Use a coarse optimization routine to find values for other rate constants (k_0, k_1, k_3, k_4, $k_{f,5}$, $k_{r,5}$) so that the simulated steady-state concentrations correspond to literature data.
- Perform a final fine-tuning of all the parameters so that it reproduces the dynamic response during stimulation as measured by the in vivo sensors described in Chap. 6.

For the first step, the cerebral metabolic rates at rest and during stimulation have been measured extensively [36, 37], with the observation that the human brain consumes approximately 100–120 g of GLC per day. Moreover, energy metabolism in the brain is driven mostly by ATP consumption—i.e., an increase in energy consumption leads to a slight reduction in ATP and glycolysis activation. Thus, by setting the correct rate for the ATPase reaction (k_2 in reaction v_2), we can basically control the glycolytic flux such that our "simulated brain" consumes GLC at the experimentally observed rate. For the second step, a coarse optimization routine was used to find a set of reaction constants (k_0 to k_5) such that the error between model predictions and known steady-state concentrations (see Table 7.1) is minimized. This solution is then refined further in the third step by optimizing all the model's parameters such that the simulated LAC profile fits with in vivo data during sensory stimulation in animals (see Fig. 7.1b). For this simulation, the parameter "*S*" (see Table 7.2) is used to increase energy consumption by about 15% over a 5-min interval (e.g., the sensory stimulation period for the animal experiment). The resulting model correctly reproduces the cerebral metabolic environment, with fluxes and concentration within physiological range and a good description of the short-term LAC dynamics during neuronal stimulation (as shown in Fig. 7.1b).

The calibration of the deterministic ODE model with in vivo data from reliable biosensors (Chap. 6) is an important step in producing a realistic "baseline" model of brain energy metabolism that can then be extended by adding PD-related features. In this connection, we previously developed a relatively detailed model of PD pathways [24], for which a reduction to a two-state (ROS and αSYN*) model was possible [25]. In line with this minimalist approach, we will use only two states to describe the vicious cycle between ROS and αSYN* here. The calibration procedure is relatively straightforward and can be expressed as follows:

- Set the basal value for η_{OP} ($\eta_{OP,max}$) according to literature data—here, we use a conservative 0.5% ROS leakage or $\eta_{OP,max} = 99.5\%$. The same approach is used for αSYN*, whereby estimates from modeling work in [38, 39] are used to determine the basal misfolding rate.
- As the basal rates of ROS/αSYN* production are determined, we can set the removal rates (k_6, k_8) such that the steady-state concentrations of both species

are equal to values reported in the literature—i.e., αSYN* is in the μM range [40, 41] and ROS measurements of 1 μM are reported [42, 43].
- For the feedback exerted by αSYN* on ROS production (see η_{OP} in Table 7.2), a Hill kinetic equation of order 4, with half-saturation constant of 8.5 μM, is determined from in vitro data [18]. The maximal increase in endogenous ROS release ($\beta_{OP,\alpha SYN}$ in Table 7.2) is set such that a ≈8% leak to ROS is possible at high αSYN* concentrations—this is a conservative estimate from *postmortem* analysis of mitochondria in PD sufferers [44].

Ethical issues and technical complexities of measurement mean that experimental data on intraneuronal ROS and αSYN* dynamics over the time course of disease progression will not be available in the foreseeable future. Our approach here was rather to determine conservative estimates that ensure ROS and αSYN* in the model will remain within physiological range, whereas key parameters of the feedback interaction are determined from available data.

Simulations Results and Analysis

Simulation of Risk Factors in PD

In previous work [24, 25], we established that the modeling framework based on energy metabolism and feedback interactions between ROS/αSYN* could reproduce a wide range of disease-inducing mechanisms. The simplified model presented here was constructed and verified on the same basis. To provide a self-contained development, some features of this development will be briefly presented (see Fig. 7.2).

PD symptoms can be induced by intense transient oxidative stress [26, 45]. We implement this type of "stimulus" in the model by applying a single transient step increase for reaction v_9. Three different simulations were performed: in the first, a prolonged but low intensity stress is applied. The responses (light gray lines in Fig. 7.2a, b) show that the system operates in the range of its physiological steady state, with low levels of ROS and αSYN*. In the second simulation, a short stress pulse of medium intensity is applied and the responses (gray lines in Fig. 7.2a, b) show that the system can also recover, even though some transient damage is accumulated (see Fig. 7.2b, gray line). In the third simulation, a short but intense stress pulse is applied and the responses (black lines in Fig. 7.2a, b) show how the system is destabilized and that damaged αSYN and ROS accumulate exponentially until a physiological limit is reached. In this simulation, a critical point has been passed in the system's nonlinear feedback dynamics and the model moves to a new state where a high ROS concentration exists, sustained by corresponding high levels in αSYN*. Although the input we use (i.e., a constant step in reaction v_9) is synthetic and may not be exactly the representative of toxin exposure in the brain, the overall dynamics of the cascade of events corresponds with reports on MPTP

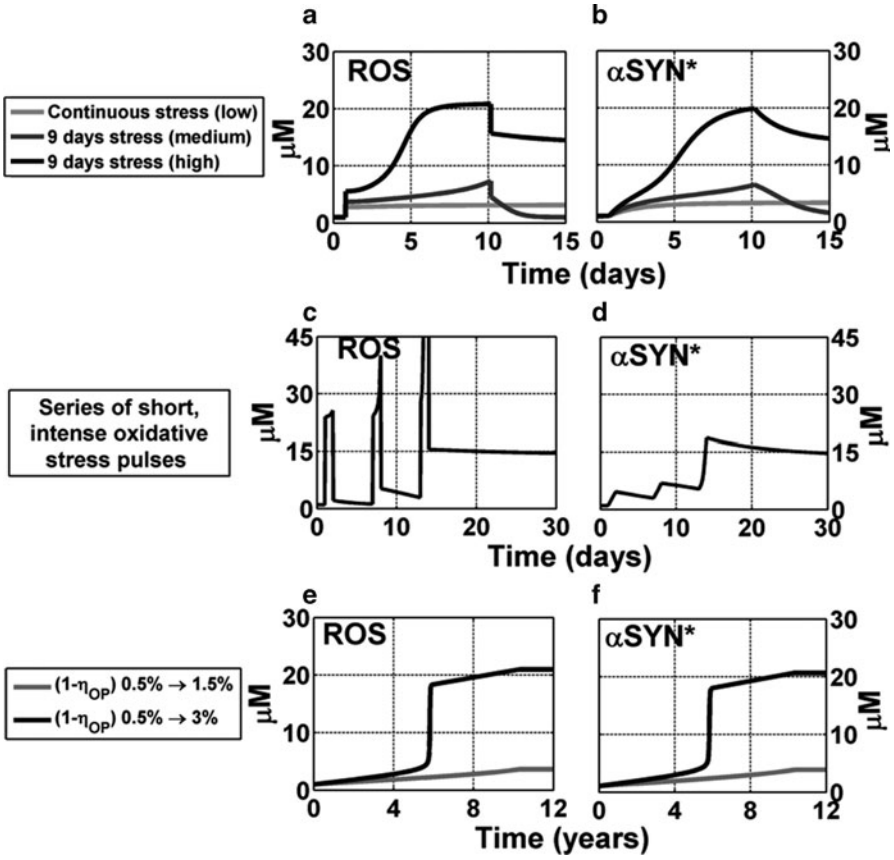

Fig. 7.2 Reproducing the effect of toxin exposure and aging. (**a**, **b**) Effect of exposure to toxins (i.e., modulation of v_9) on oxidative stress and αSYN* profiles. The exposure profiles are continuous low intensity stress (*light gray lines*), 9 days pulses starting at $t = 1$ day with medium (*gray lines*) and high intensity (*black lines*). (**c**, **d**) Effect of chronic exposure. Intense pulses of oxidative stress are implemented every 5 days. (**e**, **f**) Effect of aging on PD susceptibility. The mitochondrial release of ROS is linearly increased by 200% (*gray lines*) and 500% (*black lines*) over a period of 10 years (see Chap. 3)

usage by drug addicts, where Parkinson's symptoms were irreversibly induced within days of injection [26].

A further way to show that the disease state can be induced by drug usage is to simulate chronic exposure to periodic doses of oxidative stress. This is presented in Fig. 7.2c, d, where three intense pulses (i.e., increases in v_9) are implemented at a frequency of one every 5th day. Interestingly, the disease state is reached after a few pulses, as the system cannot recover normal αSYN* levels in between doses (its dynamics are slower than that of ROS). This feature of our model is in agreement with the observation that MPTP treatment can induce PD symptoms in mice if the drug is administered at a frequency of two doses per week [45].

Finally, as mentioned in previous chapters, advanced age is the major risk factor in PD. Although the ways in which age increases susceptibility to PD are not completely understood, there are strong grounds for arguing that brain energy metabolism compromised by age causes increased oxidative stress, mostly through the loss of Complex 1 efficiency. In our modeling framework, it is possible to show a refined form of the previous (Chap. 2) simulations, by decreasing the parameter for the mitochondrial efficiency ($\eta_{OP,MAX}$ in Table 7.2). Figure 7.2e, f presents simulation results for two linear decreases in mitochondrial efficiency ($\eta_{OP,MAX}$ decreasing over 10 years), from 0.5% to 1.5% of mitochondrial flux (gray lines) and from 0.5% to 3% of mitochondrial flux (black lines). As was the case with external stresses, we observe two possible outcomes: the system can maintain its integrity if the stress is mild (gray lines in Fig. 7.2e, f) or it is destabilized by the stress and the influence of the positive feedback dramatically increases the further release of ROS (black lines in Fig. 7.2e, f)

Bifurcation Analysis

The curves generated in the previous diagram are relatively easy to analyze and can also be compared to experimental data (e.g., Fig. 7.1b). However, an infinite number of such simulations could be made, covering all parameter values within physiological range, and still little additional insight would be obtained. The major observation from Fig. 7.2, and in coherence with the literature on MPTP, is that the feedback system of ROS and αSYN* can stabilize to damaging values even if only a transient stress is applied. This is summarized in Fig. 7.3.

First, a generic dynamical response (Fig. 7.3a) shows the three steady states: (1) healthy steady state; (2) steady state when $v_9 = 560$ mM h^{-1} is applied (i.e., the gray area); and (3) the "disease" state, with high ROS after v_9 is set back to 0. A much more compact representation is obtained by plotting only the steady states (i.e., points 1–3) as a function of a certain parameter. This plot is called a bifurcation diagram and is used frequently in the analysis of biological processes such as the cell cycle ([46, 47] and in this volume in Chap. 4). We produced this diagram for our system in Fig. 7.3b, again using v_9 (external oxidative stress) as the manipulated parameter. As can be seen the system has a relatively important range for healthy operation (i.e., the lower curve in Fig. 7.3b). In that region ($v_9 = 0$–550 mM h^{-1}), any transient stress would stabilize back to the healthy steady state. Note that $v_9 = 550$ mM h^{-1} is, roughly, 2.5 times higher than the basal release of ROS by the mitochondria. Thus, there is plenty of "head-room" for oxidative stress to vary without inducing the disease state. However, if an oxidative stress higher than $v_9 = 550$ mM h^{-1} is applied, the system will eventually switch to the higher curve (with exponential dynamics similar to Fig. 7.3a) and remain there (point 2 in Fig. 7.3a, b). This would not be so problematic if the system could "switch back" to the lower curve when v_9 is returned to zero. However, this is not possible for positive values of v_9 and consequently the switch is irreversible (i.e., the system

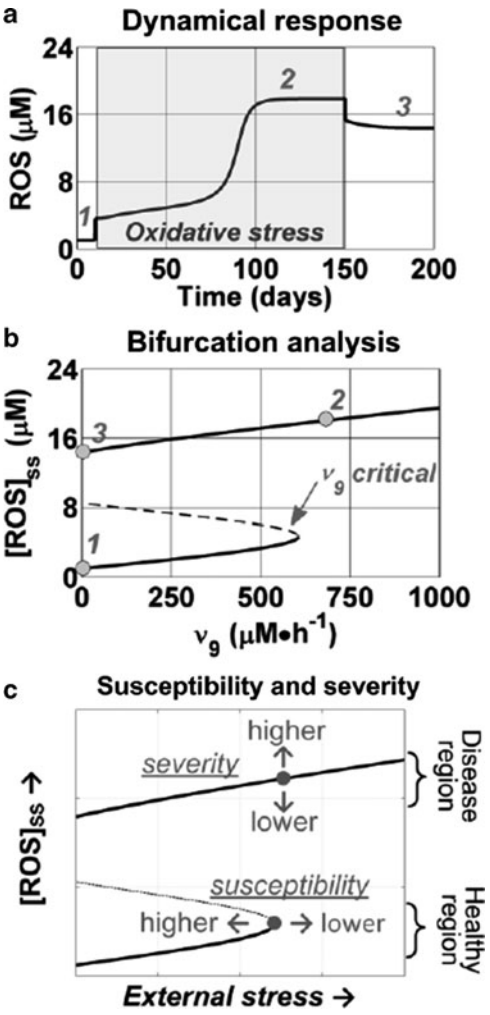

Fig. 7.3 Bifurcation analysis. (**a**) Dynamic response of the model to oxidative stress (*gray area*; $v_9 = 560\ \mu M\ h^{-1}$). (**b**) Bifurcation diagram for steady-state ROS levels (*vertical axis*) as a function of external oxidative stress (*horizontal axis*); stable (*full lines*), and unstable (*dotted line*) steady states are shown. (**c**) Susceptibility and severity of PD as properties of a bifurcation diagram

stabilizes to point #3). This key feature of the bifurcation diagram is a mathematical confirmation of experimental reports on MPTP and other PD-inducing toxins, which showed that a transient exposure can induce a continuous and irreversible progression of the disease [26, 45].

Finally, we summarize two fundamental properties of PD etiopathology with regard to the bifurcation diagram: (1) disease susceptibility and (2) severity of the condition (see Fig. 7.3c). The critical point at which the healthy steady-state curve stops refers to PD susceptibility in the sense that a higher critical v_9 implies greater resistance to external oxidative insults and thus a reduced chance of developing the disease. Conversely an extremely low (or null) critical value for v_9 would imply very high susceptibility, as any small stress could move the system away from the healthy state. Once in the disease state (i.e., the upper curve in Fig. 7.3b, c) it is

probable that the severity of the condition will correlate with the actual ROS levels. Thus, any change in physiological parameter (i.e., reduction in antioxidative metabolism, see Chap. 3) that shifts the curve to higher ROS levels would make the overall condition more aggressive.

The simulation results presented in this section show how a mathematical description of the feedback interactions between ROS and αSYN* is completely coherent with the "vicious cycle" of neurodegeneration. In systems biology terms, the model suggests that PD is triggered by an irreversible bistable neurochemical switching process. The possible shapes of the bifurcation diagram could be used to focus the investigation of pathogenesis, and as a tool for generating hypotheses on how changes in particular parameter can affect the steady states of the system.

Simulation of Neuroprotective Strategies: The Synergistic Effect of Phosphocreatine and Antioxidants

The previous section was concerned with the steady states of the system and their qualitative properties with regard to PD etiopathology. In this section, we demonstrate the importance of considering dynamical issues when investigating neuroprotective strategies.

Figure 7.1a is a generic model of PD-related biochemical processes that can be used to explore, in silico, how various neuroprotective mechanisms might improve resistance to oxidative stress or αSYN misfolding. For example, a recent study showed that a combination of CoQ_{10} and creatine can reduce PD susceptibility in animal models [48]. As these molecules are readily available as nutritional supplements, there was hope that they could provide a simple and effective neuroprotective regime. Unfortunately, clinical trials with *either* CoQ_{10} *or* creatine in human subjects have proven statistically inconclusive [49] and current clinical investigations without creatine (with results to be published in 2012–2013), rely on high dosages of CoQ_{10}. The positive results in [48] on the combined use of creatine and CoQ_{10} contrast sharply with the counter conclusions from their independent use. This apparent paradox would be resolved if there were to be a synergetic benefit from using both creatine *and* antioxidants (such as CoQ_{10}). The model can be used to examine this hypothesis in silico, and in particular, to investigate the dynamical aspects of a possible beneficial interaction between CoQ_{10} and creatine in the biochemical context of PD.

Creatine (Cr) is used in metabolic pathways to store energy in phosphorous bonds. The high-energy molecule thus obtained (phosphocreatine, PCr) can then be used to restore ATP levels during periods of high demand. The reaction is catalyzed by the enzyme creatine kinase (v_{10} in Fig. 7.4a and Table 7.2). The reaction is reversible and reaches equilibrium quite rapidly. In this form, creatine provides energy only when the ATP concentration is decreasing, a mechanism that we previously concluded was similar to the derivative action used extensively in

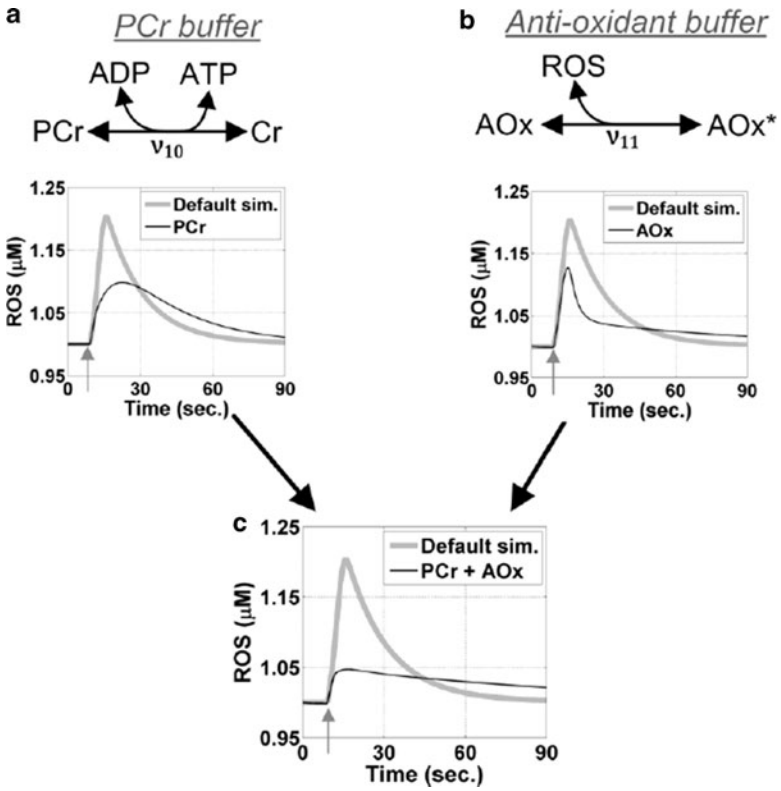

Fig. 7.4 Exploring the ROS buffering role of creatine (**a**), antioxidants (**b**), and a combination of both (**c**) in transient conditions. The default simulation (*thick gray lines*) is without creatine and antioxidants. The simulations are for short-term transient conditions in synapses, with a 1-s stimulation of energy consumption (indicated by *gray arrows*). Fluxes v_{10} and v_{11} are defined in Table 7.2

control systems [22]. This mechanism thus operates only under highly transient conditions, such as we could expect in a firing synapse.

We investigated this in silico by simulating large changes in energy demand over a very short time (i.e., about 1 s such as observed in Chap. 4) and analyzed ROS profiles with, and without, creatine buffering (see Fig. 7.4a). As can be seen, although creatine is an energy buffer, it also has an effect on ROS levels during stimulation. The reason for this is that any ATP molecule regenerated by PCr does not have to be regenerated by the mitochondrial ETC. This results in a lower mitochondrial activation during the spike in energy demand (simulations not shown) and consequently, lower mitochondrial derived ROS. However, PCr regeneration (which requires ATP) after the spike will obviously lead to a delayed production of the ROS molecules that were not produced during the stress. The overall result is thus not a reduction in total ROS production, but a "spreading out" oxidative stress over time (i.e., the areas under both curves in Fig. 7.4a are the same). In this context,

the advantage of buffering energy lies in the reduction of the ROS peak during stimulation. Since a low ROS level over a longer time is not problematic, the "spreading feature" would probably help the cells to avoid dangerous transients.

Interestingly, cells also have oxidative stress "buffer" molecules—i.e., molecules that can sequester ROS, but then need to be regenerated by oxidizing another molecule. The most abundant of such molecules is glutathione, which is regenerated by oxidizing NADPH, which is in turn regenerated by the pentose phosphate pathway [50, 51]. In addition to its role in the mitochondrial electron transport chain, CoQ_{10} is also an antioxidant that operates on a similar principle as glutathione (i.e., it is easily reduced and oxidized and can thus mediate or buffer oxidative stress). Remaining with the theme of using simple models, we implemented one generic antioxidant reaction in the model, with the antioxidant alternating between its reduced (AOx) and oxidized (AOx*) forms (see v_{11} in Fig. 7.4b and Table 7.2). Simulations presented in Fig. 7.4b show that antioxidants also have a benefit in smoothing the ROS peak, although the shape of the curve is slightly different compared to the simulation with PCr.

Finally, in keeping with the observations in [48] and the hypothesis of a synergistic effect, we also produced a simulation with both molecules present (see Fig. 7.4c). The net effect is an almost complete disappearance of the ROS peak after stimulation and a maximal ROS "disturbance" of 0.05 μM from the base level—i.e., a fourfold disturbance reduction compared to the simulation without creatine and antioxidants.

However, keeping in mind our premise on the mitigated role of creatine and antioxidants, these results must be analyzed carefully. As mentioned previously, with the buffer mechanisms, the ROS are only spread out on a longer period of time. This is most probably beneficial to some extent, but the actual improvement would depend on the dynamics of the energy budget at the synaptic level—an area that is still not fully elucidated [52]. Secondly, our model also indicates that the amounts of PCr and antioxidant available *locally* within neurons or synapses are also important (simulation not shown). Thus, the success of a PCr/antioxidant regime most probably depends on both the right dosage and dynamic regime (which we do not necessarily control). Thus, it seems clear that the approach has potential (as was shown in animal models), but that it's relative complexity means that the transposition from animals to human should be explored with great care.

Concluding Remarks

The mathematical modeling framework presented here is in line with current systems approaches developed for complex diseases. The long-term objective is to use such models in the role of a translator, such that biologist, engineers, mathematicians, and physicians can collaborate in their studies of complex diseases such as Parkinson's. Thus, one specific objective of this chapter was to show how we can "translate" the recurring and often cited "vicious cycle" of neurodegeneration

[1–7] into a compact mathematical form that can be easily analyzed, used, and communicated. The result is a bifurcation diagram highlighting how PD can be modeled by an irreversible bistable switching mechanism.

As highlighted with this model and elsewhere in the book, Parkinson's is a disease for which the dynamics of the underlying biological processes are critical. It will thus be important to pursue the development of new experimental probes (such as that described in Chap. 6) and complement them with rigorous mathematical models that can be used as in silico probes for components of the system that cannot be measured easily. The brain is a complex system with a continuously changing pattern of activity and it is obvious that a better understanding of neurodegeneration requires a full appreciation of the underlying biochemical dynamics that can be obtained through modeling. As an example, we have shown here how a model can be used to improve our understanding of the dynamic role played by creatine in alleviating oxidative stress in transient conditions.

The variability of PD implies that research into the condition and the ensuing medical treatment will require predictive and personalized approaches. This point was not discussed extensively here, but the models developed in [21–25] have already shown some predictive capacity and could thus potentially be used to direct therapy development in a predictive manner. Furthermore, these models are based on a mechanistic description of the enzymes involved energy metabolism and PD-related pathways. It will thus be possible at some point to map genetic information (i.e., obtained from mRNA microarrays or genome-wide association studies) on the reactions of the system and analyze how key properties change at a personalized level, between individuals, and over the course of their lives.

References

1. Lotharius J, Brundin P (2002) Pathogenesis of Parkinson's Disease. Nat Rev Neurosci 3:932
2. Malkus KA, Tsika E, Ischiropoulos H (2009) Oxidative modifications, mitochondrial dysfunction, and impaired protein degradation in Parkinson's disease: how neurons are lost in the Bermuda triangle. Mol Neurodegener 4:24
3. Litvan I, Halliday G (2007) The etiopathogenesis of Parkinson's disease and suggestions for future research. J Neuropathol Exp Neurol 1 66:251–257
4. Powers WJ (2008) Cerebral mitochondrial metabolism in early Parkinson's disease. J Cereb Blood Flow Metab 28:1754
5. Jenner P (2003) Oxidative stress in Parkinson's disease. Ann Neurol 53(Suppl 3):S26–S36
6. Gibb WR, Lees AJ (1998) The relevance of the Lewy body to the pathogenesis of idiopathic Parkinson's disease. J Neurol Neurosurg Psychiatry 51:745–752
7. Cookson MR (2009) Alpha-Synuclein and neuronal cell death. Mol Neurodegener 4:9
8. Devi L, Raghavendran V, Prabhu BM, Avadhani NG, Anandatheerthavarada HK (2008) Mitochondrial import and accumulation of alpha-synuclein impair complex I in human dopaminergic neuronal cultures and Parkinson disease brain. J Biol Chem 283(14):9089–9100
9. Martin LJ, Pan Y, Price AC, Sterling W, Copeland NG, Jenkins NA (2006) Parkinson's disease alpha-synuclein transgenic mice develops neuronal mitochondrial degeneration and cell death. J Neurosci 26:41–50

10. Klivenyi P, Siwek D, Gardian G, Yang L, Starkov A, Cleren C, Ferrante RJ, Kowall NW, Abeliovich A, Beal MF (2006) Mice lackin alpha-synuclein are resistant to mitochondrial toxins. Neurobiol Dis 21:541–548
11. Braak H, Ghembremedhin E, Rb U, Bratzke H, Tredici K (2004) Stages in the development of Parkinson's disease-related pathology. Cell Tissue Res 318(1):121–134
12. Hughes AJ, Daniel SE, Kilford L, Lees AJ (1992) Accuracy of clinical diagnosis of idiopathic Parkinson's disease: a clinico-pathological study of 100 cases. J Neurol Neurosurg Psychiatry 55:181–184
13. Bennett MC, Bishop JF, Leng Y, Chock PB, Chase TN, Mouradian MM (1999) Degradation of alpha-synuclein by proteasome. J Biol Chem 274:33855–33858
14. Berlett BS, Stadtman ER (1997) Protein oxidation in aging, disease, and oxidative stress. J Biol Chem 272(33):20313–20316. doi:10.1074/jbc.272.33.20313
15. Lodish H, Berk A, Kaiser CK, Krieger M, Scott MP, Bretscher A, Ploegh H, Matsudeira P (2000) Molecular cell biology, 6th edn. W.H. Freeman and Company, New York, NY
16. Mosharov EV, Larsen KE, Kanter E, Phillips KA, Wilson K, Schmitz Y, Krantz DE, Kobayashi K, Edwards RH, Sulzer D (2009) Interplay between cytosolic dopamine, calcium and alpha-synuclein causes selective death of substantia nigra neurons. Neuron 62:218–229
17. Lashuel HA, Hartley D, Petre BM, Walz T, Lansbury PT (2002) Amyloid pores from pathogenic mutations. Nat Rev Neurosci 418:291
18. van Rooijen BD, Claessens MMAE, Subramaniam V (2009) Lipid bilayer disruption by oligomeric alpha-synuclein depends on bilayer charge and accessibility of the hydrophobic core. Biochim Biophys Acta 1788:1271–1278
19. Frase H, Hudak J, Lee I (2006) Identification of the proteasome inhibitor MG262 as a potent ATP-dependent inhibitor of the Salmonella enterica serovar Typhimurium Lon Proteaseâ. Biochemistry 45(27):8264–8274. doi:10.1021/bi060542e
20. Cortes VF, Veiga-Lopes FE, Barrabin H, Alves-Ferreira M, Fontes CFL (2006) The [gamma] subunit of Na+, K+-ATPase: role on ATPase activity and regulatory phosphorylation by PKA. Int J Biochem Cell Biol 38(11):1901–1913
21. Cloutier M, Bolger FB, Lowry JP, Wellstead P (2009) An integrative dynamic model of brain energy metabolism using in vivo neurochemical measurements. J Comput Neurosci 27:391–414
22. Cloutier M, Wellstead P (2010) The control systems structures of energy metabolism. J R Soc Interface 7:651–665
23. Wellstead P, Cloutier M (2011) An energy systems approach to Parkinson's disease. WIREs Syst Biol Med 3:1–6
24. Cloutier M, Wellstead P (2011) Dynamic modelling of protein and oxidative metabolisms simulates the pathogenesis of Parkinson's disease. IET Syst Biol (In press). doi:10.1049/iet-syb.2011.0071
25. Cloutier M, Middleton RH, Wellstead P (2011) A feedback motif for the pathogenesis of Parkinson's disease. IET Syst Biol (In press). doi:10.1049/iet-syb.2011.0072
26. Stanley F (1996) The case of the frozen addicts. N Engl J Med 335:2002
27. Schmidt H, Jirstrand M (2006) Systems biology toolbox for Matlab: a computational platform for research in systems biology. Bioinformatics 22(4):514–515
28. Underwood AH, Holmes EA (1965) Properties of phosphofructokinase from rat liver and their relation to the control of glycolysis and gluconeogenesis. Biochem J 95:868–875
29. Heinrich R, Schuster S (1996) The regulation of cellular systems. ITP Chapman & Hall, New York, NY
30. Heldt HW, Klingenberg M, Milovancev M (1972) Differences between the ATP/ADP ratios in the mitochondrial matrix and in the extramitochondrial space. Eur J Biochem 30:434–440
31. Pellerin L, Magistretti PJ (1994) Glutamate uptake into astrocytes stimulates aerobic glycolysis: a mechanism coupling neuronal activity to glucose utilization. Proc Natl Acad Sci 91:10625–10629
32. Proctor CJ, Csaba S, Boys RJ, Gillespie CS, Shanley DP, Wilkinson DJ, Kirkwood BL (2005) Modelling the actions of chaperones and their role in ageing. Mech Ageing Dev 126:119–131

33. Fai Poon H, Frasier M, Shreve N, Calabrese V, Wolozin B, Butterfield DA (2005) Mitochondrial associated metabolic proteins are selectively oxidized in A30P alpha-synuclein transgenic mice—a model of familial Parkinson's disease. Neurobiol Dis 18:492–498
34. Shlomi T, Benyamini T, Gottlieb E, Sharan R, Ruppin E (2011) Genome-scale metabolic modeling elucidates the role of proliferative adaptation in causing the Warburg effect. PLoS Comput Biol 7(3):e1002018
35. Lewis NE, Schramm G, Bordbar A, Schellenberger J, Andersen MP, Cheng JK, Patel N, Yee A, Lewis RA, Eils R, Konig R, Palsson BO (2010) Large-scale in silico modeling of metabolic interactions between cell types in the human brain. Nat Biotechnol 28(12):1279–1285
36. Magistretti P (2006) Neuron-glia metabolic coupling and plasticity. J Exp Biol 209:2304–2311
37. Clark DD, Sokoloff L (1999) Circulation and energy metabolism. In: Siegel GJ, Agranoff BW, Albers RW, Fisher SK, Uhler MD (eds) Basic neurochemistry: molecular, cellular, and medical aspects, 6th edn. Lippincott Williams & Wilkins, Philadelphia, PA, pp 638–669
38. Proctor CJ, Tsirigotis M, Gray DA (2007) An in silico model of the ubiquitin-proteasome system that incorporates normal homeostasis and age-related decline. BMC Syst Biol 1:17
39. Sneppen K, Lizana L, Jensen MH, Pigolotti S, Otzen D (2009) Modelling proteasome dynamics in Parkinson's disease. Phys Biol 6:036005
40. Raichur A, Vali S, Gorin F (2006) Dynamic modeling of alpha-synuclein aggregation for the sporadic and genetic forms of Parkinson's disease. Neuroscience 142:859–870
41. Bharathi P, Nagabhushan P, Rao KSJ (2008) Mathematical approach to understand the kinetics of alpha-synuclein aggregation: relevance to Parkinson's disease. Comput Biol Med 38:1084–1093
42. Lei B, Adachi N, Arai T (1998) Measurement of the extracellular H2O2 in the brain by microdialysis. Brain Res Protocols 3:33–36
43. Desagher S, Glowinski J, Premont J (1996) Astrocytes protect neurons from hydrogen peroxide toxicity. J Neurosci 16:2553–2562
44. Schapira AH, Cooper JM, Dexter D, Clark JB, Jenner P, Mardsen CD (1990) Mitochondrial complex I deficiency in Parkinson's disease. J Neurochem 54:823–829
45. Song DD, Shults CW, Sisk A, Rockenstein E, Masliah E (2004) Enhanced substantia nigra mitochondrial pathology in human alpha-synuclein transgenic mice after treatment with MPTP. Exp Neurol 186:158–172
46. Tyson JJ, Chen KC, Novak B (2003) Sniffers, buzzers, toggles and blinkers: dynamics of regulatory and signalling pathways in the cell. Curr Opin Cell Biol 15:221–231
47. Aguda BD, Kim Y, Piper-Hunter MG, Friedman A, Marsh CB (2009) MicroRNA regulation of a cancer network: consequences of the feedback loops involving miR-17-92, E2F and Myc. Proc Natl Acad Sci 105:19678–19683
48. Yang L, Calingasan NY, Wille EJ, Cormier K, Smith K, Ferrante RJ, Flint Beal M (2009) Combination therapy with Coenzyme Q10 and creatine produces additive neuroprotective effects in models of Parkinson's and Huntington's diseases. J Neurochem 109(5):1427–1439. doi:10.1111/j.1471-4159.2009.06074.x
49. Parashos SA, Swearingen CJ, Biglan KM, Bodis-Wollner I, Liang GS, Ross GW, Tilley BC, Shulman LM, for the NETPDI (2009) Determinants of the timing of symptomatic treatment in early Parkinson disease: the national institutes of health exploratory trials in parkinson disease (NET-PD) experience. Arch Neurol 66(9):1099–1104. doi:10.1001/archneurol.2009.159
50. Ben-Yoseph O, Camp DM, Robinson TE, Ross BD (1995) Dynamic measurements of cerebral pentose phosphate pathway activity in vivo using [1,6-13 C2,6,6-2 H2] glucose and microdialysis. J Neurochem 64(3):1336–1342
51. Vali S, Mythri RB, Jagatha B, Padiapu J, Ramanujan KS, Andersen JK, Gorin F, Bharath MMS (2007) Integrating glutathione metabolism and mitochondrial dysfunction with implications for Parkinson's disease: a dynamic model. Neuroscience 149:917–930
52. Attwell D, Laughlin SB (2001) An energy budget for signaling in the grey matter of the brain. J Cereb Blood Flow Metab 21(10):1133–1145

Chapter 8
Mathematical Models of Dopamine Metabolism in Parkinson's Disease

Zhen Qi, Gary W. Miller, and Eberhard O. Voit

Abstract As discussed in Chap. 1 and elsewhere in this volume, a feature of Parkinson's disease (PD) is a reduction in dopamine concentration in the striatum, caused by progressive loss of dopamine neurons in the substantia nigra pars compacta. Dopamine is a crucial neurotransmitter that is involved in numerous physiological functions, and its role in PD has been studied extensively. However, the dynamics of dopamine in situ are not fully understood because it is affected by a large number of metabolites, other biological components, and an ill-characterized spectrum of environmental and genetic factors. This chapter describes the state of the art in mathematical models of dopamine metabolism and signal transduction.

Z. Qi (✉)
Department of Biomedical Engineering, Georgia Institute of Technology, 313 Ferst Drive, Atlanta, GA 30332, USA

Center for Neurodegenerative Disease, Emory University, 201 Dowman Drive, Atlanta, GA 30322, USA

Integrative BioSystems Institute, Georgia Institute of Technology, Atlanta, GA 30332, USA
e-mail: zhen.qi@gatech.edu

G.W. Miller
Center for Neurodegenerative Disease, Emory University, 201 Dowman Drive, Atlanta, GA 30322, USA

Department of Environmental Health, Rollins School of Public Health, Emory University, Atlanta, GA 30322, USA

E.O. Voit
Department of Biomedical Engineering, Georgia Institute of Technology, 313 Ferst Drive, Atlanta, GA 30332, USA

Integrative BioSystems Institute, Georgia Institute of Technology, Atlanta, GA 30332, USA

P. Wellstead and M. Cloutier (eds.), *Systems Biology of Parkinson's Disease*,
DOI 10.1007/978-1-4614-3411-5_8,

First, the topology of the dopamine pathway is reviewed. Second, the construction of two types of models is discussed. The first of these models targets dopamine metabolism in the presynaptic terminal, while the second describes dopamine-based signal transduction at the synapse and signal integration in the postsynaptic target neurons. The construction phase of symbolic models is followed by numerical configurations based on data. The resulting parameterized models are then compared with experimental and clinical observations as a means of testing their validity and predictive power. The best model is utilized to analyze ill-understood aspects of the role of dopamine in PD and to identify critical molecules and processes that might be potential therapeutical targets. Simulations of drugs targeting these sites are presented and evaluated with respect to their benefits, possible side effects, and downstream effects of perturbations in dopamine dynamics.

Introduction

The neurotransmitter dopamine plays a critical role in the development and treatment of Parkinson's disease (PD) [1]. With respect to development issues, it has been suggested that the loss of dopaminergic neurons can be induced by the generation of toxic species and by oxidative stress associated with abnormal dopamine metabolism [2–5]. For instance, nigral neurons are damaged by the toxin 1-methyl-4-phenyl-1,2,5,6-tetrahydropyridine (MPTP) and its oxidation product MPP+, in a way that induces cell loss and PD [6, 7]. Specifically, MPTP perturbs dopamine metabolism and recruits the components of the dopamine pathway for its toxic effects [8–10]. To restore dopamine function, treatment options have mostly relied on (1) the replacement of dopamine precursors, (2) inhibition of its degradative enzymes, and (3) dopamine agonists. L-DOPA, the precursor of dopamine and main PD medication for over 30 years, operates by dopamine replacement in a way that mitigates motor symptoms [11]. Studies have shown that injection of L-DOPA or carbidopa can reverse the motor symptoms caused by MPTP to some degree [12, 13].

The synthesis and fate of dopamine in situ involve complex and interconnected processes. First, numerous metabolic and structural components are involved. The precursor of dopamine synthesis is tyrosine, which is supplied to neurons through capillaries. Upon synthesis, dopamine is distributed among several neuronal compartments: the cytoplasm, vesicles, and synaptic cleft. Dopamine can also be degraded through various pathways, some of which have toxic by-products. Glial cells participate in dopamine metabolism.

A further complicating feature is the different timescales of dopamine metabolic and signaling processes. The tonic release of dopamine can be regarded as a relatively slow background signal. However, upon stimulation, a phasic release of dopamine transduces information, and this signaling process needs to be instantaneous and reliable. In addition to speed, the system must have enough efficiency and fidelity to interpret the signals correctly. For instance, an individual dopamine signal must be distinguished from a train of stimuli.

Also, dopamine metabolism is regulated by many components, some of which are not completely understood. These regulators affect enzymes that catalyze the synthesis and degradation of dopamine and the metabolites or transporters that distribute and recycle dopamine. For example, dopamine auto-receptors sense the dopamine level in the synaptic cleft and feed a signal back to control synthesis, release, and degradation of dopamine [14, 15].

The complexities in metabolism and signal transduction render intuition regarding details of the physiological and pathological dynamics of dopamine ineffective and unreliable. A logical step, therefore, is to complement experimentation and clinical studies with mathematical methods and computer-aided analyses of computational systems biology. In the case of dopamine, some systems biology approaches exist. Specifically, some mathematical models of dopamine metabolism, and associated phenomena, have been developed (e.g., see 16–18), and used as computational systems for analyzing the dynamic properties and design principles of dopamine regulation.

In the following, we discuss the development of mathematical models for dopamine metabolism and signaling, and discuss their application for PD. Two distinct aspects are considered: the dynamics of dopamine biosynthesis and degradation in the presynapse, and the signal transduction and interpretation in the postsynapse.

Development of a Mathematical Model of Dopamine Metabolism

Considering the complexity of metabolic systems, the development of a mathematical model may at first look daunting. However, biological systems analysis has established guidelines that subdivide the process into manageable steps [19, 20]. We follow these guidelines as follows: (1) model selection and design; (2) model validation; and (3) model applications. Though it may look quite straightforward, the first step is crucial. Here, the modeler makes decisions regarding the inclusion, or exclusion, of biological components and processes, the type of model, and the alignment of data availability and modeling needs. These decisions are driven by three major issues: (1) the purpose of the model and what questions it should address; (2) the information available; and (3) the biological components to be considered in the model.

Since our task is to model dopamine metabolism, elucidate its dynamic properties, and to screen the system for potential drug targets and biomarkers of PD, we decided on a mechanistic, dynamic, deterministic model that is as detailed and realistic as available data allow. In reality, stochastic features are present, but to restrict complexity, random effects are not considered initially. If necessary, they can be added to the model at a later stage [21]. After the selection of the model type, we determine the biological entities and processes to be included into the model. Because dopamine metabolism is our first target, its main components and processes need to be considered as outlined in the following section.

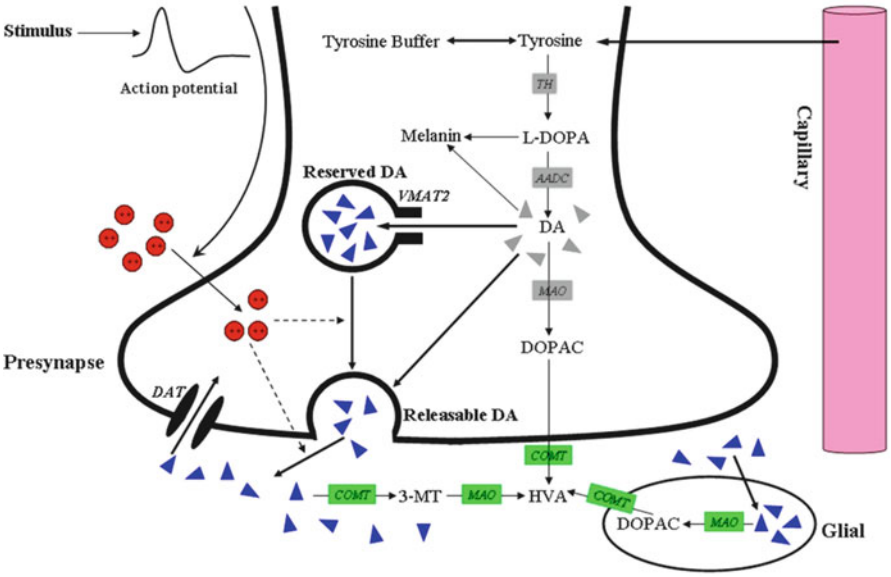

Fig. 8.1 Simplified diagram of dopamine metabolism in the presynapse. Dopamine metabolism includes the synthesis, storage, release, recycling, and degradation of dopamine in the presynaptic terminal and synaptic cleft. *Blue triangles* show dopamine and *red circles* represent calcium cations. Enzymes catalyzing relevant reactions are shown in italics with green background. *TH* tyrosine hydroxylase; *AADC* DOPA decarboxylase; *MAO* monoamine oxidase; *COMT* catechol *O*-methyltransferase; *DA* dopamine; *3-MT* 3-methoxytyramine; *DOPAC* 3,4-dihydroxy phenylacetate; *HVA* homovanillic acid; *DAT* dopamine transporter; *VMAT2* vesicular monoamine transporter

The Metabolic Pathway of Dopamine Metabolism

The dopamine dynamics in the presynapse includes synthesis, degradation, compartmentalization, release, and reuptake, as well as numerous regulatory mechanisms. A simplified diagram is presented in Fig. 8.1, with a more detailed pathway representation in [17]. Dopamine is synthesized from the precursor L-DOPA produced from tyrosine supplied through the brain capillaries. Most of the synthesized dopamine is packed into storage vesicles through vesicular monoamine transporters (VMAT2). The vesicles are divided into two classes: one is used as a temporary pool for later dopamine release into the synaptic cleft, and another as a reserve pool (in case the temporary release pool is depleted). Once released into the synaptic cleft, dopamine executes its signaling function—this property is discussed later in the chapter. Some of the released dopamine diffuses out of the cleft, while some is retrieved by dopamine transporter (DAT) proteins and carried back to the presynaptic terminal for recycling. Dopamine can also be enzymatically converted into other metabolites, such as 3,4-dihydroxyphenylacetate (DOPAC) and homovanillic acid (HVA).

Dopamine is released into the cleft in two different ways: one pathway is the constant, low-rate background release, and the other is activated release induced by action potential stimulus. The fundamental processes discussed above are included in the conceptual dopamine model, as are all known regulatory processes, such as inhibition signals that affect certain enzyme-catalyzed reaction steps. Modeled entities are dopamine species in several compartments, its precursors and degradation products, plus enzymes and transporters.

Mathematical Framework for the Presynaptic Dopamine Model

The design of a mathematical model for the dopamine pathway described above consists of building a symbolic model of the metabolic system by mapping its structure of the pathway onto corresponding equations. For this purpose, we use three equation formalizations, namely, mass action kinetics [22], Michaelis–Menten kinetics [23], and models from biochemical systems theory (BST) [24–26], to convert the dopamine pathway into a symbolic mathematical model. This symbolic model was subsequently parameterized, thereby making it specific for the available data. The model was then tested through algebraic and computational diagnostics, as well as a variety of simulation studies. Indeed, most numerical values for concentrations, rate constants, kinetic orders, and Michaelis constants were obtained from experimental measurements reported in the literature. Remaining parameters were estimated by fitting the model to experimental data.

Validation of the Dopamine Model

Once the model of dopamine metabolism is fully configured and parameterized, it is ready for simulations and analyses. In this validation phase, the model is subjected to rigorous tests that try to confirm its reliability and correctness, before it is used in applications. Specifically, the model is first checked in terms of the internal consistency (stability and sensitivity), which is expected of most biological systems. Next the model is tested against experimental and clinical data associated with the biochemistry, pharmacology, and electrophysiology of the system. Both static and dynamic behaviors are compared as described below.

Internal Consistency of the Dopamine Model

Due to the complexity of the dopamine model, the algebraic computation of eigenvalues, as indicators of the stability of the system, is not applicable. Instead, numerical simulations were used to analyze the stability of the system. For a wide

range and number of simulations covering different operating regimes, a small perturbation was applied to a different component to check if the system would return back to its steady state. These tests confirmed the stability of the model.

Stability analysis targets the capability of the system to tolerate small, temporary changes in components that might be caused by changes in the environment or by external interventions. There could also be structural changes, where processes or components in the system are permanently altered, for instance, due to genetic mutations or pharmacological interventions. The characteristics of a system in response to such structural changes are described by sensitivity analysis. Our simulation results show that the dopamine model has a low sensitivity profile, which indicates that the system is robust to structural changes as long as they are small or moderate in magnitude. The sensitivity analysis also revealed that some components and processes are comparatively more influential than others. These sensitive components are mainly involved in dopamine recycling processes, and as such are potentially valuable as drug targets.

External Consistency of the Dopamine Model

External consistency tests address the performance of a model against experimental observations in response to perturbations or stimuli. The model response can be separated into static responses and dynamic responses as follows.

Static responses. A static response focuses on the change in a steady state following a persistent perturbation or stimulus, while a dynamic response focuses on the transient curve between the stimulus and the completion of the system's response. We investigated the performance of the dopamine model in response to genetic mutations and electrical stimulations. The genetic mutations included heterozygous deletions, homozygous knockouts, and gene hypomorphs of some components of dopamine metabolism. The results show that model-based predictions of the changes in steady state are consistent with experimental observations (Fig. 8.2). The correlation coefficient between predictions by the dopamine model and experimental observations is 0.845.

Dynamic responses. Electrical stimulations included a 10-s stimulation applied to brain tissue and a short single stimulation applied to DAT transgenic (DAT-tg), DAT wild-type (DAT +/+), DAT heterozygote (DAT +/–), and DAT knockout (DAT –/–) mice. Following the 10-s stimulation, large amounts of dopamine is released into the synaptic cleft such that the dopamine level in the cleft quickly climbs to about 35 μM. The dynamic responses of the dopamine model to these electrical stimulations match the existing experimental observations quantitatively, although the timing shows some differences (Fig. 8.3). Specifically, for genetically mutated and wild-type mice, the model reproduces the rapid raise in dopamine levels within a few seconds of stimulation, followed by a decrease. However,

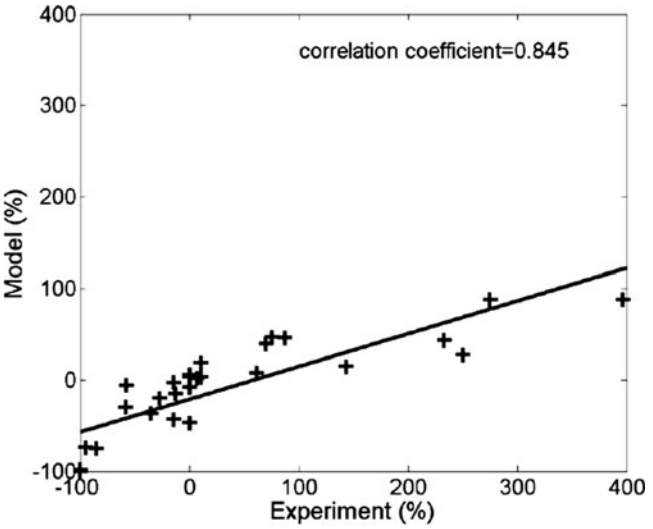

Fig. 8.2 Comparison between static responses of the dopamine model and experimental observations with respect to genetic mutations. Each data point represents the relative change (percentage) of a metabolite following an experimental (or corresponding simulated) manipulation, such as a heterozygous deletion or homozygous knockout of one of the central components of dopamine metabolism, including TH, MAO, VMAT2, DAT, and COMT. The *x*-coordinate reflects the experimental measurements, while the *y*-coordinate shows the corresponding model predictions. The consistency between the model predictions and observations is quantified by their correlation coefficient

the model simulations exhibit a lag in the descending phases in response to single stimulation of DAT-tg, DAT +/+, and DAT +/– mice.

Applications of the Presynaptic Dopamine Model

After the dopamine model has been tested and proved to have sufficient internal consistency and the ability to reproduce experimental observations, it is ready for various applications. These applications can typically be categorized into three groups: (1) explanation, (2) exploration, and (3) prediction. First, a mathematical model should be able to explain (at least key aspects of) the underlying mechanisms of the phenomenon under investigation. It should reveal connections, qualitative or quantitative, between model inputs and outputs and provide deeper insights into the investigated system. Second, a mathematical model offers the opportunity to explore a system through simulations, which incurs almost no costs and only a moderate amount of time. Compared to model simulations, any corresponding biological experiments or clinical investigations are expensive and time consuming. Furthermore, some experiments are difficult to perform and others are not feasible because of ethical concerns or limitations with current technologies. A mathematical model allows effective exploration of these scenarios. Third, a mathematical model should be able to make predictions and generate hypotheses that can be

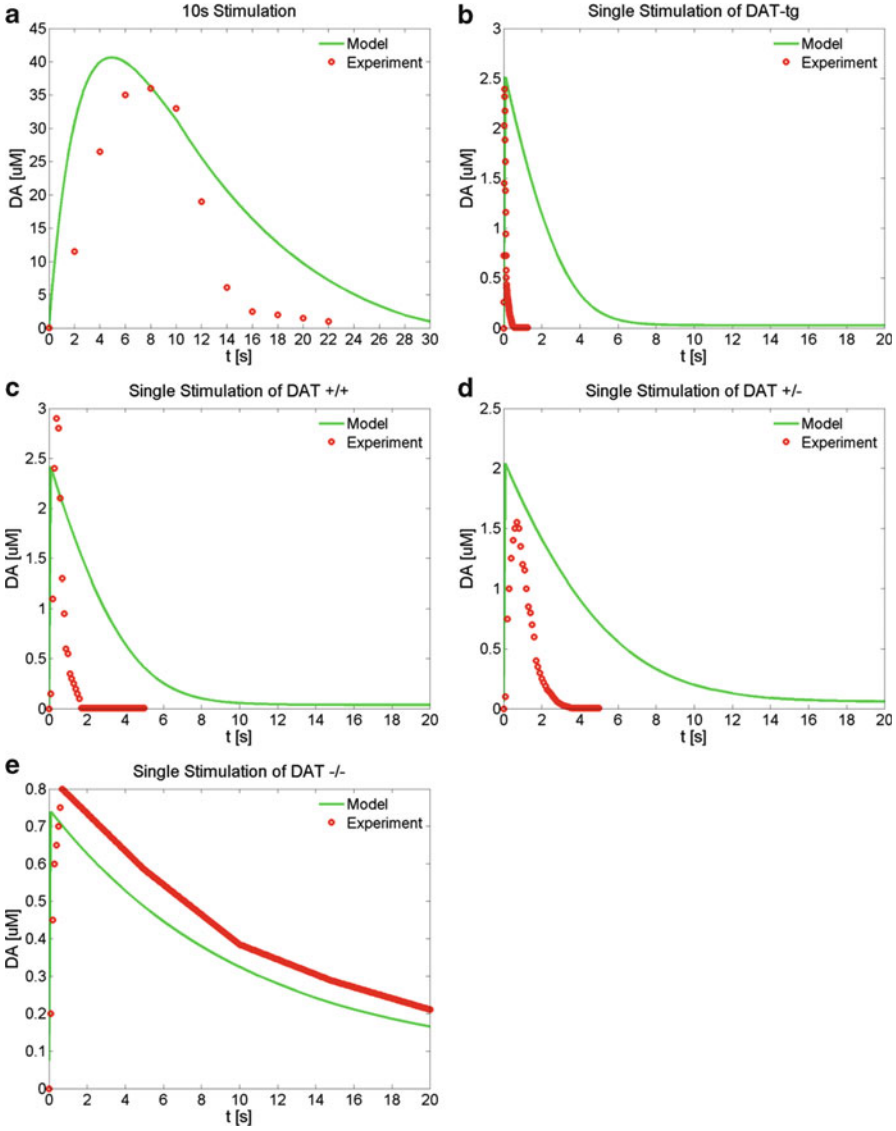

Fig. 8.3 Comparison between dynamic responses of the dopamine model and experimental observations with respect to electrical stimuli. Electrical stimulations include a 10-s stimulation applied to brain tissue and a short single stimulation applied to DAT transgenic (DAT-tg), DAT wild-type (DAT +/+), DAT heterozygous deletion (DAT +/–), and DAT knockout (DAT –/–) mice. The *y*-coordinate is the dopamine level (μM) in the synaptic cleft

tested by biological and clinical means. For example, a model might identify potential drug targets associated with human disease. Hypotheses generated by a mathematical model may assist in the design of new experiments or clinical trials. Examples of some of these aspects are discussed below.

Explanations Provided by the Dopamine Model

L-DOPA and Tyrosine as Treatments of PD

L-DOPA has been the main medication of PD motor symptoms for decades. Since L-DOPA is synthesized from tyrosine and the enzyme tyrosine hydroxylase (TH), which catalyzes this conversion, is regarded to be the rate-limiting enzyme of dopamine metabolism, one may ask the question: Why don't we supply PD patients with tyrosine or enhance the activity of TH to convert more tyrosine into L-DOPA, which will consequently be converted into more dopamine? Manipulating the enzyme activity of TH may not be easy, but tyrosine could be supplied through the bloodstream and the tyrosine level in blood vessels could probably be affected through diet, oral medication, or injection. Thus, tyrosine administration may seem to be a reasonable candidate for PD medication.

We compared the efficacy of L-DOPA and tyrosine treatment with respect to increases in dopamine level, utilizing the mathematical model of dopamine metabolism. The simulation results demonstrated that tyrosine administration can indeed increase dopamine level, and this result is also supported by experiments showing that levels of the dopamine metabolite HVA in PD patients increase after the administration of tyrosine [27]. However, the simulations also show that L-DOPA administration is much more effective than the tyrosine administration in elevating the dopamine level. Mechanistically, tyrosine usage for other purposes such as protein synthesis buffers the tyrosine level against alterations, and this buffering action appears to be the main reason for the difference in efficacy. In addition, end-production inhibition and substrate inhibition contribute to the inferior efficacy of tyrosine administration.

HVA and DOPAC as Indicators of Dopamine Levels

Many experiments utilize the dopamine metabolites HVA and DOPAC as indicators of the dopamine level in situ. The reason for this practice is that HVA and DOPAC are breakdown metabolites of dopamine and their levels are much easier to monitor than dopamine itself. However, one should ask: Do HVA and DOPAC indeed provide a reliable estimation of the in situ dopamine concentration under various conditions? As discussed previously, dopamine is located in different compartments so that there are several different dopamine levels. Among these, the dopamine level in the synaptic cleft is most important because it carries the information of a stimulus and transduces it into the postsynapse. For this reason, the dopamine level in the synaptic cleft, eDA, is used here for an investigation of the consistency between changes in cleft dopamine level and in the levels of HVA and DOPAC.

As an initial investigation, the activity of the rate-limiting enzyme TH is doubled. The model simulations show that eDA, DOPAC, and HVA are all elevated along with the manipulation, though the magnitudes of increases are different

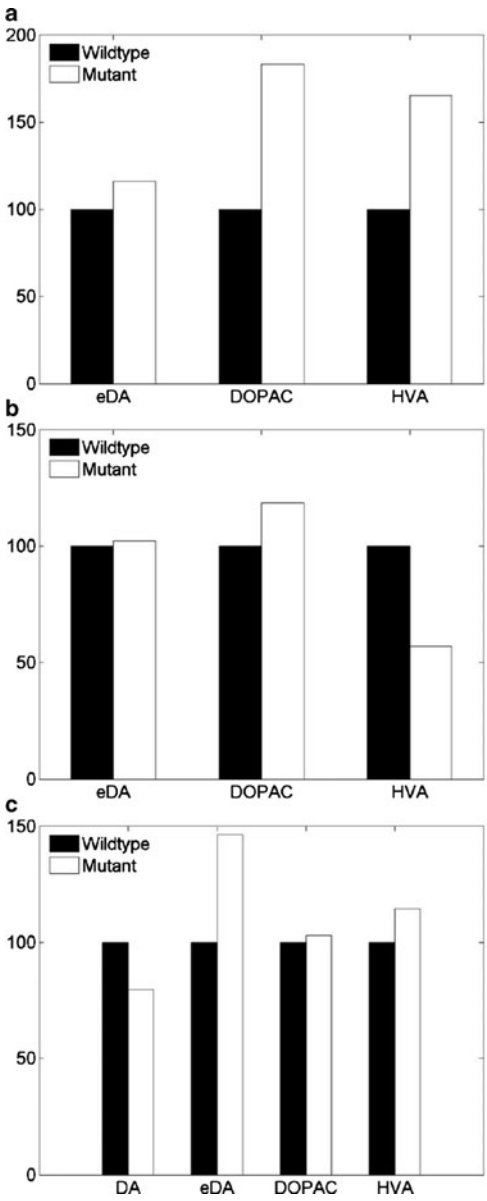

Fig. 8.4 Comparison between changes in dopamine and its metabolites. DOPAC and HVA are not always appropriate indicators of the in situ dopamine level, as indicated by model responses to various genetic alterations in comparison to wild type, namely: (**a**) TH activity is doubled; (**b**) a heterozygote of COMT is introduced; and (**c**) DAT has a heterozygote mutation. All wild types are normalized to 100 for ease of comparison. *DA* tissue dopamine; *eDA* external dopamine in the synaptic cleft; *DOPAC* 3,4-dihydroxyphenylacetate; *HVA* homovanillic acid

(Fig. 8.4a). In this case, DOPAC and HVA can qualitatively act as indicators of the eDA level. In a second experiment, we alter the enzyme catechol *O*-methyltransferase (COMT) which catalyzes DOPAC into HVA and converts dopamine into 3-methoxytyramine (3-MT). Specifically, we simulated a heterozygote mutant of COMT so that the level of COMT in the mutant is half of that in the wild type. The result shows that eDA is almost unaffected, whereas the DOPAC

level is noticeably elevated (Fig. 8.4b), while HVA is significantly decreased. In this case, DOPAC and HVA exhibit opposite responses. Thus, at least one, if not both, cannot be a good indicator of eDA. Third, we simulate a heterozygote mutant of DAT, which functions as the transporter recycling eDA back into the cytoplasm. This simulation shows that eDA increases significantly while DOPAC is almost unaffected (Fig. 8.4c). Interestingly, in response to this perturbation, the tissue dopamine decreases in a way that contrasts the increase in eDA. Thus, dopamine in different compartments can change in the opposite directions, and DOPAC and HVA do not necessarily exhibit changes that are consistent with that of eDA.

These simulation results suggest that caution is necessary in the design and analysis of experiments involving dopamine metabolism. With respect to indicator variables, DOPAC and HVA may accurately reflect the true dopamine level under some conditions, but sometimes this correlation fails. This type of inconsistency reflects one of the complexities of biological systems, such as dopamine metabolism. Dopamine is distributed among several compartments, namely, the cytoplasm, release vesicles, reserve vesicles, and synaptic cleft. Depending on the specific compartment, dopamine can have distinct fates. Dopamine in the cytoplasm and the synaptic cleft may be degraded or diffuse. Even the degradation processes are distinct due to different spectra of enzymes in the two compartments [28].

Vesicles generally sequester cytoplasmic dopamine and store it. Some vesicles release dopamine into the synaptic cleft, while other vesicles act as a reserve for dopamine when the release vesicles are depleted. Thus, due to compartmentalization and different enzyme compositions in different locations, dopamine levels will not necessarily correlate with breakdown metabolites DOPAC and HVA, and trends may even run in opposite directions.

Exploration of Experimentally Untested Scenarios

Dopamine is distributed among several compartments. This compartmentalization is interesting and important because it may have implications for the search of more efficient PD medications. Current PD medications, such as L-DOPA administration, aim to restore dopamine neuron functionality by supplying dopamine precursors, inhibiting its degradation, and activating its receptors. The efficacy of these dopamine-based PD medications is clearly affected by the spatial dopamine distribution. The dopamine level in the synaptic cleft is presumably most critical; however, this level is maintained by the release process from vesicles and is reduced by transport through DAT back into the cell. An ideal medication would increase the dopamine level in the synaptic cleft while minimizing perturbations in other components of the system.

Experimentalists can use voltammetry to record the dopamine level in the synaptic cleft and acquire tissue homogenates to measure the tissue dopamine level. However, it is difficult to monitor the cytoplasmic and vesicular dopamine concentrations in vivo. The mathematical model of dopamine metabolism, by contrast, enables easy

separation of dopamine in different compartments. Thus, to investigate the effects of a possible manipulation on the dopamine distribution among compartments, we can employ the model to trace (albeit in silico) the various dopamine levels under different intervention scenarios.

As an illustration, we present some results of dynamic changes in the dopamine distribution among compartments following interventions on TH, VMAT2, or DAT. Two types of interventions are applied: double activation and a heterozygote mutation. Increases in the activity of TH raise the dopamine levels in all compartments and consequently elevate the tissue dopamine level (Fig. 8.5a). However, the greatest change occurs in the cytoplasmic dopamine, while the change in the crucial dopamine level in the synaptic cleft is only modest, with the same being true for the change in the vesicular dopamine. Thus, because a large portion of the increase in tissue dopamine comes from cytoplasmic dopamine, the efficacy of the intervention is low, and even if experimentalists measure a significant increase in the tissue dopamine level, the critical dopamine level in the synaptic cleft may not increase much.

Second, the activation of VMAT2, which sequesters cytoplasmic dopamine into vesicles, can increase both the vesicular and synaptic cleft dopamine concentrations (Fig. 8.5b). Meanwhile, it reduces the cytoplasmic dopamine, which can be beneficial because dopamine degradation produces reactive oxygen species and toxic quinones. The tissue dopamine level also increases, but changes less in comparison with the vesicular dopamine. Finally, inhibition of DAT causes a strong and immediate elevation of the dopamine in the synaptic cleft while it reduces the cytoplasmic, vesicular, and tissue dopamine levels (Fig. 8.5c). This intervention looks very advantageous because it increases the desired signal and reduces the dopamine levels in other compartments. However, dopamine in vesicles is stored for its release so that any significant decrease in the stored dopamine may compromise the capacity of neurons to maintain dopamine supply during sequences of repeated stimuli.

Predictions and Hypothesis Generation

The hallmark of a good mathematical model is its ability to make predictions that are testable in the laboratory. As mentioned before, one purpose of our dopamine model is to identify potential drug targets for PD. Predicting a target requires a sequence of steps. First, we need to define an objective function to determine the effect of a manipulation of a candidate component or process. Since the scope of this study is limited to dopamine metabolism, we select the dopamine level in the synaptic cleft as an important (positive) indicator because it carries the neuronal signals, and select reactive oxygen species and quinones as secondary (negative) indicators because they are toxic and should be kept under control. Second, we need

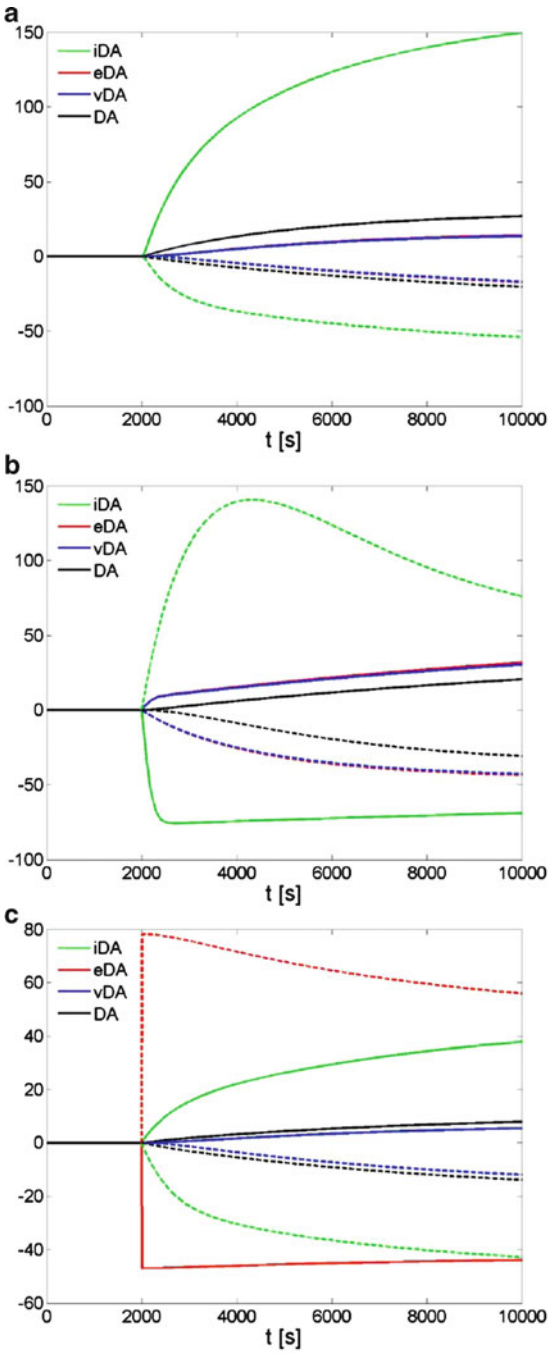

Fig. 8.5 Dopamine distribution among different compartments, following various manipulations. Dopamine is distributed among several compartments, namely, the cytoplasm, vesicles, and synaptic cleft. Changes in compartmentalized dopamine levels following some interventions are traced. *Green*

to use appropriate mathematical methods and computational algorithms for drug target screening. Because multiple criteria are required for the assessment of drug targets, a manipulation acting on a single site is usually insufficient and multisite interventions tend to be more promising. Because of the synergy between multisite interventions and the nonlinearity of the synergy, we need to use an appropriate and efficient method that can sample a parameter space instead of using single-value evaluations and extrapolations around a single, "normal" point. A good option is a stochastic Monte-Carlo simulation that utilizes (pseudo-) random numbers to sample large parameter spaces [29]. Specifically, each sample represents an intervention with a certain magnitude in a particular location of the system. A simulation of this type is performed for a sample and the process is repeated thousands or millions of times. For one-site, two-site, and multisite interventions, relevant simulation results are assessed according to predefined criteria, and particularly good or bad potential drug targets are identified.

Results of simulations of this type show that VMAT2, DAT, and the enzyme monoamine oxidase (MAO) are critical for the dopamine level in the synaptic cleft. By contrast, iron cations, MAO, DAT, catalase, glutathione peroxidase, glutathione, and VMAT2 have the greatest influence on the accumulation of hydroxyl radical. For toxic quinones, iron cations, DAT, MAO, COMT, and VMAT2 are the most significant determinants. Interestingly, MAO, DAT, and VMAT2 are critical with respect to all three indicators. However, a single-site intervention at one of these three targets turns out to be insufficient to meet all criteria. For example, inhibition of MAO alone can effectively increase the dopamine level in the synaptic cleft, but as a side effect this inhibition also increases toxic quinone species, which need to be controlled or eliminated.

As an alternative, we can combine multiple manipulations to minimize possible side effects while maximizing potential benefits. Among these combinations, the two combinations MAO/VMAT2 and COMT/DAT are discussed in detail. Simulation results show that activating VMAT2 in combination with an inhibition of MAO can increase the dopamine level in the synaptic cleft while alleviating highly reactive hydroxyl radical and controlling toxic quinones. By comparison, inhibition

Fig. 8.5 (continued) lines: cytoplasmic dopamine (iDA); *red line*: dopamine in the synaptic cleft (eDA); *blue lines*: vesicular dopamine (vDA); *black lines*: tissue dopamine (DA); *solid lines*: twofold activation; and *dashed lines*: reduction to 50% in heterozygote mutations. Interventions are applied at time point 2,000. Values on the *y* axes are changes in compartmentalized dopamine relative to their original steady states. (**a**) Doubled activation and heterozygote mutation in TH. The greatest change is seen in the cytoplasmic dopamine. The change in the dopamine level in the synaptic cleft is only modest. (**b**) Double activation and heterozygote mutation in VMAT2. Both the vesicular dopamine and the dopamine in the synaptic cleft are increased following the activation of VMAT2. Meanwhile, VMAT2 activation reduces the cytoplasmic dopamine, which may be beneficial because its degradation produces reactive oxygen species and toxic quinones. (**c**) Doubled activation and heterozygote mutation in DAT. The inhibition of DAT causes great and immediate elevation of the dopamine in the synaptic cleft while it reduces the cytoplasmic, vesicular, and tissue dopamine levels

of both COMT and DAT increases the dopamine level in the synaptic cleft and concomitantly keeps hydroxyl radical and toxic quinones under control. Not only can the mathematical model predict potential drug targets, but it can also compare interventions at these targets in terms of efficiency, side effects, and their sensitivity to the imprecision with which such interventions can be implemented [30]. In the given case, the model prediction of potential drug targets is indirectly supported by experimental observations and drug studies. For instance, Selegiline, an MAO inhibitor, has long been used as a therapeutic agent for PD [31–34]. Recent findings also show that a reduction of VMAT2 causes a severe reduction of dopamine, nigrostriatal neurodegeneration, increased vulnerability to various toxicants, and motor behavior deficits [35–38]. Also, a clinical study shows that gene polymorphisms associated with increased VMAT2 expression reduce the incidence of PD in women [39].

A Mathematical Model for Dopamine-Based Signal Transduction

The signals carried by dopamine through the synaptic cleft are received by specialized dopamine receptors on the postsynaptic membrane and downstream signaling cascades are triggered. Similarly, signals are received through receptors for other neurotransmitters such as glutamate. Once the postsynapse receives these signal combinations, it integrates and interprets them. In order to understand this process, we need to characterize the features and capabilities of the receiver in the postsynapse in greater detail.

The nigrostriatal pathway of dopamine, which is associated with PD, projects neurons from the substantia nigra pars compacta to the striatum (see Chap. 1). The striatum consists primarily of medium spiny neurons, which serve as key mediators of signal processing. In particular, these neurons contain the protein DARPP-32 (dopamine- and cAMP-regulated phosphoprotein with 32-kDa molecular weight) [40], which processes dopamine and glutamate signals and translates them into specific biochemical, cellular, and physiological actions [41–44]. The integration of signals by DARPP-32 constitutes a complex system of phosphorylation and dephosphorylation events. Briefly, dopamine in the synaptic cleft binds to its receptors and induces the production of the secondary messenger cAMP, which then activates protein kinase A (PKA). PKA phosphorylates a threonine residue of DARPP-32 and this phosphorylation inhibits protein phosphatase 1 (PP1). In contrast, a glutamate signal causes calcium cations to flow into the neuron through ion channels (see Chaps. 4 and 5). This calcium influx activates protein phosphatase 2B (PP2B), which dephosphorylates DARPP-32 at the same threonine site, thereby reducing DARPP-32's inhibition of PP1. In addition, the calcium influx stimulates protein phosphatase 2A (PP2A) and cyclin-dependent kinase 5 (CDK5), which, respectively, control the phosphorylation and dephosphorylation of

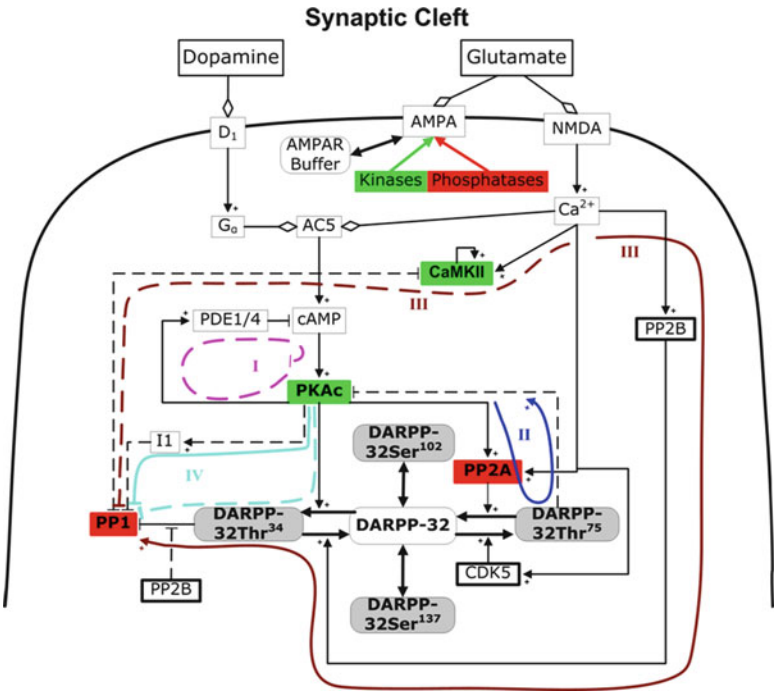

Fig. 8.6 Simplified representation of the DARPP-32 system and identified important mechanisms for its signal transduction in medium spiny neurons of the striatum. Dopamine and glutamate are generated in their presynaptic terminals and released into the synaptic cleft, where they bind to specialized receptors on the postsynaptic membrane. This binding triggers signal transduction processes, which regulate activities of various protein kinases and phosphatases. The protein kinases and phosphatases regulate phosphorylation of AMPA receptors and thereby modify the synaptic plasticity of GABAergic medium spiny neurons. *Colored* and *dotted lines* represent critical mechanisms for the signal transduction. I: negative feedback loop PKA–PDE–cAMP–PKA (*lavender line*); II: positive feedback loop of PKA–PP2A–DARPP-32-Thr75–PKA (*blue line*); III: alternative pathways of glutamate–PP2B–PP1 vs. glutamate–-CaMKII–PP1 (*brown lines*); and IV: alternative pathways of PKA–DARPP-32-Thr34–PP1 vs. the pathway PKA–I1–PP1 (*cyan lines*)

DARPP-32 at another threonine site. Phosphorylation of DARPP-32 at this threonine site inhibits PKA.

Based on previous work [45–47], we developed a mathematical model of the DARPP-32 signal transduction system that allowed us to study its properties in more detail [48, 49]. The model analysis revealed, explained, or quantified the following characteristics of the DARPP-32 signal transduction system. First, the DARPP-32 system has the capability of discerning surprisingly many neurotransmission scenarios and converting them into appropriate responses. In our simulations, input signals were considered individually or in combination, transient or sustained, one-shot or repetitive pulses, with varying time periods, and of either high or low amplitude. The DARPP-32 system faithfully interpreted these different

configurations of signals and converted them into distinct activity profiles of kinases and phosphatases. For example, the model showed that signals with different amplitudes can induce distinct steady states of PKA and PP1 or cause qualitative differences in their dynamics, such as overshoot vs. undershoot. Because kinases and phosphatases can regulate the density and conductance of AMPA receptors which are used as an indicator of synaptic plasticity of medium spiny neurons in the striatum, the distinction of various input signals by the DARPP-32 system also resulted in different types of synaptic plasticity, such as potentiation and depression.

The model also allowed the clarification of mechanistic motifs that are critical to the capability of the DARPP-32 system to discern signal types. A few highlights are the following: the negative feedback loop PKA–PDE–cAMP–PKA (I, Fig. 8.6) is critical for proper dopamine signaling. Inhibition of this mechanism can switch medium spiny neurons from synaptic potentiation to synaptic depression in response to concurrent dopamine and glutamate signals. The positive feedback loop of PKA–PP2A–DARPP-32-Thr75–PKA (II, Fig. 8.6) is critical to both dopamine signals and glutamate signals. Typically, this mechanism enhances dopamine signals and counteracts glutamate signals. Glutamate signals regulate PP1 activity through the pathway glutamate–PP2B–PP1 and the pathway glutamate–CaMKII–PP1 (III, Fig. 8.6). Both mechanisms are important to dopamine signals and glutamate signals, but they are antagonistic to each other. Dopamine regulation of PP1 activity through the two mechanisms PKA–DARPP-32-Thr34–PP1 and PKA–I1–PP1 (IV, Fig. 8.6) is critical to dopamine signaling, and the former mechanism is more effective.

Discussion

This chapter presented an overview of the processes needed to develop a systems model of dopamine metabolism in the context of PD. These processes can be categorized into distinct phases, which lead to the following guidelines. First, one determines the type of model that seems most effective and selects the biological entities and processes to be included in the model. This step requires consideration of the specific modeling purposes and the available data. In the present case, we decided to develop a mechanistically based, dynamic, and deterministic model of dopamine metabolism that was as simple and yet as realistic as possible. Second, a symbolic model is developed, based on the known or alleged topology of the system. This model shows which components are associated with which processes and identifies whether the association is fundamentally positive or negative. In our case, two distinct models of dopamine metabolism and dopamine signaling were developed. Also in this phase, mathematical representations for all processes are selected. We chose mass action, Michaelis–Menten, and generalized mass action models of BST. Once selected, these representations are numerically configured, which requires specific data analyses and computational methods for parameterization. Third, the numerically parameterized model is subjected to validation tests that assess the model's internal consistency (e.g., stability and sensitivity) and external consistency (e.g., similarity to clinical data or

experimental observations of the biochemical, pharmacological, and electrophysiological features of the system). Finally, the mathematical model is used to explain observed phenomena, reveal the design motifs of internal subsystems for specific purposes, explore new scenarios, and make predictions. As an example, our model of dopamine metabolism provides explanations for the difference in efficacy of L-DOPA and tyrosine as PD medication. The model also explains why HVA and DOPAC are sometimes, but not always, good indicators of the dopamine levels in situ. The model of dopamine metabolism in the presynapse was also used to explore the organizational dopamine distribution among several compartments under various conditions. Moreover, the model was used to predict potential drug targets and compare interventions at these targets in terms of efficacy, side effects, and their sensitivity to possible inaccuracies in the implementation of interventions.

The model of dopamine dynamics in the presynapse focuses on the biochemical level, while the postsynaptic model addresses signal transduction. Obviously, PD involves processes at other levels of organization. For instance, multiple brain regions are associated with the disease, and each of them contains millions of neurons that communicate through multiple neurotransmitters. Moreover, mechanisms underlying this disease span many levels, from genetics, biochemistry, and physiology to lifestyle and environmental exposure. Corresponding to this wide range is a huge amount of data with diverse characteristics. Considering how complicated the network of processes is even at a single level, it is clear (as discussed in the Preface to this volume) that disease phenomena spanning several levels are beyond the grasp of intuition. As was detailed elsewhere in this volume, these phenomena include aging (Chap. 3) and impairments in ions balance (Chaps. 4 and 5) as well as deregulation of energy metabolism (Chaps. 2 and 7). Integration of the dynamic biological processes of PD pathology will thus be important, and in this regard, Systems biology offers valuable tools that should be used to meet this challenge. At present, the methods of systems biology are not quite sufficient to the task, but rapid progress has been made during the past decade. Eventually, there is a good chance that mathematical models will be valuable, complementary tools to medical diagnostics, clinical decision making, and development of new treatment strategies. This will be of critical importance for research on PD, where model-based improvements in understanding the complex dynamics of dopamine can improve the forms and uses of therapies.

Acknowledgments This work was supported by a grant from the National Institutes of Health (P01-ES016731, G.W.M., PI) and a grant from the University Systems of Georgia (E.O.V., PI). Any opinions, findings, and conclusions or recommendations expressed in this material are those of the authors and do not necessarily reflect the views of the sponsoring institutions.

References

1. de Lau LM, Breteler MM (2006) Epidemiology of Parkinson's disease. Lancet Neurol 5:525–535
2. Graham DG (1978) Oxidative pathways for catecholamines in the genesis of neuromelanin and cytotoxic quinones. Mol Pharmacol 14:633–643

3. Stokes AH, Hastings TG, Vrana KE (1999) Cytotoxic and genotoxic potential of dopamine. J Neurosci Res 55:659–665
4. Yuan H, Zheng JC, Liu P, Zhang SF, Xu JY et al (2007) Pathogenesis of Parkinson's disease: oxidative stress, environmental impact factors and inflammatory processes. Neurosci Bull 23:125–130
5. Przedborski S (2005) Pathogenesis of nigral cell death in Parkinson's disease. Parkinsonism Relat Disord 11(Suppl 1):S3–S7
6. Davis GC, Williams AC, Markey SP, Ebert MH, Caine ED et al (1979) Chronic Parkinsonism secondary to intravenous injection of meperidine analogues. Psychiatry Res 1:249–254
7. Langston JW, Ballard P, Tetrud JW, Irwin I (1983) Chronic Parkinsonism in humans due to a product of meperidine-analog synthesis. Science 219:979–980
8. Burns RS, Chiueh CC, Markey SP, Ebert MH, Jacobowitz DM et al (1983) A primate model of parkinsonism: selective destruction of dopaminergic neurons in the pars compacta of the substantia nigra by N-methyl-4-phenyl-1,2,3,6-tetrahydropyridine. Proc Natl Acad Sci U S A 80:4546–4550
9. Cohen G, Mytilineou C (1985) Studies on the mechanism of action of 1-methyl-4-phenyl-1,2,3,6-tetrahydropyridine (MPTP). Life Sci 36:237–242
10. Chang GD, Ramirez VD (1986) The mechanism of action of MPTP and MPP+ on endogenous dopamine release from the rat corpus striatum superfused in vitro. Brain Res 368:134–140
11. Toulouse A, Sullivan AM (2008) Progress in Parkinson's disease-where do we stand? Prog Neurobiol 85:376–392
12. Fredriksson A, Plaznik A, Sundstrom E, Jonsson G, Archer T (1990) MPTP-induced hypoactivity in mice: reversal by L-dopa. Pharmacol Toxicol 67:295–301
13. Doudet D, Gross C, Lebrun-Grandie P, Bioulac B (1985) A model of Parkinson's disease: effect of L-dopa therapy on movement parameters and electromyographic activity in monkeys treated with 1-methyl-4-phenyl-1,2,3,6-tetrahydropyridine (MPTP). C R Seances Soc Biol Fil 179:85–97
14. Kennedy RT, Jones SR, Wightman RM (1992) Dynamic observation of dopamine autoreceptor effects in rat striatal slices. J Neurochem 59:449–455
15. Pothos EN, Przedborski S, Davila V, Schmitz Y, Sulzer D (1998) D2-Like dopamine autoreceptor activation reduces quantal size in PC12 cells. J Neurosci 18:5575–5585
16. Justice JB Jr, Nicolaysen LC, Michael AC (1988) Modeling the dopaminergic nerve terminal. J Neurosci Methods 22:239–252
17. Qi Z, Miller GW, Voit EO (2008) Computational systems analysis of dopamine metabolism. PLoS One 3:e2444
18. Best JA, Nijhout HF, Reed MC (2009) Homeostatic mechanisms in dopamine synthesis and release: a mathematical model. Theor Biol Med Model 6:21
19. Qi Z, Miller GW, Voit EO (2010) Computational modeling of synaptic neurotransmission as a tool for assessing dopamine hypotheses of schizophrenia. Pharmacopsychiatry 43(Suppl 1): S50–S60
20. Voit EO, Qi Z, Miller GW (2008) Steps of modeling complex biological systems. Pharmacopsychiatry 41(Suppl 1):S78–S84
21. Wu J, Qi Z, Voit EO (2010) Investigation of delays and noise in dopamine signaling with hybrid functional Petri nets. In Silico Biol 10.
22. Curto R, Voit EO, Sorribas A, Cascante M (1998) Mathematical models of purine metabolism in man. Math Biosci 151:1–49
23. Palsson BO, Lightfoot EN (1984) Mathematical modelling of dynamics and control in metabolic networks. I. On Michaelis-Menten kinetics. J Theor Biol 111:273–302
24. Savageau MA (1969) Biochemical systems analysis. II. The steady-state solutions for an n-pool system using a power-law approximation. J Theor Biol 25:370–379
25. Savageau MA (1969) Biochemical systems analysis. I. Some mathematical properties of the rate law for the component enzymatic reactions. J Theor Biol 25:365–369
26. Savageau MA (1970) Biochemical systems analysis. 3. Dynamic solutions using a power-law approximation. J Theor Biol 26:215–226

27. Growdon JH, Melamed E, Logue M, Hefti F, Wurtman RJ (1982) Effects of oral L-tyrosine administration on CSF tyrosine and homovanillic acid levels in patients with Parkinson's disease. Life Sci 30:827–832
28. Myohanen TT, Schendzielorz N, Mannisto PT (2010) Distribution of catechol-O-methyltransferase (COMT) proteins and enzymatic activities in wild-type and soluble COMT deficient mice. J Neurochem 113:1632–1643
29. Bolch WE (2010) The Monte Carlo method in nuclear medicine: current uses and future potential. J Nucl Med 51:337–339
30. Qi Z, Miller GW, Voit EO (2009) Computational analysis of determinants of dopamine (DA) dysfunction in DA nerve terminals. Synapse 63:1133–1142
31. Fernandez HH, Chen JJ (2007) Monamine oxidase inhibitors: current and emerging agents for Parkinson disease. Clin Neuropharmacol 30:150–168
32. Youdim MB, Bakhle YS (2006) Monoamine oxidase: isoforms and inhibitors in Parkinson's disease and depressive illness. Br J Pharmacol 147(Suppl 1):S287–S296
33. Stocchi F, Vacca L, Grassini P, De Pandis MF, Battaglia G et al (2006) Symptom relief in Parkinson disease by safinamide: Biochemical and clinical evidence of efficacy beyond MAO-B inhibition. Neurology 67:S24–S29
34. Tyce GM, Dousa MK, Muenter MD (1990) MAO and L-dopa treatment of Parkinson's disease. J Neural Transm Suppl 29:233–239
35. Caudle WM, Richardson JR, Wang MZ, Taylor TN, Guillot TS et al (2007) Reduced vesicular storage of dopamine causes progressive nigrostriatal neurodegeneration. J Neurosci 27:8138–8148
36. Colebrooke RE, Humby T, Lynch PJ, McGowan DP, Xia J et al (2006) Age-related decline in striatal dopamine content and motor performance occurs in the absence of nigral cell loss in a genetic mouse model of Parkinson's disease. Eur J Neurosci 24:2622–2630
37. Mooslehner KA, Chan PM, Xu W, Liu L, Smadja C et al (2001) Mice with very low expression of the vesicular monoamine transporter 2 gene survive into adulthood: potential mouse model for parkinsonism. Mol Cell Biol 21:5321–5331
38. Takahashi N, Miner LL, Sora I, Ujike H, Revay RS et al (1997) VMAT2 knockout mice: heterozygotes display reduced amphetamine-conditioned reward, enhanced amphetamine locomotion, and enhanced MPTP toxicity. Proc Natl Acad Sci U S A 94:9938–9943
39. Glatt CE, Wahner AD, White DJ, Ruiz-Linares A, Ritz B (2006) Gain-of-function haplotypes in the vesicular monoamine transporter promoter are protective for Parkinson disease in women. Hum Mol Genet 15:299–305
40. Walaas SI, Aswad DW, Greengard P (1983) A dopamine- and cyclic AMP-regulated phosphoprotein enriched in dopamine-innervated brain regions. Nature 301:69–71
41. Svenningsson P, Nishi A, Fisone G, Girault JA, Nairn AC et al (2004) DARPP-32: an integrator of neurotransmission. Annu Rev Pharmacol Toxicol 44:269–296
42. Greengard P, Allen PB, Nairn AC (1999) Beyond the dopamine receptor: the DARPP-32/protein phosphatase-1 cascade. Neuron 23:435–447
43. Spencer HJ (1976) Antagonism of cortical excitation of striatal neurons by glutamic acid diethyl ester: evidence for glutamic acid as an excitatory transmitter in the rat striatum. Brain Res 102:91–101
44. Girault JA, Spampinato U, Savaki HE, Glowinski J, Besson MJ (1986) In vivo release of [3H] gamma-aminobutyric acid in the rat neostriatum—I. Characterization and topographical heterogeneity of the effects of dopaminergic and cholinergic agents. Neuroscience 19:1101–1108
45. Lindskog M, Kim M, Wikstrom MA, Blackwell KT, Kotaleski JH (2006) Transient calcium and dopamine increase PKA activity and DARPP-32 phosphorylation. PLoS Comput Biol 2: e119
46. Barbano PE, Spivak M, Flajolet M, Nairn AC, Greengard P et al (2007) A mathematical tool for exploring the dynamics of biological networks. Proc Natl Acad Sci U S A 104:19169–19174

47. Fernandez É, Schiappa R, Girault JA, Le Novère N (2006) DARPP-32 is a robust integrator of dopamine and glutamate signals. PLoS Comput Biol 2:e176
48. Qi Z, Miller GW, Voit EO (2010) The internal state of medium spiny neurons varies in response to different input signals. BMC Syst Biol 4:26
49. Qi Z, Kikuchi S, Tretter F, Voit EO (2011) Effects of dopamine and glutamate on synaptic plasticity: a computational modeling approach for drug abuse as comorbidity in mood disorders. Pharmacopsychiatry 44(Suppl 1):S62–S75

Index

P. Wellstead and M. Cloutier (eds.), *Systems Biology of Parkinson's Disease*,
DOI 10.1007/978-1-4614-3411-5,